

**ELECTRICAL POWER SUPPLY  
TO OFFSHORE OIL INSTALLATIONS  
BY  
HIGH VOLTAGE DIRECT CURRENT  
TRANSMISSION**

Jørgen Chr. Myhre

A thesis submitted to  
Norwegian University of Science and Technology  
Faculty of Electrical Engineering and Computer Science  
Department of Electrical Power Engineering  
in partial fulfilment of the requirements for the degree: doktor ingeniør.

April 2001

ISBN 82-7948-186-5  
ISSN 0809-103X  
2001:24

Have you taken the Devil on your back, you must carry him to the destination.

## ACKNOWLEDGEMENTS

This study was initiated in 1992 as a part of the Strategic Technology Programme “Norge som energinasjon” (Norway as Energy Nation), based on cooperation between the Department of Electrical Power Engineering at Norwegian Institute of Technology (NTH) and the Norwegian Electric Power Research Institute (EFI). The programme was financed by the Royal Norwegian Council for Scientific and Industrial Research (NTNF).

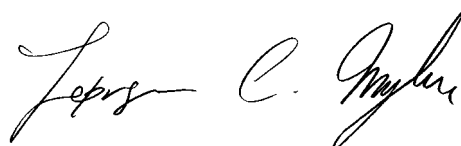
A lot of water has flowed through the turbines since then, NTNF has become the Research Council of Norway, NTH has become part of the Norwegian University of Science and Technology and EFI has become SINTEF Energy Research. The scholarship ended and I had to go back to my former workplace by Siemens in Norway at the Department of Industry, Maritime and Transportation Services for financial reasons and complete my thesis in my spare time, which turned out scarce.

Thus I have to express my sincere gratitude to my scientific advisers, Professor Tore Undeland, Dept. of Electrical Power Engineering, and Adjunct Professor/ specialist Henry B. Raphael, Statoil, not the least for their infinite patience with my slow progress. I also wish to express my gratitude to Adjunct Associate Professor/ senior engineer Asle Skjellnes, Siemens, for bringing in many good ideas, even though they often led to extra work. I also wish to thank the rest of the staff and my fellow doctoral students at the department for support, help and encouragement during almost a decade.

I also thank Stewart Clark at NTNU for his help with the final English Editing.

Last, but not least I must thank my wife Nina for her patience and my children Birgitte, Julie and Rolf, who have almost forgotten how a father should act.

Trondheim, April 2001



*Acknowledgements*

# SUMMARY

This study was initiated to investigate if it could be feasible to supply offshore oil installations in the North Sea with electrical power from land. A prestudy of alternative converter topologies indicated that the most promising solution would be to investigate a conventional system with reduced synchronous compensator rating.

The study starts with a summary of the state of power supply to offshore installations today, and a short review of classical HVDC transmission. It goes on to analyse how a passive network without sources influences the inverter. The transmission, with its current controlled rectifier and large inductance, is simulated as a current source. Under these circumstances the analysis shows that the network frequency has to adapt in order to keep the active and reactive power balance until the controllers are able to react. The concept of firing angle for a thyristor is limited in a system with variable frequency, the actual control parameter is the firing delay time.

Sensitivity analysis showed some astonishing consequences. The frequency rises both by an increase in the active and in the reactive load. The voltage falls by an increase in the active load, but rises by an increase in the inductive load.

Two different control principles for the system of inverter, synchronous compensator and load are defined. The first takes the reference for the firing delay time from the fundamental voltage at the point of common coupling. The second takes the reference for the firing delay time from the simulated EMF of the synchronous compensator. Of these, the second is the more stable and should be chosen as the basis for a possible control system.

Two simulation tools are applied. The first is a quasi-phasor model running on Matlab with Simulink. The other is a time domain model in KREAN. The time domain model is primarily used for the verification of the quasi-phasor model, and shows that quasi-phasors is still a valuable tool for

making a quick analysis of the main features when the details of the transients are of less importance.

The study indicates that power supply by HVDC transmission from land to offshore oil installations could be technically feasible, even without the large synchronous compensators normally required. It has been shown that in a network only supplied by an inverter, variations of active and reactive loads have significant influence on both voltage and frequency. Particularly it should be noted that the frequency shows a positive sensitivity to increases in load. This could make the system intrinsically unstable in the case of a frequency dependent load such as motors.

It was not a part of the study to optimize controllers, but even with simple controllers it was possible to keep the frequency within limits given by norms and regulations, but the voltages were dynamically outside the limits, though not very far. These voltage overswings take place in the first few instances after a disturbance, so it takes unrealistically fast controllers to handle them. They are partly due to the model, where the land based rectifier and the DC reactors are simulated by a constant current source, but partly they have to be handled by overdimensioning of the system.

The simulations indicate that it should be technically possible to supply an oil platform with electrical power from land by means of HVDC transmission with small synchronous compensators. Whether this is financially feasible has not been investigated. Neither has it been considered whether the necessary equipment can actually be installed on an oil platform.

Recently both ABB and Siemens have presented solutions for HVDC transmission in the lower and medium power range based on voltage source converters based on IGBTs. Fully controllable voltage source HVDC converters have properties that may be better suited than conventional line commutated current source thyristor inverters, to supply weak or passive networks, such as offshore oil installations, with electrical power. But they also have some disadvantages, and a complete technical and financial comparison must be performed in order to decide about any potential project.

# TABLE OF CONTENTS

Acknowledgements .....	iii
Summary.....	v
List of symbols and abbreviations.....	xiii
Abbreviations.....	xiii
Symbols .....	xiv
Subscripts.....	xv
1 Introduction .....	1
1.1 Environmental aspects .....	1
1.2 Financial aspects.....	2
1.3 Recent developments .....	3
1.4 Scope of the thesis .....	3
1.5 Structure of thesis .....	4
2 Offshore power supply systems.....	7
2.1 Power sources of today .....	7
2.2 Electric power systems .....	9
2.2.1 Main power system .....	9
2.2.2 Emergency power system .....	9
2.2.3 Essential power supply.....	10
2.3 Technical requirements for power supply to offshore installations.....	10
2.3.1 Norms and regulations .....	10
2.4 Types of load .....	11
2.4.1 Drives for process- and auxiliary systems .....	11
2.4.2 Process heating systems .....	11
2.4.3 Electrochemical systems .....	11
2.4.4 Lighting-, heating- and ventilation systems .....	12
2.4.5 Typical consumers .....	12
2.5 Electric Power Supply from Land .....	13

*Table of contents*

2. 5. 1	Power ratings.....	13
2. 5. 2	Transmission methods.....	13
2. 6	Summary.....	14
3	Models for electric machines and drives .....	15
3. 1	Levels of models.....	15
3. 2	Induction motors .....	16
3. 2. 1	Transient model.....	16
3. 2. 2	Subtransient model.....	22
3. 3	Induction motors at start-up.....	22
3. 4	Synchronous machines .....	23
3. 4. 1	Transient model.....	23
3. 4. 2	Subtransient model.....	27
3. 5	Adjustable speed drives .....	27
3. 5. 1	Current source inverters, transient model .....	27
3. 5. 2	Voltage source inverters, transient model.....	30
3. 5. 3	Subtransient model.....	30
3. 6	Summary.....	30
4	Conventional HVDC transmission .....	31
4. 1	General.....	31
4. 1. 1	HVDC transmission systems .....	31
4. 1. 2	HVDC converters.....	33
4. 1. 3	HVDC converter stations .....	34
4. 2	Basic control principles .....	35
4. 2. 1	DC transmission control.....	35
4. 2. 2	Converter current/voltage characteristics.....	36
4. 2. 3	Tap changer control .....	40
4. 2. 4	Master control system and telecommunications .....	42
4. 3	Quasi-stationary model of HVDC systems.....	42
4. 4	Summary.....	44
5	HVDC supply to weak AC networks .....	45
5. 1	Voltage stability.....	45
5. 2	Temporary overvoltages .....	53
5. 3	Summary.....	53
6	HVDC supply to offshore oil installations .....	55
6. 1	Introduction.....	55
6. 2	Simulation programs.....	56
6. 3	Simulation model.....	57
6. 3. 1	Distributed load behind transformers.....	57
6. 3. 2	Rotating large induction motor load .....	58



6.3.3	Motor to be started .....	59
6.3.4	Adjustable speed drives load.....	59
6.3.5	Harmonic filters .....	60
6.3.6	Static Var Compensator .....	61
6.3.7	Synchronous compensator .....	61
6.3.8	HVDC transmission .....	62
6.3.9	Supply network with filter circuits on land.....	62
6.3.10	Control of HVDC transmission, SVC and synchronous compensator .....	62
6.4	summary.....	63
7	Analysis of a network with an RC load.....	65
7.1	Introduction.....	65
7.2	Unstabilized RC network fed by line commutated inverter .....	66
7.2.1	Unstabilized systems.....	66
7.2.2	Sensitivity of frequency and voltage for variations in load .....	76
7.2.3	Physical analysis of positive sensitivity of frequency for variations in conductance.....	79
7.2.4	Sensitivities of frequency and voltage for variations in firing delay time and network capacity .....	84
7.2.5	Relative sensitivity .....	88
7.2.6	Example, small signal sensitivity.....	92
7.3	RC networks fed by controlled inverter with controllable capacitance.....	96
7.3.1	Control theory .....	96
7.3.2	Base case example .....	99
7.4	Summary .....	115
8	Consequences of a synchronous compensator .....	117
8.1	Introduction.....	117
8.2	Reactive power production characteristics of capacitors and synchronous compensators .....	118
8.2.1	Capacitors.....	118
8.2.2	Synchronous compensators.....	119
8.3	Inverter network with both capacitors and synchronous compensators .....	121
8.4	Conclusion .....	132
8.4.1	Conditions for solution.....	132
8.4.2	Stationary conditions.....	132
8.4.3	Bypassing critical areas.....	132
8.4.4	Consideration of the compensator inertia .....	133
8.4.5	Relation to classical theory .....	134

*Table of contents*

9	Quasi-phasor simulations of a system with a synchronous compensator and a passive load, without controllers.....	135
9.1	Introduction.....	135
9.2	About the model.....	136
9.3	System to be simulated .....	138
9.4	Quasi-phasor simulations.....	140
9.4.1	System with reference for the firing pulses given by the voltage at PCC .....	140
9.4.2	System with reference for the firing pulses given by the EMF of the compensator .....	148
9.4.3	Conclusion .....	156
9.5	Verification simulations by Krean.....	156
9.5.1	Voltage at PCC as reference .....	156
9.5.2	EMF in the synchronous compensator as reference.....	161
9.5.3	Comparison of results .....	165
9.6	Conclusion .....	170
10	Quasi-phasor simulations of a system with a synchronous compensator and induction motor starting directly on line .....	173
10.1	System to be simulated .....	173
10.2	Simulations of system with reference for the firing pulses given by the voltage at PCC .....	174
10.3	Simulations of system with reference for the firing pulses given by the EMF of the compensator.....	177
10.3.1	Connecting the motor, at $t=1$ s .....	180
10.3.2	The motor reaches full speed, at $t\approx 19$ s .....	186
10.3.3	Loading the motor, at $t=23$ s .....	188
10.3.4	Conclusion .....	188
10.4	Verification simulations by KREAN.....	190
10.4.1	Voltage at PCC as reference .....	190
10.4.2	EMF in the synchronous compensator as reference.....	193
10.5	Conclusion .....	195
11	Practical implementation of HVDC transmission from land to an offshore installation .....	197
11.1	Introduction.....	197
11.2	Necessary equipment on board the offshore installation .....	198
11.2.1	The inverter .....	200
11.2.2	Inverter transformer .....	200
11.2.3	Harmonic filters .....	201
11.2.4	Capacitor banks.....	201
11.2.5	Synchronous compensator .....	203
11.2.6	The motor to be started .....	204

11. 2. 7	Running DOL motors.....	204
11. 2. 8	Control strategy on board.....	204
11. 2. 9	Land-based rectifier .....	205
11. 2. 10	Rectifier control .....	206
11. 2. 11	Telecommunications .....	207
11. 2. 12	Worst case variation of reactive power.....	207
11. 2. 13	Procedure for starting a large motor .....	208
11. 3	Summary.....	209
12	KREAN simulations on model with inverter, synchronous compensator and load .....	211
12. 1	Simulation conditions .....	211
12. 2	Model with resistive base load.....	212
12. 3	Conclusion .....	218
13	Conclusions .....	221
13. 1	Background.....	221
13. 2	Frequency must vary.....	221
13. 3	Two models.....	222
13. 4	Two simulation tools .....	222
13. 5	Simulation results .....	222
13. 6	Practical implementations.....	223
13. 7	Recent development.....	223
Appendix A	Calculation of active and reactive power of an induction motor based on curves for torque and current during start-up.....	225
Appendix B	Machine data for a typical offshore generator.....	229
Appendix C	Machine data for a typical large induction motor .....	231
Appendix D	Comparison of Systems for HVDC Power Supply to Offshore Oil Installations with Emphasis on the Double Bridge Inverter.....	235
	References .....	243

*Table of contents*

# LIST OF SYMBOLS AND ABBREVIATIONS

## ABBREVIATIONS

AC	Alternating Current
CO <sub>2</sub>	Carbon Dioxide
DC	Direct Current
EMF	Electromotoric Force, Induced Voltage
ESC	Equivalent Short Circuit Power
ESCR	Equivalent Short Circuit Ratio
HVDC	High Voltage Direct Current
IGBT	Insulated Gate Bipolar Transistor
MAP	Maximum Available Power
NPD	Norwegian Petroleum Directorate
PCC	Point of Common Coupling
PI	Proportional+Integral
PLL	Phase Locked Loop
RMS	Root Mean Square
SC	Short Circuit Power
SCR	Short Circuit Ratio
Sm <sup>3</sup>	Standard Cubic metre
SVC	Static VAR Compensator
TCR	Thyristor Controlled Reactor
TOV	Temporary Overvoltages

## SYMBOLS

$\alpha$		Firing angle
$\beta$		Pole wheel angle
$b$	B	Susceptance
$c$	C	Capacitance
$\Delta t$		Firing delay time
	D	Damping constant
$d_{xN}$		Rated relative inductive voltage drop
$e$	E	Induced voltage, EMF
$e_k$		Relative short circuit voltage
	ESC	Equivalent short circuit power
	ESCR	Equivalent short circuit ratio
$\gamma$		Extinction angle
$g$	G	Conductance
$i_{s0}$		Initial short circuit current
$j$		Complex operator
	J	Inertia
$k$		Constant
$l$	L	Inductance
$m$	M	Torque
$p$	P	Active power
$q$	Q	Reactive power
$r$	R	Resistance
$r_a$	$R_a$	Stator resistance
$\sigma$		Slip
$s$	S	Apparent power
	SC	Short circuit power
	SCR	Short circuit ratio
$\tau$		Period
	T	Time constant
$u$	U	Voltage
$u_{dio}$	$U_{dio}$	Ideal no-load direct voltage
$\omega$		Angular frequency
$x$	X	Reactance
$x_{ad}$	$X_{ad}$	Mutual reactance
$x_k$	$X_k$	Commutation reactance
$\psi$		Magnetic flux
$y$	Y	Admittance
$z$	Z	Impedance
	$\Omega$	Rotational speed
*		Complex conjugate

## SUBSCRIPTS

0	Initial value, Before disturbance
1	Stator
1	After disturbance
2	Rotor
A	Converter A
B	Converter B
c	Capacitor
con	Converter
d	Air-gap (Torque, Power)
d	d-axis
d	DC-side
e,el	Electrical
E	Effective
f	Exciter
i	Inverter
l	Load, Network
m	Magnetizing
m,mek	Mechanical
n,N	Nominal, rated
p	Pull-Out
q	q-axis
r	Rectifier
ref	Reference
s	Source
sc	Synchronous compensator
v	AC-side

*List of symbols and abbreviations*



# 1 INTRODUCTION

This chapter is intended to give a brief overview of the content of the thesis.

## 1.1 ENVIRONMENTAL ASPECTS

From its beginning, oil production in the North Sea and North Atlantic has, with a few exceptions, based its consumption of electric energy on local production by means of generators powered by gas turbines. Additionally, turbines have been the prime mover of many compressors and pumps in the MW range. On mobile or small units, diesel engines have also been used for electric power production or as the prime mover of machines. Power production based on combustion of gas was a natural solution, the gas is always present in sufficient amounts, on an oil production unit it was sometimes even considered a waste, which one had to get rid of anyway. Lots of gas was just flared off.

Gradually, this gas acquired a value. It could be used for reinjection to increase the amount of oil that could be extracted from a reservoir, or eventually, with the necessary infrastructure coming in place, it can be processed and sold at a profit. At the same time, people became aware of the threatening greenhouse effects; they fear a global increase in the temperature, mainly due to increased concentration of carbon dioxide (CO<sub>2</sub>) in the atmosphere. Protection of the environment came into the political agenda, and as a part of the efforts to stabilize the production of CO<sub>2</sub>, the Norwegian Government imposed a tax on the emission of CO<sub>2</sub> on Norwegian offshore installations, as well as onshore facilities related to the oil industry. The flaring of gas on offshore installations has almost come to an end, and the oil companies are looking at other possibilities to reduce CO<sub>2</sub>-emissions.

The largest source of CO<sub>2</sub>-emissions in Norway and Norwegian waters is offshore gas turbines for power production and directly driven machines. Altogether, 196 gas and diesel turbines with a total power rating of approximately 2780 MW turbine power were installed or planned in the Norwegian Economic Zone at the beginning of 1995 [35], which represents a yearly emission of 8.9 million tonnes CO<sub>2</sub> or about 24 % of the total Norwegian CO<sub>2</sub> emission of 37.5 million tonnes yearly. If some of the energy needed for the operation of Norwegian oil production could be replaced by electricity from hydroelectric power plants on land, it would be a substantial step towards the goal of reducing the CO<sub>2</sub>-emissions to 1989-level, where they should be in year 2000, according to national obligations, taken on after the Rio World climate conference.

## 1.2 FINANCIAL ASPECTS

*(All cost comparisons are based on the exchange rate USD1.00=NOK7.00)*

The financial aspects are perhaps just as important as the environmental ones. The gas price on the European market was approximately USD0.10/Sm<sup>3</sup> in 1995. If transportation costs are neglected, this can be regarded as the maximum value of the gas on a platform with exportation possibilities. On an oil production platform without gas exportation possibilities the gas can be re-injected into the reservoir to increase the oil yield so it still has a value. But as this value is difficult to estimate, the minimum value of the gas is zero. Based on these upper and lower limits in the gas price, a Norwegian CO<sub>2</sub>-tax of NOK 0.857 (USD0.122)/Sm<sup>3</sup> and an efficiency of a modern gas-turbine of 30 %, the cost for electric energy produced on site is between USD0.061/kWh and USD0.033/kWh. The price of bulk, long term supply of electric energy on shore in Norway was approximately USD0.029/kWh in 1995, which leaves between USD0.004/kWh and USD0.032/kWh to pay for the difference in investment between gas turbine generators and transmission system from ashore.

One very important factor in the investment cost is the total weight of the system installed on a platform. A rule of thumbs in the Norwegian oil industry is that 1 tonne of equipment requires 10 tonnes of construction materials for support in case the platform is resting on the sea bed. In the case of a floating construction the relation can be even worse. In the case of one specific floater, the calculated price for carrying 1 extra ton equipment was approximately USD1500.

It should be kept in mind that rebuilding existing installations is not very likely, but these aspects can come into consideration for new platforms.

### **1.3 RECENT DEVELOPMENTS**

Recently, both ABB [41] and Siemens [42] have introduced concepts for HVDC transmission based on pulse width modulated IGBT converters. Still the rating of these units is fairly low, typically about 200-250 MW per unit. Transmission voltage is in the range of 145 kV, and the losses are several times higher than conventional HVDC. Still this new technology offers some interesting perspectives. As the new technology is based on voltage source converters, there is a far better possibility of constructing multiterminal systems. It is also possible to connect these units in parallel in order to increase capacity. On the other hand, the announced possibility of providing the necessary reactive may be somewhat overstated, taking into account that this requires increased current carrying capability and consequently overdimensioning. But they may offer an interesting provider of part of the reactive power required. At least they may be operated so that they do not require reactive power themselves under normal conditions.

With these new possibilities, BP has started a prestudy of supplying their installations in British Sector of the North Sea with electric power from land. Potential suppliers have already presented ideas of compact prefabricated inverter units to be lifted onto abandoned production platforms. From these inverters, electric power will then be distributed by ordinary AC cable grids for supply to clusters of platforms.

### **1.4 SCOPE OF THE THESIS**

The scope of this thesis is to evaluate possible methods of supplying power to an offshore oil/gas production installation by means of HVDC, thereby replacing local power generation by gas turbines. The solution should be feasible for use where direct AC transmission is not technically or economically possible. The system must be able to transmit the necessary power for all operations of an oil production installation, units that are directly powered by gas-turbines today are also to be electrically powered. The era of big platforms may possibly soon come to an end and smaller oil production units will be placed subsea in the future, so the system should be based on components and technology available at the start of the project.

Initially, a study of possible converter topologies [12], [13], [14] was performed, and a comparison of the most likely alternatives on the basis of weight [15]. This comparison was presented at the Stockholm Power Tech in 1995, Appendix D. Finally it was decided to perform the study for a conventional line commutated thyristor converter, with the aim to minimize the synchronous compensator. This was regarded as the most acceptable solution for oil and gas companies. Such a solution includes line commutated converters feeding power into a weak network, with the stability problems this is known to imply.

## 1.5 STRUCTURE OF THESIS

The thesis starts with an overview of traditional offshore power supply systems (Chapter 2). Some simplified models for typical motor loads are introduced (Chapter 3). After a short summary of conventional HVDC theory (Chapter 4) and problems with weak AC networks (Chapter 5), the requirements for an HVDC transmission to offshore oil production platforms are reviewed (Chapter 6).

As the norms allow for larger frequency deviations on such installations, it was decided to investigate if it could be a solution to make the most of this freedom and exploit the kinetic energy available in rotating machinery. Further it was decided to perform the analysis with a quasi-phasor model. This makes simple and fast simulations and gives sufficient quality of the results to conclude about the stability. Detailed analysis in the time domain was considered superfluous, but is applied as verification of the results in certain cases. In order to understand the consequences of an inverter feeding a weak network with variable frequency, the network is replaced by a simple RC circuit, and the behaviour investigated (Chapter 7). Surprisingly it is found that in a system without controllers the frequency will increase when the load increases. This is an inherent feature of the current source line commutated converter, which has gone largely unheeded.

Another aspect that had to be taken into consideration was the dissimilar reactive power production characteristics of capacitors and synchronous compensators (Chapter 8).

Two distinct models of a passive network fed by a thyristor inverter with reactive power supply from a small synchronous compensator together with capacitor banks are developed. In one of these, the reference for the firing pulses to the thyristors is taken from the voltage at the point of common coupling. In the other the reference is taken from the EMF of the synchronous compensator (Chapter 9). The models are analysed for operations without

controllers to investigate the intrinsic stability. Then the models are enlarged with a large induction motor to be started. (Chapter 10). The simulations show that a system consisting of initially resistive load, fed by an uncontrolled thyristor inverter and with reactive supply from capacitors and a synchronous compensator rated at 20 % of the inverter, is able to start up an induction motor with power rating 10 % of the inverter.

Conclusively some aspects of a practical implementation are discussed (Chapter 11) and a simulation of a system with active controllers is performed (Chapter 12). These simulations give an unacceptable dynamic deviation in the voltage, but the controllers are not optimized and it is assumed that better controllers can remedy some of this. It has not been a scope of this thesis to optimize the controllers.

The worst voltage overshoots take place in the first few instances after a disturbance, so it takes unrealistically fast controllers to handle them completely. They are partly due to the model, where the land based rectifier and the DC reactors are simulated by a constant current source, which may be a too stiff model. But partly they have to be handled by overdimensioning of the system.

The conclusion is that a line commutated current source thyristor inverter with minimized synchronous compensator might be a possible solution for electric power supply to offshore installations from land. Meanwhile voltage source converters for HVDC have become practically available, and may be a serious competitor to classical line commutated inverters. But the classical converters still have their good sides too, better efficiency is one vital aspect.

Anyhow, this work has hopefully brought forward some interesting aspects as to the supply of power by HVDC to networks without power generation of their own.



## **2 OFFSHORE POWER SUPPLY SYSTEMS**

In this chapter I will give a short introduction to the normal power supply systems on oil and gas platforms of today, and consequently what is required of an electric power supply from land.

### **2.1 POWER SOURCES OF TODAY**

The need for power on offshore installations in the Norwegian Economic Zone is almost without exception met by local production, mainly in two ways. Heavy machinery such as gas compressors and pumps are in most cases powered directly from gas turbines or diesel motors, if necessary with a gear in the middle. Electricity is produced from generators powered by gas turbines, occasionally by diesel engines. The main part of the electricity is then consumed by electric motors, another part is consumed in electric heating in the production process, and some goes to lighting, comfort heating and auxiliary equipment. Additionally some heating is provided from heat exchangers, and in the early years some heat was produced in direct-fired boilers, but this is not common today due to safety.

There are large variations in the total need for power on the offshore installations on the Norwegian Economic Zone. Some of the factors that decide the need for power are:

- Field size and type.
  - Temperature, pressure, oil/gas ratio
- Processing.
  - What happens to the product on the installation. Separation,

compressing, heating, cooling.

- Water and/or gas injection.

To retrieve as much oil or gas as possible from the reservoir.

- Transportation system.

Pipelines or ship transportation.

The need for power varies for different installations, from 10-100 kW for small wellhead installations to more than 100 MW for the biggest platforms. The total need for power for large fields like Ekofisk or Tampen (Statfjord/Gullfaks/Veslefrikk) is close to 500 MW each.

The choice between an electric motor and a gas turbine for powering a machine is mainly decided by the short circuit capability of the network. This decides how large squirrel cage motors can be directly started without unallowable disturbances on the network. The limit for directly started electric motors has gradually increased, from 5 MW in the early days up to 8 MW today, with increasing electric power rating in the supply systems. In the case of adjustable speed drives the start-up is far less disturbing for the network and drives up to 13 MW have been installed recently. For machines of higher ratings, gas turbines have been the main power source.

The limits on motor size are not absolute, they depend on many other factors as well, company traditions among others. So the ratio between electric powering and turbine powering varies widely. Ula, with a load of 30 MW and motors up to 4 MW, is an example of a 100 % electric powered platform. Ekofisk, with a total mechanical and heating load of 400 MW, is 90 % equipped with directly driven machines.

The cost of the drive systems is an important factor when selecting between direct turbine drives and electric drives. An interesting internal study was made by Statoil [1] regarding the Veslefrikk platform, where the choice was between three small turbines driving compressors, or to increase the generating power capability to full electric supply. The investigation proved that the cost for the drives would be equal in both cases, but there was a small saving in total for the fully electrical system due to savings regarding exhaust system etc. The total efficiency was equal, the electrical losses were compensated by a better efficiency in the larger generator turbines. There were no savings in weight and volume in either case. Finally the electric solution was selected, and afterwards savings have been reported in the processing, due to smoother operation and less maintenance.

The most important exception from the rule of local power production is the gas field Troll. The first platform, Troll A is situated approximately 70 km off the coast. As most of the gas processing is removed to Kollsnes onshore,



it had an estimated maximum load of 17 MW when it started production in 1996. Due to the relatively short distance it was decided to supply the platform with electric power from land, via a 52 kV  $U_{\max}$  AC cable connection with a transmission capability of 17.5 MW.

## 2. 2 ELECTRIC POWER SYSTEMS

The electric power supply on an oil production platform is regarded as an auxiliary system, designed to supply the platform with the necessary electric power throughout its lifetime with sufficient reliability and availability. The power systems have usually been split into the following three categories:

- Main power system.
- Essential power supply.
- Emergency power system.

### 2. 2. 1 Main power system

The main power system is designed to supply all the electric power needed for the daily operation of the platform according to certain criteria regarding redundancy, flexibility, minimum load, cost optimization and environmental considerations. There are usually 2 to 4 identical generators, normally powered by gas turbines. The generator ratings vary in steps determined by the available standard gas turbines, traditionally not more than approximately 20 MW, but recently up to 35 MW turbines have been installed. One main consideration when selecting generators is to keep the short circuit current within reasonable design limits, 40 kA by high voltage distribution, 50 kA by low voltage distribution.

### 2. 2. 2 Emergency power system

To comply with Norwegian Petroleum Directorate (NPD) requirements regarding power supply in emergency situations, there has to be an emergency power supply, normally powered by diesel engines. This system is to be completely independent of the main power system and supply necessary power for fire fighting equipment, emergency lighting, cooling systems etc. for up to 24 hours, starting automatically when the main power system fails. The rating of these systems vary widely, but is normally between 0.5 and 1.5 MW.

### **2. 2. 3 Essential power supply**

During commissioning of a new platform and in the drilling period before the platform comes into production, the power has often been provided by a separate power supply, the essential power system. This is usually powered by diesel engines, in some cases by dual-fuel gas-turbines. This system can also allow certain critical operations to be continued or to be terminated in a controlled way if a major fault occurs in the main power supply or during maintenance periods. It also keeps the living quarters habitable if the main power is down for an extended period. On large platforms the generator capacity for such systems can have a rating of up to 2x4 MW. The distribution system for essential power supply is usually part of the normal distribution system. There is a tendency to omit this category on newer platforms as the main power supplies prove their reliability. The need during commissioning can be met in several ways including dual-fuel main generator turbines, temporary diesel generator sets or supply from auxiliary vessels and hotel platforms.

## **2. 3 TECHNICAL REQUIREMENTS FOR POWER SUPPLY TO OFFSHORE INSTALLATIONS**

### **2. 3. 1 Norms and regulations**

The total responsibility for supervision of the permanent oil installations in the Norwegian Economic Zone has been transferred to the Norwegian Petroleum Directorate (NPD). NPD has prepared regulations for electrical installations on oil platforms [3]. These regulations are not technical regulations however, they refer to the regulations for electrical installations in ships and marine equipment [2] for the technical design.

During the first years the electrical installations on most platforms have been built according to American practice with voltages of 13.8 kV or 6 kV for large motors, 440 V for smaller motors and 220 V for lighting and heating. The frequency has been 60 Hz. One exception is Frigg. Here the same voltages were applied but the frequency was 50 Hz.

Now the operating oil companies in the Norwegian Zone have agreed on new norms for the electrical installations, the NORSOK-OLF specifications, for new offshore oil facilities. These specifications require standard IEC voltages, up to 11 kV for large motors (above approx. 300 kW), 690 V TT system for smaller motors and 230/400 V TN-C-S systems for lighting and heating.

The frequency is to be 50 Hz. The voltages have to be kept within  $\pm 2.5$  % stationary and are allowed to vary  $+20/-15$  % dynamically at the largest normal load switching [2] (§1306). The frequency variations are  $\pm 5$  % stationary and  $\pm 10$  % transiently (§1307).

## **2. 4      TYPES OF LOAD**

The most important types of load on an offshore installation can be split in the following categories:

- Drives for process- and auxiliary systems.
- Process heating systems.
- Electrochemical systems.
- Lighting-, heating- and ventilation systems.

### **2. 4. 1      Drives for process- and auxiliary systems**

The drives for process-systems are almost exclusively powering pumps and compressors for oil, gas, water or chemicals. The required power rating can reach as high as 20 MW per unit. Traditionally units with more than 5 to 8 MW have been directly powered by turbines, while smaller units have been powered by electric motors. On a field like Ekofisk, for example, this type of load amounts to more than 90 % of the total power consumption of 400 MW, and most of it is directly powered by turbines.

### **2. 4. 2      Process heating systems**

The need for process heating varies from installation to installation. When large amounts of heat are needed, these are mostly supplied by oil- or gas burners, but electric boilers with ratings up to 20 MW have been installed. Additionally electric heat tracing cables and heat elements are used for local needs with low rating, and for special applications.

### **2. 4. 3      Electrochemical systems**

These are typically systems for the desalination of seawater, both for drinking water and for injection into the reservoir to increase the oil yield.

### 2. 4. 4 Lighting-, heating- and ventilation systems

A large platform can have a total need for lighting of 500 kW. Power for ventilation and heating of processing areas, control rooms and living quarters can reach the MW range.

### 2. 4. 5 Typical consumers

A typical list of power consumers for an oil production platform is found in Table 2-1. It is clear that the load will consist mainly of drives, most of

**Table 2-1 Main power consumption areas on an oil production platform**

Consumption area	Power	Type
Oil processing equipment.	1 - 2 MW	Heating/drives
Oil export systems	2 -12 MW	Large drives
Glycol/methanol regeneration systems	0.5 - 3 MW	Heating/small drives
Gas recompression	2 -10 MW	Large drives
Auxiliary systems	1 - 2 MW	Small/medium drives
Water injection systems	12 -25 MW	Large drives
Drilling systems	3 - 5 MW	Medium drives
Living quarters	0.5 - 2 MW	Lighting/heating/drives
Lighting, heating and ventilation	0.2 - 2 MW	Lighting/heating/drives
Heat tracing cable installations	0.1 - 1 MW	Heating
Emergency power consumers	0.5 - 6 MW	Lighting/heating/drives

them large. If the platform is to be fully electrically powered, the drives will mostly be large induction motors and synchronous motors with adjustable speed drives. For example, a study of the load on Midgaard presupposes two synchronous motors, each 30 MW fed by two separate frequency converters, four 5.5 MW high voltage induction motors and approximately 15 MW low voltage motors and passive load.

## **2.5 ELECTRIC POWER SUPPLY FROM LAND**

### **2.5.1 Power ratings**

If the supply of electric power from land to an offshore installation is to be feasible, it should be able to provide all the power needed on that installation. No gas turbines or diesel engines should be installed for normal operation, as the marginal cost of more power transmitted from land is much lower than turbine power. If possible, all the installations in one area, for example the whole Statfjord field together with Gullfaks and Veslefrikk or the whole Ekofisk area could be connected and supplied from the same source. But as these fields are already in production, rebuilding is not likely. When looking at the existing installations on the Norwegian Economic Zone, the required rating for a transmission project can easily rise to several hundreds MW.

### **2.5.2 Transmission methods**

The electric power supply from land has to be transmitted by sea-cables. These are individually designed and their electrical parameters can be varied within wide ranges to fit the actual need. Sintef Energy Research (formerly EFI) [22] has completed a study on the feasibility of AC power supply to offshore installations, based on a case of supplying an oil field with 100 MW at 132 kV over a distance of 180 km, which they found to be just at the technical limit. Due to redundancy requirements the possible alternatives were two 240 mm<sup>2</sup> three-core copper cables or four 500 mm<sup>2</sup> single-core copper cables. Electrically the single core alternative was best, while the three-core alternative had the best reliability. The cost of the three-core cable including laying and protection, but without switchgear and transformers was as high as a complete bipolar HVDC transmission with full capacity in monopolar operation. As the AC solution has much higher losses and voltage variations this alternative was without interest in this example. The single-core AC alternative could compete economically with a bipolar HVDC transmission with 67 % capacity in monopolar operation, but the reliability would be less and the losses higher for the AC alternative.

All alternatives for electric power supply from land were found to be more expensive than a conventional offshore power supply system when the power need was as low as 100 MW. If electric power supply from land is to be feasible for distances over 100-150 km and power ratings over 100 MW, it has to be an HVDC system, but with reduced converter station costs.

As mentioned earlier, the Troll A platform, situated about 70 km from shore with a rated power need of 17 MW is supplied with electrical AC power from land transmitted by one  $3 \times 240 \text{ mm}^2$  52 kV  $U_{\max}$  copper cable. This cable also integrates an optical fibre communication link with 24 fibres, which is used as the main communication line between the platform and land.

## **2.6 SUMMARY**

Power consumption on oil and gas platforms vary in wide ranges, from some tens of kW for small wellheads to several hundreds of MW for great clusters, and is not always met with electric power. If an electric power supply from land shall be of interest, it must replace both the electric power production and combustion machines for direct drives.

Transmission must be by sea cables, and AC systems will not be technically feasible by the distances involved. This leaves HVDC transmission, which until now has been considered unfeasible, mainly due to the large and heavy synchronous compensators necessary in a traditional solution.

# **3 MODELS FOR ELECTRIC MACHINES AND DRIVES**

In this chapter I will review the traditional textbook models for motors, and modify them to be based on parameters easily available from catalogues and data sheets. I will also look at adjustable speed drives and their behaviour at variable network voltage and frequency.

## **3.1 LEVELS OF MODELS**

When analysing the behaviour of a network like that of an electrically powered oil production platform, two levels of modelling are required. When analysing system stability, the time constants of the events will be of a magnitude in the order of several periods of the network frequency. This allows us to simplify the electrical problem by neglecting the harmonics and operate only with RMS values of the fundamental. On the other hand, it will be necessary to take into account the mechanical properties of the system like load torque characteristics and machine inertia, and the influence of controllers present in the system. This can be compared to the transient model of a synchronous machine.

Additionally there is need for a subtransient level of modelling. This is required to analyse functional feasibility, for example commutation analysis of an unconventional type of converter. For such analysis the time constants are much shorter than one period, and time domain analysis will be the best tool. But in these cases, the frequency of the network and the speed of the machines can be considered constant.

## 3.2 INDUCTION MOTORS

### 3.2.1 Transient model

For electric motor drives offshore the squirrel cage induction motor is the preferred one as long as the network has sufficient short circuit power to allow direct on line (DOL) starting. The largest induction motors in the Norwegian Zone were approximately 8 MW in 1995. Such large high voltage induction motors usually have a very steep speed/torque characteristic at the operating point. Normally the operating slip is about 0.3 % to 0.7 % and the pull-out slip is only 1.5 % to 2 % [20]. Figure 3-1 shows a typical load curve for one such large induction motor (Siemens type 1RQ1805-4HN.0, 6.6 kV, 7480 kW, 1493 rpm). The same figure also presents a torque curve calculated on the basis of a motor model with constant parameters, together with a typical square load curve. The correspondence between model and reality is quite good for slip less than the pull-out slip, as shown in the blow-up of the range above pull-out in Figure 3-2. Here the curves for square load torque and constant load torque are also drawn. As can be seen, the correspondence between the linear motor model and real motor data is quite good. It is also obvious that within the normal slip range, the square load curve may be replaced by the simpler constant load curve.

The classical linear model of an induction motor is shown in Figure 3-3. Here,  $r_1$  and  $\omega l_1$  are armature resistance and leakage reactance,  $r_2$  and  $\omega l_2$  are rotor resistance and leakage reactance and  $\omega l_m$  is total magnetizing reactance.

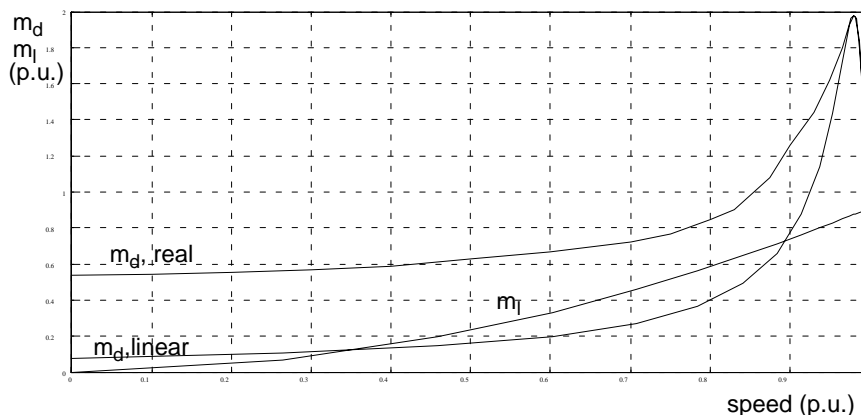


Figure 3-1 Typical torque curve for large induction motor (Siemens type 1RQ1805-4HN.0, 6.6 kV, 7488 kW, 1493 rpm), compared with calculated curve for linear model and square load torque curve.



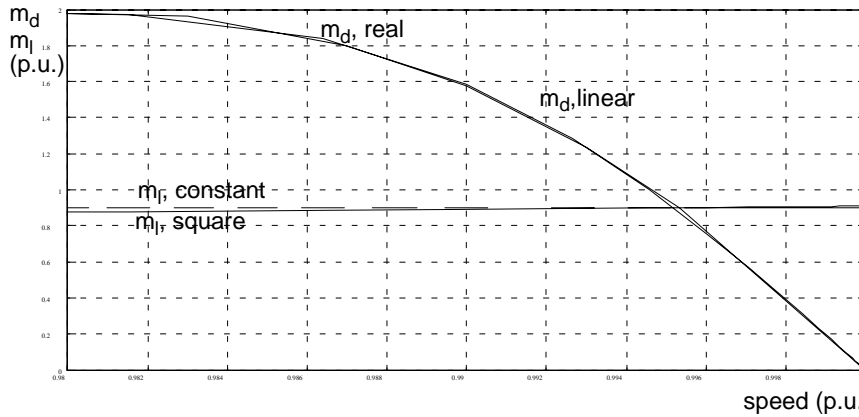


Figure 3-2 Typical torque curve for large induction motor (Siemens type 1RQ1805-4HN.0, 6.6 kV, 7488 kW, 1493 rpm), compared with calculated curve for linear model. Square load torque curve compared to constant torque load. Slip less than pull-out slip.

$r_2(1-\sigma)/\sigma$  represents the mechanical load, where  $\sigma$  is the slip. The terminal voltage is  $u$ .

A simplified model based on the linear model is shown in Figure 3-4. Here  $\omega l'$  is the sum of the leakage reactances in stator and rotor while  $r_2/\sigma$  is the sum of rotor resistance and load. The normally high magnetizing reactance in parallel is regarded as infinite and disregarded. We can use this model to find approximate values for  $\omega l'$  and  $r_2$ , and to find the relationship between voltage, current and slip. This model does not account for the time constant of the air gap voltage in the motor. In real motors of this size this time constant can be in the magnitude of 10 to 20 periods, giving the motor the ability to transiently act as a generator and support the network voltage. Disregarding this, however, gives more conservative results in the simulations.

In order to find a simple model of induction motors, which is valid for variable electrical voltage and frequency and based on readily available parameters, we make a quick review of the motor theory.

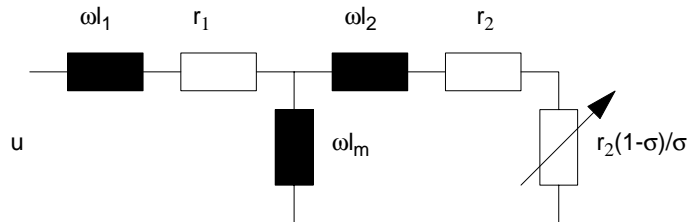


Figure 3-3 Per phase diagram of classical linear model of induction motor.

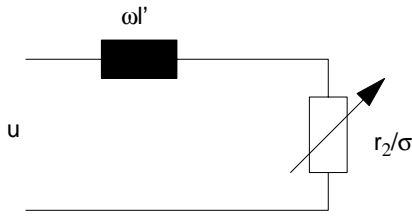


Figure 3-4 Simplified per phase diagram of classical linear model of induction motor.

At pull-out we have the maximum power transmitted through the air gap, that is the sum of rotor losses and mechanical power is maximum. That occurs when we have impedance adaptation in the rotor:

$$\frac{r_2}{\sigma_p} = \omega_{el} l' \quad (3-1)$$

where  $\sigma_p$  is the pull-out slip. The pull-out current will be

$$i_p = \frac{u}{\omega_{el} l' \cdot (1 + j)} \quad (3-2)$$

The power transmitted through the air gap at pull-out will be

$$p_p = \text{Re}(u \cdot i_p^*) = \text{Re}\left(\frac{u^2}{2 \cdot \omega_{el} l'} \cdot (1 + j)\right) = \frac{u^2}{2 \cdot \omega_{el} l'} \quad (3-3)$$

This power is transmitted through a synchronously rotating magnetic field and the pull-out torque in p.u. will be

$$m_p = \frac{p_p}{\omega_{el}} = \frac{u^2}{2 \cdot \omega_{el} \cdot \omega_{el} l'} \quad (3-4)$$

Using the rated values of voltage, frequency and pull-out torque, the inductance  $l'$  can be calculated

$$l' = \frac{1}{2 \cdot m_{pN}} \quad (3-5)$$

From (3-1) we get

$$r_2 = \sigma_{pN} \cdot l' = \frac{\sigma_{pN}}{2 \cdot m_{pN}} \quad (3-6)$$

Inserting (3-5) and (3-6) into Ohm's law for the model we find the general relationship between voltage and current in the motor for an arbitrary electrical frequency.

$$i = 2 \cdot u \cdot m_{pN} \cdot \frac{\sigma}{\sigma_{pN}^2 + (\sigma \omega_{el})^2} \cdot (\sigma_{pN} - j \cdot \sigma \omega_{el}) \quad (3-7)$$

The active power transmitted through the air gap is

$$p_d = \text{Re}(u \cdot i^*) = \text{Re} \left( 2 \cdot u^2 \cdot m_{pN} \cdot \frac{\sigma}{\sigma_{pN}^2 + (\sigma \omega_{el})^2} \cdot (\sigma_{pN} + j \cdot \sigma \omega_{el}) \right) \quad (3-8)$$

$$p_d = 2 \cdot u^2 \cdot m_{pN} \cdot \frac{\sigma \cdot \sigma_{pN}}{\sigma_{pN}^2 + (\sigma \omega_{el})^2} \quad (3-9)$$

The air gap torque for an arbitrary electrical frequency then becomes

$$m_d = \frac{p_d}{\omega_{el}} = 2 \cdot \frac{u^2 \cdot m_{pN}}{\omega_{el}} \cdot \frac{\sigma \cdot \sigma_{pN}}{\sigma_{pN}^2 + (\sigma \omega_{el})^2} \quad (3-10)$$

where  $m_d$  is air gap torque,  $m_{pN}$  is rated pull-out torque,  $\sigma$  is slip and  $\sigma_{pN}$  is rated pull-out slip. Normally, rated pull-out torque is given in relationship to nominal torque,

$$m_{pN} = k_p \cdot m_{dN} \quad (3-11)$$

and rated pull-out slip is not given in the data-sheets. Using (3-10) with rated values and inserting (3-11) gives

$$m_{dN} = 2 \cdot k_p \cdot m_{dN} \cdot \frac{\sigma_N \cdot \sigma_{pN}}{\sigma_{pN}^2 + \sigma_N^2} \quad (3-12)$$

which can be solved to give

$$\sigma_{pN} = (k_p + \sqrt{k_p^2 - 1}) \cdot \sigma_N \quad (3-13)$$

The equation for the mechanical torque balance in the motor in absolute values is

$$M_d = M_l + J \cdot \frac{d\Omega}{dt} \quad (3-14)$$

where  $M_d$  is the air gap torque,  $M_l$  is the load torque,  $J$  is the total inertia of machine and load and  $\Omega$  is the rotational speed. Introducing per unit values and the acceleration time

$$T_a = \frac{\Omega_N \cdot J}{M_{dN}}, \quad (3-15)$$

where  $M_{dN}$  is the rated air gap torque and  $\Omega_N$  is the rated rotational speed, we get

$$m_d = m_l + \frac{T_a \cdot m_{dN}}{\omega_{mekN}} \cdot \frac{d\omega_{mek}}{dt} \quad (3-16)$$

The large drives on an oil production platform will be either compressors or pumps. There may be differences in sticktion torque, but these are of minor importance and basically there is a square relation between speed and torque if the losses are ignored. So we have for the load torque:

$$m_l = k_l \cdot m_{dN} \cdot \omega_{mek}^2 \quad (3-17)$$

For simplicity we assume that the machine is fully utilized,  $k_l = 1$

$$m_l = m_{dN} \cdot \omega_{mek}^2 \quad (3-18)$$

Inserting the first part of (3-10) and (3-18) in (3-16) gives

$$\frac{p_d}{\omega_{el}} = m_{dN} \cdot \omega_{mek}^2 + \frac{T_a \cdot m_{dN}}{\omega_{mekN}} \cdot \frac{d\omega_{mek}}{dt} \quad (3-19)$$

Inserting (3-11) into (3-19) and solving for  $d\omega_{mek}/dt$  gives

$$\boxed{\frac{d\omega_{mek}}{dt} = \left( \frac{P_d}{\omega_{el} \cdot m_{dN}} - \omega_{mek}^2 \right) \frac{\omega_{mekN}}{T_a}} \quad (3-20)$$

Because both the network frequency and the mechanical speed is variable, the slip should be replaced by

$$\sigma = 1 - \frac{\omega_{mek}}{\omega_{el}} = \frac{\omega_{el} - \omega_{mek}}{\omega_{el}} \quad (3-21)$$

in the electrical equation for the current (3-7). This gives

$$i = 2 \cdot u \cdot k_p \cdot m_{dN} \cdot \frac{(\omega_{el} - \omega_{mek})}{\omega_{el} [\sigma_{pN}^2 + (\omega_{el} - \omega_{mek})^2]} \cdot [\sigma_{pN} - j(\omega_{el} - \omega_{mek})] \quad (3-22)$$

The apparent electric power becomes

$$s_m = u \cdot i^* = 2 \cdot u^2 \cdot k_p \cdot m_{dN} \cdot \frac{(\omega_{el} - \omega_{mek}) \cdot [\sigma_{pN} - j(\omega_{el} - \omega_{mek})]}{\omega_{el} [\sigma_{pN}^2 + (\omega_{el} - \omega_{mek})^2]} \quad (3-23)$$

which splits into

$$\boxed{p_d = \text{Re}(s_m) = 2 \cdot u^2 \cdot k_p \cdot m_{dN} \cdot \frac{\sigma_{pN} \cdot (\omega_{el} - \omega_{mek})}{\omega_{el} [\sigma_{pN}^2 + (\omega_{el} - \omega_{mek})^2]}} \quad (3-24)$$

and

$$\boxed{q_d = \text{Im}(s_m) = 2 \cdot u^2 \cdot k_p \cdot m_{dN} \cdot \frac{(\omega_{el} - \omega_{mek})^2}{\omega_{el} [\sigma_{pN}^2 + (\omega_{el} - \omega_{mek})^2]}} \quad (3-25)$$

where the rated pull-out slip must be calculated from (3-13).

Equations (3-24), (3-25) and (3-20) give a full quasi-stationary description of an induction motor in normal operation when voltage and/or frequency varies. This model is based on values found on the rating plate or in catalogues.

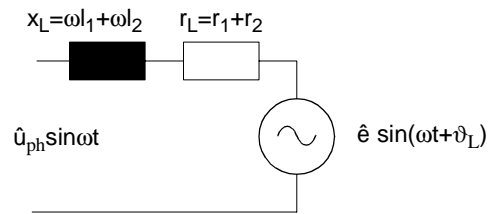


Figure 3-5 Induction motor subtransient equivalent according to [26].

### 3.2.2 Subtransient model

If a thyristor converter system shall be analysed with regard to commutation, or harmonic analysis is to be performed, another motor model is required. But as long as we are not directly interested in the detailed behaviour of the motor itself, B. K. Bose [26] has shown that both synchronous and induction motors can be modelled as an impedance in series with a sinusoidal counter electromotive force (EMF) for each phase, as shown in Figure 3-5. The reactance  $x_L$  is the sum of the leakage reactances in stator and rotor, while the resistance  $r_L$  is the sum of the stator and rotor resistances.

Large induction motors will constitute an important part of the load. If the normally high magnetizing reactance is neglected, only the leakage reactance remains. For the motor-ratings that come into question, this is typically in the magnitude of 0.2 p.u. [20]. The resistance consists of copper- and iron-losses. A traditional estimate is that each of these account for 1/3 of the total motor losses, air and bearing friction accounts for the last 1/3. With an efficiency of typically 97 %, [20], the resistance is typically 0.02 p.u. The time constant of the counter EMF amplitude is typically in the range of 500 ms or even more for these large motors. Thus the counter EMF can be regarded as constant for the short time periods in question for commutation.

## 3.3 INDUCTION MOTORS AT START-UP

From Figure 3-1 it is obvious that the linearized model cannot be applied to an induction motor during start-up. The linearized model differs from reality because the parameters in the model are constant, while they actually vary with slip frequency, due to skin-effects etc. There are several ways to get around this problem. One possibility is to create a model with more than one cage. The simplest model then is a double cage model, where the first cage is the standard linearized model, and then an additional cage is designed to

provide the missing torque during start-up. One easy way to do this is by a cage with pull-out slip equal to 1 and pull-out torque equal to the missing breakaway torque. But this easy model still does not fit well with real torque curves for intermediate speeds. Then there remains the possibility of making a multicage model, with cages that have to be adjusted and trimmed to fit the measured curve, or the much simpler method of replacing the model with a look-up table with the real figures for torque and current during start-up.

Such a table usually contains values for torque and current depending on relative speed ( $\frac{n}{n_{sync}}$ ) at rated voltage. The active and reactive power drawn from the network can be calculated as a function of the table values and the instant voltage under the following conditions:

- The losses can be ignored.
- The network frequency does not vary too far from the rated frequency.

Then we get, as shown in Appendix A

$$p = u^2 \cdot m \left( \frac{\omega_{mek}}{\omega_{el}} \Big|_{u_n} \right) \cdot \omega_{el} \quad (3-26)$$

$$q = u^2 \cdot \sqrt{\left( i \left( \frac{\omega_{mek}}{\omega_{el}} \Big|_{u_n} \right) \right)^2 - \left( m \left( \frac{\omega_{mek}}{\omega_{el}} \Big|_{u_n} \right) \cdot \omega_{el} \right)^2} \quad (3-27)$$

## 3.4 SYNCHRONOUS MACHINES

### 3.4.1 Transient model

Synchronous motors have worse starting characteristics than squirrel cage induction motors and will normally be frequency controlled. They are never connected directly to the network on oil platforms. Synchronous compensators and generators will naturally be connected directly to the network. Practically all synchronous machines offshore will be of full pole type, so this is the type we shall concentrate on. What is said will also be principally valid for salient pole machines.

The traditional model of a synchronous machine is the Thevenin equivalent, Figure 3-6, where the electromotoric force (EMF) and the impedance

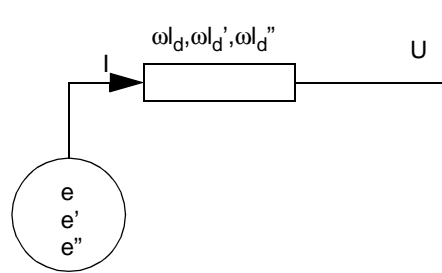


Figure 3-6 Thevenin equivalent of synchronous machine.

applied will vary according the problem. They can be subtransient, transient or stationary. In this case the time constants of the disturbance is in the magnitude of 1 s, so it is the transient values that are to be applied. The phasors for the model are shown in Figure 3-7, transient as well as subtransient and stationary values. The phasors are drawn for an overmagnetized full-pole generator with motoric reference, (consumed power is positive).

To find how the machine behaves during a disturbance it is feasible to analyse it by two axis theory [38]. The following equations (in p.u.) describes a synchronous machine with motoric reference, disregarding the damper windings [39].

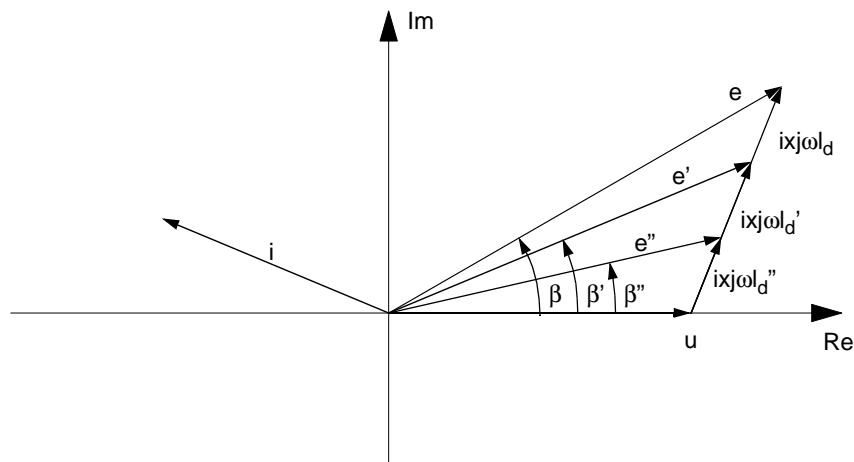


Figure 3-7 Phasor diagram of full pole synchronous machine, drawn for overmagnetized generator, with motoric reference (consumed power is positive).



Disregarding the null-system, which we normally can in a symmetric system, we have for the voltages:

$$u_d = r_a i_d + \frac{d\psi_d}{\omega_N dt} - \omega_m \psi_q \quad (3-28)$$

$$u_q = r_a i_q + \frac{d\psi_q}{\omega_N dt} + \omega_m \psi_d \quad (3-29)$$

$$u_f = r_f i_f + \frac{d\psi_f}{\omega_N dt} \quad (3-30)$$

The fluxes are given by:

$$\psi_d = x_d i_d + x_{ad} i_f \quad (3-31)$$

$$\psi_q = x_q i_q \quad (3-32)$$

$$\psi_f = x_{ad} i_d + x_f i_f \quad (3-33)$$

Inserting the flux equations into the voltage equations and rearranging, we arrive at the following explicit differential equations for the currents in the machine

$$\frac{d}{\omega_N dt} i_d = \frac{u_d + \omega_m x_q i_q - r_a i_d - \frac{x_{ad}}{x_f} (u_f - r_f i_f)}{x_d'} \quad (3-34)$$

$$\frac{d}{\omega_N dt} i_q = \frac{u_q - \omega_m (x_d i_d + x_{ad} i_f) - r_a i_q}{x_q} \quad (3-35)$$

$$\frac{d}{\omega_N dt} i_f = \frac{x_d (u_f - r_f i_f) - x_{ad} (u_d + \omega_m x_q i_q - r_a i_d)}{x_d' x_f} \quad (3-36)$$

where we have defined the transient d-axis reactance as:

$$x_d' = x_d - \frac{x_{ad}^2}{x_f} \quad (3-37)$$

The air gap torque can be expressed by:

$$m_d = x_{ad} i_f i_q + (x_d - x_q) \cdot i_d i_q \quad (3-38)$$

The mechanical torque equation for a synchronous machine is, in p.u.

$$m_N \cdot T_a \cdot \frac{d^2 \beta}{dt^2} - D \cdot \frac{d\beta}{dt} = m_d - m_l \quad (3-39)$$

where  $\beta$  is the pole angle between the rotor EMF and the terminal voltage,  $D$  is the damping constant which substitutes the damper windings, and  $m_l$  is the load torque. In the case of a synchronous compensator,  $m_l = 0$ . For a generator,  $m_l$  and  $m_d$  is negative (motoric reference).

The instantaneous active power delivered or consumed by a synchronous machine is given by

$$p = u_d \cdot i_d + u_q \cdot i_q \quad (3-40)$$

and the reactive power can be expressed as

$$q = u_d \cdot i_q - u_q \cdot i_d \quad (3-41)$$

The machine rotates with a speed  $\omega_{mek}$ , while the electrical frequency is  $\omega_{el}$ . These two are equal in the stationary state, but can vary transiently. The difference between electrical frequency and machine speed gives the variations in the pole angle.

$$\frac{d\beta}{dt} = (\omega_{el} - \omega_{mek}) \quad (3-42)$$

$$\beta = \int_{t_0}^t (\omega_{el} - \omega_{mek}) dt + \beta_0 \quad (3-43)$$

where  $\beta_0$  has to be calculated from the steady state before the disturbance. For a synchronous compensator,  $\beta_0 = 0$ .

Equations (3-34), (3-35), (3-36), (3-38), (3-39), (3-40), (3-41) and (3-43) constitute a model of the synchronous machine with properties that are similar to a phasor model. This is further discussed in Section 9. 2. and Section 9. 4. 2

### **3. 4. 2 Subtransient model**

The same model as described in Section 3. 2. 2 can, as mentioned, be used for synchronous machines with regard to analysis of commutation or harmonic analysis. For synchronous machines of salient pole type the d- and q-axis inductance are of the same value, and this value is applied in the model.

For synchronous machines of salient pole type a common simplification, especially when dealing with several motors together, will be to apply the average of the d- and q-axis inductance.

The subtransient time constant is typically in the range of 20 to 50 ms, while a commutation period will be in the range of 0.5 to 1 ms. So it is the subtransient inductance that is relevant for commutation analysis due to the short time spans involved. This inductance will be in the range of 0.15 to 0.25 p.u. In the model of a synchronous machine the resistance will be the stator resistance, the inductance will be the subtransient inductance and the EMF will be the subtransient air-gap voltage.

A load consisting of several motors can be represented by a lumped motor, with p.u. ratings a weighted average of the individual p.u. ratings. The EMF has to be adjusted to represent the true load factor of the motors, but, being a sinusoidal source of fundamental frequency, this only has influence on the fundamental currents and voltages.

## **3. 5 ADJUSTABLE SPEED DRIVES**

### **3. 5. 1 Current source inverters, transient model**

If the process requires adjustable speed or the power rating for an electric motor is so high that an induction motor cannot be directly started, adjustable speed drives are applied. For large drives synchronous motors are usually applied with inverters of current link type with controlled rectifiers. The drives are normally operated to keep a constant speed independent of the network frequency and voltage variation and independent of load variations.

The DC link current is proportional to the load torque, i.e. with stable mechanical conditions the absolute value of the AC current drawn from the grid is constant. The voltage of the link is directly proportional to the speed which implies that a controlled rectifier with constant load has a power factor proportional to relative speed at constant network voltage. If the grid voltage drops, the rectifier must reduce its firing angle  $\alpha$  to keep the link voltage and the speed constant. The active power required by the drive will be constant, independent of the voltage. Altogether the active current will be inversely proportional to the voltage, the absolute value of the current will remain constant and the reactive current will decrease proportional to  $\sin\alpha$ , as shown in Figure 3-8. The half circle over  $u_{v1}$  is the geometrical place for  $u_{v1}\sqrt{\cos\alpha_1^2 + \sin\alpha_1^2}$ , where the phasor  $u_{v1}\cos\alpha_1$  must end. The half circle over  $u_{v2} = u_{v1} - \Delta u_v$  is the geometrical place for  $(u_{v1} - \Delta u_v)\sqrt{\cos\alpha_2^2 + \sin\alpha_2^2}$ , where the new phasor  $u_{v2}\cos\alpha_2$  must end. The DC link voltage has to remain constant to keep the speed constant, i. e.  $|u_{v2}\cos\alpha_2| = |u_{v1}\cos\alpha_1|$ . This gives the new firing angle  $\alpha_2$ . The DC link current has to remain constant to keep the torque constant, i. e.  $|i_2| = |i_1|$ .

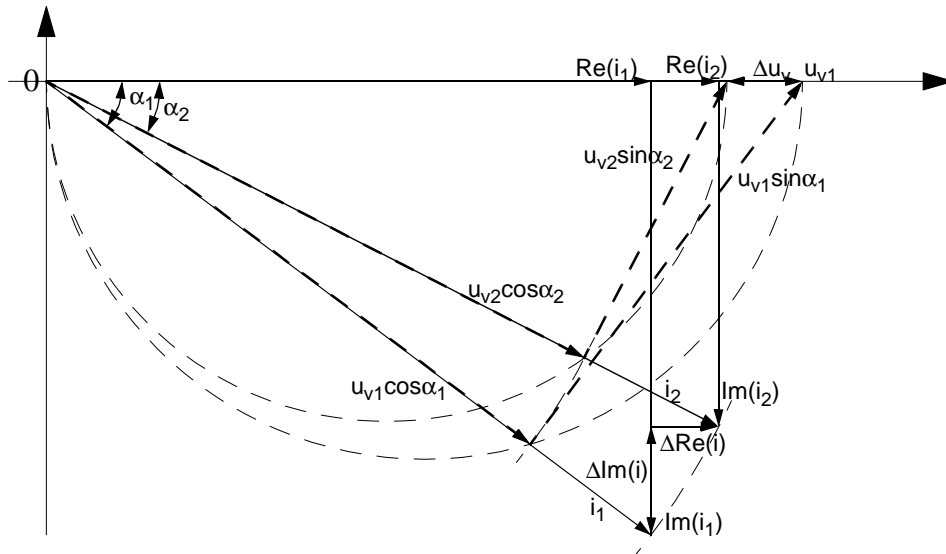


Figure 3-8 Phasor diagram of voltage and current drawn by a current source, constant speed drive after a voltage drop of  $\Delta u_v$ .

Thus it is possible to find the new the active and reactive current,  $Re(i_1) + \Delta Re(i)$  and  $Im(i_1) + \Delta Im(i)$ .

$$|i_{v1}| = |i_{v2}| = const \quad (3-44)$$

$$u_d = \frac{3\sqrt{2}}{\pi} u_{v2} \cos \alpha_2 = \frac{3\sqrt{2}}{\pi} u_{v1} \cos \alpha_1 \quad (3-45)$$

$$\cos \alpha_2 = \frac{u_{v1}}{u_{v2}} \cos \alpha_1 \quad (3-46)$$

$$i_{v2} = |i_{v1}| (\cos \alpha_2 - j \sin \alpha_2) \quad (3-47)$$

$$i_{v2} = |i_{v1}| \left[ \frac{u_{v1}}{u_{v2}} \cos \alpha_1 - j \sqrt{1 - \left( \frac{u_{v1}}{u_{v2}} \cos \alpha_1 \right)^2} \right] \quad (3-48)$$

$$p_2 = \sqrt{3} u_{v2} Re(i_{v2}) = \sqrt{3} u_{v2} |i_{v1}| \frac{u_{v1}}{u_{v2}} \cos \alpha_1 \quad (3-49)$$

$$\boxed{p_2 = \sqrt{3} u_{v1} |i_{v1}| \cos \alpha_1 = p_1} \quad (3-50)$$

$$q_2 = -\sqrt{3} u_{v2} Im(i_{v2}) = \sqrt{3} u_{v2} |i_{v1}| \sqrt{1 - \left( \frac{u_{v1}}{u_{v2}} \cos \alpha_1 \right)^2} \quad (3-51)$$

$$\boxed{q_2 = \sqrt{3} |i_{v1}| \sqrt{u_{v2}^2 - u_{v1}^2 \cos^2 \alpha_1}} \quad (3-52)$$

Equation (3-52) makes it obvious that normal operation cannot be continued if the AC voltage drops below  $u_{v1} \cos \alpha_1$ . Normally such a drive is designed to operate in the normal mode down to where the rectifier reaches a minimum firing angle  $\alpha_{min}$ . It can even operate at lower voltages, but then the DC link voltage cannot be kept up and the speed has to be reduced proportional to the voltage. If the load torque is constant, like a hoist, the inverter acts as a constant current load on the network. If the load torque is proportional to the square of the speed, as in pumps and compressors, the current is

reduced likewise and the inverter acts as a voltage proportional admittance with  $\cos\phi$  near one.

### 3. 5. 2 Voltage source inverters, transient model

Normally, voltage source inverters are made with diode rectifiers and PWM inverters. Under stable mechanical conditions they represent a constant active power load with  $\cos\phi$  very near one when seen from the network. This means that they consume an active current inversely proportional to the terminal voltage, and no fundamental reactive current. If the voltage drops below the level where the current reaches maximal value, the mechanical load is reduced by slowing the speed, and the network current is kept at maximum.

### 3. 5. 3 Subtransient model

Both the current source and voltage source drives draw an approximately square wave current (6-pulse converters) or stepped wave current (12-pulse converters) from the AC source. So for subtransient analysis this type of load can be modelled by a current source with the correct form. If several variable speed drives are present an analysis can be based upon a square wave current source with current and displacement angle equal to the resulting current and displacement angle of the sum of the drives.

## 3. 6 SUMMARY

In this chapter we have found simple models for electric machines and drives, to be used in building a model of the total oil platform to be supplied with electric power by HVDC transmission from land. The models do not aim at exact descriptions of the machines, they are intended to give adequate description of the load that the inverter sees.

# 4 CONVENTIONAL HVDC TRANSMISSION

In this chapter I will give a short review of traditional HVDC transmission theory. The review is based mainly on [4] and [5].

## 4.1 GENERAL

### 4.1.1 HVDC transmission systems

There are different ways to build an HVDC transmission system, as shown in the following figures. Figure 4-1 presents the simplest solution, a monopolar system where earth is used as a return path for the current. Since the earth current has a tendency to cause corrosion in underground metallic structures, this mode of operation is only allowed for short time periods for overhead lines in most countries. For sea cable transmissions, however, this arrangement is often used due to the high cable costs, as only one conductor is required. In such cases the earth electrode is located in the sea and

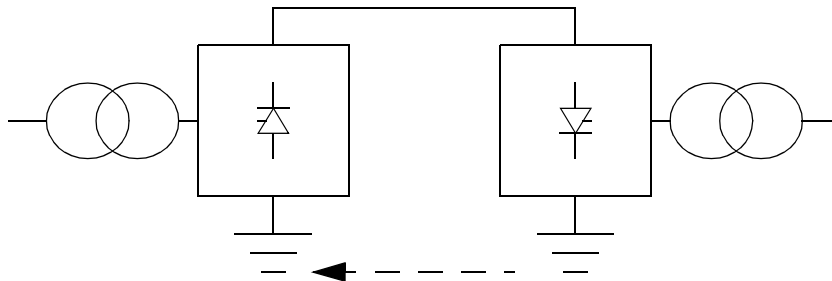


Figure 4-1 Monopolar HVDC transmission with earth return.

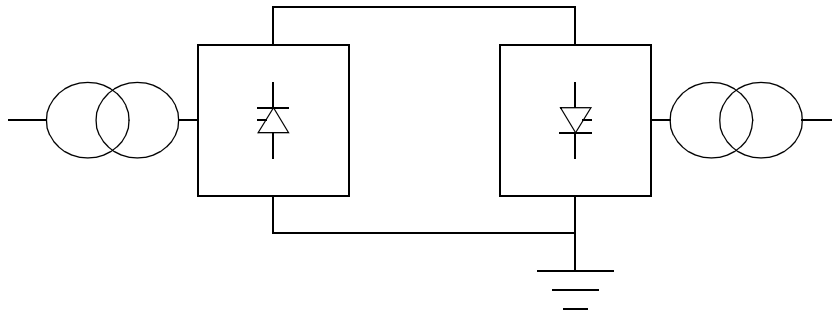


Figure 4-2 Monopolar HVDC transmission with metallic return.

connected to the converter by an electrode line insulated from ground over land to avoid corrosion. This solution has increasingly come under question in shallow waters with heavy ships traffic, like the North Sea, as it among other factors may have serious influence on magnetic compasses. Additionally in the North Sea, both oil companies and public authorities will not be happy for uncontrolled earth currents flowing in and around their highly sophisticated equipment.

If it is required to avoid the earth current, a natural extension of this system is the monopolar system with metallic return, which is shown in Figure 4-2. A special case of the monopolar transmission with metallic return is the HVDC back-to-back link. The HVDC back-to-back link is often used on the border between two asynchronous grids or grids of different frequencies to allow power transmission from one system to the other.

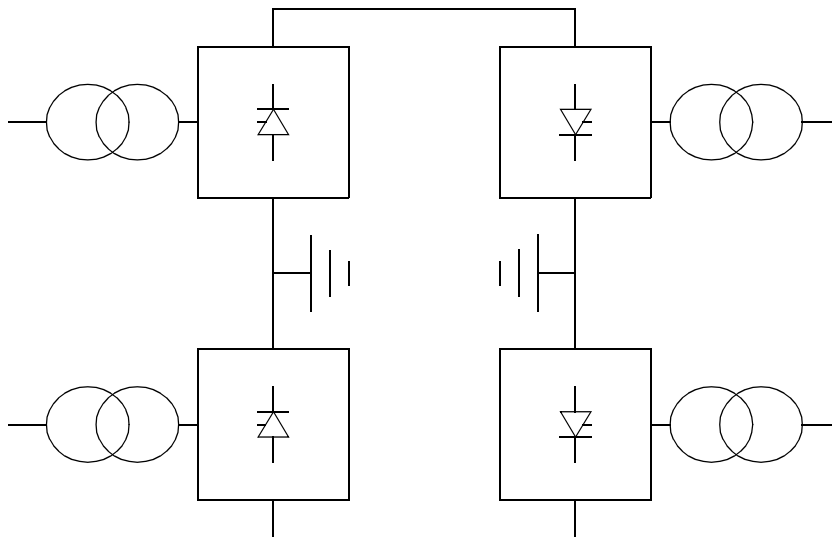


Figure 4-3 Bipolar HVDC transmission.



For overhead lines the system is normally bipolar as in Figure 4-3. In each converter station two converters are connected in series and the middle point is connected to earth. The insulation level for each line has only to be the voltage of one converter and the capacity of the transmission is doubled. This bipolar system can be operated at 50 % capacity as a monopolar system in case of faults. If one pole is out of operation for an extended period, the system can usually be reconnected to form a monopolar system with metallic return.

#### 4. 1. 2 HVDC converters

The basic design for practically all HVDC converters is the 12-pulse double bridge converter which is shown in Figure 4-4. The converter consists of two 6-pulse bridge converters connected in series on the DC side. One of them is connected to the AC side by a YY-transformer, the other by a YD-transformer. The AC currents from each 6-pulse converter will then be phase shifted  $30^\circ$ . This will reduce the harmonic content in the total current drawn from the grid, and leave only the characteristic harmonics of order  $12m \pm 1$ ,  $m=1,2,3,\dots$ , or the 11th, 13th, 23th, 25th etc. harmonic. The non-characteristic harmonics will still be present, but considerably reduced. Thus the need for filtering is substantially reduced, compared to 6-pulse converters.

The 12-pulse converter is usually built up of 12 thyristor valves. Each valve consists of the necessary number of thyristors in series to withstand the required blocking voltage with sufficient margin. Normally there is only one string of thyristors in each valve, no parallel connection. Four valves are built together in series to form a quadruple valve and three quadruple valves,

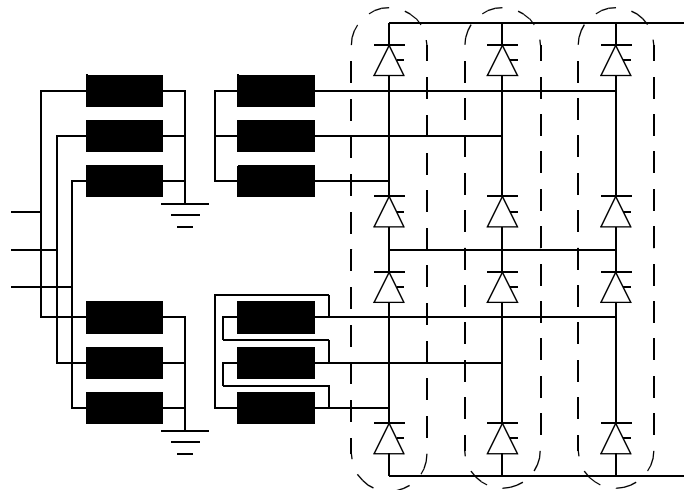


Figure 4-4 12-pulse converter.

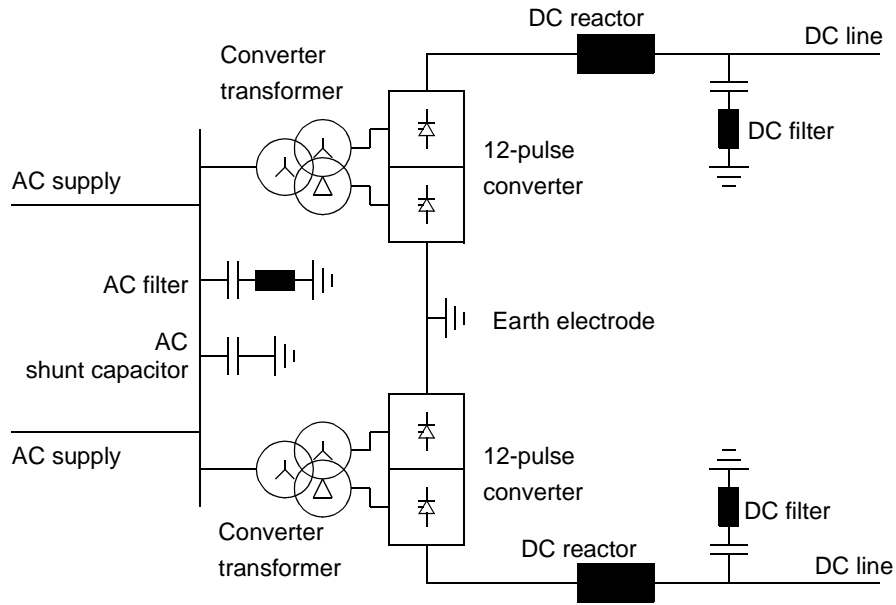


Figure 4-5 Main elements of a HVDC converter station with one bipole consisting of two 12-pulse converter unit.

together with converter transformer, controls and protection equipment, constitute a converter.

The converter transformers are usually three winding transformers with the windings in YydN-connection. There can be one three-phase or three single-phase transformers, according to local circumstances. In order to optimize the relationship between AC- and DC voltage the converter transformers are equipped with tap changers.

### 4. 1. 3 HVDC converter stations

An HVDC converter station (Figure 4-5) is normally built up of one or two 12-pulse converters as described above, depending on the system being mono- or bipolar. In some cases each pole of a bipolar system consists of two converters in series to increase the voltage and power rating of the transmission. It is not common to connect converters directly in parallel in one pole. The poles are normally as independent as possible to improve the reliability of the system, and each pole is equipped with a DC reactor and DC filters.

Additionally the converter station consists of some jointly used equipment. This can be the connection to the earth electrode, which normally is situated

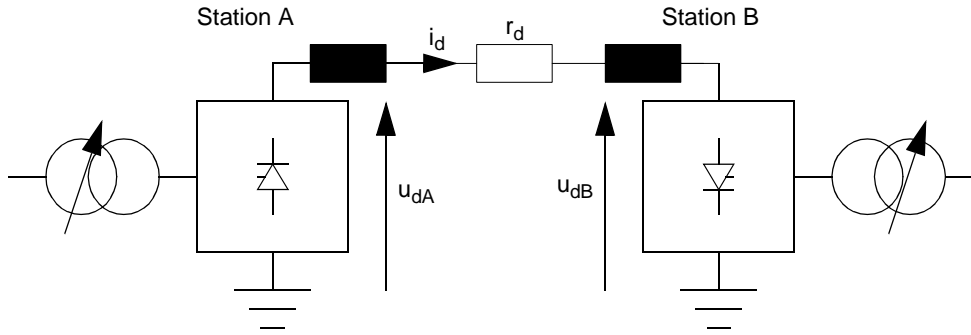


Figure 4-6 Monopolar HVDC transmission.  
Voltage in station B according to reversed polarity convention.

some distance away from the converter station area, AC filters and equipment for supply of the necessary reactive power.

## 4.2 BASIC CONTROL PRINCIPLES

### 4.2.1 DC transmission control

The current flowing in the DC transmission line shown in Figure 4-6 is determined by the DC voltage difference between station A and station B. Using the notation shown in the figure, where  $r_d$  represents the total resistance of the line, we get for the DC current

$$i_d = \frac{u_{dA} - u_{dB}}{r_d} \quad (4-1)$$

and the power transmitted into station B is

$$P_d = u_{dB} \cdot i_d = u_{dB} \cdot \frac{u_{dA} - u_{dB}}{r_d} \quad (4-2)$$

In rectifier operation the firing angle  $\alpha$  should not be decreased below a certain minimum value  $\alpha_{\min}$ , normally  $3^\circ$ - $5^\circ$  [4], [5], in order to make sure that there really is a positive voltage across the valve at the firing instant. In inverter operation the extinction angle should never decrease below a certain

minimum value  $\gamma_{\min}$ , normally  $17^\circ$ - $19^\circ$  [4], [5], otherwise the risk of commutation failures becomes too high.

On the other hand, both  $\alpha$  and  $\gamma$  should be as low as possible to keep the necessary nominal rating of the equipment to a minimum. Low values of  $\alpha$  and  $\gamma$  also decrease the consumption of reactive power and the harmonic distortion in the AC networks.

To achieve this, most HVDC systems are controlled to maintain  $\gamma = \gamma_{\min}$  in normal operation. The DC voltage level is controlled by the transformer tap changer in inverter station B. The DC current is controlled by varying the DC voltage in rectifier station A, and thereby the voltage difference between A and B. Due to the small DC resistances in such a system, only a small voltage difference is required, and small variations in rectifier voltage gives large variations in current and transmitted power.

The DC current through a converter cannot change the direction of flow. So the only way to change the direction of power flow through a DC transmission line is to reverse the voltage of the line. But the sign of the voltage difference has to be kept constantly positive to keep the current flowing.

To keep the firing angle  $\alpha$  as low as possible, the transformer tap changer in rectifier station A is operated to keep  $\alpha$  on an operating value which gives only the necessary margin to  $\alpha_{\min}$  to be able to control the current.

#### 4.2.2 Converter current/voltage characteristics

The resistive voltage drop in converter and transformer, as well as the non-current voltage drop in the thyristor valves are often disregarded in practical analysis, as they are normally in the magnitude of 0.5 % of the normal operating voltage. The commutation voltage drop, however, has to be taken into account as this is in the magnitude of 5 to 10 % of the normal operating voltage. The direct voltage  $U_d$  from a 6-pulse bridge converter can then be expressed by

$$u_d = u_{dio} \cdot \left[ \cos \alpha - d_{xN} \cdot \frac{i_d}{i_{dN}} \cdot \frac{u_{dioN}}{u_{dio}} \right] \quad (4-3)$$

where  $\alpha$  is the firing angle,

$$d_{xN} = \frac{3}{\pi} \cdot \frac{i_{dN} \cdot x_k}{u_{dioN}} \approx \frac{1}{2} \cdot e_k \text{ is the rated relative inductive voltage drop,}$$

$i_d$  and  $i_{dN}$  are the actual and rated direct current respectively

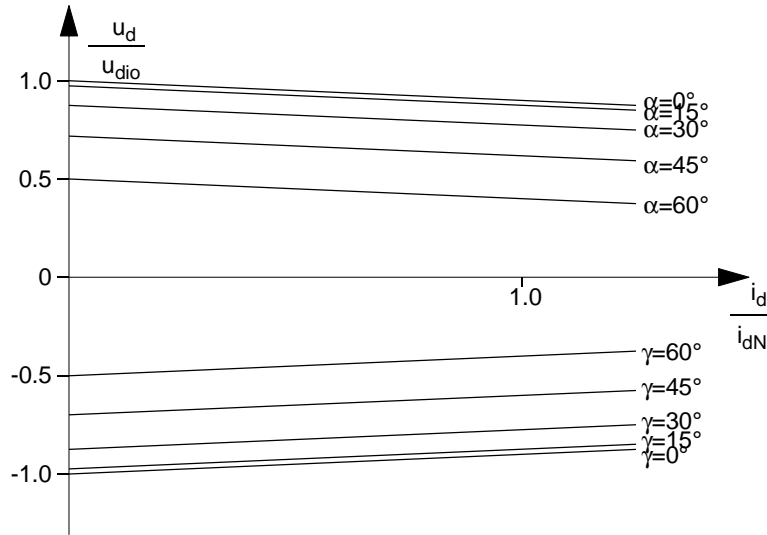


Figure 4-7 Principal current/voltage characteristics for a converter. Firing angle  $\alpha$  and extinction angle  $\gamma$  as parameter.

$u_{dio}$  and  $u_{dioN}$  are the actual and rated no-load direct voltage at  $\alpha = 0$

$x_k$  is the commutation reactance, normally the transformer short circuit reactance and

$e_k$  is the relative short circuit voltage of the transformer.

If the converter is operating as inverter it is more convenient to operate with extinction angle  $\gamma$  instead of firing angle  $\alpha$ . The extinction angle is defined as the angle between the end of commutation to the next zero crossing of the commutation voltage. Firing angle  $\alpha$ , commutation angle  $\mu$  and extinction angle  $\gamma$  are related by

$$\alpha + \mu + \gamma = 180^\circ \quad (4-4)$$

In inverter mode, the direct voltage from the inverter can be written as

$$u_d = -u_{dio} \cdot \left[ \cos\gamma - d_{xN} \cdot \frac{i_d}{i_{dN}} \cdot \frac{u_{dioN}}{u_{dio}} \right] \quad (4-5)$$

The current/voltage characteristics expressed in (4-3) and (4-5) are shown principally in Figure 4-7 for normal values of  $i_d$  and  $d_{xN}$ . In order to create a characteristic diagram for the complete transmission, it is usual to define positive voltage in inverter operation in the opposite direction compared to rectifier operation, as shown in Figure 4-6. Doing this and drawing only the

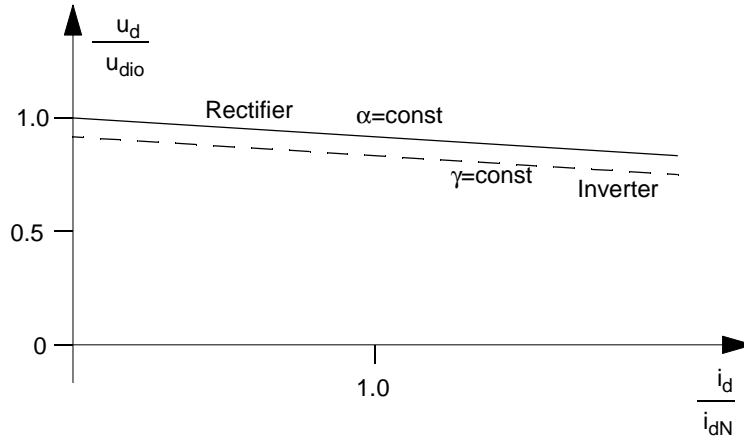


Figure 4-8 Typical current/voltage characteristics for rectifier and inverter (reversed polarity convention).

limit characteristics we get the typical diagram in Figure 4-8, where the rectifier characteristic is continuous and the inverter characteristic is dashed.

It is clear that to operate both converters on a constant firing/extinction angle principle is like leaving them without control. This will not give a stable point of operation, as both characteristics have approximately the same slope. Small differences appear due to variations in transformer data and voltage drop along the line. To gain the best possible control the characteristics should cross at as close to a right angle as possible. This means that one of the characteristics should preferably be constant current. This can only be achieved by a current controller.

If the current/voltage diagram of the rectifier is combined with a constant current controller characteristic we get the steady state diagram in Figure 4-9 for converter station A. A similar diagram can be drawn for converter station B. If we apply the reversed polarity convention for the inverter and combine the diagrams for station A and station B we get the diagram in Figure 4-10.

In normal operation, the rectifier will be operating in current control mode with the firing angle  $\alpha > \alpha_{min}$ . The inverter has a slightly lower current command than the rectifier and tries to decrease the current by increasing the counter voltage, but cannot decrease  $\gamma$  beyond  $\gamma_{min}$ . Thus we get the operating point A. We assume that the characteristic for station B is referred to station A, that is it is corrected for the voltage drop along the transmission line. This voltage drop is in the magnitude of 1-5 % of the rated DC voltage.

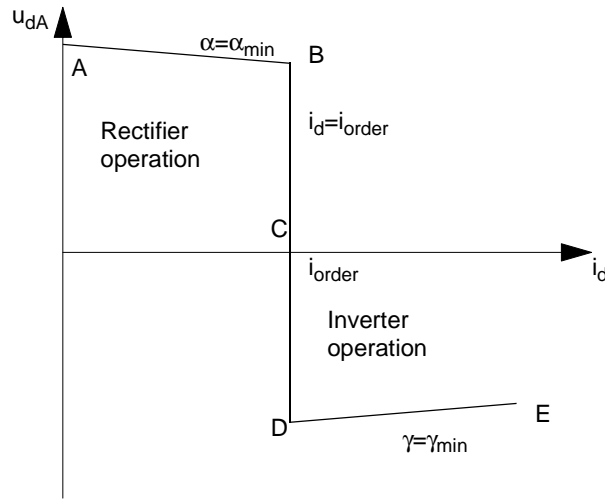


Figure 4-9 Steady state  $u_d/i_d$  diagram for converter station A.

If the AC voltage at the rectifier station drops, due to some external disturbance, the voltage difference is reduced and the DC current starts to sink. The current controller in the rectifier station starts to reduce the firing angle  $\alpha$ , but soon meets the limit  $\alpha_{min}$ , so the current cannot be upheld. When the current sinks below the current command of the inverter, the inverter control reduces the counter voltage to keep the current at the inverter current command, until a new stable operating point B is reached.

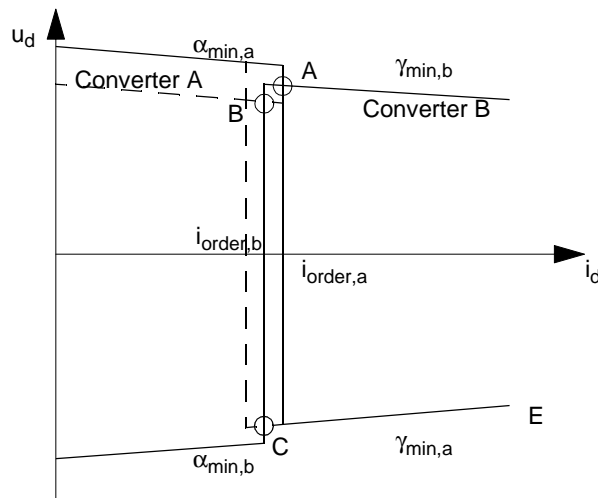


Figure 4-10 Steady state  $u_d/i_d$  characteristic for converter station A and station B.

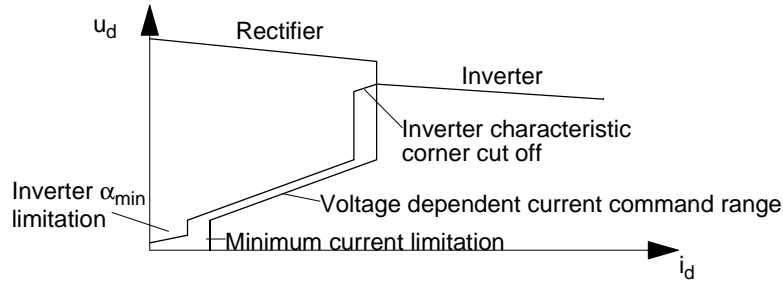


Figure 4-11 Complete  $u_d/i_d$  characteristics for HVDC transmission.

If the current command at station A is decreased below that of station B, station A will see a current that is too high and start to increase the firing angle  $\alpha$ , to reduce the voltage. Station B will see a diminishing current and try to keep it up by increasing the extinction angle  $\gamma$  to reduce the counter voltage. Finally station A meets the  $\gamma_{min}$  limit and cannot reduce the voltage any further and the new operating point will be at point C. Here the voltage has been reversed to negative while the current is still positive, that is the power flow has been reversed. Station A is operating as inverter and station B as rectifier. The difference between the current commands of the rectifier and the inverter is called the current margin.

It is possible to change the power flow in the transmission simply by changing the sign of the current margin, but in practice it is desirable to do this in more controllable ways. Therefore the inverter is normally equipped with a  $\alpha_{min}$  limitation in the range of  $95-105^\circ$ . To avoid current fluctuations between operating points A and B at small voltage variations the corner of the inverter characteristic is often cut off. Finally, it is not desirable to operate the transmission with high currents at low voltages, and most HVDC controls are equipped with voltage dependent current command limitation. The final complete  $u_d/i_d$  characteristics of the transmission then look like those shown in Figure 4-11.

### 4.2.3 Tap changer control

The preferred operation of an HVDC transmission system is, as described, with the inverter in  $\gamma_{min}$ -control to minimize reactive power need. Additionally it is required to operate the system as close to the rated voltage as possible to minimize the resistive power losses. The rectifier needs to be operated with as small  $\alpha$  as possible and still keep sufficient margin. This requires the commutation voltage, both for the rectifier and the inverter, to be controlled



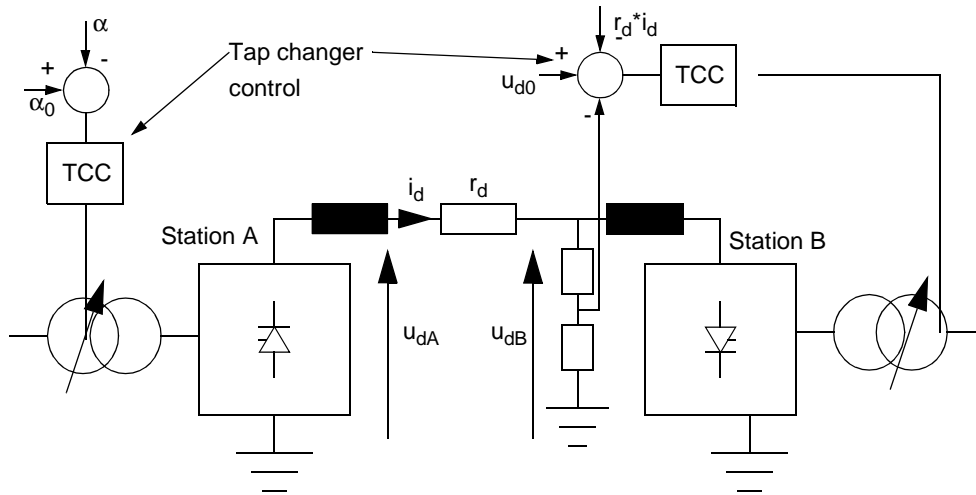


Figure 4-12 Tap changer control.

according to the DC current. Additionally the normal variations of the AC voltages have to be considered. All this is taken care of by the tap changer control of the converter transformers. The tap changers have to have a rather wide range of operation, often  $\pm 15\%$ . The function of the tap changer control is shown in Figure 4-12. With the inverter in constant extinction angle (CEA) control, the inverter tap changer is controlled in such a way that the DC voltage at the rectifier end is close to its rated value. This is achieved by compensating the measured voltage at the inverter by an amount calculated from the measured DC current. To avoid hunting of the tap changer, the control deadband has to be wider than the size of one tap step. The rectifier tap changer is controlled in such a way that if  $\alpha$  gets too close to  $\alpha_{min}$  it raises the commutation voltage, and if  $\alpha$  gets too large it lowers the voltage. Typically the control tries to keep  $\alpha$  between  $10^\circ$  and  $20^\circ$  [4]. These limits give a voltage band of  $\Delta u_d = u_d \cdot (\cos 10^\circ - \cos 20^\circ) = 0,045 u_d$ . Allowing for some error in the measurement of the angles reduces this band to about 2.5-3 % of  $u_{d0}$ . The tap steps have to be less than this band, typically 1.3-2 %. The tap steps naturally have to be the same for both rectifier and inverter, as the system normally is designed to carry power in both directions.

Mechanical tap changers are still the normal solution, and the speed of operation is still considerably slower than the firing control system. The cooperation between the two controls thus does not cause any problems.

#### 4.2.4 Master control system and telecommunications

The controls described above are basic and fairly standardized and similar for all HVDC converter stations. The master control, however, is usually system specific and individually designed. Depending on the requirements of the transmission, the control can be designed for constant current or constant power transmitted, or it can be designed to help stabilizing the frequency in one of the AC networks by varying the amount of active power transmitted.

The control systems are normally identical in both converter systems in a transmission, but the master control is only active in the station selected to act as the master station, which controls the current command. The calculated current command is transmitted by a communication system to the slave converter station, where the pre-designed current margin is added if the slave is to act as rectifier, subtracted if it is to act as inverter. In order to synchronize the two converters and assure that they operate with same current command (apart from the current margin), a telecommunications channel is required. Should the telecommunications system fail for any reason, the current commands to both converters are frozen, thus allowing the transmission to stay in operation. Special fail-safe techniques are applied to ensure that the telecommunications system is fault-free. The requirements for the telecommunications system are especially high if the transmission is required to have a fast control of the transmitted power, and the time delay in processing and transmitting these signals will influence the dynamics of the total control system.

### 4.3 QUASI-STATIONARY MODEL OF HVDC SYSTEMS

The characteristic equations for rectifier, (4-3), and inverter, (4-5), can be modified and expressed in p.u. form as:

$$u_{d,r} = u_{dio,r} \cdot \cos \alpha - \frac{3}{\pi} \cdot x_{k,r} \cdot i_d \quad (4-6)$$

and

$$u_{d,i} = -u_{dio,i} \cdot \cos \gamma + \frac{3}{\pi} \cdot x_{k,i} \cdot i_d \quad (4-7)$$

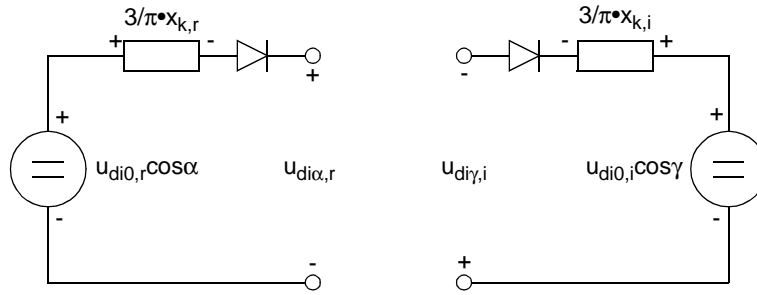


Figure 4-13 Rectifier and inverter modelled as quasi-stationary voltage sources and series resistors.

These equations each represent a controlled voltage source and a series resistor, as shown in Figure 4-13. The diode is inserted to indicate that current can only flow in one direction. In the case of an HVDC transmission to an offshore oil or gas field, the frequency of the supplying network on shore can be regarded as constant and hence the resistor representing the commutation voltage drop in the rectifier can be regarded as constant. On the platform, however, the frequency is allowed to vary and thus the resistor representing the commutation voltage drop in the inverter has to vary accordingly. Equation (4-7) must be modified to:

$$u_{d,i} = -u_{dio,i} \cdot \cos \gamma + \frac{3}{\pi} \cdot \omega_{el} \cdot l_{k,i} \cdot i_d \quad (4-8)$$

where  $\omega_{el}$  is the p.u. frequency at the platform.

The DC current can vary in time, thus we have to consider the inductance of the circuit, also outside the commutation interval. Then there are always two phases conducting in a bridge converter, and the internal inductance of a converter in this interval is:

$$l_i = 2l_k \quad (4-9)$$

Additionally there will be a large inductance  $l_d$  present in the DC circuit to provide smoothing of the current. The resistance of the transmission line is so small (1 % - 5 %) that it can practically be neglected for dynamic analysis and

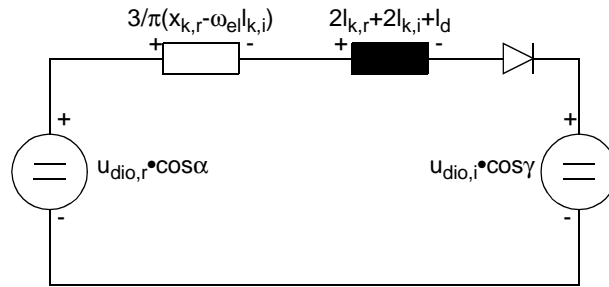


Figure 4-14 Final model of HVDC transmission.

stability analysis. The final circuit can be remodelled as in Figure 4-14. This circuit can be described by:

$$\frac{di_d}{dt} = \frac{u_{dio,r} \cdot \cos\alpha - u_{dio,i} \cdot \cos\gamma - \frac{3}{\pi} \cdot (x_{k,r} - \omega_{el} \cdot l_{k,i}) \cdot i_d}{2l_{k,r} + 2l_{k,i} + l_d} \quad (4-10)$$

where the firing angle  $\alpha$  for the rectifier and extinction angle  $\gamma$  for the inverter are determined by the control system as previously described.

## 4.4 SUMMARY

This chapter summarizes the conventional construction and control of HVDC transmission and the cooperation of the different controllers involved. A quasi-stationary description of an HVDC transmission, which can be used in a complete model, is given by (4-10).

# **5 HVDC SUPPLY TO WEAK AC NETWORKS**

In this chapter I will briefly introduce the traditional stability analysis of HVDC transmission into weak AC networks.

## **5.1 VOLTAGE STABILITY**

An important parameter when we consider supply to an AC network by means of HVDC, is the ‘strength’ of the AC network. This ‘strength’ reflects the sensitivity of the AC system to disturbances, a strong system is not significantly disturbed by changes in load power or faults. The short circuit ratio, which will be defined below, in a system is normally a good measure of the strength of the system.

The mechanical inertia is another indicator of the strength of the AC system. A system with low mechanical inertia may suffer large frequency deviations as a result of the disturbances. In order to simplify the analysis of the voltage stability in this chapter the mechanical inertia is assumed to be so large that the network frequency is kept constant during load transients.

A model for analysing the interactions between an HVDC converter and a weak AC network is shown in Figure 5-1. This model has been extensively analysed, among others by Joint Task Force, Cigré 14.07/ IEEE15.05.05 [28], [29], [30].

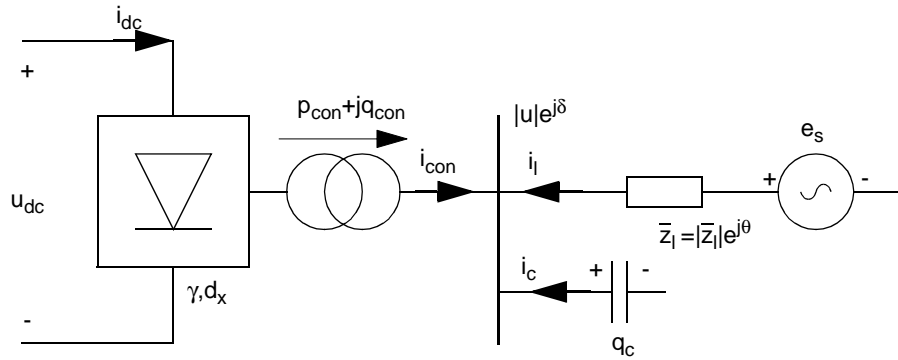


Figure 5-1 Simplified model of an HVDC converter connected to an AC network.

The definition of short circuit power (SC) at a given busbar in an AC network is, according to IEC:

$$SC = \frac{U_N^2}{Z_l} \quad (5-1)$$

where  $U_N$  is the nominal voltage and  $Z_l$  is the equivalent network impedance. When calculating the equivalent network impedance for this analysis the transient impedances of synchronous machines should be used due to the magnitude of the time constants involved. The short circuit power of a network, according to this definition, is a fictitious parameter. When calculating the real short circuit current, for example, one must consider the equivalent source voltage  $E_s$ , which is normally higher than the rated voltage.

When analysing the connection of a converter to a network when there is a shunt compensation capacitor bank present, this unit has to be taken into consideration as well. To the converter, the shunt compensator will look like a part of the network. The new, effective equivalent impedance  $Z_{lE}$  is found according to the Thevenin theorem by zeroing all sources in the network to be replaced, thus the resulting impedance will be the parallel connection of the original network impedance  $Z_l$  and the shunt compensator impedance  $Z_c$ .

$$\vec{Z}_{lE} = \frac{\vec{Z}_l \cdot \vec{Z}_c}{\vec{Z}_l + \vec{Z}_c} \quad (5-2)$$

The equivalent source voltage  $E_s$  will also have to be corrected, in order to supply the correct open terminal voltage and short circuit current.

$$\vec{E}_{sE} = E_s \cdot \frac{\vec{Z}_c}{\vec{Z}_l + \vec{Z}_c} \quad (5-3)$$

The effective short circuit power (ESC) can be calculated from the effective network impedance:

$$ESC = \left| \frac{\vec{U}_N \cdot \vec{U}_N^*}{\vec{Z}_{IE}^*} \right| = \left| \frac{\vec{U}_N \cdot \vec{U}_N^*}{\vec{Z}_l^*} + \frac{\vec{U}_N \cdot \vec{U}_N^*}{\vec{Z}_c^*} \right| = |\vec{SC} + \vec{Q}_c| \quad (5-4)$$

where  $Q_c$  is the reactive power produced by the filters and shunt compensation capacitors in the converter station. Bearing in mind that the network impedance is almost purely inductive and the shunt compensator impedance is almost purely capacitive, with good accuracy, the effective short circuit power becomes,:

$$ESC = SC - |Q_c| \quad (5-5)$$

where the absolute value signs are to remind us that ESC is reduced when shunt compensating capacitors are applied.

The per unit value of the short circuit power, the short circuit ratio (SCR), in an AC system in conjunction with HVDC converters is calculated on the basis of the rated active power of the converter station, not the apparent power as usually in AC calculations. Then the short circuit ratio can be calculated from

$$SCR = \frac{SC}{P_{N,con}} \quad (5-6)$$

where  $P_{N,con}$  is the rated power of the converter station. An alternative expression is

$$SCR = \frac{1}{z_l} \quad (5-7)$$

with the network impedance  $z_l$  expressed in p.u. based on the rated active power of the converter station.

Taking the influence of the filters and shunt compensation capacitors into account, we find the effective short circuit ratio (ESCR) in the same way, defined as:

$$ESCR = \frac{SC - |Q_c|}{P_{N, con}} \quad (5-8)$$

or alternatively

$$ESCR = \frac{1}{z_{lE}} \quad (5-9)$$

with the effective network impedance  $z_{lE}$  likewise expressed in p.u. based on the rated active power of the converter station.

In this model, synchronous motors should be represented by their transient reactance, due to the magnitude of the time constants present.

The phasor diagram for the circuit in Figure 5-1 will be as shown in Figure 5-2, where the phase angle  $\varphi_{con}$  of the converter is given by:

$$\varphi_{con} = a \cos \frac{\cos \gamma + \cos(\gamma + \mu)}{2} \quad (5-10)$$

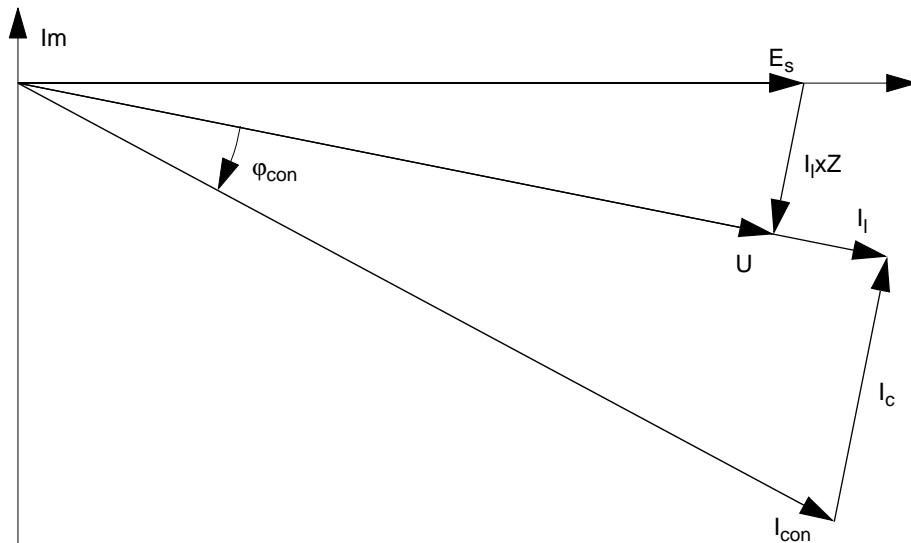


Figure 5-2 Phasor diagram for model of HVDC converter and net.



If the network impedance is nearly inductive, as indicated in the phasor diagram, there will be a voltage drop from the stiff source  $E_s$  to the converter terminal voltage  $U$ . This voltage drop will increase with increasing need for reactive power at the converter, while variations in active power per se have minor influence on the terminal voltage. But variations in active power from a line commutated converter inevitably cause variations in reactive power, thus they indirectly influence the terminal voltage.

If we assume a converter operating at a typical constant extinction angle  $\gamma = 18^\circ$  and having a relative inductive voltage drop (See Chapter 4)  $d_x = 0.075$ , there will be a need for a reactive power compensation  $q_c = 0.54$  to have unity power factor towards the network at nominal operating conditions. If this converter is connected to a network with a given short circuit capacity, the terminal voltage can be calculated and plotted as a function of the DC current. This has been done for networks with varying SCR. The result for a network with SCR=4.5 is shown in Figure 5-3. If this HVDC transmission system is controlled in the most usual way, to transmit constant power around nominal operating conditions it is obvious that increasing the current will increase the transmitted power. A simple controller will be sufficient to keep the transmitted power constant. This network can be considered as 'strong' in this context.

If the transmission is connected to a network with SCR=2.5, the results will be as shown in Figure 5-4. Still, an increase in current from the nominal oper-

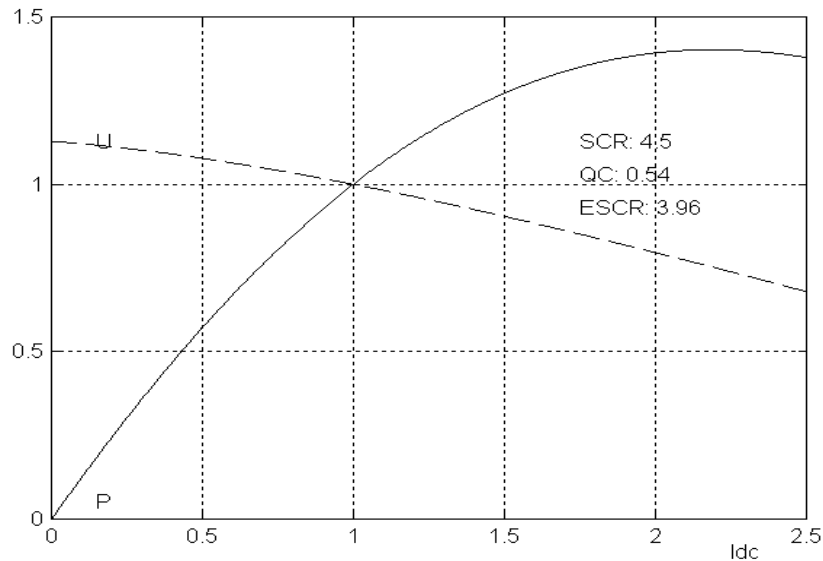


Figure 5-3 Terminal voltage  $U$  and transmitted power  $P$  from a converter connected to a strong network, as a function of DC current  $i_{dc}$ .

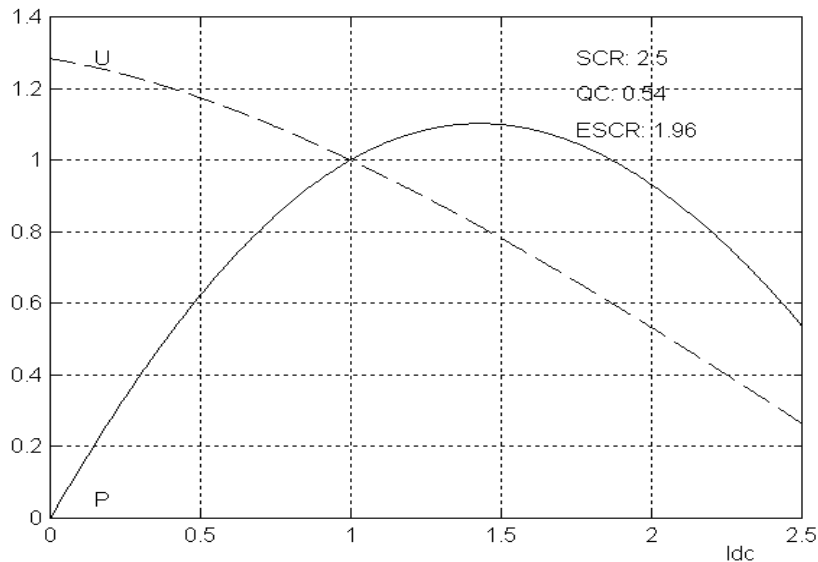


Figure 5-4 Terminal voltage  $U$  and transmitted power  $P$  from a converter connected to a weak network, as a function of DC current  $i_{dc}$ .

ating point will bring an increase in the power transmitted, but there is a significantly reduced margin to the peak of the power curve. If the current is increased beyond this point of maximum available power (MAP), the voltage drop will be greater than the increase in current, and the power transmitted will start to drop if the current is increased further. This network will be considered weak, and the feasibility of the HVDC transmission must be investigated closely.

If the network only has  $SCR=1.25$ , it may be that the nominal operating point is beyond the MAP point, as shown in Figure 5-5. In this case, any attempt to increase the power from the operating point by increasing the current will lead to a reduction of power transmitted, and the system is clearly unstable in the case of constant power control, which is a part of most normal master control schemes for HVDC transmissions today [5]. In this context it may be noted that it will be of no help increasing the rating of the HVDC transmission, as the active power rating of this is the basis for the p.u. values. An increase of the rating will only decrease the ESCR twofold, first the SCR value will decrease as the p.u. basis increases, and secondly the larger converter needs more shunt compensation, thereby decreasing ESCR further.

The voltage drop is mainly due to the reactive power needed by the converter. The apparently obvious way to try to remedy the problem of a weak AC system would be to reduce this need by producing the reactive power where it is needed, that is close to the converter. Unfortunately this also makes

things worse. As can be seen from the expression for the effective short circuit ratio (5-8), increasing the reactive compensation only reduces the effective short circuit ratio. The reason for this is that by increasing the compensation, the source voltage can be correspondingly reduced, and hence the short circuit capacity is reduced.

Fortunately there are some possibilities to solve the problem. It has been assumed that the source voltage and network impedance will be constant during the disturbance, while the voltage control of the system in reality acts precisely through these parameters. If the power control is relatively slow, compared to the voltage control system, the converter will operate in approximately constant current control during disturbances. A converter operated in constant current control mode will be significantly more stable in case of voltage disturbances as long as there is a control margin in the rectifier. So if slow power control can be accepted, this will be helpful.

If slow power control cannot be accepted, or the voltage control system is not sufficiently effective, a simple, but usually not very practical solution is to increase the ESCR of the AC system by more generation capacity, addition of supply lines or installation of synchronous compensators, or by reducing the power rating of the HVDC transmission. The installation of fast acting voltage controllers on the commutation busbar is a better solution. A Static Var Compensator (SVC) is such a device that can compensate voltage deviations fast. One study [18] indicates that by the introduction of SVCs on an

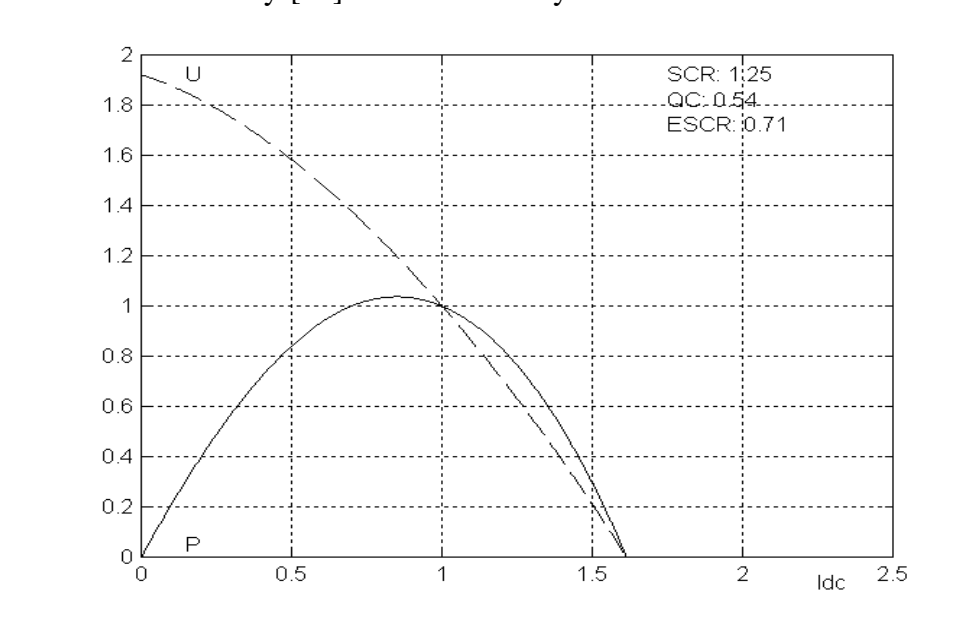


Figure 5-5 Terminal voltage  $U$  and transmitted power  $P$  from a converter connected to a very weak network, as a function of DC current  $i_{dc}$ .

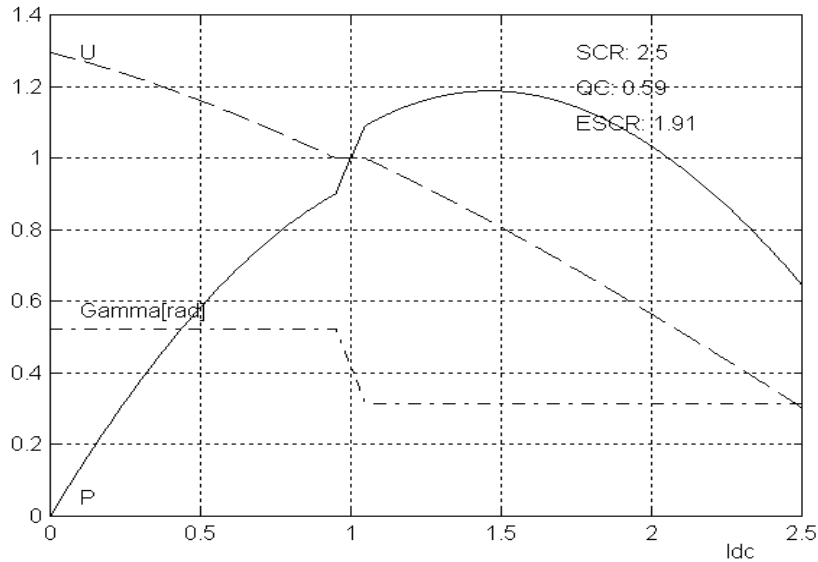


Figure 5-6 Terminal voltage  $U$  and transmitted power  $P$  from a converter with  $\gamma$ -control connected to a weak network, as a function of DC current  $i_{dc}$ .

offshore installation, the synchronous compensator rating could be reduced from the usual 60 % of the transmission rating to approximately 25 %.

Stable operation can also be achieved by modification of the HVDC control. Disregarding the slow tap-changers, the relation between AC- and DC voltage is controlled by the inverter extinction angle  $\gamma$ . Operating the system at a fixed, minimum  $\gamma$  control indeed gives the benefit of minimum reactive power consumption, but the cost is lack of control capability. On the other hand, a controllable  $\gamma$  gives increased voltage control, at the cost of reactive power consumption and some increase in valve ratings.

The weak network shown in Figure 5-4 has been recalculated with  $\gamma$ -control. The rated extinction angle  $\gamma_N$  has been set to  $24^\circ$  with an allowed range of variation from  $18^\circ$  to  $30^\circ$ . The shunt compensation capacitor has been increased to  $q_c = 0.59$  in order to compensate for increased reactive power demand, thereby weakening the ESCR further. The results of the calculations are shown in Figure 5-6. Compared to Figure 5-4 there is a significant improvement in the stability, seen as the distance to the MAP-point. Additionally the figure shows the variations of  $\gamma$  (in radians). To simplify the calculations in this example,  $\gamma$  is kept stable at  $30^\circ$  for currents below the rated current. Above the rated current,  $\gamma$  is kept stable at  $\gamma = \gamma_{min} = 18^\circ$ . Just around the rated operating point,  $\gamma$  varies from max to min., thereby control-

ling the power transmitted by means of the DC voltage and the AC power factor while the current shows little variation.

## 5.2 TEMPORARY OVERVOLTAGES

As seen from the curves presented in the previous section, load reductions in a converter results in increased voltages before the voltage control of the network manages to reduce the source voltage. The maximum voltages will be the value of the voltage curve at  $I_{dc} = 0$ , which is the effective source voltage  $E_{sE}$ . For weak networks, the temporary overvoltages may reach as high as 130 % or more, as seen from Figure 5-4/Figure 5-6, in this example. The duration will last until the voltage controllers are able to regain control, which normally may take many periods. In comparison, the transient voltages deviations allowed on an offshore oil installation will be +20/-15 %.

The values which are shown in the curves are naturally only the RMS value of the fundamental harmonic. If the voltages exceed the saturation voltages of transformers etc., harmonic distortion can give considerably higher peak values.

## 5.3 SUMMARY

In traditional HVDC systems the inverter normally operates in constant  $\gamma$ -min. control mode, in order to save reactive power, minimize transmission losses and to minimize the inverter rating. The price is to give up one degree of freedom in the control of the system. This, together with the normal operating mode, which is power control, of the master controller is one important reason for the problems with HVDC transmission to weak AC networks.



# **6 HVDC SUPPLY TO OFFSHORE OIL INSTALLATIONS**

In this chapter, the simulation tool for evaluation of HVDC transmission to offshore oil platforms will be selected. Further, the models for electric machines and drives from Chapter 3 will be put together with quasi-phasor models for the other elements which together constitute the whole platform network, to show a possible model for simulation of the stability of the HVDC supply and the platform AC network.

## **6.1 INTRODUCTION**

If an HVDC transmission is to be connected to a network, there must be a certain short circuit ratio (SCR) present to avoid stability problems, as seen from Chapter 5. The aim of supplying offshore oil installations with electric power from land is precisely the opposite, to get rid of the power production (and consequently the intrinsic SCR) on board. In the traditional case of HVDC power supply to a weak network with low power production capacity, SCR has been increased by means of synchronous compensators, usually with a reactive power rating of about 60 % of the nominal rating of the HVDC transmission. These have had the additional task of supplying inertia to keep frequency deviations within limits. One study [18] have shown by simulations that it is possible to reduce the size of the synchronous compensators to approximately 25 % by introducing Static Var Compensators (SVC) with fast voltage control.

These are, however, still too heavy synchronous compensator units to give an economically feasible solution. The maximum that should be accepted is a synchronous machine that can serve the dual purpose of essential generator at start-up and in case of faults, and synchronous compensator in normal opera-

tion. The size of this generator will in many cases not be more than in the range of 10 % of the normal power requirements. On the other hand, the requirements for the frequency stability are not as high as on land. The regulations [2] demand the frequency variations to be kept within  $\pm 5$  % stationary and  $\pm 10$  % transiently. The voltage is allowed to vary within  $\pm 2.5$  % stationary and  $+20/-15$  % transiently at the largest normal load switching. If these limits are fully utilized, it might be possible to keep the system stable.

## 6.2 SIMULATION PROGRAMS

The simulations to be performed in order to decide the possibility of keeping the system stable can be performed in several ways, with varying degrees of exactness. The basic difference is between methods based on instantaneous values, and methods based on average values, like phasors. The event which is of interest in this case is network stability of frequency and voltage, with a typical time span in the range of seconds. Thus simulation methods based on instantaneous values, while more exact, will give too much information that is not really needed, thus clouding the relevant results. These methods also require too much simulation time and resources to be feasible in this case.

Phasor calculation, on the other hand, is formally a representation of constant sinusoidal values. If, however, the changes in current, voltage, impedance or frequency are slow compared to the system frequency, the errors arising from a quasi-stationary calculation are negligible. One must keep in mind that the results are only correct for the fundamental harmonic, the influence of higher harmonics must be investigated separately. Phasor calculation requires the possibility of complex calculations, or at least parallel processing of real and imaginary parts of complex numbers.

There are several possible programs which are more or less suited to perform the simulations required. Those immediately available in the Department of Electrical Power Engineering at NTNU at the start of this project were:

- Matlab with Simulink
- KREAN
- EMTP
- EMTDC
- SIMPOW



- EDSA

Of these, SIMPOW and EMTP operate by instantaneous values, giving an precision that is not required in this feasibility study. SIMPOW is also able to simulate time-varying phasor-values, while EMTP is only able to calculate a stationary starting point. Additionally our experience is that both have fairly high entrance thresholds, requiring more time for learning than could be spent in this case. EMTDC was very recently acquired, and still under evaluation.

KREAN is well known by us and has a reasonably low threshold, but, like EMTP, it is based on instantaneous values. The computing time and resources required for long time domain analysis of complex three-phase circuits will quickly become prohibitive. At present it does not have the ability to operate with complex numbers, making it unfit for phasor calculations. EDSA is a fairly easy accessible simulation program, but it seems to lack the necessary modules for simulation of modern power electronics in power utility context.

Matlab with Simulink is a well known, simple and efficient simulation program, which is easy to learn. It is well suited for phasor-based simulations, as it is relatively easy to implement the parallel processing of real and imaginary parts.

In this work, Matlab with Simulink was selected as the tool for the simulations based upon a quasi stationary model related to phasors, while KREAN was used for control simulations in order to verify the simpler model, and in other cases when a time domain simulation is required.

## 6.3 SIMULATION MODEL

The system to be simulated is shown on Figure 6-1. All loads are connected to the main busbar.

The model could consist of the following elements:

### 6.3.1 Distributed load behind transformers

This will sum up to approximately 30 % of the total power on the platform. From this 1/3 can be stipulated as heating and light. This load can be regarded as frequency independent, with voltage/power relationship:

$$p = k \cdot u^2 \quad (6-1)$$

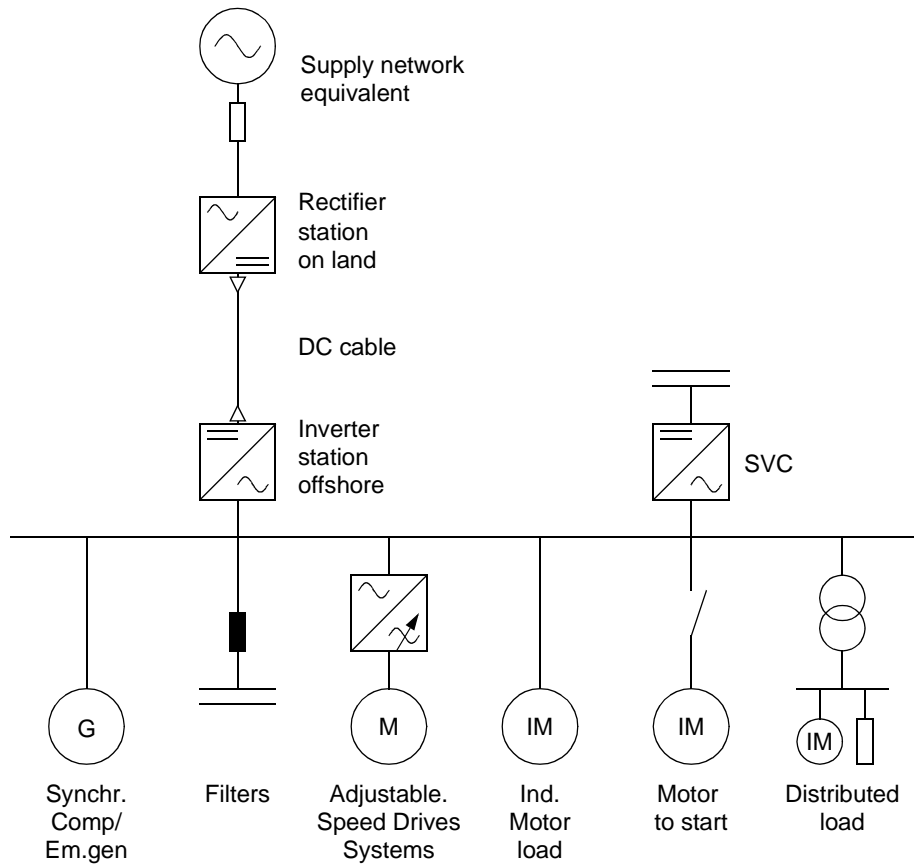


Figure 6-1 Model of HVDC supply to an offshore oil-installation.

The remaining 2/3 of the load can be stipulated as ‘small motor’ load, practically exclusively pumps/fans with square speed/torque characteristics, which gives the frequency/power relationship:

$$p = k \cdot f^3 \quad (6-2)$$

This load is practically voltage independent. The inertia of these motors will be disregarded.

### 6.3.2 Rotating large induction motor load

This will constitute of approximately 20 % of the total load on the platform. These motors will be powering the large pumps and compressors on the platform with square speed/torque characteristics. These motors will have relatively small deviations from nominal slip and can be described by clas-

sical linearized models around nominal load. The relevant equations are found in Chapter 3 to be:

$$\frac{d\omega_{mek}}{dt} = \left( \frac{P_d}{\omega_{el} \cdot m_{dN}} - \omega_{mek}^2 \right) \frac{\omega_{mekN}}{T_a} \quad (3-20)$$

$$p_d = \text{Re}(s_m) = 2 \cdot u^2 \cdot k_p \cdot m_{dN} \cdot \frac{\sigma_{pN} \cdot (\omega_{el} - \omega_{mek})}{\omega_{el} [\sigma_{pN}^2 + (\omega_{el} - \omega_{mek})^2]} \quad (3-24)$$

and

$$q_d = \text{Im}(s_m) = 2 \cdot u^2 \cdot k_p \cdot m_{dN} \cdot \frac{(\omega_{el} - \omega_{mek})^2}{\omega_{el} [\sigma_{pN}^2 + (\omega_{el} - \omega_{mek})^2]} \quad (3-25)$$

### 6.3.3 Motor to be started

This is assumed to be a large induction motor constituting approximately 10 % of the total load. As this motor has to run through the whole speed range from standstill to normal slip, the simple linear model is not sufficient. Instead, the best alternative is to make use of typical speed/torque and speed/current curves for relevant motors. Based on these curves, active and reactive power can be calculated as shown in Chapter 3:

$$p = u^2 \cdot m \left( \frac{\omega_{mek}}{\omega_{el}} \Big|_{u_n} \right) \cdot \omega_{el} \quad (3-26)$$

and

$$q = u^2 \cdot \sqrt{\left( i \left( \frac{\omega_{mek}}{\omega_{el}} \Big|_{u_n} \right) \right)^2 - \left( m \left( \frac{\omega_{mek}}{\omega_{el}} \Big|_{u_n} \right) \cdot \omega_{el} \right)^2} \quad (3-27)$$

Together with the speed/torque equation (3-20), these equations describe the motor during start-up, also during varying voltage and network frequency.

### 6.3.4 Adjustable speed drives load

This will constitute of approximately 40 % of the total load on the platform. This type of load may in some cases be rectifiers powering DC motors, but consist mainly of current source converters today, powering adjustable speed synchronous motors. The rating of voltage source converters are steadily growing, and this type of converters will probably be dominating in the future. As the motors powered by a frequency converter always will run with a controlled speed independent of the network frequency, the load is frequency independent. By normal control, current source converters and rectifiers draw a constant active power from the network at a given point of work, independent of both frequency and voltage, while the reactive power varies with the network voltage. The equations are given in Chapter 3:

$$p_2 = \sqrt{3}u_{v1}|i_{v1}|\cos\alpha_1 = p_1 \quad (3-50)$$

and

$$q_2 = \sqrt{3}|i_{v1}|\sqrt{u_{v2}^2 - u_{v1}^2 \cos^2\alpha_1} \quad (3-52)$$

At line voltages below a given level the current source converters are no longer able to maintain the terminal voltage of the motors. Normally they maintain operation in the torque control mode while the speed is allowed to drop with the voltage for another voltage span, until finally they are disconnected at a minimum voltage. In this low-voltage range, current source converters act as a constant current load on the network, with a displacement power factor near 1.

Voltage source converters do not normally control the voltage of the voltage link, they are in fact often equipped only with a diode rectifier. Thus they draw a constant active power load from the network with a displacement power factor close to 1.

Adjustable speed drives may be equipped with additional control features acting with automatic load reductions at large disturbances in the network, but this will not be included in this modelling.

### 6.3.5 Harmonic filters

These will be passive tuned filters for harmonic cancellation. They will act as shunt capacitors for the fundamental harmonic. They will supply reactive power according to

$$q = u \cdot \left( \frac{1}{\omega_{el} \cdot c} - \omega_{el} \cdot l \right) \quad (6-3)$$

### 6.3.6 Static Var Compensator

This will be modelled as a controlled source supplying the necessary reactive power. This source must act together with the filters to avoid resonance phenomena or other adverse effects.

### 6.3.7 Synchronous compensator

This is assumed to be an ordinary synchronous machine with transient reactances. In Chapter 3, the following equations were found, which are valid for a synchronous machine in a network where mechanical as well as electrical frequencies may vary.

$$\frac{d}{\omega_N dt} i_d = \frac{u_d + \omega_m x_q i_q - r_a i_d - \frac{x_{ad}}{x_f} (u_f - r_f i_f)}{x_d'} \quad (3-34)$$

$$\frac{d}{\omega_N dt} i_q = \frac{u_q - \omega_m (x_d i_d + x_{ad} i_f) - r_a i_q}{x_q} \quad (3-35)$$

$$\frac{d}{\omega_N dt} i_f = \frac{x_d (u_f - r_f i_f) - x_{ad} (u_d + \omega_m x_q i_q - r_a i_d)}{x_d' x_f} \quad (3-36)$$

$$p = u_d \cdot i_d + u_q \cdot i_q \quad (3-40)$$

$$q = u_d \cdot i_q - u_q \cdot i_d \quad (3-41)$$

$$\beta = \int_{t_0}^t (\omega_{el} - \omega_{mek}) dt + \beta_0 \quad (3-43)$$

$$m_d = x_{ad} i_f i_q + (x_d - x_q) \cdot i_d i_q \quad (3-38)$$

$$m_N \cdot T_a \cdot \frac{d^2 \beta}{dt^2} - D \cdot \frac{d\beta}{dt} = m_d - m_l \quad (3-39)$$

One of the purposes of the simulation is to determine the necessary size of this machine in order to keep the system dynamically stable within the requirements of the regulations [2] regarding frequency and voltage variations.

### 6.3.8 HVDC transmission

The current flow through an HVDC transmission line was found in Chapter 4 to be:

$$\frac{di_d}{dt} = \frac{u_{dio,r} \cdot \cos \alpha - u_{dio,i} \cdot \cos \gamma - \frac{3}{\pi} \cdot (x_{k,r} - \omega_{el} \cdot l_{k,i}) \cdot i_d}{(2l_{k,r} + 2l_{k,i} + l_d)} \quad (4-10)$$

By proper selection of base values it is achieved that  $u_{dio} = u_v$  and  $i_d = i_v$ . This only describes the power part of the transmission. The control part is expressed through expressions for  $\alpha$  and  $\gamma$ . The tap-changer control will be disregarded in this context, as this control is acting too slow to be of any interest for stability purposes. The control part will be treated below.

### 6.3.9 Supply network with filter circuits on land

The supplying network can be modelled as a Thevenin equivalent, consisting of a stiff voltage source and an inductive series impedance. If the filter circuits on land are incorporated with the series impedance, the total impedance will reflect the effective short circuit capacity of the network with filters. If the filters are modelled separately as shunt capacitors, the Thevenin equivalent reflects the proper short circuit capacity of the network. As this

study does not aim at the events on land, the simplest model is chosen, and the filters are incorporated in the Thevenin equivalent. The effective series impedance must be added to the leakage inductance of the converter transformer to form the total commutation inductance of the converter.

### 6.3.10 Control of HVDC transmission, SVC and synchronous compensator

Traditional control has been to keep  $\gamma$  constant at  $\gamma_{\min}$  and control  $\alpha$  to keep constant power flow or sometimes a constant current flow. If this HVDC transmission is going to supply an offshore installation, the first extension of control would be to control the power flow by means of controlling  $\alpha$  to match the power needs on the platform. This will require measurements on the platform and a certain amount of calculations to be performed before the need for power can be transmitted to land. The calculations can be performed quickly using the calculation tools available today, but some time is inevitably required to transmit the signals to land and verify them. An estimated typical time lag will be in the magnitude of 20 to 30 ms [21].

The interaction between the HVDC transmission, supplying active power while consuming reactive, and the SVC, supplying reactive power needed both by the transmission and the consumers on the platform has to be analysed. A very efficient way of decoupling active and reactive power is to apply d-q-transformation of voltage and current and control active and reactive power independently on this basis [31]. To simplify the simulations, and also due to the slower voltage controller of the synchronous compensator, this will be kept on a constant magnetization, and mainly act as inertia in the system.

## 6.4 SUMMARY

This chapter has shown the reason to choose Matlab with Simulink as the tool for my simulations. Further it has discussed quasi-phasor models of most of the elements that constitute the HVDC transmission and platform network to be used in a complete model of the whole system. But the further work brought forth so many other interesting aspects that the simulation of the total system never was completed. This will have to remain to another thesis, but in my opinion it certainly should be done.





# **7 ANALYSIS OF A NETWORK WITH AN RC LOAD**

In this chapter we shall initially investigate the fundamental behaviour of an inverter feeding power into a passive network consisting of resistors and capacitors. It will be shown that in a system with fixed firing delay time and fixed DC link current, both voltage and frequency will vary if either resistance or capacitance is changed. The sensitivities of frequency and voltage for change in network parameters, as well as for a change in firing delay time are found. The concept of relative sensitivity is introduced and the relative sensitivities are discussed. Especially it shall be noted that there is a positive sensitivity in frequency with regard to change in load, represented by network conductance. This implies a possible instability for all types of load which increase by frequency, like motors.

Further, a base case inverter is analysed for small signal sensitivities, and an example system where voltage and frequency are controlled by means of variations in network capacitance and firing delay time is simulated. The simulations are performed both in a quasi-phasor model and a time domain model. Both models give the same results, and show that this type of control is possible, as well as confirms that quasi-phasors are a useful way of modelling.

## **7.1 INTRODUCTION**

In order to analyse the behaviour of low inertia network when supplied from an HVDC inverter, the frequency sensitivity of the networks must be found. This will be done by starting with a simple RC load on the inverter. Then the capacitor size and the firing delay time will be controlled in order to stabilize the frequency and voltage. Finally a synchronous compensator will

be introduced to add inertia to the system. The aim of the KREAN simulations is primarily to verify the proposed model and quantify the reactive power needed by the inverter.

It may be helpful to start with some very elementary conditions to clarify the approach to the model that will be developed. In any network there has to be maintained a balance between produced and consumed power, active as well as reactive. If there is balance between produced and consumed reactive power,

$$Q_{produced} + Q_{consumed} = 0 \quad (7-1)$$

the sum of inductive and capacitive susceptance in the network has to be zero. Both these parameters are frequency dependent, but they can be expressed by means of the frequency and the frequency independent parameters capacitance and inductance.

$$j\omega C + \frac{1}{j\omega L} = 0 \quad (7-2)$$

If the balance is disturbed by a change in capacitance or inductance, the only possibility to regain the balance is to allow the system to oscillate with a new resonance frequency.

$$\omega = \frac{1}{\sqrt{LC}} \quad (7-3)$$

It must be noted that in the case of active components, like inverters, the capacitance and/or inductance may be voltage dependent. Thus the frequency may vary with the voltage. In general, any load disturbance in a network can be regarded as a change in the network impedance.

## **7.2 UNSTABILIZED RC NETWORK FED BY LINE COMMUTATED INVERTER**

### **7.2.1 Unstabilized systems**

Line commutated converters need reactive power in order to perform commutation. That makes them look like equivalent inductors to the network. If the rest of the network is able to supply reactive power, looking like an

equivalent capacitor, there will be a stable oscillation with frequency given by (7-3). In order to see how such a system will behave, with simple simulations, the model shown in Figure 7-1 is established. The network is represented by a resistor R and capacitor C in parallel. The resistor represents all the active load in the system. The capacitance represents the net surplus of reactive load. A parallel connection is chosen, as this is the closest representation of the load in parallel with filters and parallel compensating capacitors which is the usual configuration.

For simplicity, the converter is a simple 6-pulse thyristor bridge inverter, while in reality the inverter will certainly be 12-pulse. The commutation is considered ideal and the DC current  $I_d$  is without ripple and kept constant. In the following, the consequences of changing the firing delay time of the thyristors will be analysed.

The analysis will be performed in absolute values, in order to avoid the problems of defining suitable base values.

An inverter requires reactive power from the AC system it supplies. Thus the inverter can be described as an active source in parallel with a reactive load. The active and reactive fundamental power drawn from the AC network are given by:

$$P = \sqrt{3}U_v I_v \cos \alpha \tag{7-4}$$

$$Q = \sqrt{3}U_v I_v \sin \alpha \tag{7-5}$$

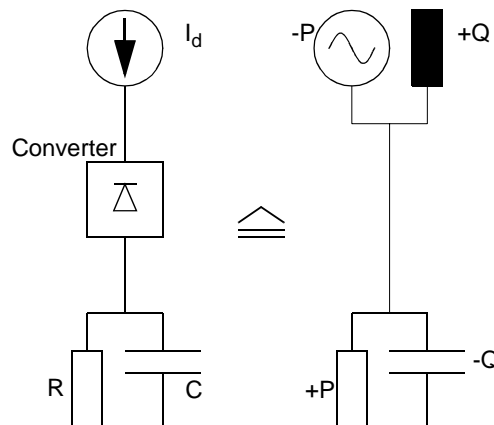


Figure 7-1 Model of simple capacitive load fed by inverter, and its equivalent impedance model. Power consumption is defined positive and production negative.

The relationship between the fundamental RMS AC current and smooth DC current in a 6-pulse thyristor bridge inverter is

$$I_v = \frac{\sqrt{6}}{\pi} \cdot I_d \quad (7-6)$$

The voltage relationship is

$$U_d = \frac{3\sqrt{2}}{\pi} U_v \cdot \cos \alpha \quad (7-7)$$

The resulting frequency is unknown, consequently the firing delay angle is also unknown. Therefore we select the firing delay time  $\Delta t$  as parameter for the following analysis. From the firing delay time  $\Delta t$  and the unknown period time  $\tau$  we get

$$\alpha = \frac{\Delta t}{\tau} \cdot 2\pi = \Delta t \cdot \omega \quad (7-8)$$

Combining (7-6), (7-7) and (7-8) with the active power balance gives, when disregarding the harmonics:

$$P_{inv} = I_d \cdot U_d = I_d \cdot \frac{3\sqrt{2}}{\pi} U_v \cdot \cos(\Delta t \cdot \omega) = -U_v^2 G = -P_{load} \quad (7-9)$$

The minus sign arises from motoric references with the system operating in the 2<sup>nd</sup> quadrant and the DC voltage being defined negative in inverter operation. The conductance description is chosen to better suit parallel connection of loads later. Solving (7-9) gives:

$$\cos(\Delta t \cdot \omega) = -\frac{U_v}{I_d} \cdot \frac{\pi}{3\sqrt{2}} \cdot G \quad (7-10)$$

The fundamental reactive power balance gives:

$$Q_{inv} = \sqrt{3} I_v U_v \sin \alpha = \frac{3\sqrt{2}}{\pi} \cdot I_d U_v \sin(\Delta t \cdot \omega) = U_v^2 \cdot \omega C = -Q_{load} \quad (7-11)$$

which gives:

$$\sin(\Delta t \cdot \omega) = \frac{U_v}{I_d} \cdot \frac{\pi}{3\sqrt{2}} \cdot \omega C \quad (7-12)$$

Dividing (7-12) with (7-10) gives

$$\tan(\Delta t \cdot \omega) = -\frac{\omega C}{G} \quad (7-13)$$

This equation cannot be solved to find  $\omega$  as an explicit function of  $\Delta t$ , but  $\Delta t$  can be found as a function of  $\omega$ .

$$\Delta t = \frac{\text{atan}\left(-\frac{\omega C}{G}\right)}{\omega} \quad (7-14)$$

where

$$\frac{\pi}{2\omega} \leq \Delta t \leq \frac{\pi}{\omega} \quad (7-15)$$

in inverter operation

Inserting (7-14) into (7-10) gives the resulting AC voltage as:

$$U_v = \frac{3\sqrt{2}}{\pi} \cdot I_d \cdot \frac{1}{\sqrt{G^2 + (\omega C)^2}} \quad (7-16)$$

Inserting (7-16) into (7-9) gives the corresponding DC voltage:

$$U_d = -\frac{U_v^2 \cdot G}{I_d} = -\left(\frac{3\sqrt{2}}{\pi}\right)^2 \cdot I_d \cdot \frac{G}{G^2 + (\omega C)^2} \quad (7-17)$$

### Base Case Example:

To give a numerical example a base case is defined. This will be an inverter with rated power 100 MW. Nominal operating frequency is 50 Hz and nominal extinction angle  $\gamma$  is  $20^\circ$ . Commutation is considered ideal, which is a common simplification when studying the principal operation of a converter. Then an extinction angle  $\gamma$  of  $20^\circ$  is equivalent to a firing angle of

160°. The nominal operating voltage is 120 kV. The rest of the data appear from Table 7-1.

**Table 7-1 Main data of base case inverter.**

Inverter nominal power rating at 50 hz	100 MW
Inverter nominal firing angle $\alpha$ at 50 hz	160°
AC nominal voltage at 50 hz	120 kV
AC nominal current	512 A
Inverter nominal reactive power rating at 50 hz	36.4 MVAr
AC network equivalent resistance, per phase	144 $\Omega$
AC network equivalent capacitance, per phase	8.05 $\mu$ F
DC current	657 A
DC nominal voltage	-152.3 kV

Inserting these values in (7-14) and solving gives the relationship between frequency  $f=2\pi\omega$  and firing delay time  $\Delta t$  shown in Figure 7-2, where the axes have been exchanged to depict frequency as function of firing delay time. In order to prove the mathematics to be valid for the whole inverter range, the calculation aims to establish the limits for firing angles near 90° and 180°,

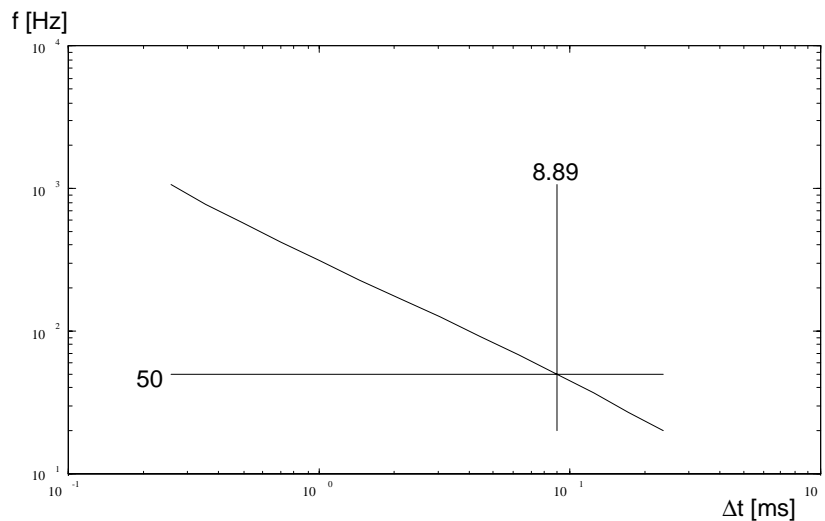


*Figure 7-2 Frequency as a function of firing time delay for the circuit in Figure 7-1.*

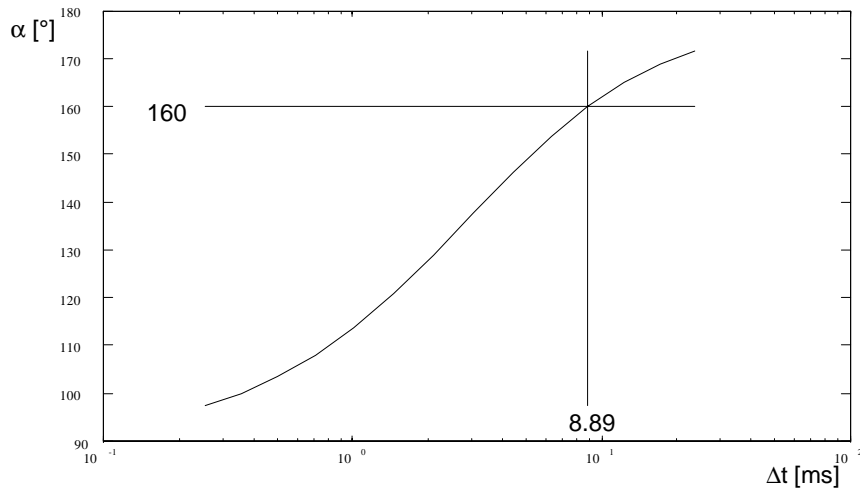


Figure 7-3 Resulting firing delay angle for the circuit in Figure 7-1, calculated from the frequencies in Figure 7-2.

giving a wide frequency range. Naturally, it is only the frequency range around 50 or 60 Hz which is of practical interest.

The resulting firing angle can be calculated using (7-8). The result is shown in Figure 7-3. The resulting AC and DC voltages can be calculated from (7-16) and (7-17). The results of this are displayed in Figure 7-4. As can be seen from the curves, a frequency of 50 Hz corresponds to a delay time of 8.89 ms and a firing angle of  $160^\circ$  as was presupposed. Furthermore, feeding a DC current of 657 A, corresponding to a fundamental current of 512 A into

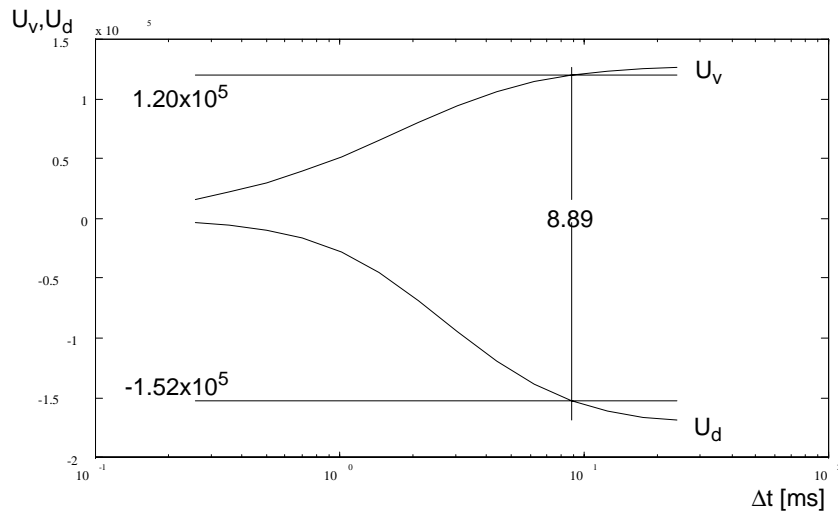


Figure 7-4 AC and DC voltages in the circuit of Figure 7-1 as functions of the firing delay time  $\Delta t$

the network at 50 Hz gives the line voltage of 120 kV and DC voltage of -152 kV, as expected.

Figure 7-2 shows that the frequency decreases by increasing firing delay time, while Figure 7-3 shows that the resulting firing angle increases from near  $90^\circ$  at short firing delay times to near  $180^\circ$  at long firing delay times. Figure 7-4 shows that the absolute values of the AC and DC voltage increase from near zero at short firing delay times to above nominal values at long firing delay times.

The physical explanation is that at high frequencies the capacitive part of the network practically short-circuits the fixed current. The AC voltage drops and only a small amount of active power is consumed. The power factor is close to zero, capacitive. To provide balance of active and reactive power the inverter has to have a power factor close to zero, inductive, i. e. a firing angle near  $90^\circ$  and a short firing delay time. But the firing delay time cannot be shorter than somewhat more than a quarter of a period, thus when the firing delay time decreases further, the frequency must increase correspondingly. Contrary, at low frequencies the capacitive part almost disappears. The network seems purely resistive, forcing the inverter to a firing angle near  $180^\circ$ . But the firing delay time cannot be longer than somewhat less than a half of a period, thus when the firing delay time increases further, the frequency must decrease correspondingly.

The basic circuit in Figure 7-1 has been modelled in KREAN and simulated to verify if the simple mathematical model based on RMS-values of the fundamental harmonic is acceptable. The simulations were performed by setting the AC circuit in oscillations by means of a three-phase voltage source with frequency and amplitude equal to the calculated at the point to investigate. When the circuit has started to oscillate, the voltage source is disconnected and the circuit left to stabilize. As can be expected, the resulting voltage is rather distorted, and the zero crossing of the voltages, giving the natural commutation points, differs from those of the fundamental harmonic. This amounts to a shift in the firing delay time, resulting in a frequency deviating from the expected. To correct this the voltages have to be filtered through a phase-locked loop, and the firing delay time has to be measured from the zero crossing of the filtered voltage. The phase locked loop was designed to give voltages in phase with the fundamental of the phase voltages. The current and voltage forms at approximately 50 Hz are shown in Figure 7-5 and Figure 7-6.

The results of the KREAN simulations have been post-processed in Matlab. The real firing delay times corrected for the error due to the phase locked loop have been determined. The resulting frequencies and RMS values of the fundamental voltage based on Fourier analysis, as well as the phase



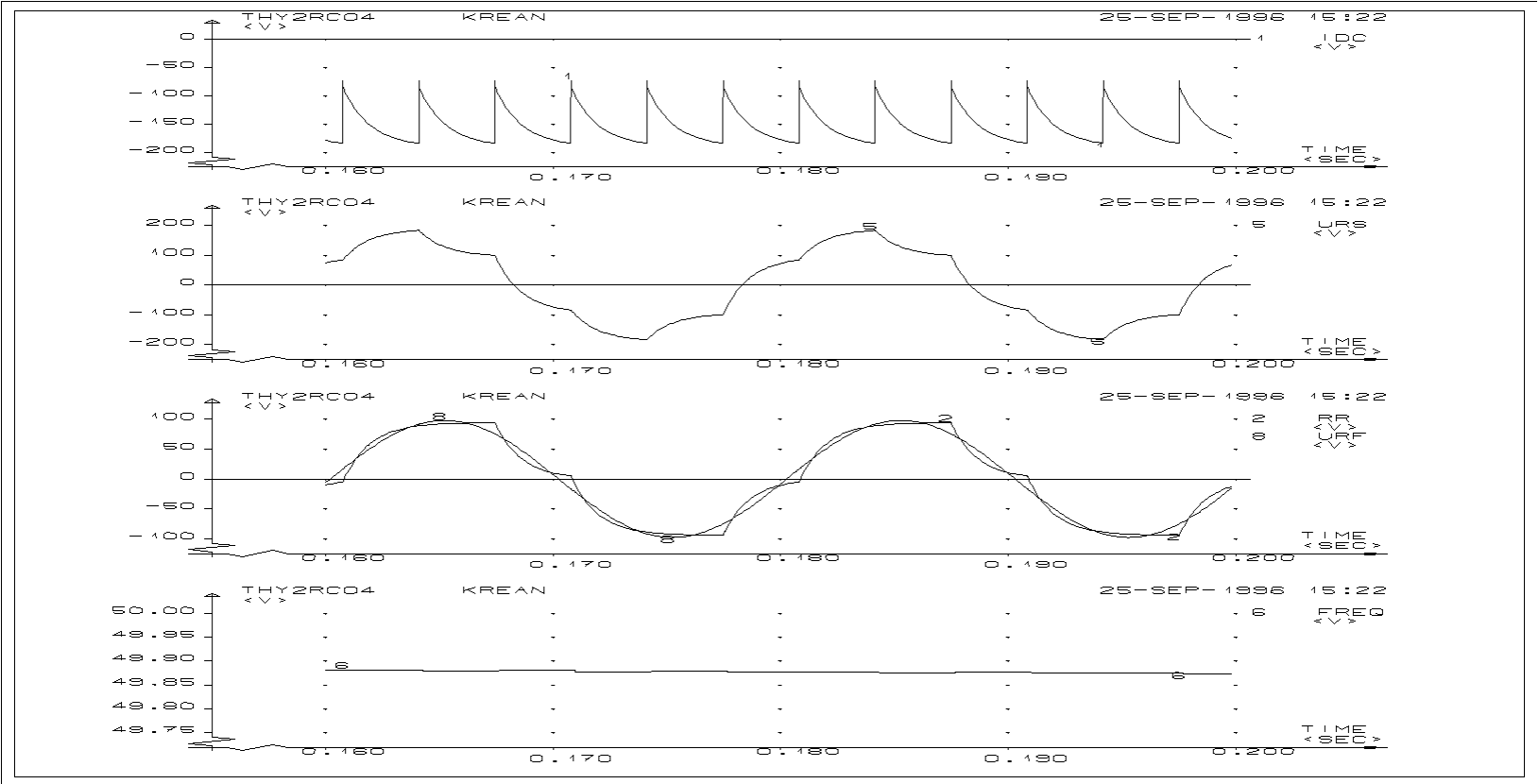


Figure 7-5 DC voltage at source (upper curve), line voltage (second curve), instantaneous and fundamental phase voltage (third curve) and frequency (lower curve) in a passive RC circuit fed by an inverter at approximately 50 Hz.

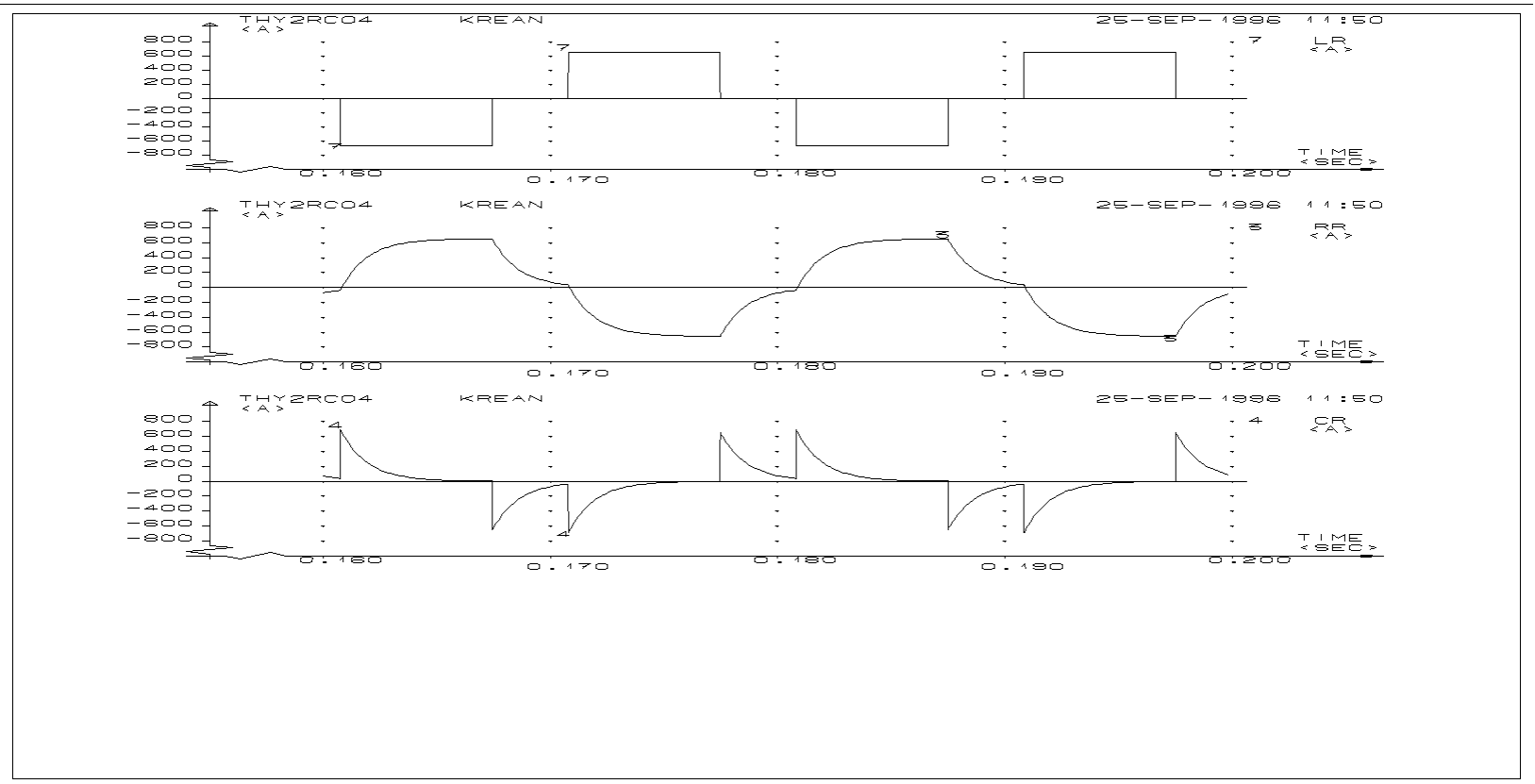


Figure 7-6 Total phase current from the inverter (upper curve), current in the resistor (second curve) and current in the capacitor (third curve) in a passive RC circuit fed by an inverter at approximately 50 Hz.

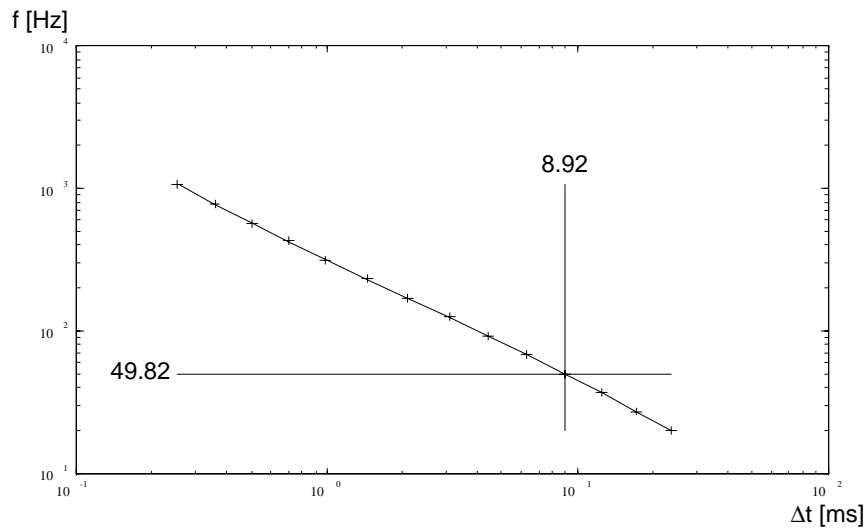


Figure 7-7 Frequency as a function of firing time delay in KREAN simulation, compared to computed values.

angle between voltage and current as a measure for the firing angle have been compared to the theoretically calculated values in Figure 7-7, Figure 7-8 and Figure 7-9, where the KREAN results are presented as crosses.

The agreement is quite good. These simulations show that there is a unique relationship between firing delay time, frequency and voltages for a given circuit. The relationship is described by (7-14), (7-16) and (7-17) with good accuracy. A model based on these equations will probably give satisfactory results for the problem under investigation.

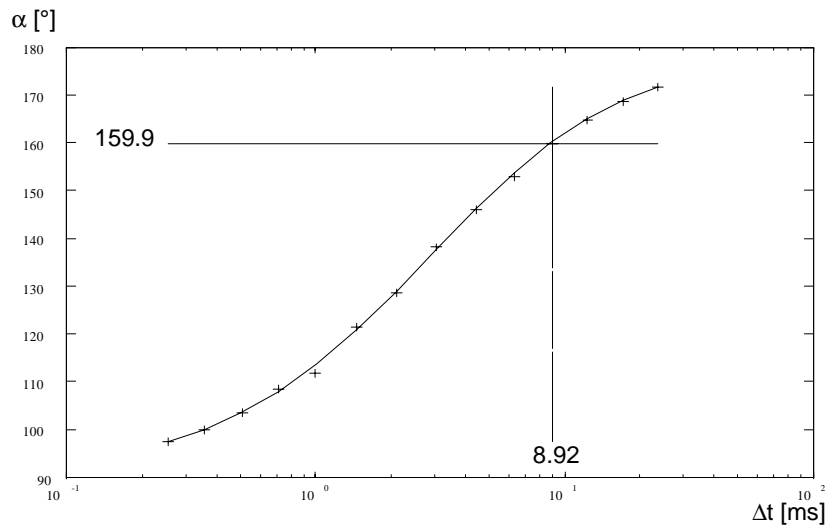


Figure 7-8 Resulting firing delay angle for the circuit in Figure 7-1. Results from KREAN simulations compared to computed values

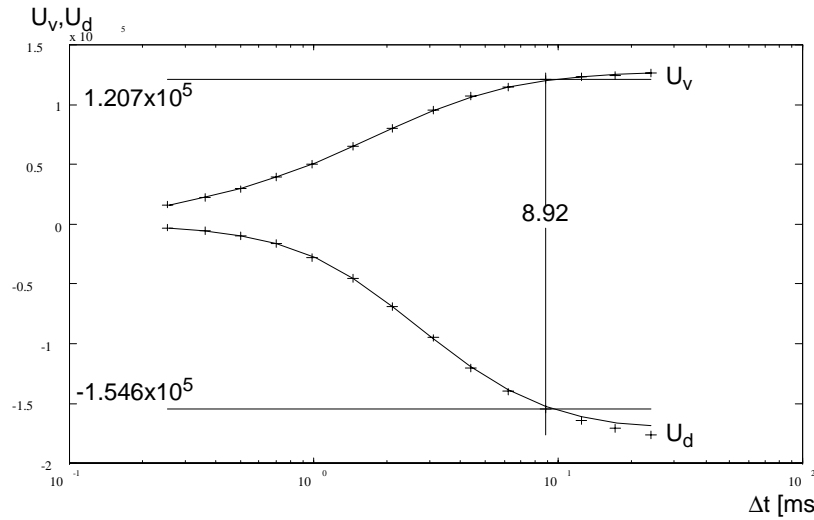


Figure 7-9 AC and DC voltages in the circuit of Figure 7-1. Results from KREAN simulations compared to computed values

### 7. 2. 2 Sensitivity of frequency and voltage for variations in load

A basic question in a circuit where the real load consists for a very large part of rotating machines is how the frequency behaves for a change in the load. If, for instance, the frequency drops when the load is reduced it leads to a speed reduction in the machines. This will, in turn, lead to a further load reduction, leading to a further frequency reduction, and so there is clearly the possibility of an unstable situation. The same will be the case if the voltage drops for a load reduction. It is necessary to find the sensitivities of frequency and voltage for a change in load conductance.

The dependence of the frequency of the load conductance is given implicitly in:

$$\tan(\Delta t \cdot \omega) = \frac{-\omega C}{G} \quad (7-13)$$

and the dependence of the voltage of the load conductance is given in:

$$U_v = \frac{3\sqrt{2}}{\pi} \cdot I_d \cdot \frac{1}{\sqrt{G^2 + (\omega C)^2}} \quad (7-16)$$

Partial derivation of these equations with regard to conductance  $G$  will show how angular frequency  $\omega$  and voltage  $U_v$  depend on the load. (7-13) is an implicit equation, but partial derivation on both sides and performing some algebra gives the result. For the partial derivative of the angular frequency with regard to the load conductance we rewrite slightly and get:

$$\frac{\partial}{\partial G}[G \tan(\Delta t \omega)] = \frac{\partial}{\partial G}(-\omega C) \quad (7-18)$$

$$\tan(\Delta t \omega) + \frac{G \Delta t}{\cos(\Delta t \omega)^2} \cdot \frac{\partial \omega}{\partial G} = -C \frac{\partial \omega}{\partial G} \quad (7-19)$$

$$\frac{\partial \omega}{\partial G} = \frac{-\tan(\Delta t \omega)}{\frac{G \Delta t}{\cos(\Delta t \cdot \omega)^2} + C} \quad (7-20)$$

By application of (7-13) to eliminate  $C$  this can be rewritten as:

$$\frac{\partial \omega}{\partial G} = \frac{-\tan(\Delta t \omega)}{\frac{G \Delta t}{\cos(\Delta t \cdot \omega)^2} - \frac{G}{\omega} \tan(\Delta t \omega)} \quad (7-21)$$

This reforms to:

$$\frac{\partial \omega}{\partial G} = \frac{-\tan(\Delta t \omega) \cos(\Delta t \cdot \omega)^2}{\Delta t \omega - \tan(\Delta t \omega) \cos(\Delta t \cdot \omega)^2} \cdot \frac{\omega}{G} \quad (7-22)$$

which, by application of some sine and cosine manipulation, simplifies to:

$$\boxed{\frac{\partial \omega}{\partial G} = \frac{-\sin(2\Delta t \omega)}{2\Delta t \omega - \sin(2\Delta t \omega)} \cdot \frac{\omega}{G}} \quad (7-23)$$

In inverter operation  $\frac{\pi}{2} \leq \Delta t \omega \leq \pi$  and  $\sin(2\Delta t \omega) \leq 0$ . Thus both the numerator and denominator of (7-23) is positive. The conductance and frequency is defined positive. Therefore the sensitivity of the frequency is positive for a change in load conductance. This means that an increase in conductance, which is equivalent to an increase in load, leads to a rise in frequency. In the case where the load is frequency dependent, like rotating

machines, this implies a possibly unstable situation, which perhaps may be solved by a controller. As it later will appear that the situation really is unstable, this entitles a closer investigation in the next section.

For the voltage we have:

$$\frac{\partial U_v}{\partial G} = \frac{\partial}{\partial G} \left( \frac{3\sqrt{2}}{\pi} \cdot I_d \cdot \frac{1}{\sqrt{G^2 + (\omega C)^2}} \right) \quad (7-24)$$

which can be developed to

$$\frac{\partial U_v}{\partial G} = \frac{-\left(\frac{3\sqrt{2}}{\pi} \cdot I_d\right)}{2(\sqrt{G^2 + (\omega C)^2})^3} \frac{\partial}{\partial G} [G^2 + (\omega C)^2] \quad (7-25)$$

and further to

$$\frac{\partial U_v}{\partial G} = \frac{-\frac{3\sqrt{2}}{\pi} \cdot I_d}{\sqrt{G^2 + (\omega C)^2}^2} \left( \frac{2G + 2\omega C^2 \frac{\partial \omega}{\partial G}}{2[G^2 + (\omega C)^2]} \right) \quad (7-26)$$

The part outside the parentheses can be recognized from (7-16). Following the insertion of (7-23), this can be simplified to:

$$\frac{\partial U_v}{\partial G} = -\frac{U_v}{G} \cdot \frac{G^2 - (\omega C)^2 \left( \frac{\sin(2\Delta t \omega)}{2\Delta t \omega - \sin(2\Delta t \omega)} \right)}{[G^2 + (\omega C)^2]} \quad (7-27)$$

Insertion of (7-13) and application of some sine and cosine manipulation gives:

$$\boxed{\frac{\partial U_v}{\partial G} = -\left(1 - \frac{\Delta t \omega (1 - \cos(2\Delta t \omega))}{2\Delta t \omega - \sin(2\Delta t \omega)}\right) \cdot \frac{U_v}{G}} \quad (7-28)$$

In inverter operation the conductance is defined positive and then (7-28) is negative when the expression inside the parentheses is positive. This is the case when

$$\Delta t \omega > \tan(\Delta t \omega) \quad (7-29)$$

which is always fulfilled in inverter operation, because  $\Delta t\omega > 0$  and  $\tan(\Delta t\omega) \leq 0$  in the 2<sup>nd</sup> quadrant.

In inverter operation, the sensitivity of the voltage is negative for a change in load conductance. This means that an increase in conductance, which is equivalent to an increase in load, leads to a fall in voltage, which counteracts the load increase. This indicates an inherent stable situation. But also here a controller will be required to keep the voltage within required limitation. The design of the controllers will be discussed later.

### 7. 2. 3 Physical analysis of positive sensitivity of frequency for variations in conductance

In order to understand why the frequency increases when conductance increases, a number of KREAN simulations were performed. In this section we will consider resistance instead of conductance, as this is the way in KREAN. In the first case an inverter with time controlled thyristor firing pulses was feeding the RC load from the base case numerical example. By means of time controlled thyristor firing pulses the frequency of the AC current is locked. The frequency of the voltage was registered as previously described, as the mean value of the inverse of the time between the last registered zero crossings of the line voltages. The results are shown in Figure 7-10, Figure 7-11, Figure 7-12 and Figure 7-13. Figure 7-10 gives an overview of the simulation. The system is started in the usual way by means of auxiliary voltage sources, this is omitted in the figure. At time  $t=0.2$  s, the resistance of the load was increased to the double value. After allowing some time for the system to stabilize, the load capacitance was reduced to half the value at time  $t=0.35$  s. When the resistance increases, the voltage rise. This is because the system is powered by a current source. The RMS current in the capacitor rise, due to the increased voltage. Thus the RMS current in the resistor is decreased, and the RMS voltage rise does not get as high as the increase in resistance would imply. It can also be seen that the increase of current in the capacitor falls in the first part of the half-period, thus shifting the phase of the fundamental of the resistive current backwards. The phase voltage of the load is in phase with the resistive current, and thus is also shifted backwards. This phase shifting is registered by the frequency measurement as a passing dip in frequency.

When the capacitance is reduced, the opposite takes place. The capacitive current is reduced, leading to increased resistive current in the beginning of the half period and a phase shifting of resistive current and voltage forward. This phase shifting is registered as a transient increase in frequency.

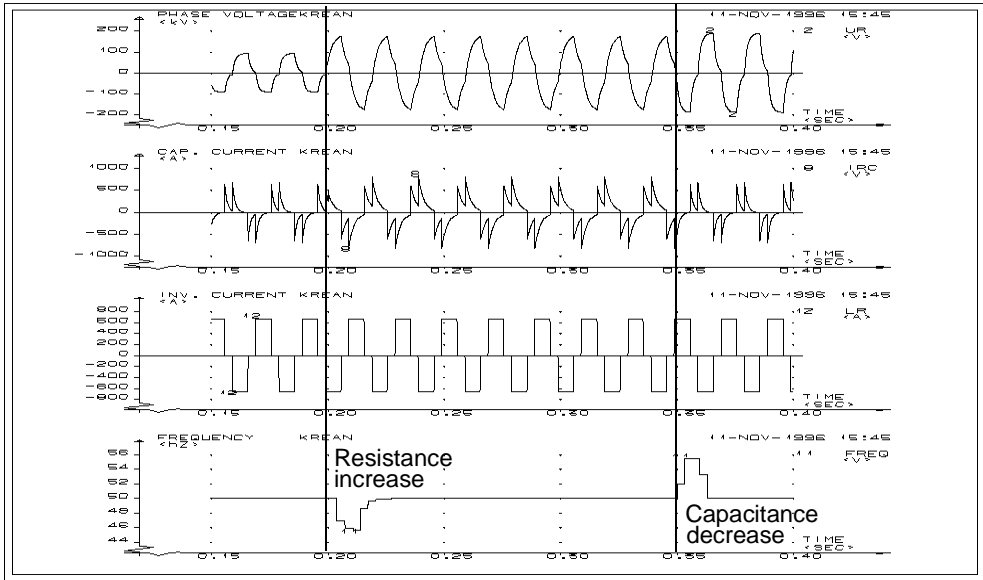


Figure 7-10 Phase voltage, capacitor current and inverter current in phase R, and system frequency based on line voltages. Resistance is doubled at time  $t=0.2$  s and capacitance is halved at time  $t=0.35$  s. Time controlled firing pulses.

Figure 7-11 shows a blow-up of inverter current  $i_R$  phase and the phase voltages of the load, together with their fundamentals, before the resistance is

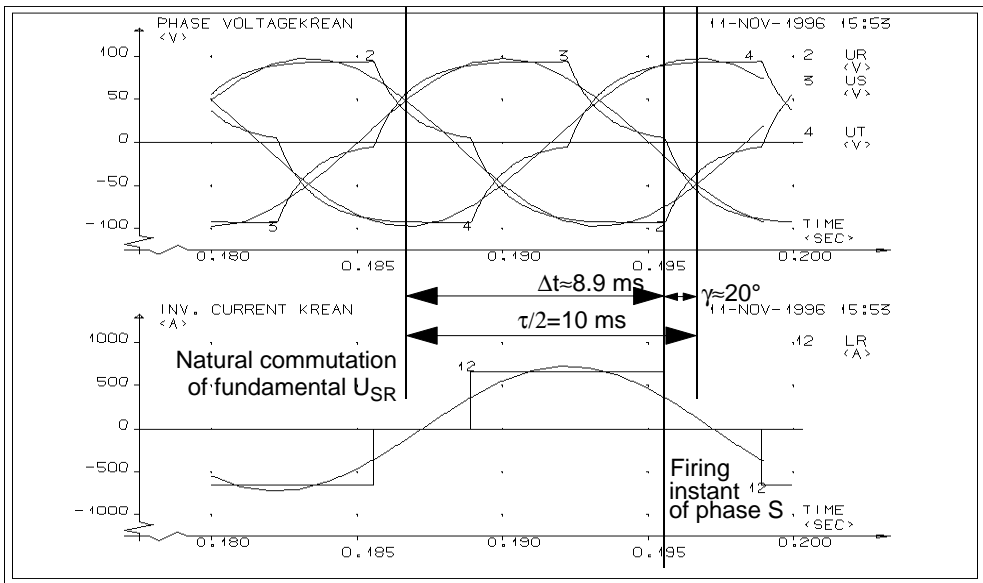


Figure 7-11 Phase voltages in RST and inverter current in phase R, together with fundamentals, before resistance is doubled at time  $t=0.2$  s. Time controlled firing pulses.



increased. The system is operating with nominal values of DC current, resistance, capacitance and frequency. The figure depicts that the voltage and extinction angle also take on nominal values.

The situation after the increase in resistance, but before the decrease in capacitance is presented in Figure 7-12. The duration of the half period is the same, given by the time controlled firing pulses. But the voltages have shifted backwards in phase, thereby decreasing the firing delay time and increasing the extinction angle. The magnitude of the voltage has increased, and the shape has shifted somewhat. This is better seen in Figure 7-10.

Finally, in Figure 7-13 the situation after reduction of the capacitance is shown. This figure is quite similar to Figure 7-11, except that the voltage is doubled. The reason for this is of course that by doubling the resistance and halving the capacitance the real and imaginary part of the impedance are changed in the same scale, keeping the phase angle constant.

Then the simulation was repeated, but this time the frequency was allowed to vary, while the firing delay time was kept constant. An overview of the simulation after the initial start-up is shown in Figure 7-14. The situation before the increase of the resistance is identical to the previous simulation shown in Figure 7-10. When the resistance is increased, the same phase shift and transient dip in frequency occurs. But now there is a phase difference between the actual voltages and the phase locked loop which is the reference for the firing pulses, which forces the PLL to start reducing its frequency. After a time delay, which partly consists of the firing delay time and partly of

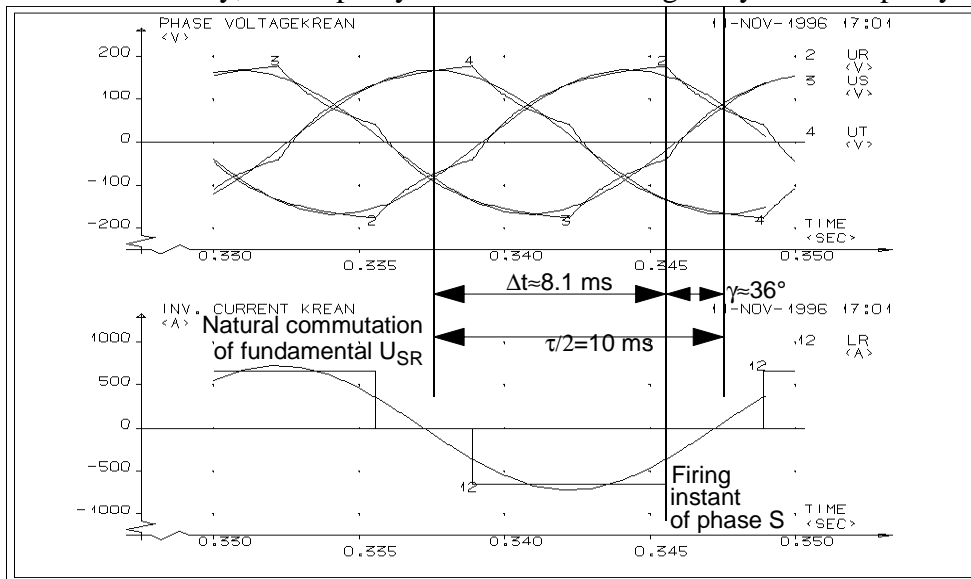


Figure 7-12 Phase voltages in RST and inverter current in phase R, together with fundamentals, after resistance is doubled at time  $t=0.2$  s and before capacitance is halved at time  $t=0.35$  s. Time controlled firing pulses.

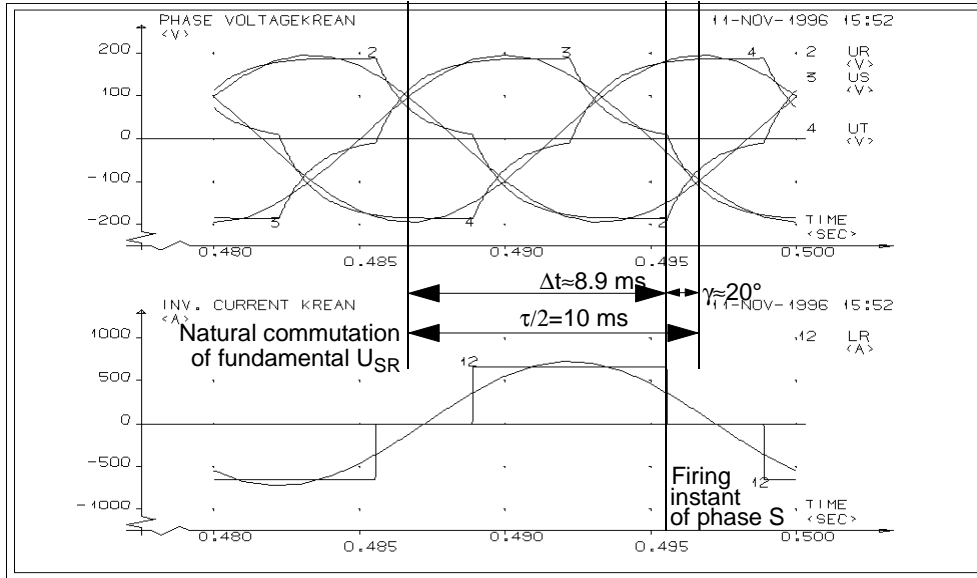


Figure 7-13 Phase voltages in RST and inverter current in phase R, together with fundamentals, after resistance is doubled at time  $t=0.2$  s and capacitance is halved at time  $t=0.35$  s. Time controlled firing pulses.

the delay in frequency measurement, the changed frequency also appears in the measured frequency. Correspondingly, when the capacitance is decreased, there is first a phase shift leading to a transient frequency rise, just similar to the previous simulation, and then secondly the PLL increases the frequency

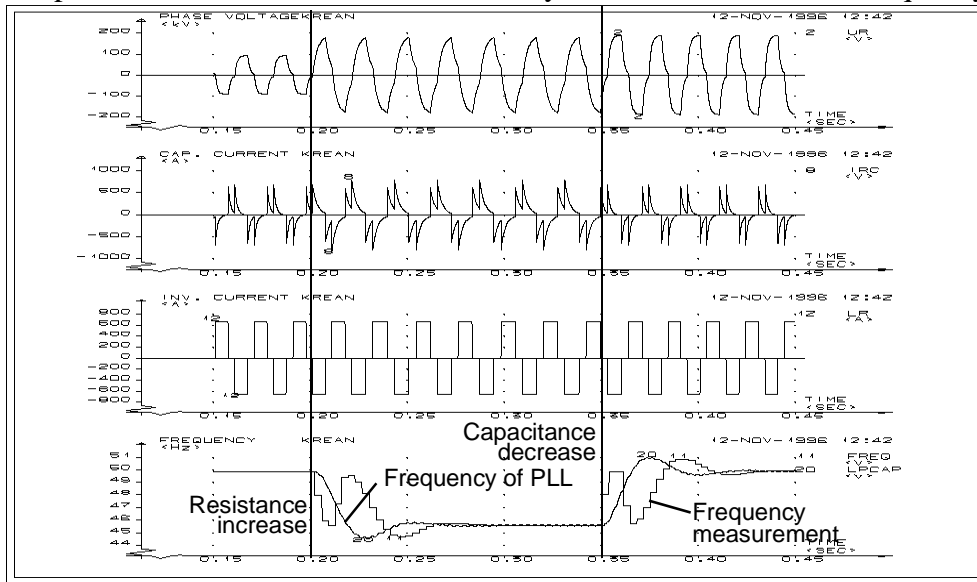


Figure 7-14 Phase voltage, capacitor current and inverter current in phase R, and system frequency based on line voltages. Resistance is doubled at time  $t=0.2$  s and capacitance is halved at time  $t=0.35$  s. Constant firing delay time.

of the system back to the initial value. When the system has stabilized again, the situation is once more identical with the previous simulation. The situation before the capacitance is decreased is shown in Figure 7-15. The shape of the curves is quite similar to the situation in Figure 7-12, but the frequency is reduced. The extinction angle  $\gamma$  is not exactly the same, this is due to the fact that the frequency is reduced and thus the imaginary part of the impedance is somewhat greater.

The different situations can be described by phasor diagrams as shown in Figure 7-16. In all the diagrams the inverter current is chosen as real and constant. Diagram I) shows the initial condition, as in Figure 7-11. Diagram IIa) shows the situation with double resistance and time controlled firing pulses, as in Figure 7-12, while diagram IIb) shows the situation with double resistance and constant firing delay time, as in Figure 7-15. Angular frequency  $\omega_{2b}$  is lower than  $\omega_0$ . Therefore the capacitive current  $I_{c2b}$  is less than  $I_{c2a}$  and consequently the phase angle  $\phi_{2b}$  is less than  $\phi_{2a}$ . Diagram III) shows the situation with double resistance and half capacitance, as in Figure 7-14. Currents, frequency and phase angle are as in the initial situation, while the voltage has been doubled.

It should be noted that these simulations of course do not represent real situations, they are performed to clarify what happens when the system parameters, like resistance, are varied under different conditions.

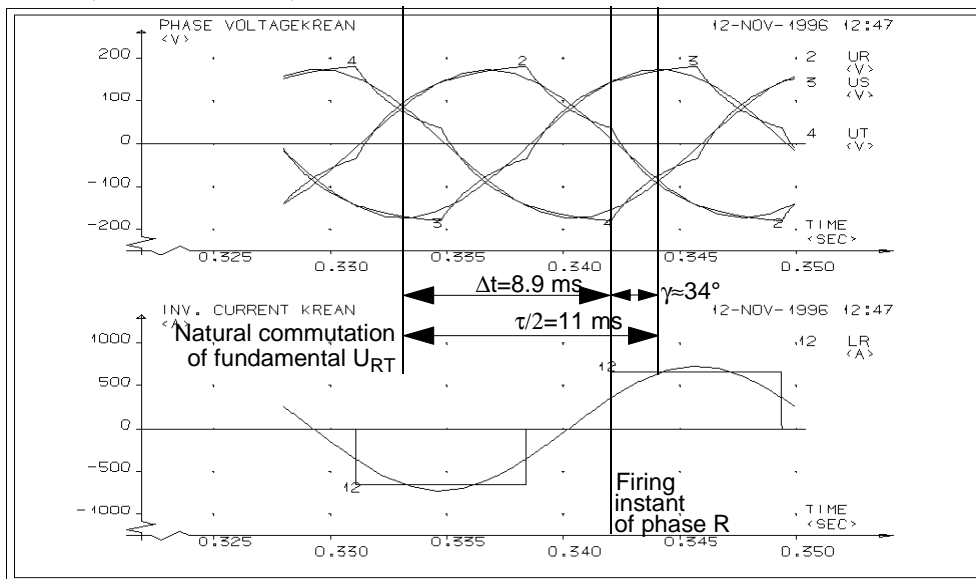


Figure 7-15 Phase voltages in RST and inverter current in phase R, together with fundamentals, after resistance is doubled at time  $t=0.2$  s and before capacitance is halved at time  $t=0.35$  s. Constant firing delay time.

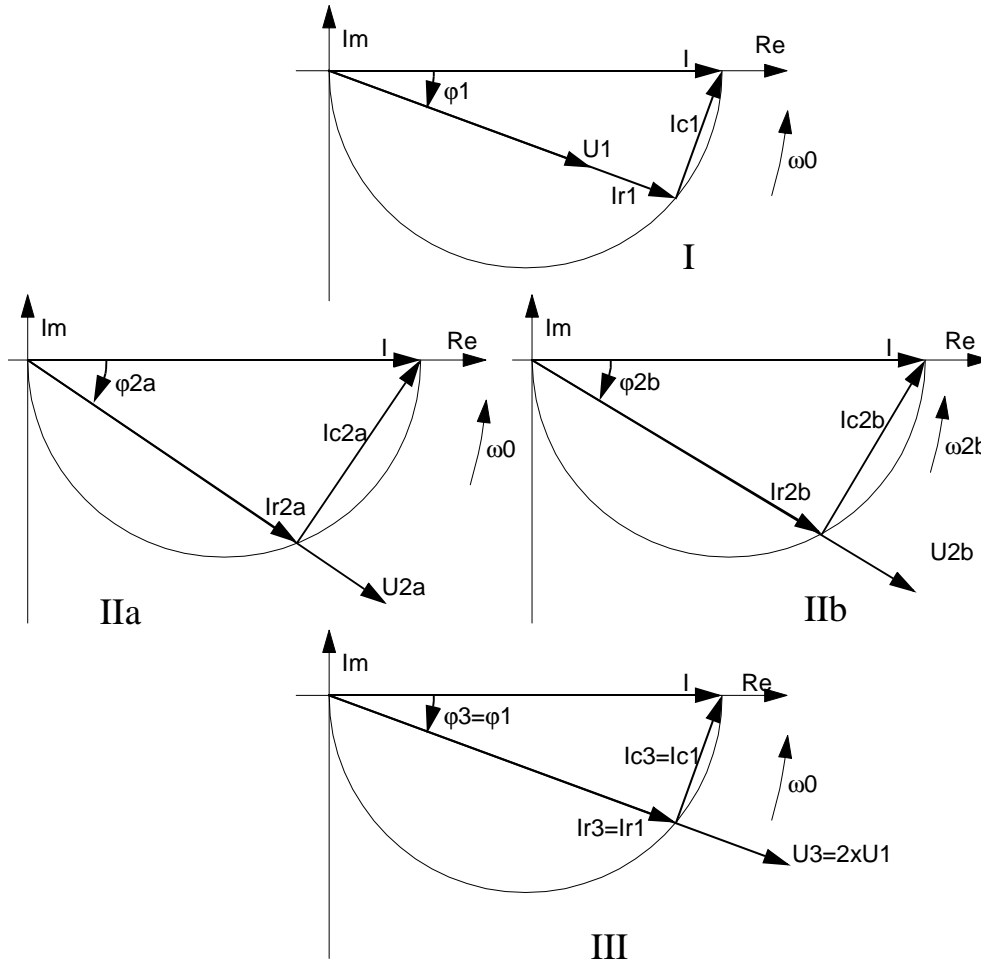


Figure 7-16 Phasor diagrams for inverter feeding RC load

I) Initial condition,  $R=R_N$ ,  $C=C_N$ ,  $\omega=\omega_0$ ,  $\Delta t=\Delta t_N$ .

IIa) Constant frequency,  $R=2R_N$ ,  $C=C_N$ ,  $\omega=\omega_0$ .

IIb) Constant firing delay time,  $R=2R_N$ ,  $C=C_N$ ,  $\Delta t=\Delta t_N$ .

III) End conditions,  $R=2R_N$ ,  $C=0.5C_N$ ,  $\omega=\omega_0$ ,  $\Delta t=\Delta t_N$ .

#### 7. 2. 4 Sensitivities of frequency and voltage for variations in firing delay time and network capacity

In the real world a basic requirement to a power supply is to keep voltage and frequency within limits given by norms and specifications when the load varies. The analysis in Section 7. 2. 1 indicates that this can be done by controlling firing delay time and network capacity to keep the frequency and voltage constant when the load varies. A variation in network load can be regarded as a variation in network conductance. In order to find the necessary capacitance and firing delay time to keep voltage and frequency constant we

can solve (7-16) to find the capacitance as a function of conductance with angular frequency and voltage as parameters, which gives:

$$C = \frac{\sqrt{\left(\frac{3\sqrt{2}}{\pi} \cdot \frac{I_d}{U_{v,N}}\right)^2 - G^2}}{\omega_N} \quad (7-30)$$

The required firing delay time is given by for instance (7-10), which can be transformed to:

$$\Delta t = \frac{\arccos\left(-\frac{U_{v,N}}{I_d} \cdot \frac{\pi}{3\sqrt{2}} \cdot G\right)}{\omega_N} \quad (7-31)$$

The variables to be controlled are the voltage and frequency. The parameters which are controllable are firing time delay and net network capacitance. In order to determine the most efficient control strategy it is of interest to determine the sensitivity of the frequency and voltage for variations in firing delay time and network capacitance. This is done by partial derivation. The equation best suited for partial derivation of the angular frequency is (7-13). This is an implicit equation, but partial derivation on both sides and performing some algebra gives the result. For the partial derivative of the angular frequency with regard to the firing delay time we get:

$$\frac{\partial}{\partial \Delta t} \tan(\Delta t \omega) = \frac{\partial}{\partial \Delta t} \left(-\frac{\omega C}{G}\right) \quad (7-32)$$

$$\frac{1}{\cos(\Delta t \omega)^2} \left(\omega + \Delta t \frac{\partial \omega}{\partial \Delta t}\right) = -\frac{C}{G} \frac{\partial \omega}{\partial \Delta t} \quad (7-33)$$

$$\frac{\partial \omega}{\partial \Delta t} = \frac{-\omega}{\Delta t + \frac{C}{G} \cdot \cos(\Delta t \omega)^2} \quad (7-34)$$

By application of (7-13) and some sine and cosine manipulation we get:

$$\boxed{\frac{\partial \omega}{\partial \Delta t} = \frac{-2\Delta t \omega}{2\Delta t \omega - \sin(2\Delta t \omega)} \cdot \frac{\omega}{\Delta t}} \quad (7-35)$$

In the same way we find for the partial derivative of the angular frequency with regard to the network capacitance:

$$\frac{\partial}{\partial C} \tan(\Delta t \omega) = \frac{\partial}{\partial C} \left( -\frac{\omega C}{G} \right) \quad (7-36)$$

$$\frac{1}{\cos(\Delta t \omega)^2} \Delta t \frac{\partial \omega}{\partial C} = -\frac{1}{G} \left( \omega + C \frac{\partial \omega}{\partial C} \right) \quad (7-37)$$

$$\frac{\partial \omega}{\partial C} = \frac{-\frac{\omega}{G} \cos(\Delta t \omega)^2}{\Delta t + \frac{C}{G} \cos(\Delta t \omega)^2} \quad (7-38)$$

Inserting (7-13) and sorting gives:

$$\frac{\partial \omega}{\partial C} = \frac{\tan(\Delta t \omega) \cos(\Delta t \omega)^2}{\Delta t \omega - \tan(\Delta t \omega) \cos(\Delta t \omega)^2} \cdot \frac{\omega}{C} \quad (7-39)$$

which by sine and cosine manipulation gives:

$$\boxed{\frac{\partial \omega}{\partial C} = \frac{\sin(2\Delta t \omega)}{2\Delta t \omega - \sin(2\Delta t \omega)} \cdot \frac{\omega}{C}} \quad (7-40)$$

The best starting point for the partial derivative of the voltage with regard to the network capacitance is (7-16), we have:

$$\frac{\partial U_v}{\partial C} = \frac{\partial}{\partial C} \left( \frac{3\sqrt{2}}{\pi} \cdot I_d \cdot \frac{1}{\sqrt{G^2 + (\omega C)^2}} \right) \quad (7-41)$$

$$\frac{\partial U_v}{\partial C} = \left( \frac{3\sqrt{2}}{\pi} \cdot I_d \right) \frac{\partial}{\partial C} \frac{1}{\sqrt{G^2 + (\omega C)^2}} \quad (7-42)$$

$$\frac{\partial U_v}{\partial C} = \frac{-\frac{3\sqrt{2}}{\pi} \cdot I_d}{2\sqrt{(G^2 + (\omega C)^2)^3}} \cdot 2\omega C \left( \omega + C \frac{\partial \omega}{\partial C} \right) \quad (7-43)$$

Inserting (7-40) and sorting we get:

$$\frac{\partial U_v}{\partial C} = \frac{-\frac{3\sqrt{2}}{\pi} \cdot I_d}{\sqrt{G^2 + (\omega C)^2}} \cdot \frac{(\omega C)^2 \left(1 + \frac{\sin(2\Delta t \omega)}{2\Delta t \omega - \sin(2\Delta t \omega)}\right)}{C(G^2 + (\omega C)^2)} \quad (7-44)$$

We recognize the first part from (7-16) and get, by application of (7-13) and some sine and cosine manipulation:

$$\boxed{\frac{\partial U_v}{\partial C} = -\frac{\Delta t \omega (1 - \cos(2\Delta t \omega))}{2\Delta t \omega - \sin(2\Delta t \omega)} \cdot \frac{U_v}{C}} \quad (7-45)$$

To find the partial derivative of the voltage with regard to the firing delay time it is best to start by rewriting (7-10):

$$U_v = -\frac{3\sqrt{2}I_d}{\pi G} \cos(\Delta t \omega) \quad (7-46)$$

$$\frac{\partial U_v}{\partial \Delta t} = \frac{\partial}{\partial \Delta t} \left( -\frac{3\sqrt{2}I_d}{\pi G} \cos(\Delta t \omega) \right) \quad (7-47)$$

$$\frac{\partial U_v}{\partial \Delta t} = \frac{3\sqrt{2}I_d}{\pi G} \sin(\Delta t \omega) \left( \omega + \Delta t \frac{\partial \omega}{\partial \Delta t} \right) \quad (7-48)$$

By inserting (7-35) and sorting, together with some sine and cosine manipulation, we get

$$\frac{\partial U_v}{\partial \Delta t} = -\frac{3\sqrt{2}I_d}{\pi G} \cos(\Delta t \omega) \cdot \frac{2 \sin(\Delta t \omega)^2}{2\Delta t \omega - \sin(2\Delta t \omega)} \cdot \omega \quad (7-49)$$

The first part is recognized from (7-46)

$$\frac{\partial U_v}{\partial \Delta t} = U_v \cdot \frac{2 \sin(\Delta t \omega)^2}{2\Delta t \omega - \sin(2\Delta t \omega)} \cdot \omega \quad (7-50)$$

$$\boxed{\frac{\partial U_v}{\partial \Delta t} = \frac{\Delta t \omega (1 - \cos(2\Delta t \omega))}{2\Delta t \omega - \sin(2\Delta t \omega)} \cdot \frac{U_v}{\Delta t}} \quad (7-51)$$

The found sensitivities indicate how the process responds to small variations in the controllable parameters. They will be used later in the design of a simple controller for the system.

### 7.2.5 Relative sensitivity

In order to be able to compare the sensitivities of the frequency to the sensitivity of the voltage it may be meaningful to define a relative sensitivity, that is the variation of a variable divided by the variable itself, for a relative disturbance.

$$\frac{\partial y}{y_0} = f(x, y, z) \frac{\partial x}{x_0} \quad (7-52)$$

It must be noted that this relative sensitivity is not to be regarded as p.u. sensitivity. It is based on the values of the parameters immediately before the disturbance, not on the p.u. reference values.

The relative sensitivity of the frequency for a relative disturbance in the load is, from (7-23):

$$\frac{\partial \omega}{\partial G} \cdot \frac{G}{\omega} = \frac{-\sin(2\Delta t\omega)}{2\Delta t\omega - \sin(2\Delta t\omega)} \quad (7-53)$$

for a relative change in the firing delay time, from (7-35):

$$\frac{\partial \omega}{\partial \Delta t} \cdot \frac{\Delta t}{\omega} = \frac{-2\Delta t\omega}{2\Delta t\omega - \sin(2\Delta t\omega)} \quad (7-54)$$

and for a relative change in the network capacitance, from (7-40)

$$\frac{\partial \omega}{\partial C} \cdot \frac{C}{\omega} = \frac{\sin(2\Delta t\omega)}{2\Delta t\omega - \sin(2\Delta t\omega)} \quad (7-55)$$

The relative sensitivity of the voltage for a relative disturbance in the load is from (7-28):

$$\frac{\partial U_v}{\partial G} \cdot \frac{G}{U_v} = -\left(1 - \frac{\Delta t\omega(1 - \cos(2\Delta t\omega))}{2\Delta t\omega - \sin(2\Delta t\omega)}\right) \quad (7-56)$$



for a relative change in the firing delay time, from (7-45)

$$\frac{\partial U_v}{\partial C} \cdot \frac{C}{U_v} = -\frac{\Delta t \omega (1 - \cos(2\Delta t \omega))}{2\Delta t \omega - \sin(2\Delta t \omega)} \quad (7-57)$$

and for a relative change in the network capacitance, from (7-51)

$$\frac{\partial U_v}{\partial \Delta t} \cdot \frac{\Delta t}{U_v} = \frac{\Delta t \omega (1 - \cos(2\Delta t \omega))}{2\Delta t \omega - \sin(2\Delta t \omega)} \quad (7-58)$$

First it must be noted that all the relative sensitivities are functions only of the product of firing delay time and frequency, in other words, functions of firing angle  $\alpha$ . This means that the relative sensitivities for small disturbances from a working point will only depend on the firing angle in that point.

It appears from (7-53) and (7-55) that the frequency has the same relative sensitivity to a change in load as to a change in network capacitance, but with opposite sign.

$$\frac{\partial \omega}{\partial G} \cdot \frac{G}{\omega} = -\frac{\partial \omega}{\partial C} \cdot \frac{C}{\omega} \quad (7-59)$$

It also appears that the sensitivity of the voltage to a change in capacitance (7-57) is the same as the sensitivity to a change in firing delay time (7-58) but with opposite sign.

$$\frac{\partial U_v}{\partial C} \cdot \frac{C}{U_v} = -\frac{\partial U_v}{\partial \Delta t} \cdot \frac{\Delta t}{U_v} \quad (7-60)$$

The relative sensitivity of frequency and voltage for a disturbance in load, represented with the conductance, as a function of the firing angle  $\alpha$  is shown in Figure 7-17.

From (7-60) it appears that the voltage has the same magnitude of sensitivity for a relative change in capacitance as for a relative change in firing delay time. This indicates that there is no preference with regard to whether delay time or capacitance should be used for voltage control. The relative sensitivity of the voltage with regard to change in firing delay time and network capacitance as a function of the firing angle  $\alpha$  is shown in Figure 7-18.

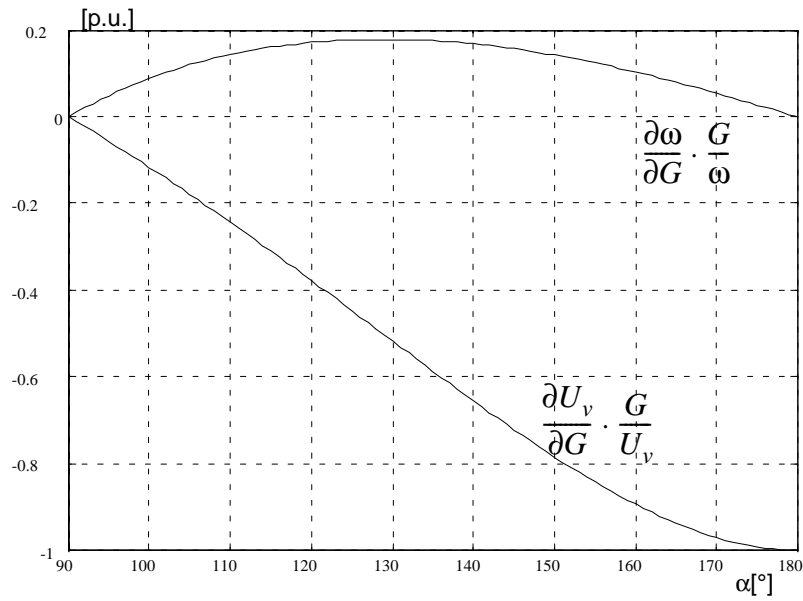


Figure 7-17 Relative sensitivity of the frequency (upper curve) and the voltage (lower curve), with regard to load conductance, as functions of the firing angle  $\alpha$ .

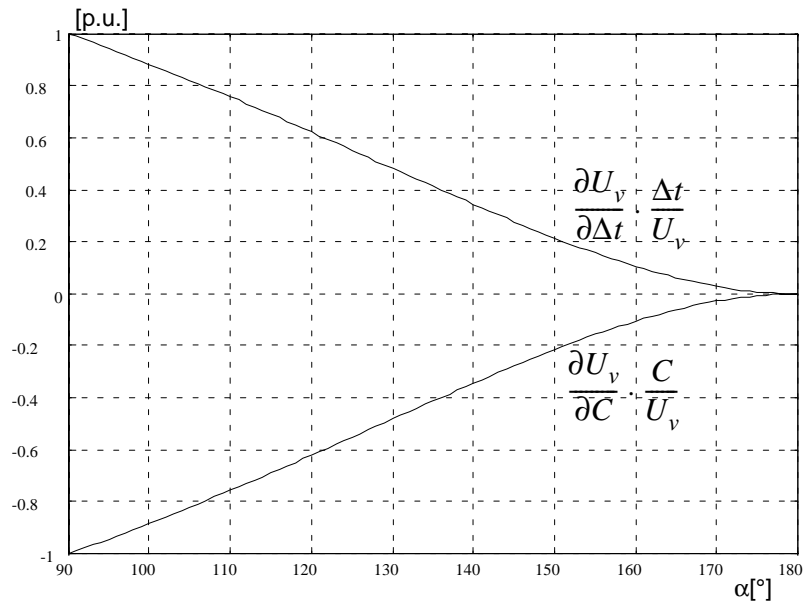


Figure 7-18 Relative sensitivity of the voltage with regard to the firing delay (upper curve) and the capacitance (lower curve), as functions of the firing angle  $\alpha$ .

Then it remains to decide which is the most sensitive of (7-54) and (7-55), that is which has the greater absolute value. The denominator is the same, it remains to compare the numerators. In inverter operation we have

$$\frac{\pi}{2} \leq \omega\Delta t \leq \pi \quad (7-61)$$

and consequently

$$\pi \leq 2\omega\Delta t \leq 2\pi \quad (7-62)$$

while

$$|\sin(2\omega\Delta t)| \leq 1 \quad (7-63)$$

This shows that the frequency will be more sensitive to a change in the firing delay angle of an inverter than a change in system capacitance. Therefore the firing delay angle is selected to control the frequency. This leaves the capacitance to control the voltage. The relative sensitivity of the frequency with regard to change in firing delay time and network capacitance as a function of the firing angle  $\alpha$  is shown in Figure 7-19. It is assumed that the required control speed can be achieved by the available control mechanisms.

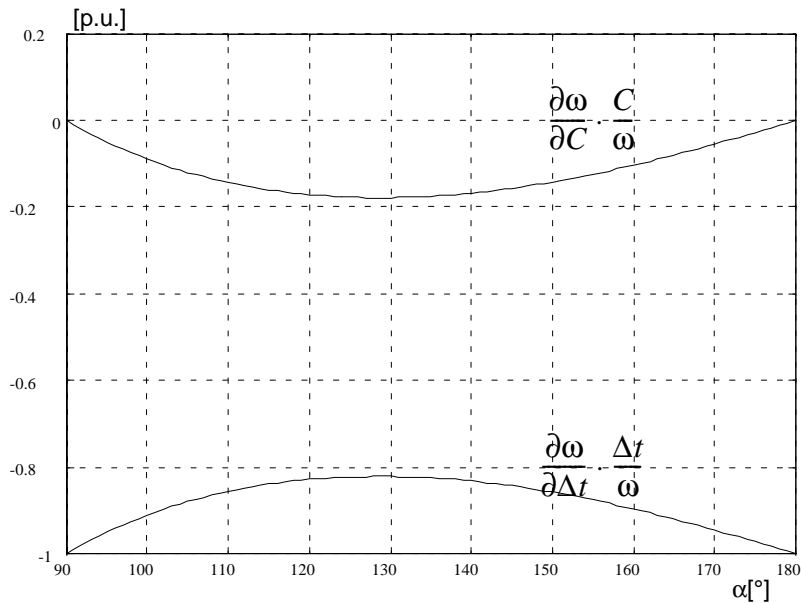


Figure 7-19 Relative sensitivity of the frequency with regard to the capacitance (upper curve) and the firing delay (lower curve), as functions of the firing angle  $\alpha$ .

### 7. 2. 6 Example, small signal sensitivity

Considering the base case inverter previously described, we want to find the sensitivity of frequency and voltage for a small change in the active load and for small variations in firing delay time and capacitor size at different loads. A realistic way of operating the transmission system is to keep the extinction angle  $\gamma$  constant by slow regulation of DC current. With constant  $\gamma$  and disregarding commutation, we also have constant  $\alpha$ , and the relative sensitivities remain constant. The absolute sensitivities, however, depend partly on the load situation, which decides the size of G and C. The relationships are fairly simple, however. Assuming voltage, frequency and firing delay angle to be controlled at nominal values, we get the following expressions for  $G_0$  and  $C_0$ .

$$G_0 = \frac{P_0}{3} / \left( \frac{U_{vN}}{\sqrt{3}} \right)^2 = \frac{P_0}{U_{vN}^2} \quad (7-64)$$

$$\frac{1}{\omega_N C_0} = \frac{U_{v,N}^2}{Q_0} = \frac{U_{vN}^2}{P_0 \cdot \tan \gamma_N} \quad (7-65)$$

$$C_0 = \frac{P_0 \cdot \tan \gamma_N}{\omega_N \cdot U_{vN}^2} \quad (7-66)$$

An extinction angle  $\gamma = 20^\circ$  is equivalent to a firing angle  $\alpha_N = 160^\circ = 2.793[\text{rad}]$ . Inserting the numerical values into (7-64) and (7-66) gives:

$$G_0 = \frac{P_0}{14400 \times 10^6} \quad (7-67)$$

$$C_0 = \frac{P_0 \cdot \tan 20^\circ}{100\pi \cdot 14400 \times 10^6} = P_0 \cdot 8.05 \times 10^{-14} \quad (7-68)$$

We get for the sensitivity of frequency for a disturbance in the load, from (7-23):

$$\frac{\partial \omega}{\partial G} = \frac{-\sin(2\alpha_N)}{2\alpha_N - \sin(2\alpha_N)} \cdot \frac{\omega_N}{G_0} = \frac{4.669 \times 10^{11}}{P_0} \left[ \frac{\text{rad/s}}{\text{mho}} \right] \quad (7-69)$$

for a change in the firing delay time, from (7-35):

$$\frac{\partial \omega}{\partial \Delta t} = \frac{-2\alpha_N}{2\alpha_N - \sin(2\alpha_N)} \cdot \frac{\omega_N}{\Delta t_N} = -3.17 \times 10^4 \left[ \frac{\text{rad/s}}{\text{s}} \right] \quad (7-70)$$

and for a change in the network capacitance, from (7-40):

$$\frac{\partial \omega}{\partial C} = \frac{\sin(2\alpha_N)}{2\alpha_N - \sin(2\alpha_N)} \cdot \frac{\omega_N}{C_0} = \frac{-4.03 \times 10^{14}}{P_0} \left[ \frac{\text{rad/s}}{\text{F}} \right] \quad (7-71)$$

We get for the sensitivity of the voltage for a disturbance in the load, from (7-28):

$$\frac{\partial U_v}{\partial G} = - \left( 1 - \frac{\alpha_N(1 - \cos(2\alpha_N))}{2\alpha_N - \sin(2\alpha_N)} \right) \cdot \frac{U_{vN}}{G_0} = \frac{-1.546 \times 10^{15}}{P_0} \left[ \frac{\text{V}}{\text{mho}} \right] \quad (7-72)$$

for a change in the network capacitance, from (7-45):

$$\frac{\partial U_v}{\partial C} = - \frac{\alpha_N(1 - \cos(2\alpha_N))}{2\alpha_N - \sin(2\alpha_N)} \cdot \frac{U_{vN}}{C_0} = \frac{-1.56 \times 10^{17}}{P_0} [\text{V/F}] \quad (7-73)$$

and for a change in the firing delay time, from (7-51):

$$\frac{\partial U_v}{\partial \Delta t} = \frac{\alpha_N(1 - \cos(2\alpha_N))}{2\alpha_N - \sin(2\alpha_N)} \cdot \frac{U_{vN}}{\Delta t_N} = 1.42 \times 10^6 [\text{V/s}] \quad (7-74)$$

Equation (7-69) is shown graphically in Figure 7-20, and (7-72) is shown graphically in Figure 7-21. Equations (7-71) and (7-73) are shown graphically in Figure 7-22. Equations (7-70) and (7-74) are independent of the load.

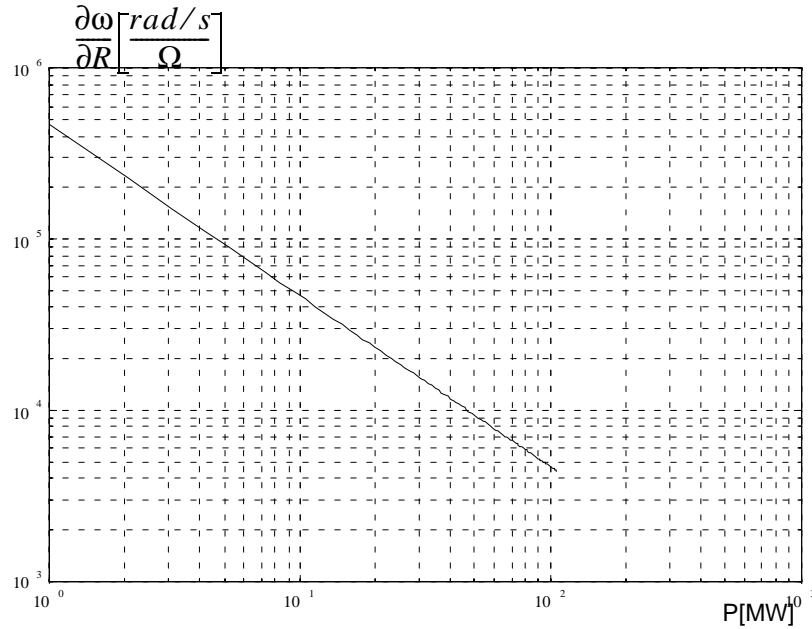


Figure 7-20 Sensitivity of angular frequency for variations in load conductance as a function of load. Voltage, frequency and firing angle at nominal values.

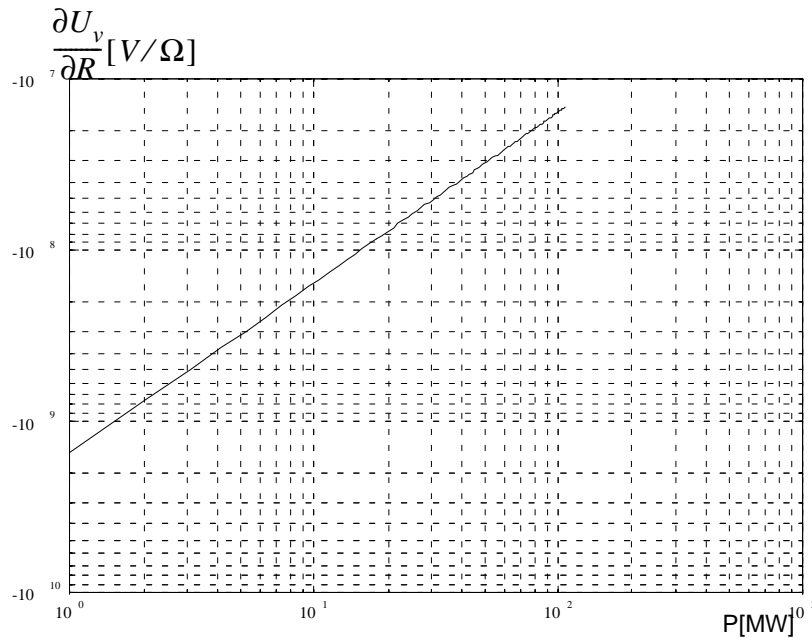


Figure 7-21 Sensitivity of line voltage for variations in load conductance as a function of load. Voltage, frequency and firing angle at nominal values.

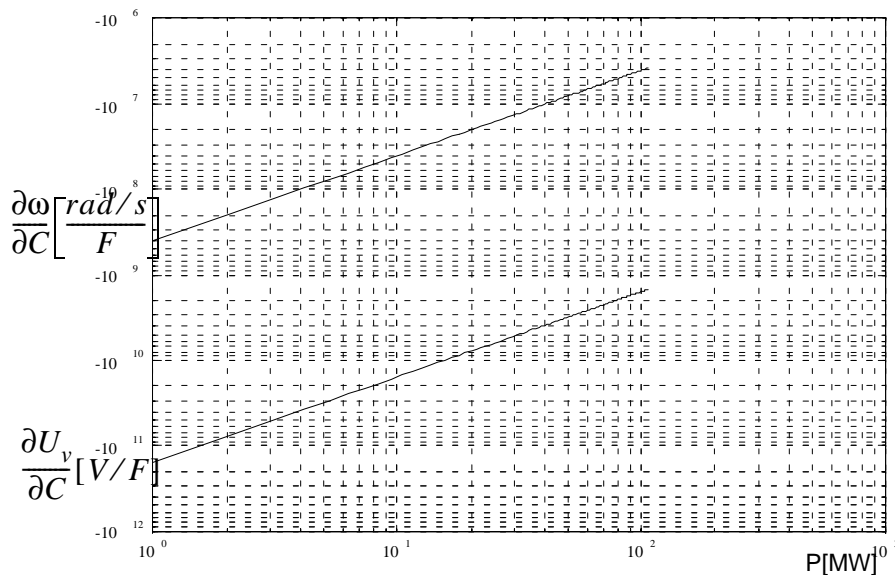


Figure 7-22 Sensitivity of line voltage and angular frequency for variations in network capacitance as functions of load. Voltage, frequency and firing angle at nominal values.

This example shows that if the voltage, frequency and firing delay time (firing angle) are kept at nominal values, the sensitivities of frequency and voltage with regard to the firing delay time are independent of the load conditions. The sensitivities with regard to change in load (conductance) increase in absolute values with increasing loads and the sensitivities to change in capacitance decrease with increasing loads. The consequence of this is that the system initially responds more for a given absolute disturbance in load at full load, and has less power to force the controlled parameters back, resulting in a slower responding system at full load than at low load. On the other hand, the higher sensitivities for variation in control variables can make the system unstable at low load, for the same controller parameters that give a stable system at full load. Fortunately, modern control technology is able to handle such problems. Keywords for this can be adaptive controllers and parameter estimation. However, these kinds of sophisticated controllers are outside the scope of this thesis.

In the next section it will be investigated if a simple controller can be found at all that can give the system any stability.

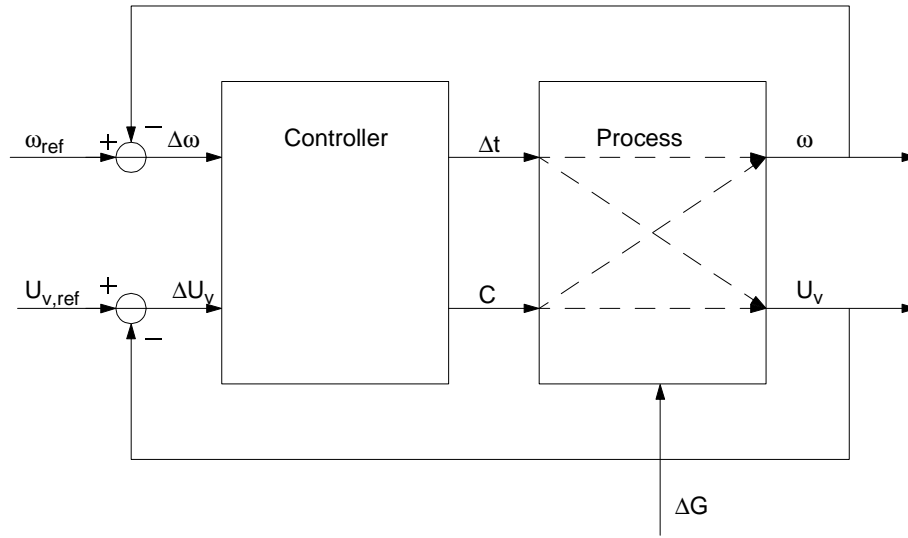


Figure 7-23 Basic concept of voltage and frequency controller.

## 7.3 RC NETWORKS FED BY CONTROLLED INVERTER WITH CONTROLLABLE CAPACITANCE

### 7.3.1 Control theory

In the previous section we found the response of the controlled parameters, voltage and frequency, to variations in the controllable parameters, firing delay time and network capacitance, in a system consisting of an inverter feeding into an RC parallel load. Having found the sensitivities, we now have the foundation to design a controller to keep voltage and frequency constant. The basic system is shown in Figure 7-23. The process to be controlled is the simple model shown in Figure 7-1. An inverter is supplied by a constant DC current source and feeds into an RC load, where the capacitance  $C$  is controllable. Presently, we are not taking a stand on how this capacitance is made controllable, we simply assume that the capacitance is directly and instantaneously controllable. Physically, the closest resemblance will probably be some sort of Static Var Compensator.

The sensitivity analysis has told us that there is a cross-coupling between the inputs and outputs in the process. A change in the firing delay time or the capacitance will lead to a change both in frequency and voltage. The system



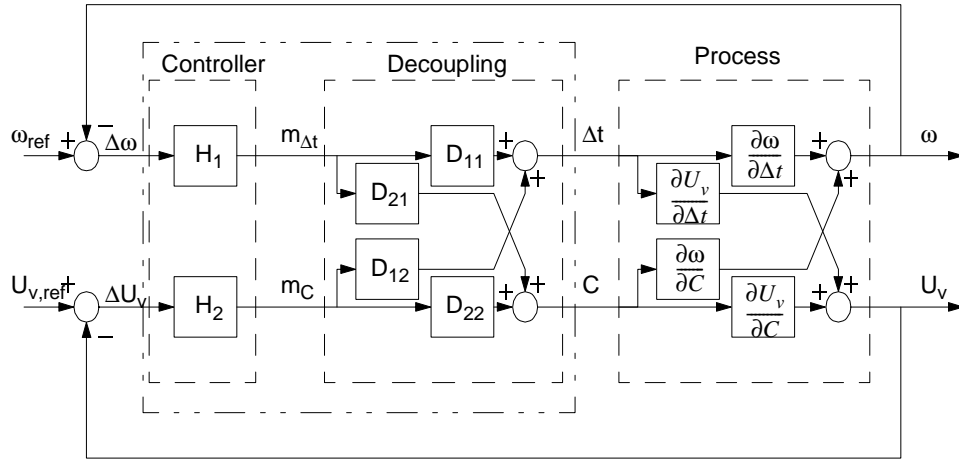


Figure 7-24 Process with decoupling and controller, disregarding process disturbances. Small signal analysis.

is multivariable as well as non-linear. The simplest way to solve the problem is to linearize at a working point. Then it becomes a classical decoupling problem from elementary control theory [37]. The solution is to introduce a decoupling between the proper controllers and the process, in such a way that when one of the controllers acts on an error, the decoupling counteracts the influence on the other variables. In terms of control theory it can be expressed as: The transfer matrix of the process with decoupling is diagonalized. The resulting system is shown in Figure 7-24. Here the unspecified controller in Figure 7-23 is split in two parts, the frequency and voltage controllers and the decoupling. They are connected by the auxiliary variables  $m_{\Delta t}$  and  $m_C$ .

In terms of matrix algebra we can designate the linearized transfer matrix of the process as  $\mathbf{A}$ . Then we have the following expression for  $\mathbf{A}$ :

$$\mathbf{A} = \begin{bmatrix} \frac{\partial \omega}{\partial \Delta t} & \frac{\partial \omega}{\partial C} \\ \frac{\partial U_v}{\partial \Delta t} & \frac{\partial U_v}{\partial C} \end{bmatrix} \quad (7-75)$$

The decoupling system is characterized with the decoupling matrix  $\mathbf{D}$ :

$$\mathbf{D} = \begin{bmatrix} D_{11} & D_{12} \\ D_{21} & D_{22} \end{bmatrix} \quad (7-76)$$

We search for a decoupling matrix  $D$  such that the resulting transfer function is a diagonal matrix  $A_d$ .

$$AD = A_d = \begin{bmatrix} A_{d\omega} & 0 \\ 0 & A_{dU_v} \end{bmatrix} \quad (7-77)$$

If the original transfer matrix  $A$  can be inverted we find the decoupling matrix  $D$  by:

$$D = A^{-1}A_d \quad (7-78)$$

In the case of a small signal analysis around a working point the transfer matrix  $A$  is reduced to consist of constants. The decoupled transfer function matrix  $A_d$  can be chosen fairly freely, one selection is to keep the sensitivities on the main diagonal unchanged:

$$A_d = \begin{bmatrix} A_{d\omega} & 0 \\ 0 & A_{dU_v} \end{bmatrix} = \begin{bmatrix} \frac{\partial\omega}{\partial\Delta t} & 0 \\ 0 & \frac{\partial U_v}{\partial C} \end{bmatrix} \quad (7-79)$$

Then the decoupling matrix  $D$  can be found from (7-78). However, one must be aware that this does not imply that the auxiliary variables  $m_{\Delta t}$  and  $m_C$ , which are the output of the controllers, become equal to the physical variables  $\Delta t$  and  $C$ . Vector  $m$  is found by:

$$m = \begin{bmatrix} m_{\Delta t} \\ m_C \end{bmatrix} = D^{-1} \begin{bmatrix} \Delta t \\ C \end{bmatrix} \quad (7-80)$$

The previous development has been done for the small signal case. The theory is not restricted to this, but can be applied for more complicated transfer matrices, consisting of transfer functions, as long as the original transfer function matrix  $A$  is invertible.

Now the control problem has degenerated into the simple problem of dimensioning two individual control loops, as shown in Figure 7-25. As the aim of the thesis is to prove the feasibility and not to optimize the system, the simplest possible controller is selected for the simulations. A proportional (P) controller is not able to achieve zero error. Furthermore this system is

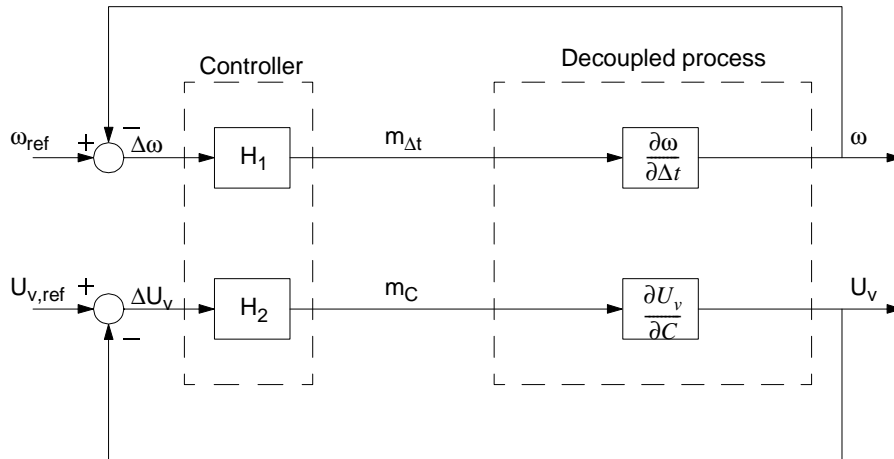


Figure 7-25 Degenerated process after decoupling and disregarding process disturbances. Small signal analysis.

neither linear nor ideally decoupled. A Proportional + Integral (PI) controller may do the job, if the response requirements are not too high. Other, far more complicated controllers can, and in fact should be applied in the case of a real implementation. But it is not the task of this thesis to optimize the controller of this system, and a PI controller is selected for the simulations.

### 7.3.2 Base case example

As stated in Section 4.2.4 and Section 6.3 there are strong requirements on the communication system between any two HVDC converters and yet they have to be designed in a way that allows continued operation in case of communication faults. This is normally done by keeping the reference value for the current fixed when communication is down. Even with communication operating, the delay imposed is in the magnitude of 20 to 30 ms. Furthermore, due to large inductances in the DC transmission, the DC current cannot be controlled fast. Therefore the system has to be designed to operate on constant DC current, and only use the DC current control for optimization purposes. This DC current control should be a fast controller per se, but the current order will vary relatively slow.

The assumption that the DC current is not to be changed during a load shift puts a restriction on the maximum load increase that can be made. If an inverter is operating with an extinction angle  $\gamma_0$  we have from (7-9)

$$I_d \cdot \frac{3\sqrt{2}}{\pi} U_v \cdot \cos(\gamma_0) = U_v^2 G_0 = P_0 \quad (7-81)$$

If the current is kept constant we then have

$$I_d = \frac{P_0}{\frac{3\sqrt{2}}{\pi} U_v \cdot \cos(\gamma_0)} = \frac{P_0 + \Delta P}{\frac{3\sqrt{2}}{\pi} U_v \cdot \cos(\gamma_1)} \quad (7-82)$$

Consequently, it will not be possible to make a larger theoretical load increase from the working point  $P_0$  than

$$\Delta P = \left( \frac{P_0}{\cos\gamma_0} - \frac{P_0}{\cos\gamma_{min}} \right) \cdot \cos\gamma_{min} = \left( \frac{\cos\gamma_{min}}{\cos\gamma_0} - 1 \right) \cdot P_0 \quad (7-83)$$

for any value of  $P_0$ . If a load increase larger than  $\Delta P$  is required, the extinction angle must be increased accordingly before the extra load is connected.

Returning to the base case example, there are four distinct cases to analyse in order to select a controller that will operate under all conditions. To avoid possible numerical problems arising from firing angles too close to  $90^\circ$  we select the four cases as

- Load change from  $0.8P_N$  to  $1P_N$ .  $\gamma = \gamma_N$  after the load change.
- Load change from  $1P_N$  to  $0.8P_N$ .  $\gamma = \gamma_N$  before the load change.
- Load change from  $0.1P_N$  to  $0.3P_N$ .  $\gamma = \gamma_N$  after the load change.
- Load change from  $0.3P_N$  to  $0.1P_N$ .  $\gamma = \gamma_N$  before the load change.

The previously described dimensioning of the control system is strictly speaking only valid for very small load variations, but will be used as a starting point to find useful controller parameters.

The necessary extinction angle before a load increase can be calculated from (7-83):

$$\gamma_0 = \pi - \alpha_0 = \arccos\left(\frac{P_0}{P_0 + \Delta P} \cos \gamma_1\right) \quad (7-84)$$

From (7-8) we calculate the firing delay time:

$$\Delta t_0 = \frac{\alpha_0 \cdot \tau}{2\pi} \quad (7-85)$$

From the power equation we find the conductance before the disturbance:

$$G_0 = \frac{P_0}{U_{vN}^2} \quad (7-86)$$

and the change in conductance for a load increase of  $\Delta P$ :

$$\Delta G = \frac{P_1}{U_{vN}^2} - \frac{P_0}{U_{vN}^2} \quad (7-87)$$

The DC current, which is to remain unchanged during the simulations, is found by rewriting the right-hand half of (7-9):

$$I_{d0} = -\frac{\pi}{3\sqrt{2}} \cdot \frac{P_0}{U_{vN} \cdot \cos(\alpha_0)} \quad (7-88)$$

The network capacitance before the disturbance is found from (7-13)

$$C_0 = -\frac{G}{\omega} \tan(\alpha_0) \quad (7-89)$$

Inserting numerical values into these equations and equations (7-69) to (7-74) for the sensitivities, gives the results presented in Table 7-2. Here the angular frequency  $\omega$  in radians/s is replaced by frequency  $f$  in Hz. It must be noted that the wide range of the exponents in Table 7-2 is due to the absolute magnitude of the figures involved, like kilovolts being controlled by  $\mu$ Farads etc. Thus 10 to the power of -3 is just as significant as 10 to the power of +9.

**Table 7-2 Initial conditions and sensitivities for different load shift cases.**

	(0.8+0.2)P <sub>N</sub>	(1-0.2)P <sub>N</sub>	(0.1+0.2)P <sub>N</sub>	(0.3-0.2)P <sub>N</sub>
γ <sub>0</sub> [°]	41.3	20.0	71.7	20.0
Δt <sub>0</sub> [ms]	7.71	8.89	6.01	8.89
I <sub>d0</sub> [A]	656.7	656.7	197.0	197.0
G <sub>0</sub> [mho]	5.56x10 <sup>-3</sup>	6.94x10 <sup>-3</sup>	0.69x10 <sup>-3</sup>	2.08x10 <sup>-3</sup>
ΔG [mho]	1.39x10 <sup>-3</sup>	-1.39x10 <sup>-3</sup>	1.39x10 <sup>-3</sup>	-1.39x10 <sup>-3</sup>
C <sub>0</sub> [μF]	15.51	8.05	6.70	2.41
∂f/∂Δt[Hz/s]	-5.38x10 <sup>3</sup>	-5.04x10 <sup>3</sup>	-7.18x10 <sup>3</sup>	-5.04x10 <sup>3</sup>
∂f/∂C[Hz/F]	-5.48x10 <sup>5</sup>	-6.41x10 <sup>5</sup>	-10.1x10 <sup>5</sup>	-21.4x10 <sup>5</sup>
∂f/∂G[Hz/mho]	1.53x10 <sup>3</sup>	0.74x10 <sup>3</sup>	9.79x10 <sup>3</sup>	2.48x10 <sup>3</sup>
∂U <sub>v</sub> /∂Δt[V/s]	5.62x10 <sup>6</sup>	1.42x10 <sup>6</sup>	15.55x10 <sup>6</sup>	1.42x10 <sup>6</sup>
∂U <sub>v</sub> /∂C[V/F]	-2.79x10 <sup>9</sup>	-1.56x10 <sup>9</sup>	-13.95x10 <sup>9</sup>	-5.21x10 <sup>9</sup>
∂U <sub>v</sub> /∂G[Hz/mho]	-1.38x10 <sup>7</sup>	-1.55x10 <sup>7</sup>	-3.82x10 <sup>7</sup>	-5.16x10 <sup>7</sup>

Table 7-2 shows that on the whole, the load increase from low load is the most sensitive situation. Therefore the case with 0.2P<sub>N</sub> load increase from initially 0.1P<sub>N</sub> is selected as the dimensioning case. The small signal transfer matrix at 0.1P<sub>N</sub>, nominal voltage and frequency and firing delay angle prepared for a load increase of 0.2P<sub>N</sub> is:

$$\mathbf{A} = \begin{bmatrix} \frac{\partial f}{\partial \Delta t} & \frac{\partial f}{\partial C} \\ \frac{\partial U_v}{\partial \Delta t} & \frac{\partial U_v}{\partial C} \end{bmatrix} = \begin{bmatrix} -7.18 \times 10^3 & -1.01 \times 10^6 \\ 15.55 \times 10^6 & -13.95 \times 10^9 \end{bmatrix} \quad (7-90)$$

If we wish to keep the diagonal elements constant during decoupling we have the required decoupled transfer matrix:

$$\mathbf{A}_d = \begin{bmatrix} \frac{\partial f}{\partial \Delta t} & 0 \\ 0 & \frac{\partial U_v}{\partial C} \end{bmatrix} = \begin{bmatrix} -7.18 \times 10^3 & 0 \\ 0 & -13.95 \times 10^9 \end{bmatrix} \quad (7-91)$$

and we find the decoupling matrix:

$$\mathbf{D} = \mathbf{A}^{-1} \mathbf{A}_d = \begin{bmatrix} 0.864 & -122.1 \\ 9.63 \times 10^{-4} & 0.864 \end{bmatrix} \quad (7-92)$$

When the decoupling system has been fixed it remains to determine the controller parameters, gain and integration time. If we keep the small signal analysis, the decoupled process has the simple transfer functions:

$$A_{df} = -7.18 \times 10^3 \quad (7-93)$$

and

$$A_{dU_v} = -13.95 \times 10^9 \quad (7-94)$$

These are pure proportional processes with a phase shift of zero. Together with a PI controller the phase shift of the controlled process will be  $-90^\circ$  at low frequencies increasing to zero at high frequencies. Thus there should be no stability problem with the phase margin.

It is known from the earlier simulations on the KREAN model that both voltage and frequency measurement contain a certain amount of 6th harmonic ripple. As these simulations are not aimed at the optimization of the control system, the speed requirements are not important and in the first try the controller will be designed to give the closed loop a damping of 50 % or -6 dB at the ripple frequency. The ripple frequency is chosen as breakpoint to keep the gain as high as possible at lower frequencies. Bearing in mind that the difference between the asymptotic approximation and the exact gain is 3dB in a Bode diagram, we need a gain in the frequency controller of

$$K_f = \frac{1}{-4.51 \times 10^4} \cdot \frac{0.5}{\sqrt{2}} = -4.94 \times 10^{-5} \quad (7-95)$$

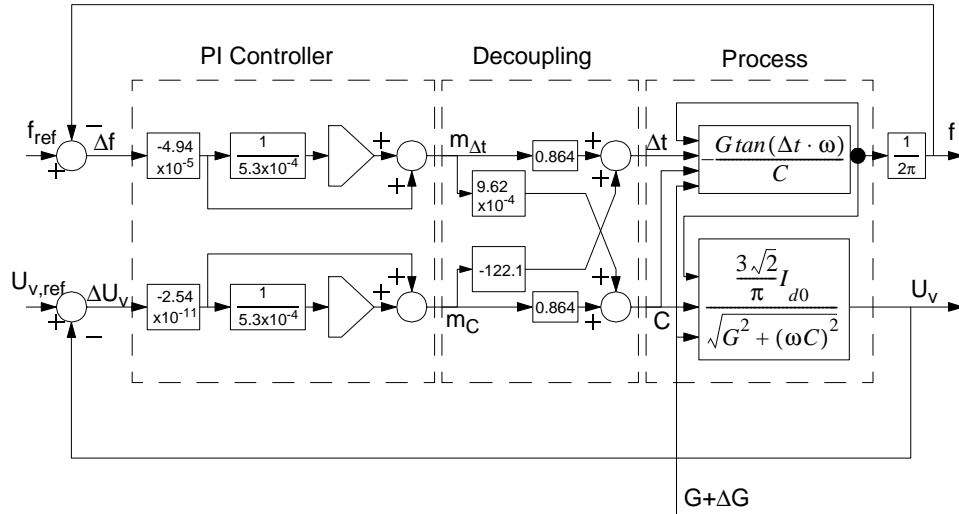


Figure 7-26 Process with decoupling and PI controller, initial values of the parameters.

and a gain in the capacitance controller of

$$K_{U_v} = \frac{1}{-13.95 \times 10^9} \cdot \frac{0.5}{\sqrt{2}} = -2.54 \times 10^{-11} \quad (7-96)$$

The time constant for both controllers is the inverse of the breakpoint angular frequency:

$$T_f = T_{U_v} = \frac{1}{300 \cdot 2\pi} = 5.3 \times 10^{-4} \quad (7-97)$$

The controlled system now becomes like Figure 7-26. This system has been modelled in KREAN to test the found controller parameters.

From the initial values of the firing delay time and capacitance we can calculate the initial values of the auxiliary variables  $m_{\Delta t}$  and  $m_C$ , which are the initial outputs of the integrators. The auxiliary variables are found by (7-80) and the results for the different test cases are listed in Table 7-3:

The parameters for a load shift from  $0.1P_N$  to  $0.3P_N$  were entered into the KREAN model and simulated, without entering any extra disturbances. As in previous KREAN simulations, the system is started by an auxiliary three-phase 50 Hz voltage source, which is disconnected after 20 ms. The system showed to be unstable with heavy oscillations with a frequency of approxi-



**Table 7-3 Initial values of controller outputs for different load shift cases.**

	$(0.8+0.2)P_N$	$(1-0.2)P_N$	$(0.1+0.2)P_N$	$(0.3-0.2)P_N$
$m_{\Delta t}$	$9.90 \times 10^{-3}$	$1.00 \times 10^{-2}$	$6.96 \times 10^{-3}$	$9.23 \times 10^{-3}$
$m_C$	$6.92 \times 10^{-6}$	$-1.86 \times 10^{-6}$	0	$-7.49 \times 10^{-6}$

mately 50 Hz. As the two loops of the system are dimensioned for the same total gain and breakpoint frequency, they have the same total gain at 50 Hz, consequently:

$$H_{50} = A_{df} \cdot K_f \cdot \left| \frac{1 + j\omega T_f}{j\omega T_f} \right| = 2.24 = 7dB \quad (7-98)$$

which confirms that any tendency towards natural oscillation with this frequency will be amplified. To remedy this the gain of the controller is reduced by shifting the breakpoint frequency from 300 Hz to 50 Hz, giving a damping of 6dB at this frequency. These parameters give stable conditions when each controller is tested individually, but with both controllers active, the system still oscillates. Shifting the breakpoint frequency further down to 25 Hz, which only gives about 2.7dB extra damping, but increases the phase margin by about  $30^\circ$ , seems to give the system sufficient damping of the 50 Hz oscillations. Testing the system with the required load shift of  $0.2P_N$ , however, proves that the damping is still too weak when the amplitude increases. To avoid slowing the response too much, the additional damping is done by reduction of the proportional gain by 12dB or 75%, thereby shifting the breakpoint frequency back to 100 Hz. This gives the system sufficient damping after a load shift of  $0.2P_N$ . The gain in the frequency controller is now:

$$K_f = -4.94 \times 10^{-5} \cdot 0.25 = -1.24 \times 10^{-5} \quad (7-99)$$

and a gain in the capacitance controller of

$$K_{U_v} = -2.54 \times 10^{-11} \cdot 0.25 = -6.35 \times 10^{-12} \quad (7-100)$$

The time constant for both controllers is the inverse of the breakpoint angular frequency:

$$T_f = T_{U_v} = \frac{1}{100 \cdot 2\pi} = 1.59 \times 10^{-3} \quad (7-101)$$

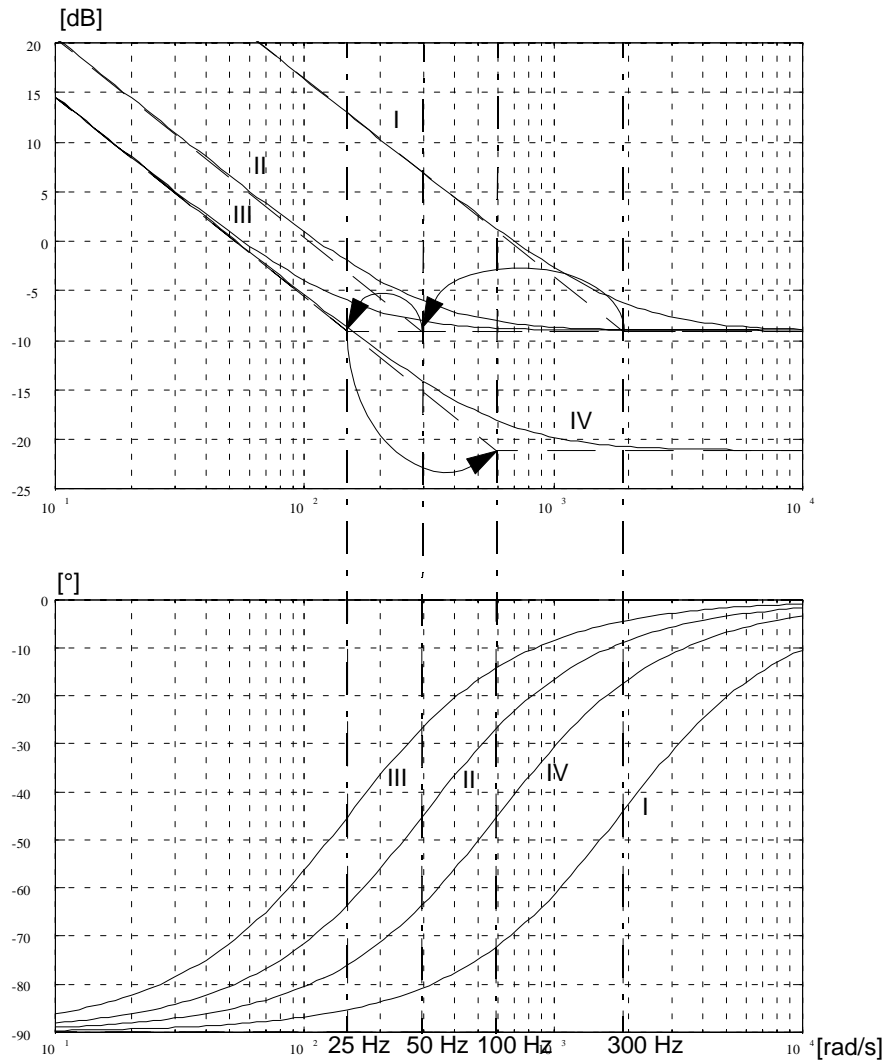


Figure 7-27 Bode plot of the small signal transfer function of the decoupled frequency control loop at  $0.1P_N$  load. I) Initial parameters. II) After moving breakpoint to 50 Hz. III) After moving breakpoint to 25 Hz. IV) After moving breakpoint to 100 Hz and reducing proportional gain. The voltage control loop has an identical Bode plot.

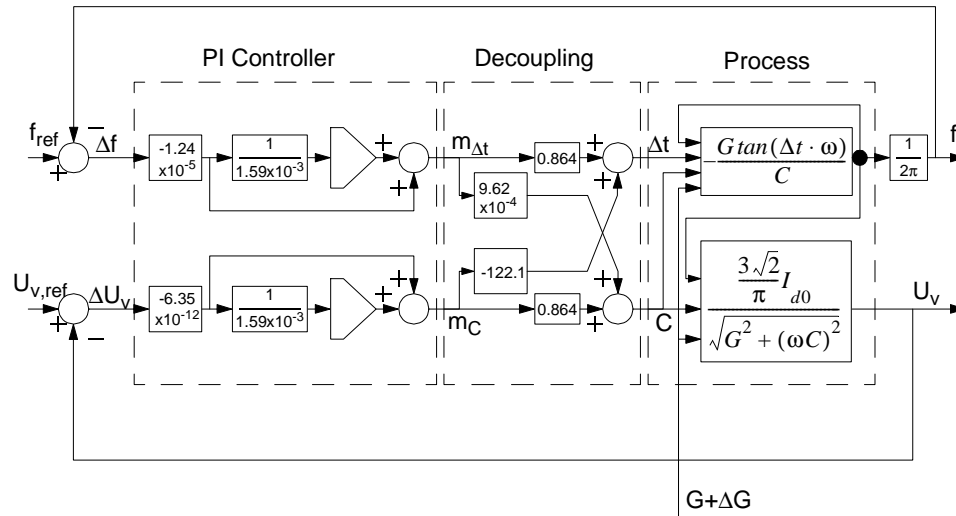


Figure 7-28 Process with decoupling and PI controller, final values of the parameters.

The Bode diagrams for the various parameter settings are shown in Figure 7-27. The system with the final set of parameters is shown in Figure 7-28

The result of the simulations of a load shift from  $0.1P_N$  to  $0.3P_N$  and back is shown in Figure 7-29. The figure shows the frequency, measured as the frequency output in Hz from the phase locked loop as the upper curve. The second curve shows the AC voltage in kV, rectified in a 6-pulse bridge and filtered through a low pass filter with breakpoint frequency at 50 Hz. The measured value is scaled to represent the RMS value at pure sinusoidal curve-form. The third curve shows the output from the frequency PI controller  $m_f$  (6), together with the actual firing time delay  $\Delta t$  (1) in ms. The last curve shows the output from the capacitance PI controller  $m_C$  (12), together with the actual capacitance  $C$  (3) in  $\mu\text{F}$ . As in the previous simulations, the system is started up by means of a three-phase sinusoidal voltage of nominal ratings for 20 ms. Then the system is left until time  $t=0.15$  s in order to damp initial imbalance. At this time the resistance is reduced, corresponding to a load increase from  $0.1P_N$  to  $0.3P_N$ . At time  $t\approx 0.3$  s, the frequency has stabilized at a nominal value, the voltage needs some more time. At time  $t=0.4$  s, the resistance is increased again, corresponding to a load decrease from  $0.3P_N$  back to  $0.1P_N$ . Now the oscillations at 50 Hz are quite pronounced, but rapidly damped. Again the frequency is controlled faster than the voltage, and at time  $t=0.8$  s the situation is stabilized again. The reason for the 50 Hz oscillations is a DC component in the phase voltages that need some time to be damped.

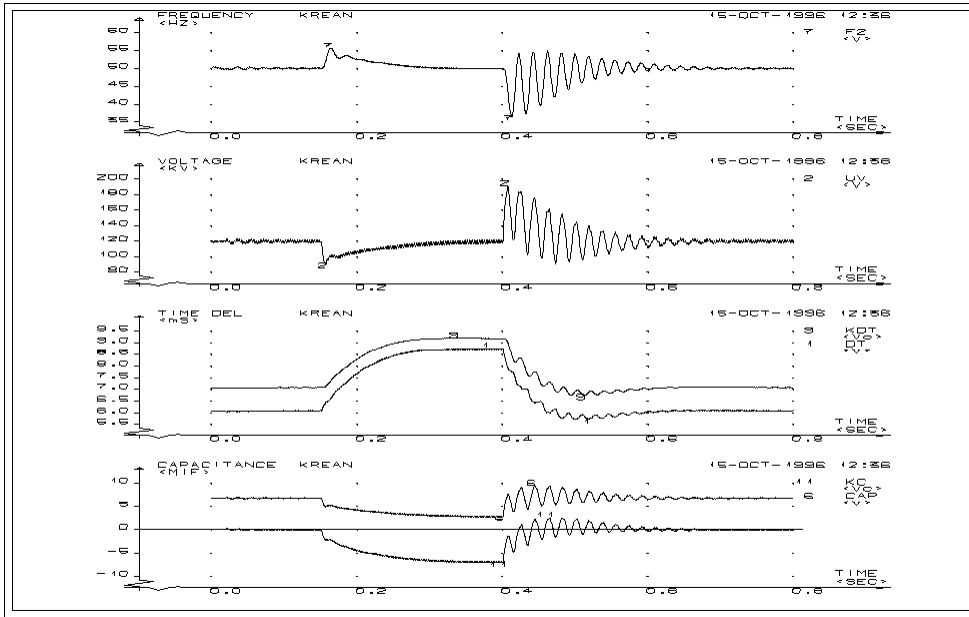


Figure 7-29 Result of KREAN simulation of process in Figure 7-26 with final set of controller parameters. Load shift from  $0.1P_N$  to  $0.3P_N$  at  $t=0.15$  s and back to  $0.1P_N$  at  $t=0.4$  s.

The peak voltage at load rejection reaches 222 kV after filtering. The real line voltages are shown in Figure 7-30, where the unsymmetry can clearly be seen. The peak amplitude values are 274 kV for  $U_{RS}$ , 344 kV for  $U_{ST}$  and 288 kV for  $U_{TR}$  in this case. The peak value is dependent on which instant of the period the switching takes place, and can theoretically reach as high as:

$$\hat{U}_v = 1.5 \cdot I_d \cdot R = 1.5 \cdot 197 \cdot 1440 = 425.5 [kV] \quad (7-102)$$

in this particular case. The oscillations in frequency are also caused by the unsymmetry of the voltages, due to the method of frequency measuring. The frequency seems to oscillate between 37 Hz and 55 Hz, but it is a question if this can be regarded as oscillations at all, as they take place within one period of the measured voltage.

Finally the found controller parameters and decoupling are tested by KREAN simulations for the case of a load shift from  $0.8P_N$  to  $P_N$  and back. The result is shown in Figure 7-31. As can be expected, due to less sensitivity, the system is much calmer, but especially the voltage is also slower in getting back to the rated value. The frequency stays between 48.5 Hz and 51.5 Hz and the voltage stays between 105 kV and 140 kV. It is to be noted that due to the slower response, the load reduction had to be delayed from  $t=0.4$  s to  $t=0.5$  s.

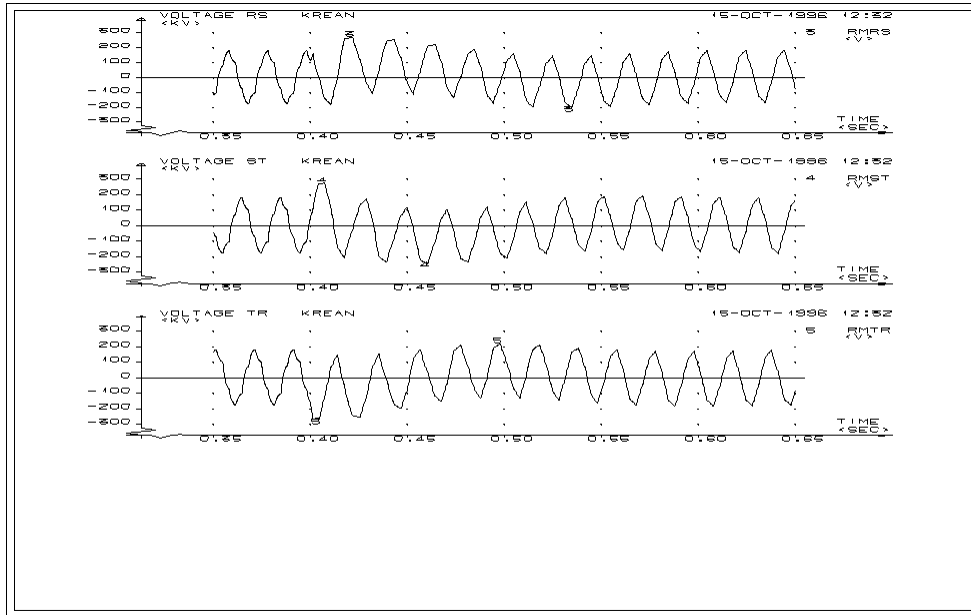


Figure 7-30 Result of KREAN simulation of process in Figure 7-26 with final set of controller parameters. Line voltages at load shift from  $0.3P_N$  to  $0.1P_N$  at  $t=0.4$  s.

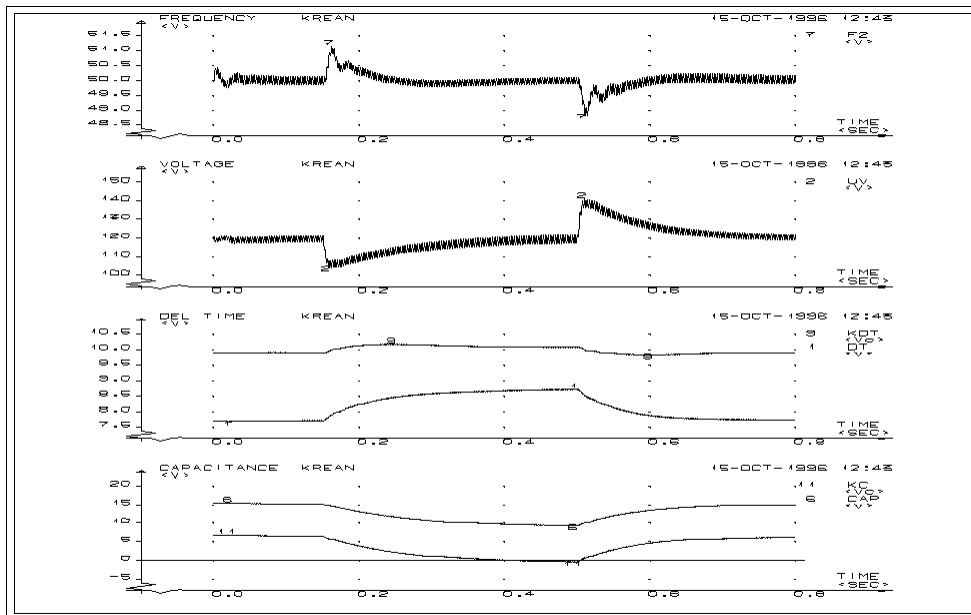


Figure 7-31 Result of KREAN simulation of process in Figure 7-26 with final set of controller parameters. Load shift from  $0.8P_N$  to  $P_N$  at  $t=0.15$  s and back to  $0.8P_N$  at  $t=0.4$  s.

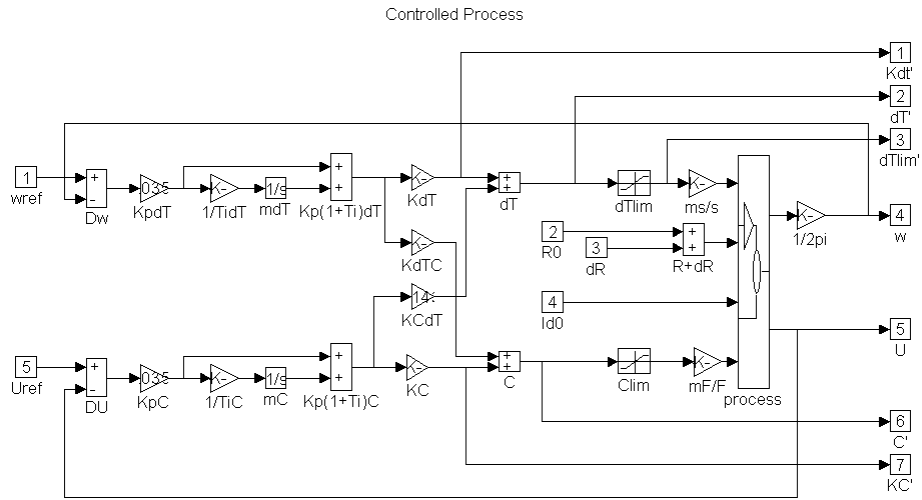


Figure 7-32 Simulink model of process in Figure 7-26.

The same system has been modelled in Matlab/Simulink, with a model which is based on the equations found in the beginning of this chapter. This model is based upon RMS-value calculations. That means that it simulates the enveloping curve of the voltage, rather than the instantaneous values. The Simulink main model is shown in Figure 7-32. The simulations will be carried out for the same two cases that have been done in KREAN. The results of the simulations, compared to the KREAN simulations are presented in the following figures.

Figure 7-33 shows the frequency. As can be expected, the idealized Simulink simulation is much smoother and does not have the 50 Hz oscillations. This is natural, as the model does not make any allowance for DC components. Furthermore, Simulink reacts instantaneously, whereas KREAN has a certain delay. This is basically due to the KREAN measurement being based on the output from the phase locked loop with its built-in controllers and filters. This has been disregarded in the Simulink model. But basically the two curves are in good accordance.

Figure 7-34 shows the voltages from KREAN and Simulink simulations. As Figure 7-33 and Figure 7-34 shows the controlled values, it is no wonder that they are equal in the stationary parts, but transiently they also follow each other well, when disregarding the oscillations due to the DC component.

Figure 7-35 shows the output of the frequency controller, the auxiliary variable  $m_{\Delta t}$ , and the actual firing delay time  $\Delta t$ . The difference between the two is the contribution from the voltage controller, due to the decoupling. The difference between Simulink and KREAN is not great, disregarding the 50 Hz

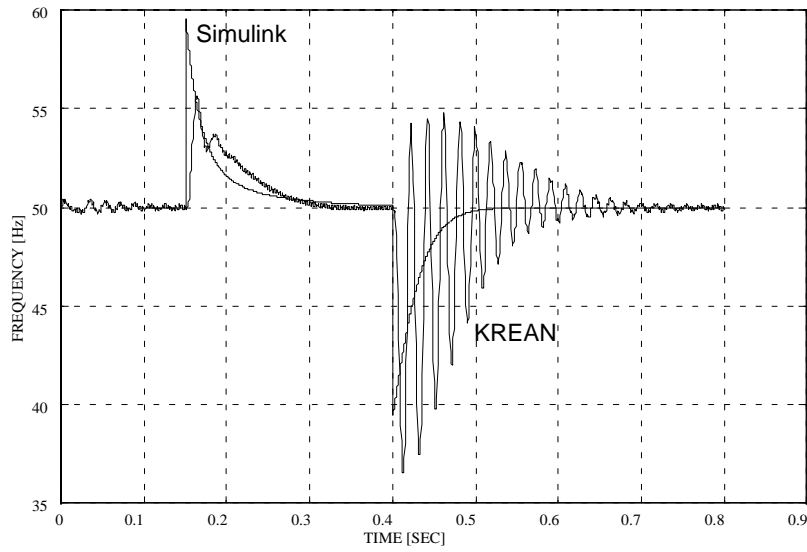


Figure 7-33 Frequency as result of Simulink simulation of process in Figure 7-26 for load shift from  $0.1P_N$  to  $0.3P_N$  and back to  $0.1P_N$ , compared to the result of KREAN simulations.

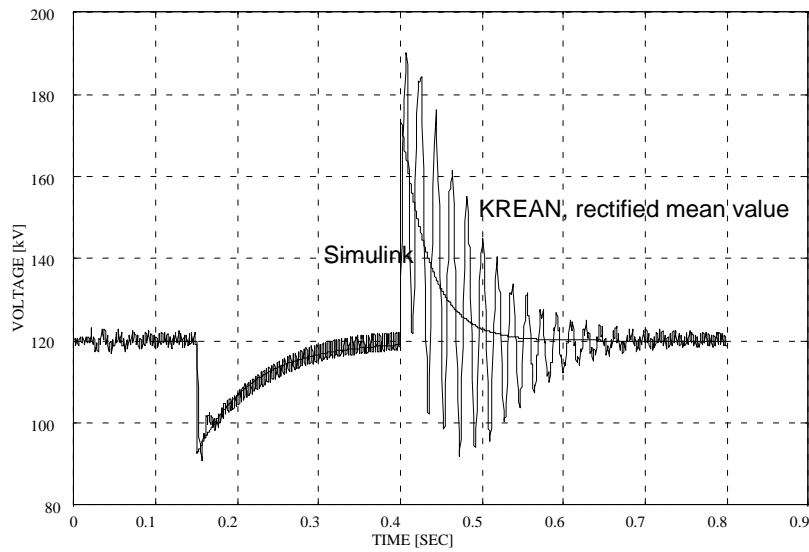


Figure 7-34 Voltage as result of Simulink simulation of process in Figure 7-26 for load shift from  $0.1P_N$  to  $0.3P_N$  and back to  $0.1P_N$ , compared to the result of KREAN simulations.

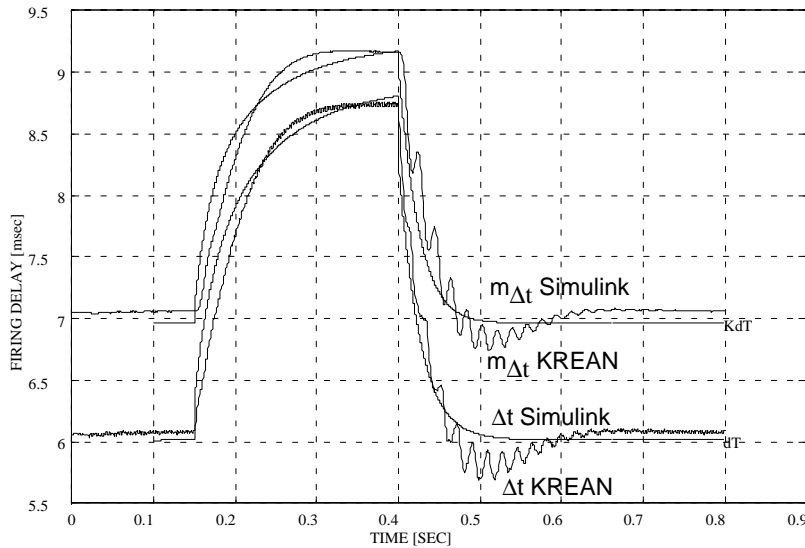


Figure 7-35 Firing delay time  $\Delta t$  and auxiliary variable  $m_{\Delta t}$  as result of Simulink simulation of process in Figure 7-26 for load shift from  $0.1P_N$  to  $0.3P_N$  and back to  $0.1P_N$ , compared to the result of KREAN simulations.

oscillations as before. But KREAN shows a tendency to overswing when returning to low load, indicating that the gain is somewhat larger than calculated. The differences in the stationary values are due to non-exact calculation of the initial values when applied to KREAN.

Figure 7-36 shows the output of the voltage controller, the auxiliary variable  $m_C$ , and the actual capacitance  $C$ . The difference between the two is the contribution from the frequency controller, due to the decoupling. The same comments apply as for the firing delay time controller.

Thereafter the comparison is made for the load shift case from  $0.8P_N$  to  $P_N$  and back to  $0.8P_N$ . The simulations and the results are basically the same as in the previous simulations and show that the system is much less sensitive at high loads. See Figure 7-37, Figure 7-38, Figure 7-39 and Figure 7-40.

These simulations show two things. First that an inverter feeding a passive load with a controllable reactive source can be controlled with regard to frequency and voltage by means of controlling the firing delay time and reactive power, in the simulations represented by the controllable capacitor. Second they show that a simple model based on RMS values gives sufficiently accuracy for a feasibility study. The transients are not recorded accurately, but peak values are within reasonable accuracy. Thus it should be possible to apply the RMS-based tool for further analysis.



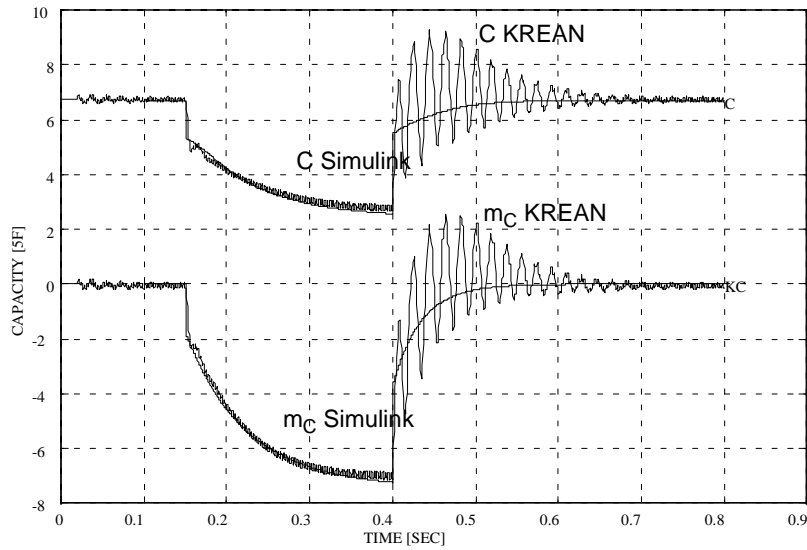


Figure 7-36 Capacitance  $C$  and auxiliary variable  $m_C$  as result of Simulink simulation of process in Figure 7-26 for load shift from  $0.1P_N$  to  $0.3P_N$  and back to  $0.1P_N$ , compared to the result of KREAN simulations.

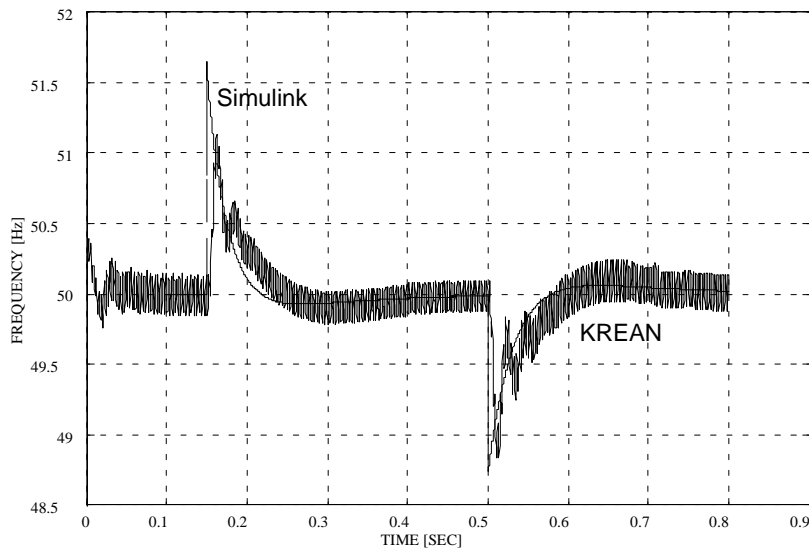


Figure 7-37 Frequency as result of Simulink simulation of process in Figure 7-26 for load shift from  $0.8P_N$  to  $P_N$  and back to  $0.8P_N$ , compared to the result of KREAN simulations.

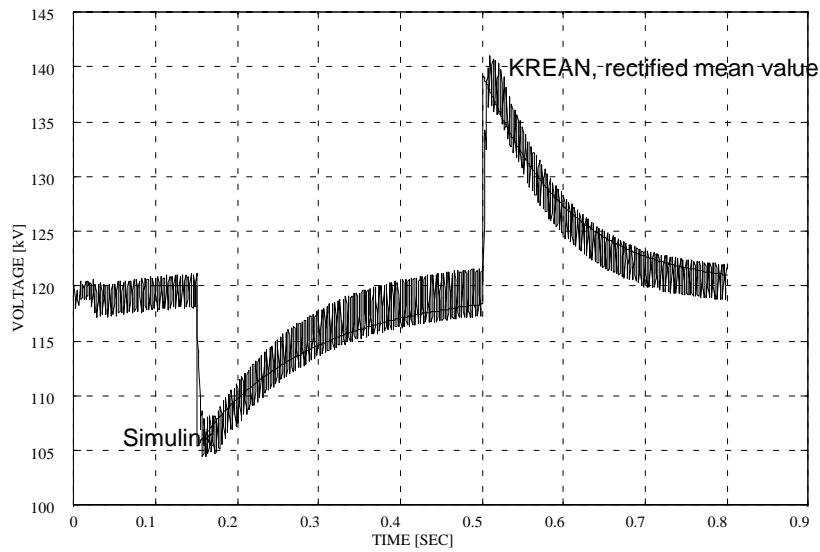


Figure 7-38 Voltage as result of Simulink simulation of process in Figure 7-26 for load shift from  $0.8P_N$  to  $P_N$  and back to  $0.8P_N$ , compared to the result of KREAN simulations.

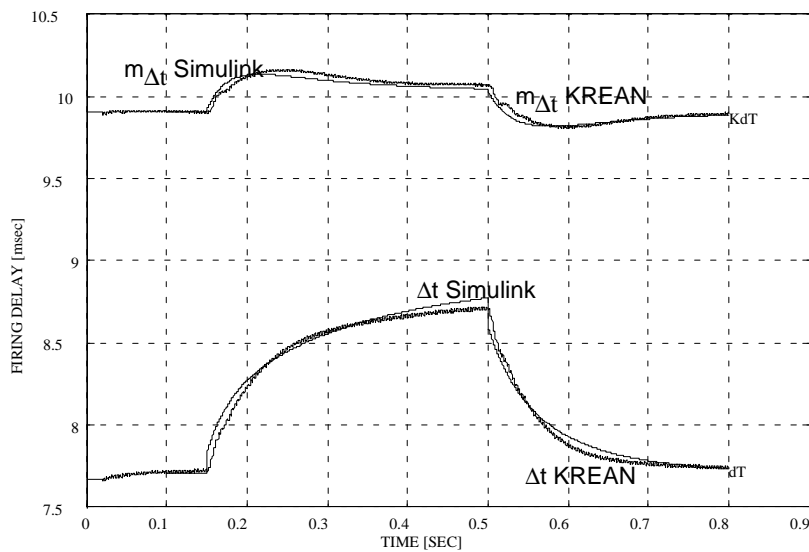


Figure 7-39 Firing delay time  $\Delta t$  and auxiliary variable  $m_{\Delta t}$  as result of Simulink simulation of process in Figure 7-26 for load shift from  $0.8P_N$  to  $P_N$  and back to  $0.8P_N$ , compared to the result of KREAN simulations.

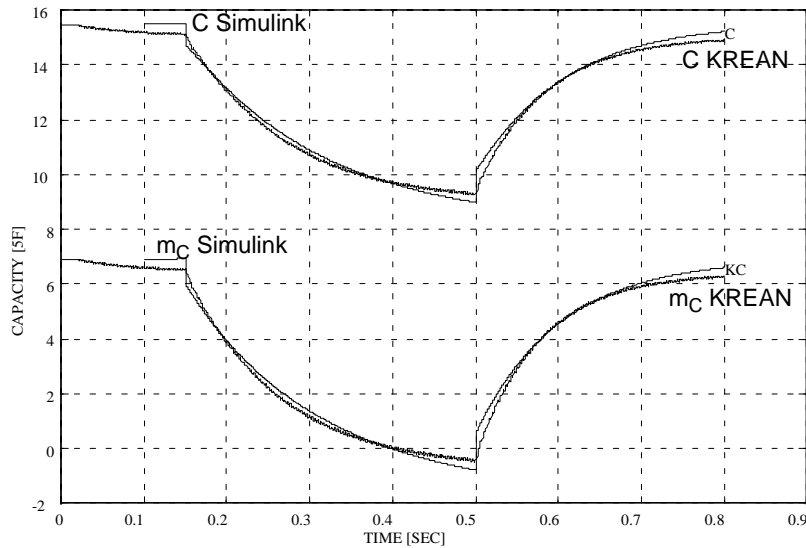


Figure 7-40 Capacitance  $C$  and auxiliary variable  $m_C$  as result of Simulink simulation of process in Figure 7-26 for load shift from  $0.8P_N$  to  $P_N$  and back to  $0.8P_N$ , compared to the result of KREAN simulations.

## 7.4 SUMMARY

In this chapter we have investigated the fundamental behaviour of an inverter feeding power into a passive RC network. It appeared that in a system with fixed firing delay time and fixed DC link current, both voltage and frequency will vary if either resistance or net capacitance is changed. The sensitivities of frequency and voltage for change in network parameters, as well as firing delay time were found. The concept of relative sensitivity is introduced and the relative sensitivities are discussed. Especially it shall be noted that there is a positive sensitivity in frequency with regard to change in load, represented by network conductance. This implies a possible instability for all types of load which increase by frequency, like motors.

Further, a base case inverter is analysed for small signal sensitivities, and an example system where voltage and frequency are controlled by means of variations in network net capacitance and firing delay time is simulated. The simulations are performed both in a quasi-phasor model and a time domain model. Both models give the same results, and show that this way of controlling is possible. The system appears stable for rather large disturbances, even with very simple controllers.



# 8 CONSEQUENCES OF A SYNCHRONOUS COMPENSATOR

In this chapter we shall discuss how the differences between reactive power production in a capacitor and in a synchronous compensator will influence the system. We will also study the consequences on the dynamic behaviour of the system.

## 8.1 INTRODUCTION

Until now it has been assumed that the source of reactive power was of minor importance, and the reactive production in the system was assumed to take place in a theoretical variable capacitor. It has been shown, however, that both voltage and frequency are prone to significant variations due to variations in load. Furthermore, a high voltage, high power variable capacitor is not easy to obtain. The nearest available today is a bank of thyristor switched capacitors, TSCs, which are able to switch on and off groups of capacitors in limited steps. For fine tuning of the production of reactive power, the most versatile unit is still the synchronous compensator, particularly because it can serve the additional role as essential generator during the start-up of the power system and in cases of breakdown in the HVDC supply. This raises the issue of how a synchronous compensator will influence the production of reactive power in the system under investigation?

## 8.2 REACTIVE POWER PRODUCTION CHARACTERISTICS OF CAPACITORS AND SYNCHRONOUS COMPENSATORS

### 8.2.1 Capacitors

The amount of reactive power produced in a capacitor connected to a network is given by:

$$q = u^2 \cdot \omega c \quad (8-1)$$

with generative reference. This equation clearly states that if the frequency of the network increases, the amount of reactive power increases linearly, as illustrated in Figure 8-1, curve 1. And if the voltage increases, the amount of reactive power increases by the square as illustrated in Figure 8-2, curve 1. The curves are drawn for a capacitor with reactive power rating of 1 p.u. at a voltage of 1 p.u. and angular frequency of 1 p.u.

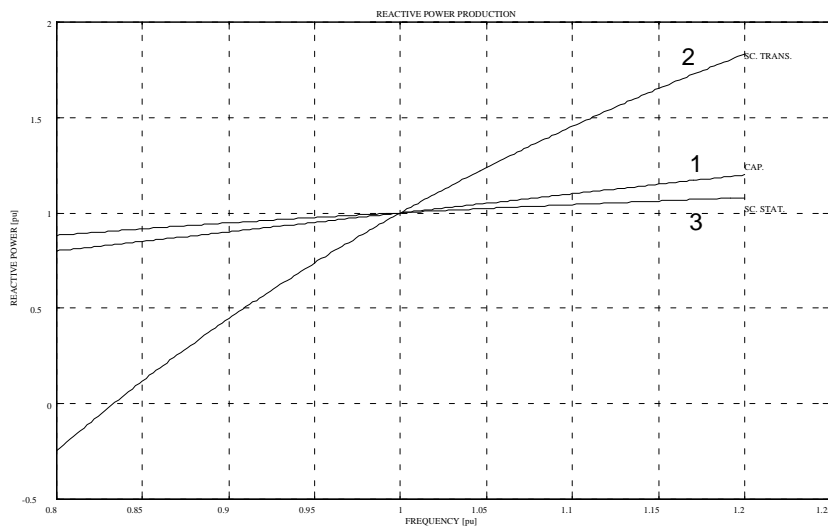


Figure 8-1 Production of reactive power in capacitor and synchronous compensator as functions of the frequency.

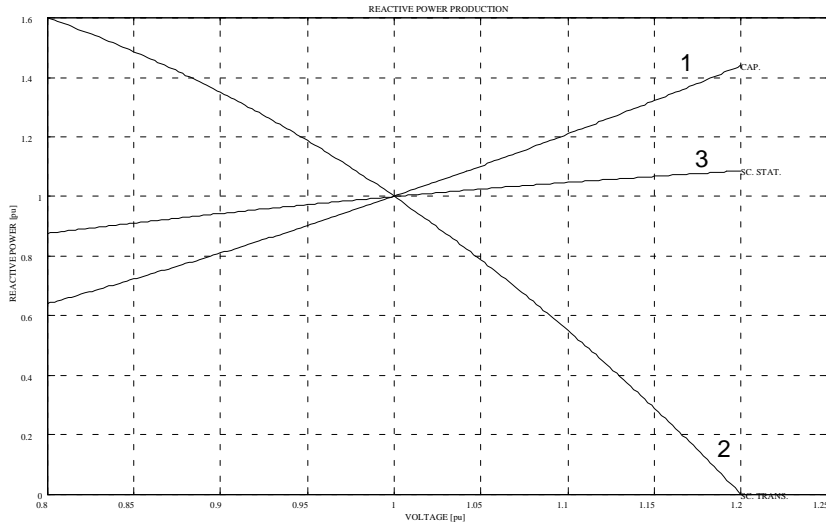


Figure 8-2 Production of reactive power in capacitor and synchronous compensator as functions of the voltage.

### 8. 2. 2 Synchronous compensators

In this chapter we are discussing synchronous compensators with constant magnetization, without their regulators, as we are only interested to study the initial period before the controllers are able to react.

The amount of reactive power produced in a synchronous compensator with constant magnetization connected to a network is given, with generative reference, by:

$$q = \frac{u \cdot \left( e_0 \cdot \frac{\omega}{\omega_0} - u \right)}{\omega l_d'} \quad (8-2)$$

This equation, with  $\omega$  as variable, is illustrated in Figure 8-1, curves 2 and 3, which show that the amount of reactive production in a synchronous compensator rises by increasing frequency. If the frequency decreases below a certain value, such that the EMF gets below the line voltage, the compensator stops producing reactive power and starts consuming. Curve 2 shows the situation for a machine with reactive power rating 1 p.u. and transient parameters  $e' = 1.2$  and  $l_d' = 0.2$ . Curve 3 shows the situation for the same machine

with stationary parameters  $e = 3.1$  and  $l_d = 2.1$ . Compared to a capacitor of the same power rating, a synchronous compensator with constant magnetization will increase production of reactive power more than a capacitor for a fast frequency increase, but as the machine turns into stationary state, the production of reactive power will drop again. (This assumes that the inertia of the machine is small, so that the machine can follow the variations in frequency)

But what is more interesting is the influence of the voltage. First, to produce any reactive power at all, the induced voltage  $e$  must be higher than the external network voltage  $u$ , i.e. the machine must be over magnetized. Secondly, if the network voltage increases, the difference between induced and external voltage decreases and the machine supplies less reactive power, as illustrated in Figure 8-2, curves 2 and 3. Curve 2 shows the situation for the above mentioned machine in transient state and Curve 3 shows the situation in stationary state.

From the curves it is obvious that a system which employs capacitors to provide the necessary reactive power, will exhibit quite different behaviour at voltage variations than a system which employs synchronous compensators. The behaviour at frequency variations however will be rather similar.

In the case where both synchronous compensators and capacitors are applied to produce the required reactive power, the system behaviour will be determined by the balance between the providers of reactive power.

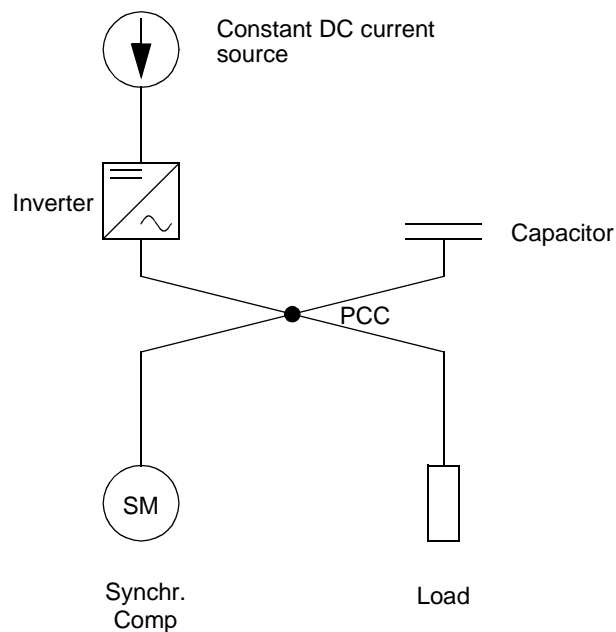


Figure 8-3 Simplified model of HVDC supply to an offshore oil-installation.



### 8.3 INVERTER NETWORK WITH BOTH CAPACITORS AND SYNCHRONOUS COMPENSATORS

The system to be discussed is shown in Figure 8-3. It consists of a constant DC current source and an inverter as model for the HVDC transmission. A capacitor and a synchronous compensator provide the reactive power needed in the system. How then will this system behave stationary when one of the parameters is changed?

The above figure can be modified to reflect Kirchoff's law in complex form, as illustrated in Figure 8-4. The figure is drawn with motoric references and the synchronous compensator is represented by its Norton equivalent. The current  $i_{sc}$  in the synchronous compensator can be split in the short circuit current  $i_{s0}$  and an inductive load current  $i_m$ , as shown in (8-4).

$$\vec{i}_{sc} = \frac{u - e}{j\omega l_d} = -j \frac{u - e_0 \frac{\omega}{\omega_0}}{\omega l_d} \quad (8-3)$$

$$\vec{i}_{sc} = -j \left( \frac{u}{\omega l_d} - \frac{e_0}{\omega_0 l_d} \right) = -j \frac{u}{\omega l_d} + j \frac{e_0}{\omega_0 l_d} = \vec{i}_m + \vec{i}_{s0} \quad (8-4)$$

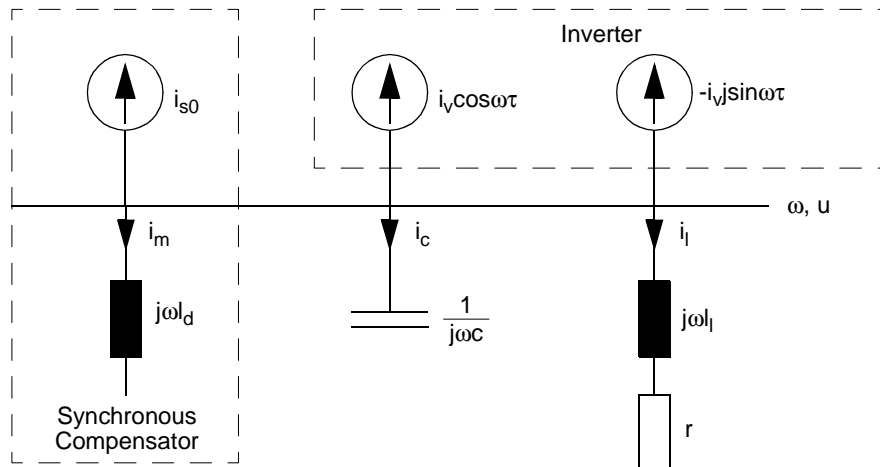


Figure 8-4 Kirchoff's law applied to simplified model of HVDC supply.

Based on Figure 8-4, the following equation can be set up:

$$\vec{i}_v + \vec{i}_{s0} + \vec{i}_m + \vec{i}_c + \vec{i}_l = 0 \quad (8-5)$$

In this equation we find the machine short circuit current:

$$\vec{i}_{s0} = j \frac{e_0}{\omega_0 l_d} \quad (8-6)$$

The machine inductive load current:

$$\vec{i}_m = -j \frac{u}{\omega l_d} \quad (8-7)$$

The capacitor current:

$$\vec{i}_c = j u \omega c \quad (8-8)$$

The external load current:

$$\vec{i}_l = u \cdot \frac{r - j\omega l_l}{r^2 + (\omega l_l)^2} = \frac{ur}{r^2 + (\omega l_l)^2} - j \frac{u\omega l_l}{r^2 + (\omega l_l)^2} \quad (8-9)$$

And the inverter current:

$$\vec{i}_v = i_v (\cos \omega \Delta t - j \sin \omega \Delta t) \quad (8-10)$$

The resulting impedance the sum of the current sources meets is the parallel connection of the three impedances

$$z_{tot} = \frac{z_m z_c z_l}{z_m z_c + z_m z_l + z_c z_l} \quad (8-11)$$

which consists of the machine impedance:

$$z_m = j\omega l_d \quad (8-12)$$

The capacitor impedance:

$$z_c = \frac{1}{j\omega c} \quad (8-13)$$

And the external load:

$$z_l = r + j\omega l_l \quad (8-14)$$

Inserting and manipulating, we arrive at:

$$z_{tot} = \frac{r + j\left[\omega l_l\left(1 + \frac{l_l}{l_d} - \omega^2 l_l c\right) + r^2\left(\frac{1}{\omega l_d} - \omega c\right)\right]}{\left(1 + \frac{l_l}{l_d} - \omega^2 l_l c\right)^2 + r^2\left(\frac{1}{\omega l_d} - \omega c\right)^2} \quad (8-15)$$

If we presuppose that the voltage in the system is linked to the real axis, the outgoing current  $i_{out}$  will have a phase angle given by the total impedance. The resulting incoming current  $i_{in}$  must have the same value and opposite direction. The incoming and outgoing currents are defined by (8-16) and (8-18).

$$\vec{i}_{in} = \vec{i}_v + \vec{i}_{s0} = i_v \cos \omega \Delta t + j(i_v \sin \omega \Delta t + i_{s0}) \quad (8-16)$$

$$\vec{i}_{out} = \vec{i}_m + \vec{i}_c + \vec{i}_l \quad (8-17)$$

$$\vec{i}_{out} = u \left[ \frac{r}{r^2 + (\omega l_l)^2} + j \left( \omega c - \frac{\omega l_l}{r^2 + (\omega l_l)^2} - \frac{1}{\omega l_d} \right) \right] = \frac{u}{z_{tot}} \quad (8-18)$$

Thus we can draw the phasor diagram in Figure 8-5 for the undisturbed case.

Now let the resulting total impedance  $z_{tot}$  be changed for some reason, normally a change in load. If no controllers are operating, the DC current will be kept constant, i. e. the magnitude of the converter current  $i_v$  is constant. The excitation of the compensator is constant and, for simplicity, the inertia of the compensator is ignored. Thus the short circuit current  $i_s$  is constant and imaginary, equal to  $i_{s0}$ . Thus the end of the new incoming current phasor  $i_{in2}$  must end somewhere on the circle given by  $i_v$  around the end of  $i_{s0}$ . The new out-

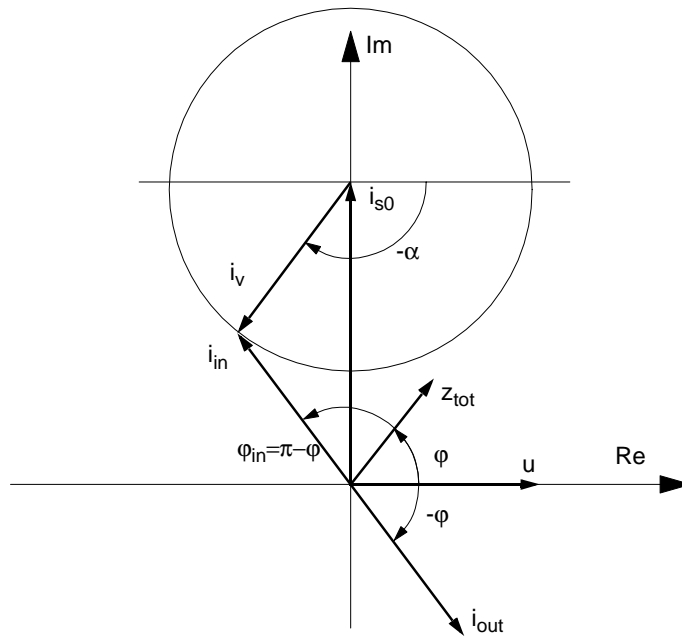


Figure 8-5 Principal phasor diagram for the currents and impedances in Figure 8-4 before disturbance.

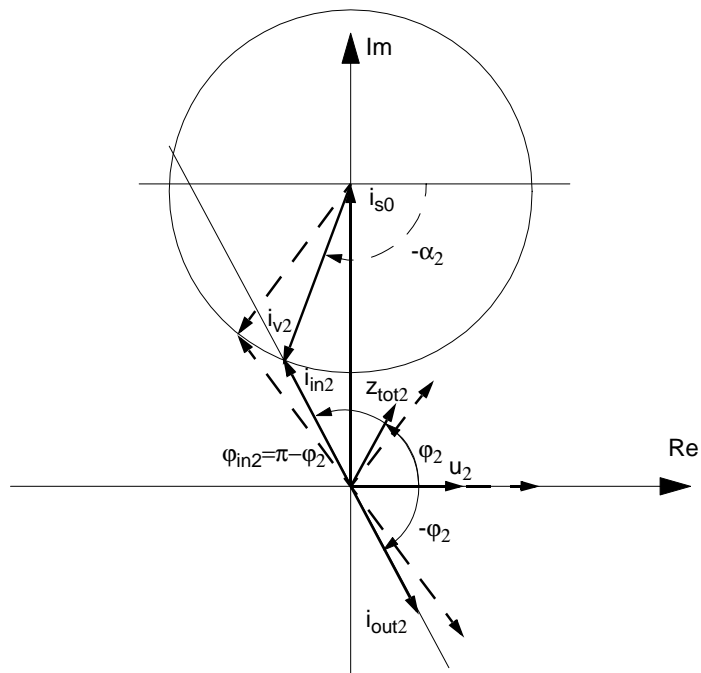


Figure 8-6 Principal phasor diagram for the currents and impedances in Figure 8-4, dashed lines indicate the situation before disturbance, continuous lines after disturbance.

going current  $i_{out2}$  is locked to the phase angle of the new total impedance  $z_{tot2}$  but the value is still unknown. According to Kirchoff's law, the new incoming current  $i_{in2}$  must be in the opposite direction. Thus the new incoming current  $i_{in2}$  is determined by the crossing of the circle of  $i_v$  by the ray from the origin in the direction of  $i_{in2}$ . But in order to move the phasor  $i_v$  to this new intersection, the firing angle  $\alpha$  must be changed. It is presupposed that no controllers are operating, thus the firing delay  $\Delta t$  is constant. The only way to change the firing angle  $\alpha$  is to change the network frequency  $\omega$ , according to  $\alpha = \omega \Delta t$ . This influences the new total impedance  $z_{tot2}$  and the solution has to be found by iterations. When the new incoming current  $i_{in2}$  is determined, the new outgoing current  $i_{out2}$  also is determined, and finally the resulting voltage  $u_2$  can be found. This has to remain purely real. The phasor diagram in Figure 8-6 shows the situation after disturbance. These phasor diagrams are principal and drawn for clarity, they do not reflect true operational conditions.

If the magnitude of the converter current  $i_v$  is less than the magnitude of the compensator short circuit current  $i_{s0}$ , as is the case in Figure 8-5 and Figure 8-6, it is obvious that for certain values of impedance phase angle  $\varphi$  there cannot be an intersection of the circle. Still Kirchoff's law has to be fulfilled. The only way to achieve this is to pull the short circuit current  $i_{s0}$  out of its pure imaginary phase. Given the operation point, the real part of the short circuit current  $i_{s0}$  has to be negative, i.e. the compensator supplies power. This has to be taken from the rotational energy, leading to a braking of the compensator and a breakdown of the network frequency.

Figure 8-6, and also Figure 8-7 show that if the magnitude of the converter current  $i_v$  is less than the magnitude of the compensator short circuit current  $i_{s0}$ , there will be two possible solutions to the requirement that the phase angles must coincide, the ray intersects the circle in two points. It is assumed that the correct solution is the one where the slope of the crossing is the same as the original. This assumption is confirmed by calculations which prove that this solution is the one which gives minimum change in active and reactive power.

If, in Figure 8-4, realistic per unit values are assigned to all parameters except the capacitance, it is easy to calculate the necessary capacitance to keep the voltage and frequency at nominal values. This can be imagined as a system where capacitor banks have been switched to adapt to the given stationary load situation. It is the relative relationship between the synchronous compensator and the load which is important for the result of these considerations. The inverter is regarded as ideal, the inverter rating has no influence on the calculated results. The capacitor size is derived from the other parameters. In

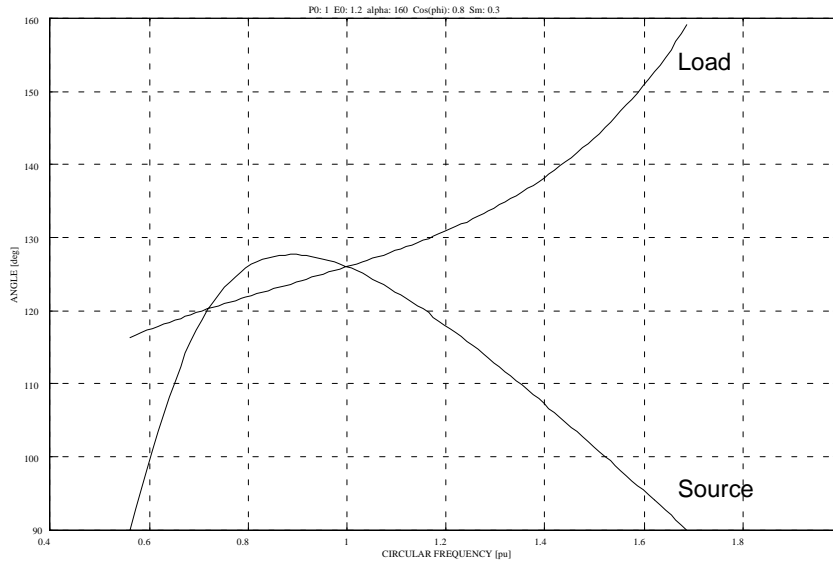


Figure 8-7 Required and offered phase angle  $\phi$  of in-feed current as functions of network circular frequency for synchronous compensator rating=0.3, before disturbance.

order to simplify the calculations, the load rating is selected to be 1 p.u. Transient values are used for the synchronous compensator. The calculations have been performed for a number of different synchronous compensator ratings between 0.1 and 2 p.u.

In Figure 8-7, the angle of the resulting impedance  $z_{tot}$  from (8-15), turned around to reflect the angle of the required in-feed current, is drawn as a function of the network circular frequency  $\omega$  for an arbitrary synchronous compensator, before disturbance. This is the curve described as “Load”. In the same diagram, the curve for the angle of the resulting in-feed current  $i_{in}$  from equation (8-16), is also drawn as a function of  $\omega$ . This is the curve described as “Source”. As expected the curves intersect for a circular frequency of 1 p.u.

Then the value of the load resistor is increased by 10 %, which is roughly equivalent of decreasing the required active power by 9 %, and the curve for the angle of the new required in-feed current is added in Figure 8-8, marked “New load”. The curve for the source current is not dependent on the change in the load. The curve for the new load angle has for the major part shifted upwards, and the new intersection point is situated at a slightly lower frequency in this case. As described before, the intersection point with the same slope as the original is assumed to be the correct solution.

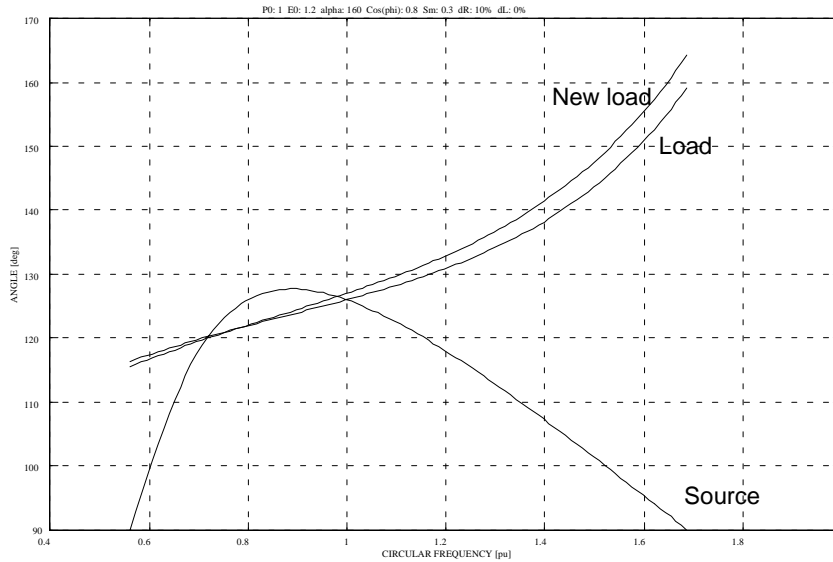


Figure 8-8 Required and offered phase angle  $\varphi$  of in-feed current as functions of network circular frequency for synchronous compensator rating=0.3, after disturbance.

The case when the magnitude of the converter current  $i_v$  is greater than the magnitude of the compensator short circuit current  $i_{s0}$ , is shown as the phasor diagram in Figure 8-9. This implies that the synchronous compensator is rather small compared to the load. This situation brings no essential news, one must only bear in mind that the required angle for the in-feed current is a ray from the origin, thus there will only be one solution in this case. The corresponding curves for the angles as functions of the network circular frequency are drawn in Figure 8-10 for the case before disturbance and in Figure 8-11 for the case after disturbance. Once more it should be reminded that these phasor diagrams are principal and drawn for clarity, they do not reflect true operational conditions.

If the operation of finding the new intersection point is performed for various values of synchronous compensator rating  $s_m$ , the resulting frequencies after the disturbance can be plotted as functions of the synchronous compensator rating. When the frequencies are determined, one also knows the current flowing from the sources through the combined impedance, and hence the resulting voltages can be calculated. This has been done and the resulting frequency and discarded solution after a 10 % increase in load resistance (9 % reduction of power), depicted as function of the synchronous compensator rating are shown in Figure 8-12. The resulting voltage is similarly shown in Figure 8-13. These curves clearly shows a discontinuity for a certain rating of

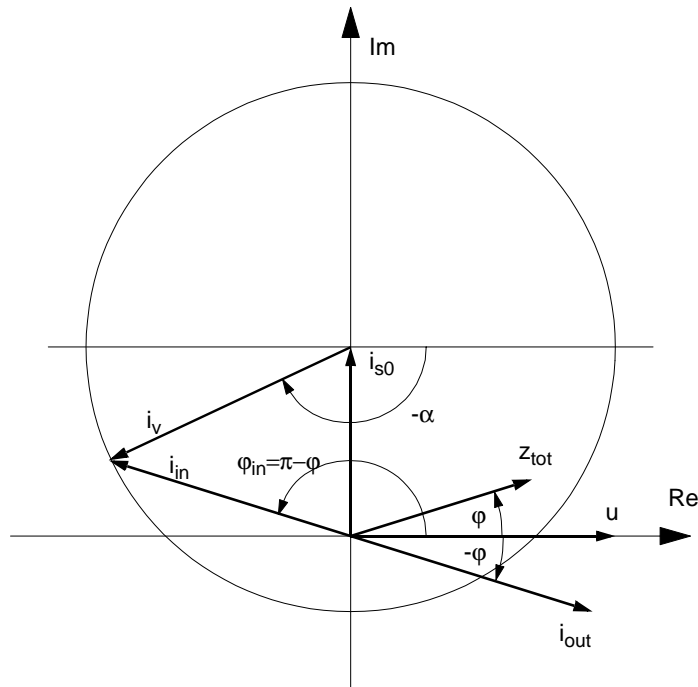


Figure 8-9 Principal phasor diagram for the currents and impedances in Figure 8-4 before disturbance,  $|i_v| > |i_{k0}|$ .

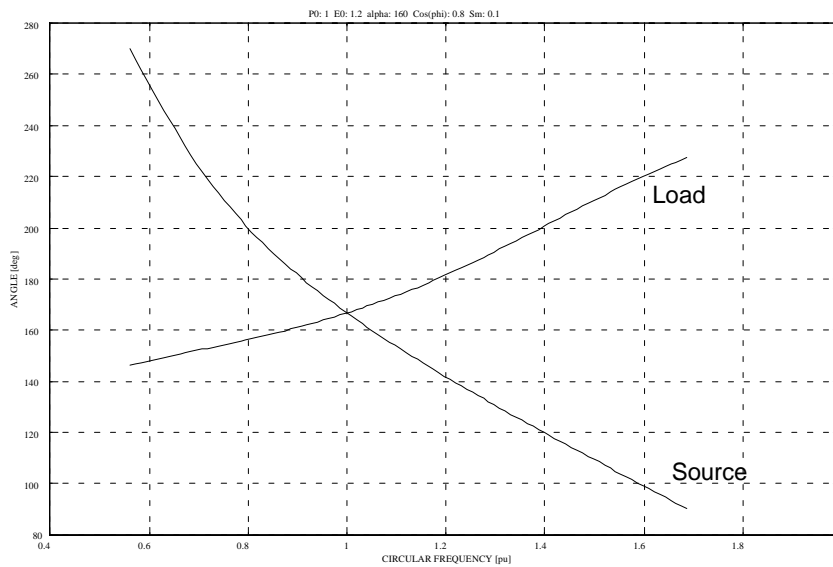


Figure 8-10 Required and offered phase angle  $\varphi$  of in-feed current as functions of network circular frequency for synchronous compensator rating=0.1, before disturbance.



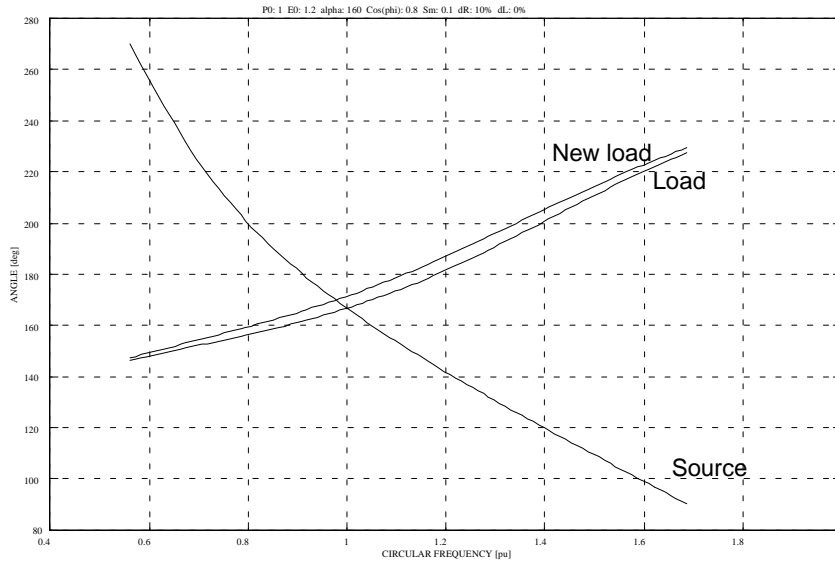


Figure 8-11 Required and offered phase angle  $\phi$  of in-feed current as functions of network circular frequency for synchronous compensator rating=0.1, after disturbance.

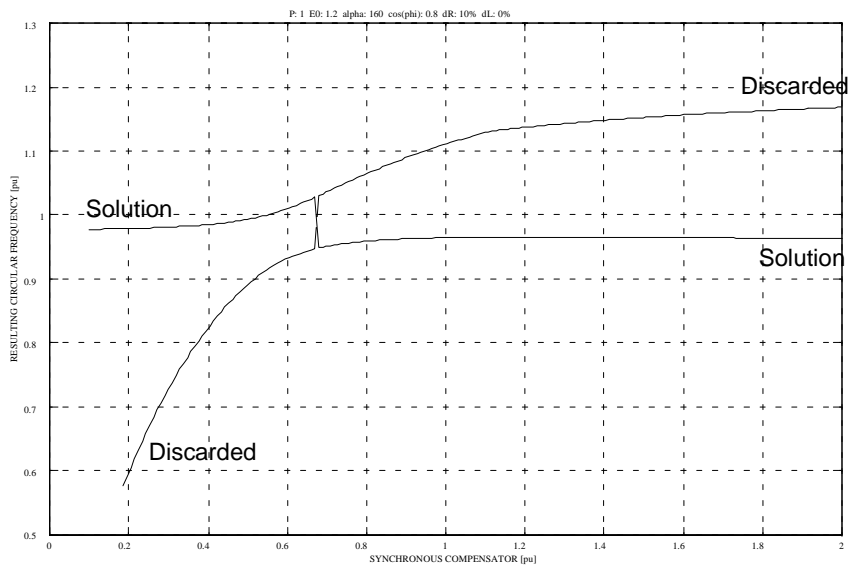


Figure 8-12 Resulting frequency and discarded solution after 10 % increase of load resistance from stationary value, as functions of synchronous compensator rating.

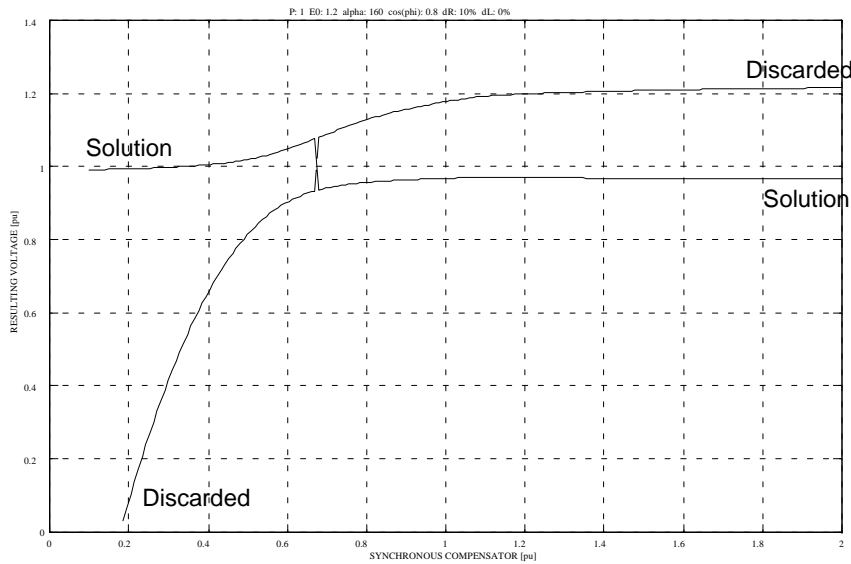


Figure 8-13 Resulting voltage and discarded solution after 10 % increase of load resistance from stationary value, as functions of synchronous compensator rating.

the synchronous compensator. This discontinuity appears where the pre-disturbance solution shifts from above to below the tangent point in the phasor diagram. It can also be seen that for most values of the synchronous compensator rating the frequency and the voltage drop for this reduction in load, as predicted by the sensitivity analysis in Chapter 7, but in a certain area near the discontinuity, the frequency and the voltage rise. This has to be taken into consideration when a controller shall be developed for a true system.

It can be seen that the discarded solution disappears for small values of synchronous compensators ratings compared to the load. This is due to the fact that in this area the magnitude of the inverter current  $i_v$  grows larger than the magnitude of the short circuit current. The circle encloses the origin and only one solution remains.

Until now, there has been no problem with missing solutions in the depicted curves. But these curves are highly dependent of the load combination and the type of disturbance, and also on the firing angle of the inverter  $\alpha$ . If, for instance the firing angle  $\alpha$  is reduced from  $160^\circ$  to  $140^\circ$ , the resulting frequency and voltage are shown in Figure 8-14 and Figure 8-15. The range for which there is no solution is now clear.

It shall be noted that a missing solution do not implicate that the situation is necessarily unstable in the working point before the disturbance, or that cer-

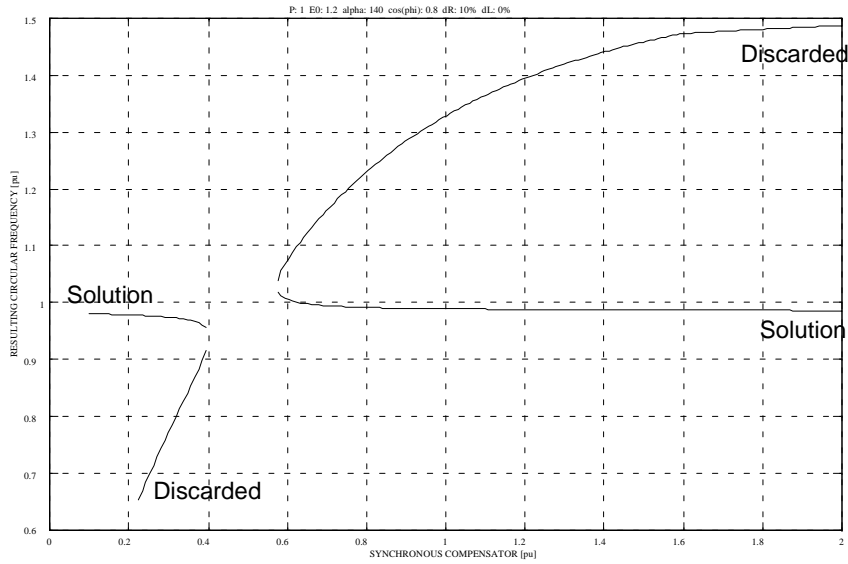


Figure 8-14 Resulting frequency and discarded solution after 10 % increase of load resistance from stationary value, as function of synchronous compensator rating.  $\alpha=140^\circ$

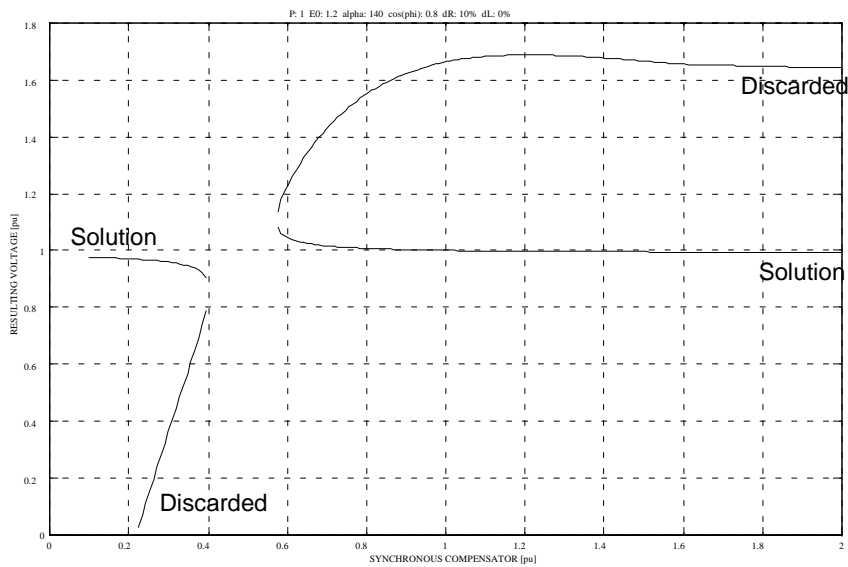


Figure 8-15 Resulting voltage and discarded solution after 10 % increase of load resistance from stationary value, as function of synchronous compensator rating.  $\alpha=140^\circ$

tain working points cannot be reached. The implication in a practical case is that the operator must always know if the system is near the critical area, and if so is the case, he should select another combination of reactive power from the synchronous compensator and from capacitor banks. It shall also be noted that the presupposition to disregard the inertia of the compensator makes the system unnecessary vulnerable, as will be further discussed in Section 8. 4. 4.

## **8. 4 CONCLUSION**

### **8. 4. 1 Conditions for solution**

As has been shown, the system will reach a new stable state after a disturbance if either the magnitude of the inverter current is greater than the magnitude of the compensator short circuit current (the circle of the inverter current encloses the origin) or the phase angle of the new load is such that there is an intersection with the circle of the inverter, even after the frequency change. In the last case, load changes that generally lead to a decrease in the phase angle of the total impedance may be critical. It can also be noted that when the circle of inverter current comes closer to the origin, the critical range of the firing angle  $\alpha$  moves towards  $90^\circ$ , this being a range that is not ordinarily in use.

### **8. 4. 2 Stationary conditions**

The calculation has been performed with transient values for the synchronous compensator. If the stationary values are applied, the short circuit current is reduced, as is the current consumed in the machine reactance. The circle of inverter current comes closer to the origin or encloses it. At the same time the resulting impedance turns less inductive or even capacitive such that the phasor balance is maintained. Calculations with stationary values should give a more stable system than those using transient values. In practice, there will also be controllers operating the system to keep stable.

### **8. 4. 3 Bypassing critical areas**

The critical area of operation is when the combination of circuit parameters is such that an expectable change of load will make the phasor diagram of the system become impossible. Fortunately there are a number of parameters to play on. In the calculations it has been assumed that the synchronous compensator has been operating at rated load and the capacitor banks have been var-

ied to supply the reactive power required. A reduction of the excitation of the compensator will have an immediate influence on the short circuit current and move the inverter current circle to a more suitable position. The reduction of reactive power production can easily be compensated by more capacitors.

For the case of an offshore power supply system with a small synchronous compensator with a rating of for example 15 %, this should bring no need for extra capacitors. In the calculated example, the problems arise at a compensator rating of 40 to 50 % of the load. By scaling, this implies that the critical range on the platform would occur in a situation where the load is about 33 %. In this case there should be sufficient spare capacitor rating to allow free play.

There is also the possibility of modifying the inverter current and firing angle, thereby modifying the inverter current circle itself. This, however, is less feasible as it will normally lead to increased losses and increased need for reactive compensation power.

#### 8.4.4 Consideration of the compensator inertia

Basically the simplification of disregarding the inverter inertia leads to the assumption that the short circuit phasor is locked to the imaginary axis. If the machine is given an inertia, this will add the possibility of an active component to the machine current. The equation for the machine current will become a modification of (8-4):

$$\vec{i}_{sc} = -j \frac{u - e_0(\cos\beta - j\sin\beta)}{\omega_0 l_d} = -j \frac{u}{\omega l_d} + \frac{e_0(\sin\beta + j\cos\beta)}{\omega_0 l_d} \quad (8-19)$$

$$\vec{i}_{sc} = -j i_m + i_{s0}(\sin\beta + j\cos\beta) \quad (8-20)$$

This shows that the active current component is linked to the short circuit current by the sine of the pole wheel angle  $\beta$ . This can be interpreted as the short circuit current phasor is no longer locked to the imaginary axis, but is allowed to “sway”, and the centre of the circle of the inverter current moves along. As the frequency deviations are shown as not being too large, the pole wheel angle variations will also be reasonable and the main conclusions of the investigation remains principally valid, even if they are too pessimistic.

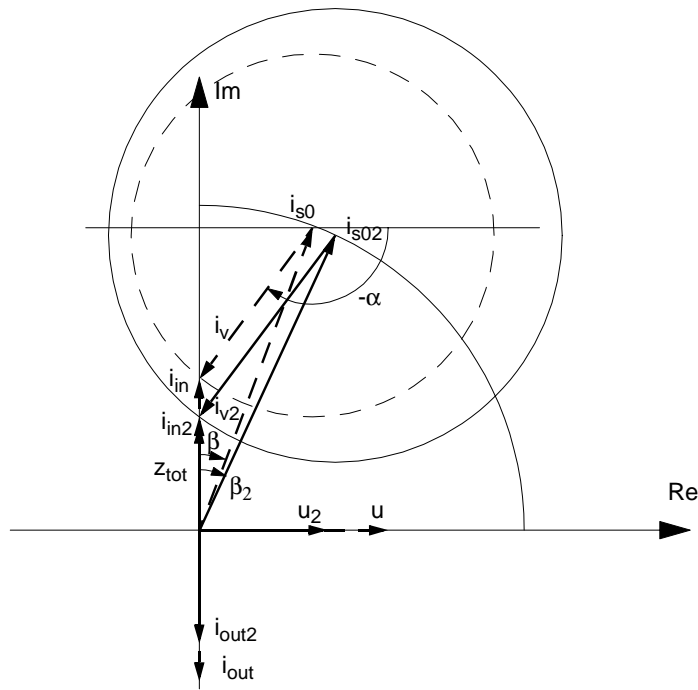


Figure 8-16 Principal phasor diagram for the currents and impedances in classical HVDC stability theory before and after increase of transmitted current.

#### 8. 4. 5 Relation to classical theory

Classical stability theory makes a number of assumptions. First it assumes that the inertia of the system is so large that there is negligible frequency variations. Second its concern is power transmission into a network represented by a Thevenin equivalent. All transmitted power is pumped into the equivalent voltage source of the network. This is the equivalent of the synchronous compensator being replaced by a machine capable of absorbing all the active power offered, and no active component in the resulting network impedance. In such a case the short circuit current phasor will have an active component with magnitude equal to the magnitude of the active component of the inverter current and opposite direction. The intersection points with the circuit will be on the imaginary axis and the problem is reduced to one dimension. The principal phasor diagram for the classical problem is shown in Figure 8-16.

# **9 QUASI-PHASOR SIMULATIONS OF A SYSTEM WITH A SYNCHRONOUS COMPENSATOR AND A PASSIVE LOAD, WITHOUT CONTROLLERS**

In this chapter we shall study the consequences of the introduction of a synchronous compensator to the formerly passive network

## **9.1 INTRODUCTION**

In Chapter 7 it was shown that the voltage and frequency of an AC system consisting of an inverter supplying power to a passive network can be controlled by variation of the reactive power supply, represented by the total network capacitance, and the inverter firing delay time. Sensitivity analysis indicated, however, the possibility of instability due to a negative sensitivity in the frequency for a change in the active load.

Furthermore it was indicated that a phasor-based simulation could give sufficiently good results to decide if the system is stable or not, and indicate the course of the transients. Now the model in Chapter 7 will first be enhanced by a 'small' synchronous compensator. In Chapter 8 it was indicated that the dynamic behaviour of a system where the reactive power is supplied by synchronous compensators may not be similar to a system where the reactive power is supplied by capacitors.

In Chapter 10 the system will be enhanced with the load of a ‘large’ induction motor to see the influence on the stability of the uncontrolled system.

## **9.2 ABOUT THE MODEL**

There is a close resemblance between the classical phasor model used in power system analysis and the dq-model used in machine analysis. The theoretical foundation is different, phasors are formally limited to represent stationary, sinusoidal quantities, while dq-transformation is, as indicated by the name, only a transformation of time-variables, which have the quality to represent stationary, sinusoidal quantities by means of constants. Phasor analysis, however, has for a long time been used to describe slowly varying quantities in power system analysis. Combining these two gives a tool that gives simple calculations. The fundamental questions of long-term stability and resulting voltage and current are solved, while the exact course of the transient, and finer points like aperiodic components are lost. Such elements though, are often dependent on the exact time of switching during a period, which cannot be known in advance. Thus they are stochastic and can in most cases be described by factors, like the well-known peak short circuit current factor  $\kappa$ .

In machine theory the dq-analysis can be stator, rotor or field oriented. Analogously our model can connect the reference axis either to the system voltage as measured in the point of common coupling, PCC, or along the synchronous compensator q-axis, the induced EMF. The reference axis will, for convenience, be called the real axis. When the real axis is connected along the synchronous compensator q-axis it rotates smoothly with the machine speed while the voltage in the PCC leads or lags as the load impedance changes. When the real axis is connected to the system voltage in PCC, it ‘jumps around’ together with the PCC voltage. The difference may seem trivial, and in fact is under stationary conditions, but acquires importance when it comes to decide which voltage to use as reference for the firing pulses of the inverter during a transient. If the EMF is used as reference, the frequency of the firing pulses and thereby the frequency of the current is given by the speed of the synchronous compensator. The amplitude and phase of the voltage is then given by the current and the impedance of the load. If the PCC voltage is selected as reference, the firing angle is given by the phase angle of the total load of the inverter, while the frequency of the system actually is a derived quantity, given by the phase angle and the firing delay time. It seems probable that the system which refers to the EMF voltage will be more stable, but this system has the drawback that the terminal voltage is phase displaced



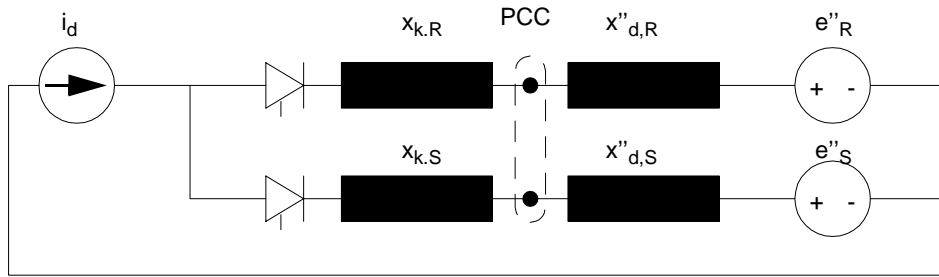


Figure 9-1 Equivalent circuit during commutation in a synchronous motor drive

by the pole wheel angle, and the risk of commutation faults is substantially increased unless extra protective effort is made.

It must be noted that this selection of reference is not only a question of modelling. It implies two different methods of control philosophy and thus two different systems, which may have totally different behaviour. In order to clarify this, both systems will be investigated.

It is also to be noted that the model using EMF as the reference for the firing pulses is basically the same principle as the classical machine commutated synchronous motor drive. The synchronous motor drive, however, has only one path for the current, through the machine and thus through the subtransient EMF which acts as the commutating voltage. In the model analysed here the situation is somewhat more complicated. There is not only one path for the current to flow, and the subtransient EMF is not the only commutating voltage. The difference is illustrated in Figure 9-1 and Figure 9-2. In Figure 9-2  $r$  and  $c$  represent the total network resistance and capacitance. This includes all sorts of loads, also motor drives. Motor drives will

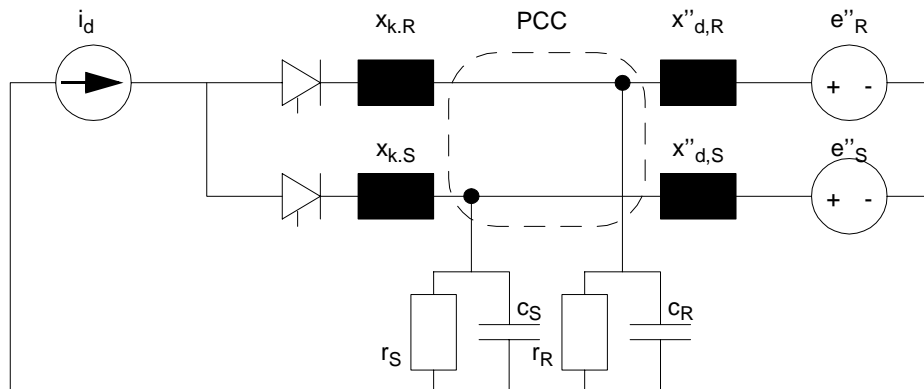


Figure 9-2 Equivalent circuit during commutation in a network with synchronous phase compensator

actually appear as subtransient voltage sources when discussing commutation. The network has to be capacitive in sum in order to facilitate commutation, the synchronous compensator will not have sufficient rating to perform commutation alone. If the network and the compensator in Figure 9-2 is collected into a Thevenin equivalent, the resulting voltage source will in general not be satisfactorily approximated by the machine subtransient EMF.

### 9.3 SYSTEM TO BE SIMULATED

The first system to be simulated is shown in Figure 9-3. It consists of a constant DC current source and a controlled inverter as model for the HVDC transmission. A controlled capacitor represents all reactive power generation in the system, it may be filters, shunt capacitors or Static Var Compensators. The exception is the 'small' synchronous compensator which is to supply mechanical inertia in the system. It is the aim to make this as small as possible.

The model is based on Kirchoff's law: The sum of all active currents into the point of common coupling is zero and the sum of all reactive currents into the point of common coupling is zero. All AC devices are connected in parallel and experience the same voltage. Therefore an admittance description is applied. The simulations are based on the previously described base case. The system has a nominal line voltage at the busbars of 120 kV and the

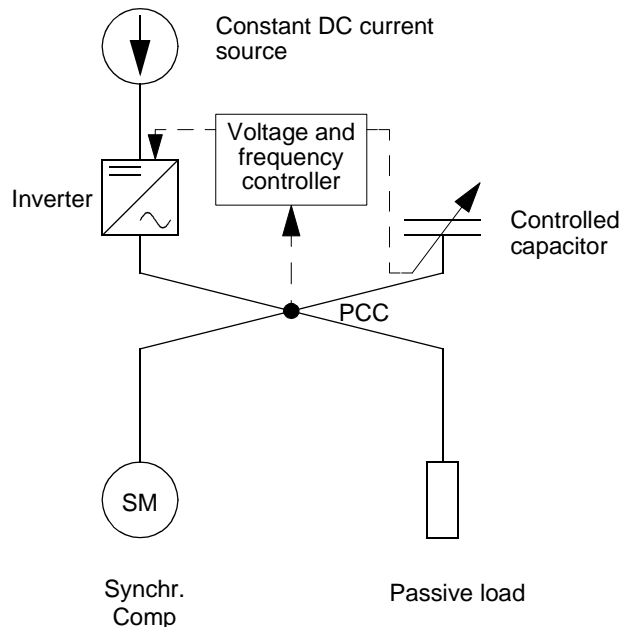


Figure 9-3 Simplified model of HVDC supply to an offshore oil-installation, to be simulated in Quasi-phasor model

inverter has power rating of 100 MW at an extinction angle  $\gamma$  of  $20^\circ$ . The controller parameters found in the previous chapter will be used initially.

The synchronous compensator is modelled in a d-axis model. The amortisseur windings have been replaced by a damping constant. This is allowable since the rest of the model is valid only for stationary and quasi-stationary events. The synchronous compensator is turbo-type, 2-pole 20 MVA, running at 10 MVar reactive supply. The excitation voltage is constant. The electrical and mechanical data are taken from a typical, existing 22 MW generator and scaled to 20 MVA, apart from the mechanical time constant, which is reduced in order to save simulation time. The data for the reference machine are given in full in Appendix B.

The rest of the system is described by a quasi-phasor model where the phasors are allowed to vary in time. The quasi-phasor model gives the enveloping curves of the fundamentals of voltage and current, but neither describes aperiodic components, nor higher harmonics. The load is modelled as a resistor with a conductance equivalent of a total load of 80 MW three phase at nominal voltage. A second load of 20 MW is switched in parallel to increase the total to 100 MW.

The capacitor can be controlled to keep the voltage constant. It is modelled as a continuously variable capacitor. The closest physical counterpart will be thyristor switched capacitors (SVCs), perhaps in combination with a thyristor controlled reactor (TCR). SVCs can only be switched in discrete steps, and only at certain instants during a period, when the voltage across the thyristor is at a minimum. But for the sake of simplicity, we disregard the physical limitations.

The firing delay can be controlled to keep the frequency constant. The initial values for the inverter at the simulation is a DC current equivalent of 100MW at nominal extinction angle, and an initial extinction angle  $\gamma=31.26^\circ$ , such that the active power output is 80 MW, to fit the load, and there is sufficient DC current available to increase the load to 100 MW at  $\gamma=20^\circ$ . The course of the simulation is to allow 1 s for stabilization of initial values. Then at  $t=1$  s the additional admittance equivalent to 20 MW load at nominal voltage is switched on and the simulation goes on until a steady state is reached at  $t=8$  s. The simulations will be performed without active controllers in order to examine the physical actions taking place.

## 9.4 QUASI-PHASOR SIMULATIONS

### 9.4.1 System with reference for the firing pulses given by the voltage at PCC

If we select the voltages at the point of common coupling (PCC) as reference for the firing pulses to the system, it will be a natural choice to select the real axis of the quasi-phasor model along the phasor of the R-phase voltage in this point.

The Simulink model of this case can be illustrated by the simplified block diagram in Figure 9-4. The block diagram includes the voltage and frequency controllers, but not all the required measurement blocks. It can immediately be seen that the model contains at least two algebraic loops, as indicated by the bold lines on the figure. These loops contain both the voltage and frequency, the two parameters that are to be controlled. There is also an algebraic connection from disturbances in the load admittance to the voltage and frequency, indicating that disturbances will give immediate response in voltage and frequency before any controller can react. To break these algebraic loops in order avoid numerical problems, filters with transfer functions

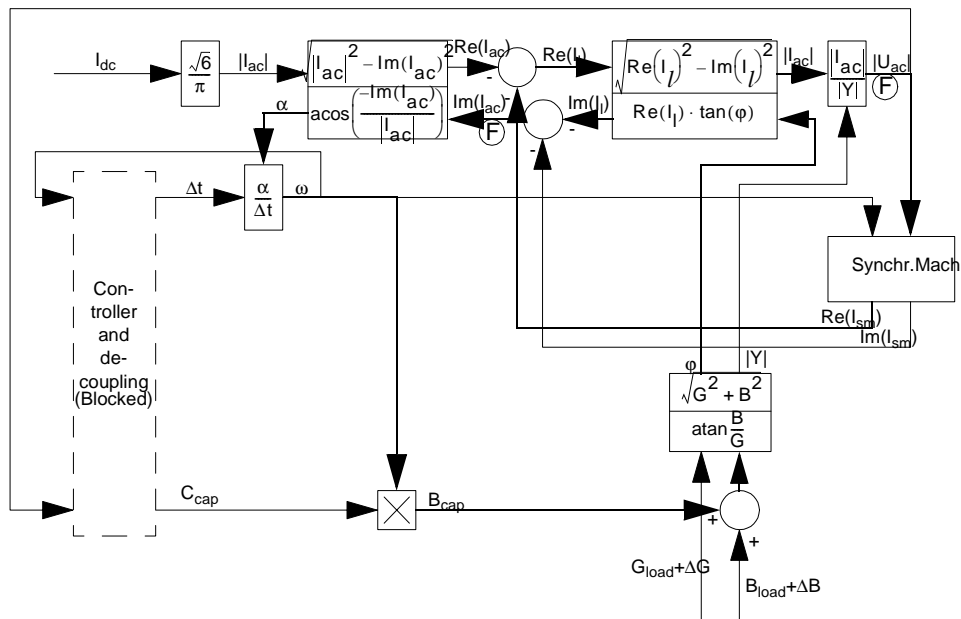


Figure 9-4 Block diagram of Simulink model with firing pulses referred to voltage at PCC.

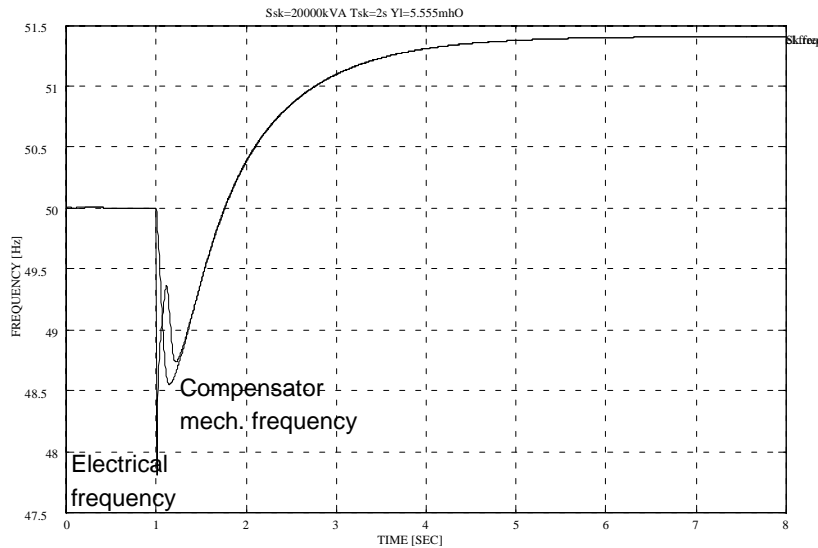


Figure 9-5 Network frequency and synchronous compensator speed after load admittance increase corresponding to a load increase from 80 MW to 100 MW. Firing pulses referred to voltage at PCC.

$\frac{1}{1 + T_f s}$  are introduced. They are placed after the calculation of the voltage and after the calculation of the imaginary part of the inverter current, at the locations marked with F. Both filters have  $T_f = 0.001 s$ .

The results of these simulations are shown in the following figures. Remember that the system is operating without controllers to check the intrinsic stability. Figure 9-5 shows the network frequency and compensator speed during the simulation, and Figure 9-6 shows the system AC RMS voltage at the point of common coupling and the DC voltage during the simulation. The depicted voltage drop and frequency rise is quite in accordance with the sign of the sensitivities found in Chapter 7. Figure 9-7 and Figure 9-8 presents the active and reactive power balance. It is noteworthy that, due to the voltage drop in this constant current system, the power dissipated in the load actually decreases when the load conductance increases. Figure 9-9 gives the extinction angle  $\gamma$  and pole wheel angle  $\beta$ . The curves shows that after some initial disturbances, both voltage and frequency drops below the initial values. As the load is resistive, the frequency has no influence on the active power consumption, which, after the switching, remains proportional to the square of the AC RMS voltage. The supplied power, however, is directly proportional to the DC voltage as the DC current is assumed to be kept constant. Even if the DC voltage drops more than proportional to the

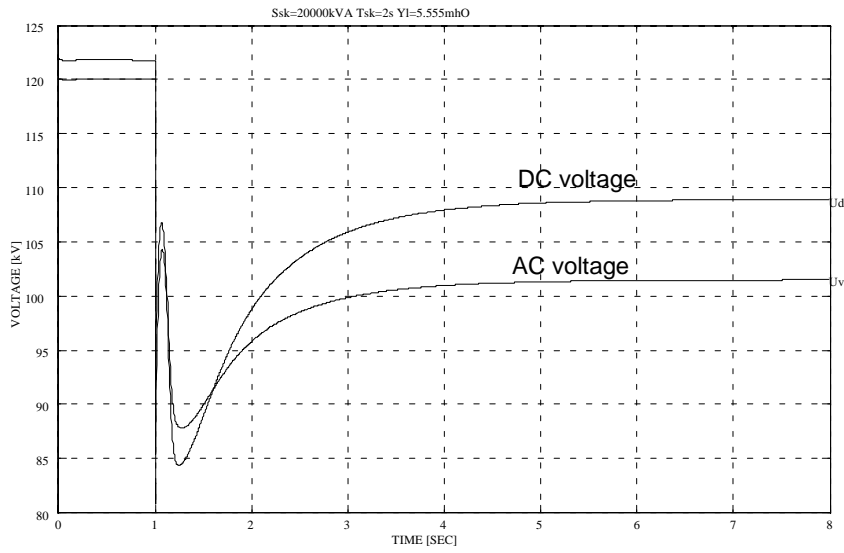


Figure 9-6 System voltages after load admittance increase corresponding to a load increase from 80 MW to 100 MW. Firing pulses referred to voltage at PCC.

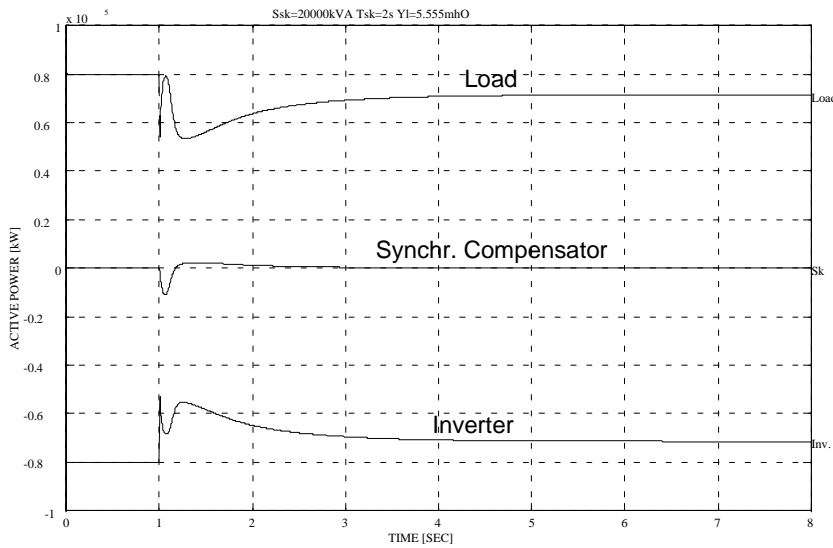


Figure 9-7 Active power balance after load admittance increase corresponding to a load increase from 80 MW to 100 MW. Firing pulses referred to voltage at PCC.

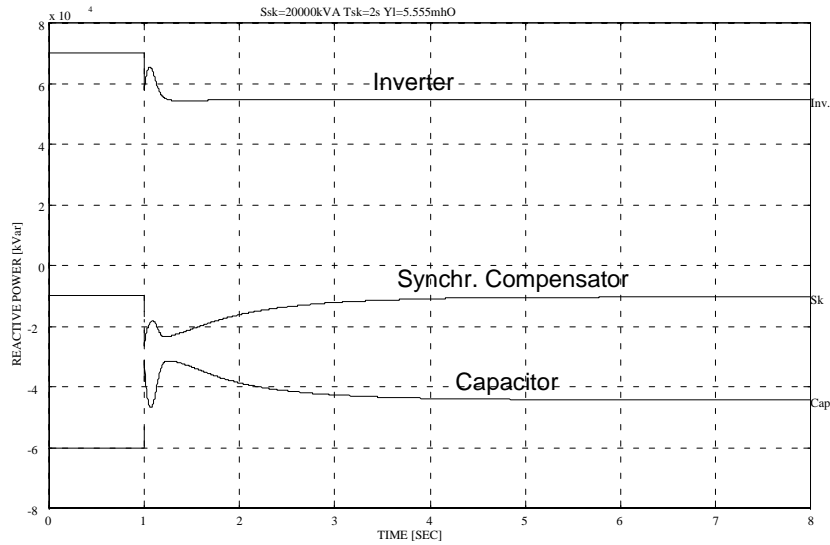


Figure 9-8 Reactive power balance after load admittance increase corresponding to a load increase from 80 MW to 100 MW. Firing pulses referred to voltage at PCC.

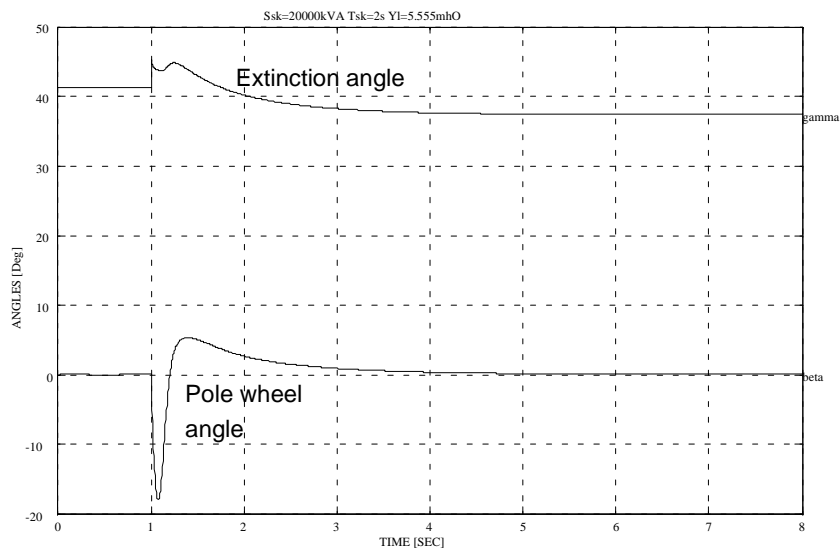


Figure 9-9 Inverter extinction angle  $\gamma$  and synchronous compensator pole wheel angle  $\beta$  after load admittance increase corresponding to a load increase from 80 MW to 100 MW. Firing pulses referred to voltage at PCC.

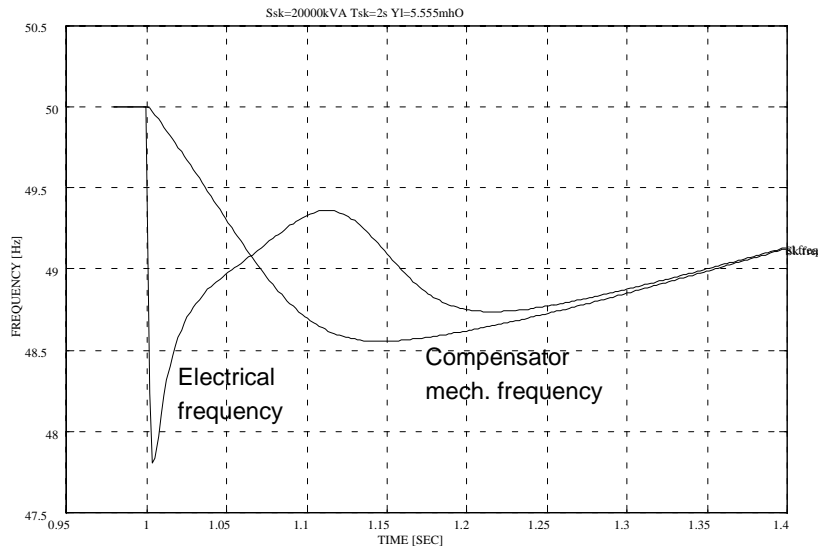


Figure 9-10 Network frequency and synchronous compensator speed during the first 0.4 s after load admittance increase corresponding to a load increase from 80 MW to 100 MW. Firing pulses referred to voltage at PCC.

AC voltage, it does not drop proportionally to the square of the AC voltage. Thus the consumed power in the load drops more than the supplied power through the DC link. The surplus of power has to be absorbed by the synchronous compensator, which accelerates accordingly after the initial drop. As the controllers are blocked, the firing delay time is kept constant and thus, due to the increasing frequency, the firing angle  $\alpha$  increases and the extinction angle  $\gamma$  decreases.

A similar development occurs for the reactive power. The produced reactive power in the capacitor drops by the square of the voltage while the consumed reactive power in the inverter drops approximately proportional to the voltage, and again, the difference has to be supplied by the compensator. In the case of reactive power, increased supply can only be achieved by increased voltage difference across the d-axis reactance. This occurs automatically when the terminal voltage drops if the excitation voltage is kept constant. In the end there must be reinstated a state where the active and reactive power are once more in balance, and this has to be achieved by a change in voltage and frequency.

As it is not easy to distinguish what happens during the first transient, Figure 9-10 shows a blow up of the frequencies and Figure 9-11 shows a blow up of the voltages during the first 0.4 s after load switch on. The curves can be interpreted as follows: Before the switching on of the additional load, it is possible to draw a phasor diagram of equivalent admittances in the network



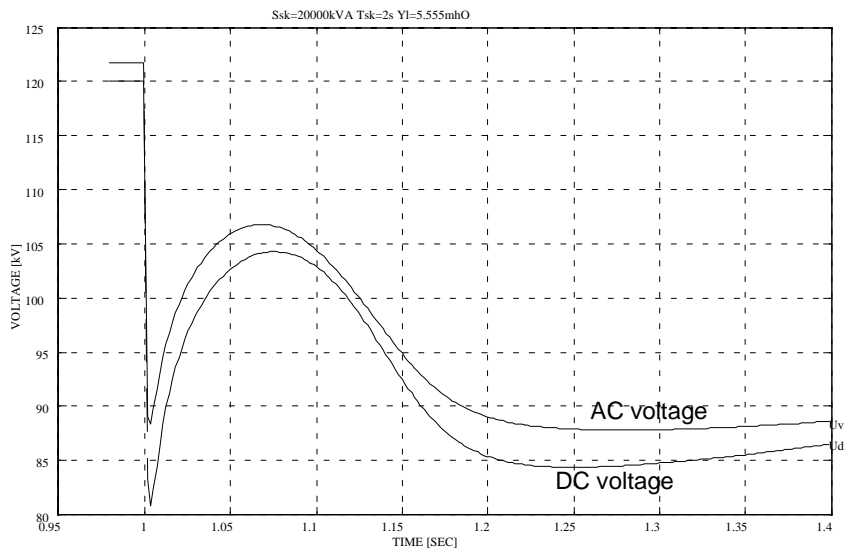


Figure 9-11 System voltages the first 0.4 s after load admittance increase corresponding to a load increase from 80 MW to 100 MW. Firing pulses referred to voltage at PCC.

as seen from the inverter terminals. This situation is shown in Figure 9-12, indicated by the indices 0. During the switching on of the additional load, the load conductance increases by  $\Delta g$  to  $g_1$ . The susceptance of the capacitors remains unchanged, but something happens to the equivalent susceptance of

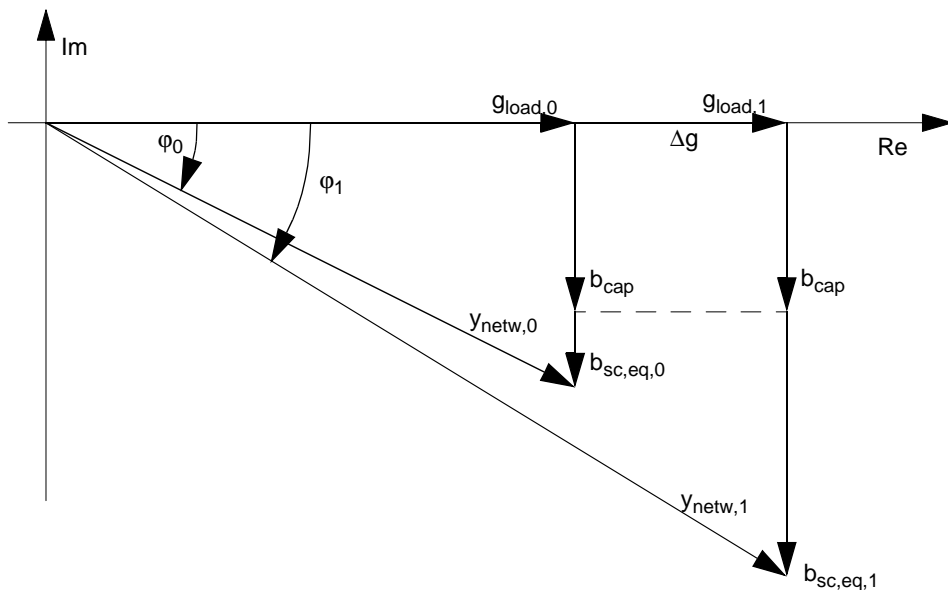


Figure 9-12 Principal phasor diagram of admittances before and some time after active load increase.

the synchronous compensator. Due to the inverter acting as a constant current source, the voltage plummets inversely proportional to the increased admittance. Due to the increased voltage difference between the unchanged (transient) EMF of the synchronous compensator and the terminal voltage, the current from the compensator increases. The fact that the compensator supplies more current at a lower terminal voltage implies a considerable increase of the equivalent susceptance of the compensator. The result is shown in Figure 9-12. The total equivalent susceptance in the network increases relatively more than the initial increase in the conductance, increasing the phase angle  $\phi$  of the network impedance. The extinction angle  $\gamma$  of the inverter must be equal to the phase angle of the network impedance. The firing delay time  $\Delta t$  is constant, and the only way to increase the extinction angle is to decrease the electrical frequency. Figure 9-10 shows that this is what happens, the frequency drops in the first instant, together with the voltage in Figure 9-11. Figure 9-13 shows that the extinction angle increases correspondingly.

The difference between the electrical and mechanical frequency is integrated into the pole wheel angle  $\beta$ , which starts to increase. This means the compensator starts to supply active power, which has to be taken from the stored kinetic energy, and the compensator starts to slow down. The supply of power from the compensator reverses the initial process and forces the voltage upwards again. The increased voltage reduces the reactive current from the compensator and thus reduces the equivalent susceptance. At the same time

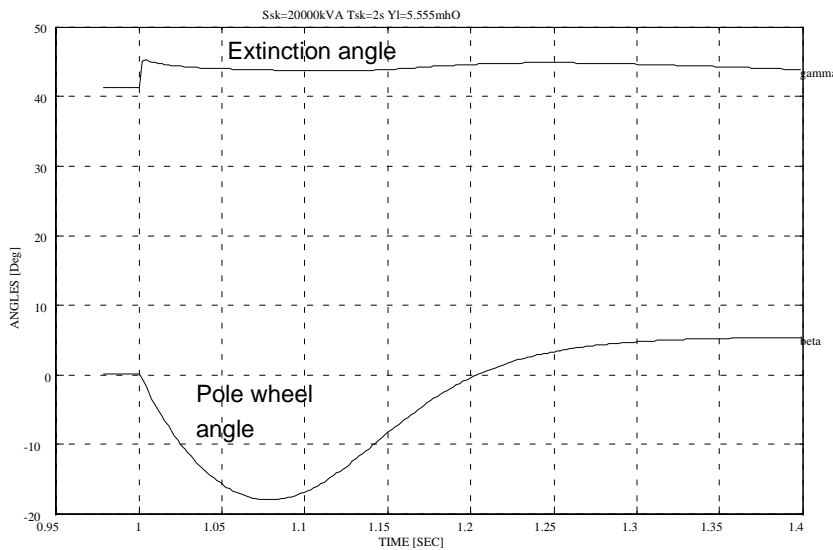


Figure 9-13 Inverter extinction angle  $\gamma$  and synchronous compensator pole wheel angle  $\beta$  in the first 0.4 s after load admittance increase corresponding to a load increase from 80 MW to 100 MW. Firing pulses referred to voltage

the active current from the compensator introduces a negative conductance in the system as seen from the inverter, but the result is a reduced network phase angle  $\varphi$  and extinction angle  $\gamma$ , and an increased firing angle  $\alpha$ , which has to be achieved by an increased electrical voltage frequency  $\omega_{el}$ . The supply of power from the compensator increases as the pole wheel angle  $\beta$  increases. This process goes on until the electrical frequency matches mechanical frequency. At this point the pole wheel angle and power supply from the compensator are at maximum. When the power from the compensator starts to drop, the voltage cannot be maintained any more and starts dropping as well. The decreasing power from the compensator further reduces the phase angle, therefore the electrical frequency continues to increase for some time, until the increase in reactive power from the compensator gets the upper hand and forces the phase angle to increase and the frequency to decrease again. Eventually the synchronous compensator ceases to supply and starts to absorb active power, and we are into the situation described earlier in this chapter. The electrical frequency stabilizes near the mechanical, leaving a negative pole wheel angle pulling the compensator and network frequency upwards until a stable working point is reached. The locus plot of the resulting impedance phasor during the first 0.4 s after load switching is shown in Figure 9-14. This can be compared to the phasor diagram in Figure 9-12.

In this section we have defined a model based on quasi-phasors. The model takes the reference for the firing pulses from the voltage at PCC. Consequently it is natural to select the real axis along the voltage phasor in this point also.

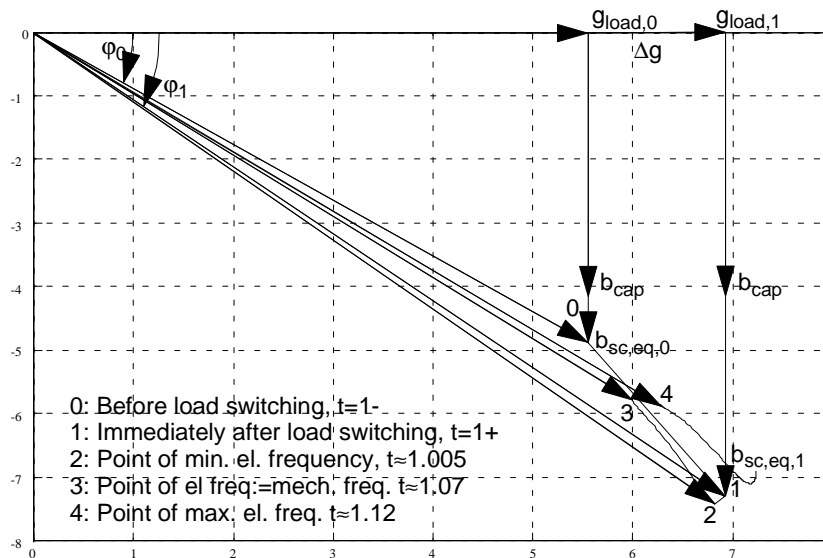


Figure 9-14 Locus plot for the resulting network impedance phasor during the first 0.4 s after load admittance increase corresponding to a load increase from 80 MW to 100 MW. Firing pulses referred to voltage at PCC.

The model gives an initially surprising result. If we increase the conductance of the load in order to increase the load, the active power actually decreases. This is due to the fact that the model is based on a current source, not a voltage source. More astounding, but in accordance with what has been found in previous chapters, the frequency of the system rises when we try to increase the load.

#### 9. 4. 2 System with reference for the firing pulses given by the EMF of the compensator

As mentioned earlier, an alternative way of controlling the system is to select the induced voltage (EMF) of the synchronous compensator as reference for the firing pulses to the thyristors. Then it will be a natural choice to select the real axis of the quasi-phasor model along the phasor of the R-phase voltage in this point. This phasor lies along the q-axis of the synchronous compensator. The choice of reference for the firing pulses makes this a different system from the previous.

By selecting the real axis of the phasor system along the q-axis of the synchronous machine, the real and imaginary parts of the EMF become equal to the q- and d-axis voltages of the machine, only the sign of the d-axis voltage must be changed. The same applies for the currents. The phase angle of the PCC voltage becomes equal to the pole wheel angle  $\beta$ . The phase angle of the current is given by the angle of the current vector in the dq-plane  $\zeta$ . The difference  $\zeta - \beta$  is the traditional phase angle  $\phi$ , see Figure 9-15.

This implies another sequence of calculations and the block schematic will then be as shown in Figure 9-16. This system also contains at least two algebraic loops in the process, indicated by the bold lines. There is also the direct algebraic connection from load admittance to voltage, giving rise to immediate responses. It shall be noted that the electrical frequency is not a state variable in this simulation, and must be calculated separately. The phase angle of the PCC voltage, compared to the EMF of the compensator is calculated in order to know the pole wheel angle  $\beta$ . The derivative of this value is the difference between electrical and mechanical frequency, which is needed to calculate the influence of the damping. Hence the electrical frequency is also calculated. To break the algebraic loops in the model, similar filters to the previous case are inserted. This time the locations are after the calculations of real and imaginary voltages. Both filters have  $T_f = 0.001 s$ . A third filter is inserted to dampen the derivative of the pole wheel angle  $\beta$ , when it steps from one value to another at load switching, thereby creating a dirac pulse in the electrical frequency which disappears in the presentation of the curves. Also here the filters are indicated by F.

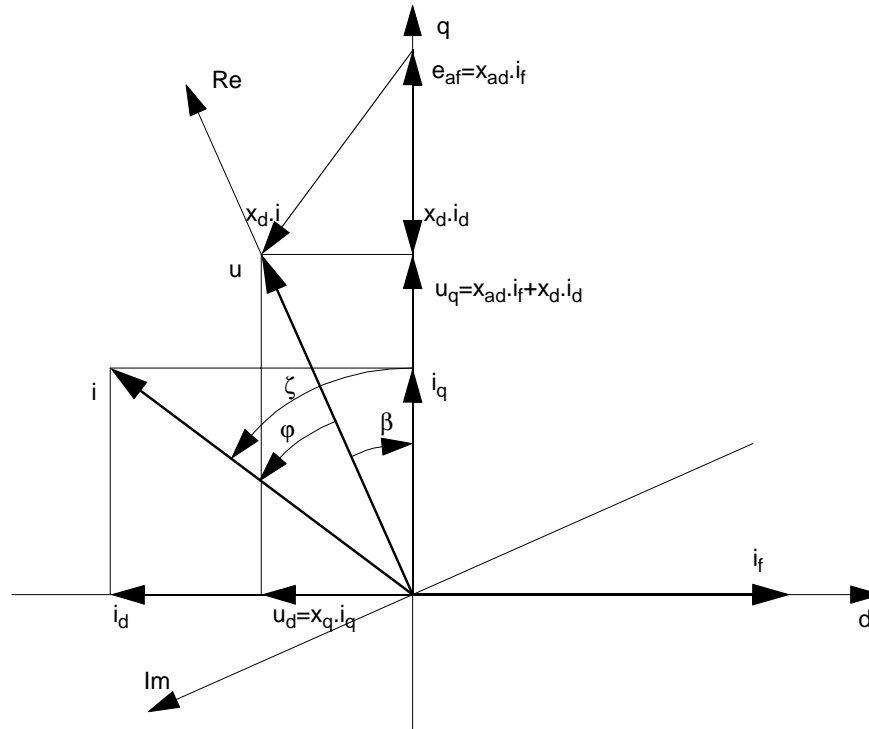


Figure 9-15 Connection between dq-vectors and quasi-phasors in the synchronous machine

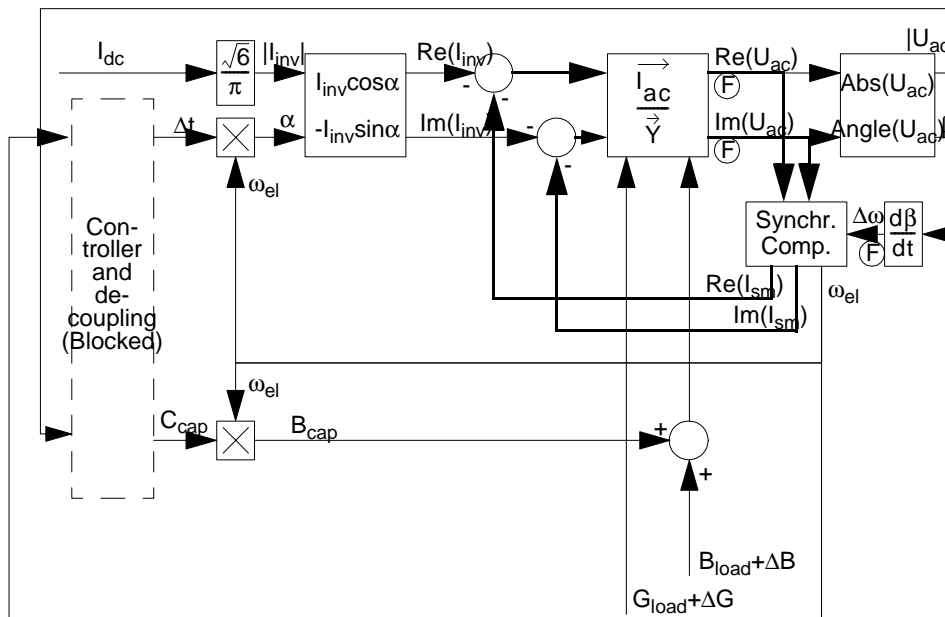


Figure 9-16 Block diagram of Simulink model with real axis given by EMF voltage

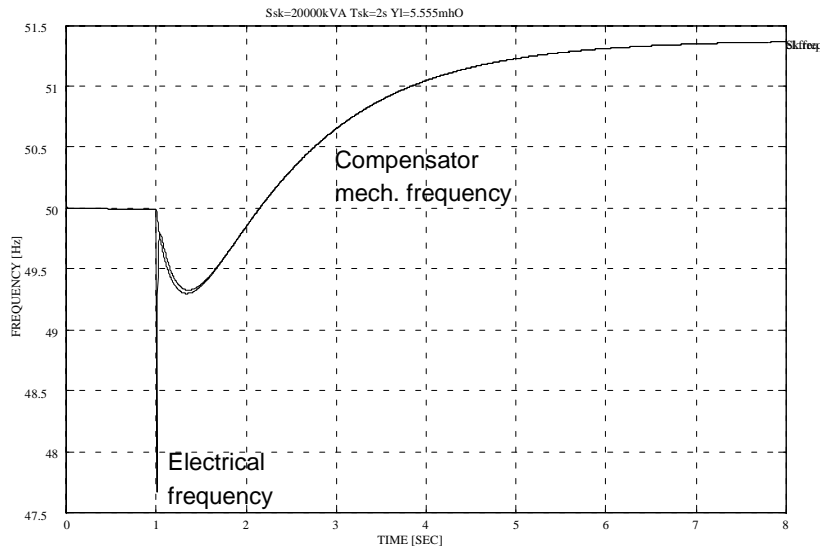


Figure 9-17 Network frequency and synchronous compensator speed after load admittance increase corresponding to a load increase from 80 MW to 100 MW. Firing pulses referred to EMF.

The system is simulated under the same conditions as the previous model and the results of this simulation are shown in the following figures. Remember that this system too is operating without controllers to check the intrinsic stability. Figure 9-17 shows the network frequency and compensator speed during the simulation of an increase of the admittance equivalent of a load increase from 80 MW to 100 MW at constant voltage. The details at load switching will be discussed later, in conjunction with the more detailed Figure 9-22, Figure 9-23 and Figure 9-24. At present it is only to be pointed out that the frequency drop, represented by the mechanical frequency, is less than in the previous case, Figure 9-5, and the difference between electrical and mechanical frequency is less after the initial disturbances. On the other hand, the system reacts slower when it comes to approach the stable state.

Figure 9-18 depicts the system AC RMS voltage at the point of common coupling and the DC voltage during the simulation. Figure 9-19 and Figure 9-20 presents the active and reactive power balance. The long-term processes governing this system are the same as described in the previous case and the principal development is the same. But, as the electrical frequency in the last example is far closer tied to the mechanical frequency, the changes in pole wheel angle are slower and smaller. Therefore the response of the total system to disturbances in load conductance is distinctly slower than the previous system, presented in Figure 9-6, Figure 9-7 and Figure 9-8.

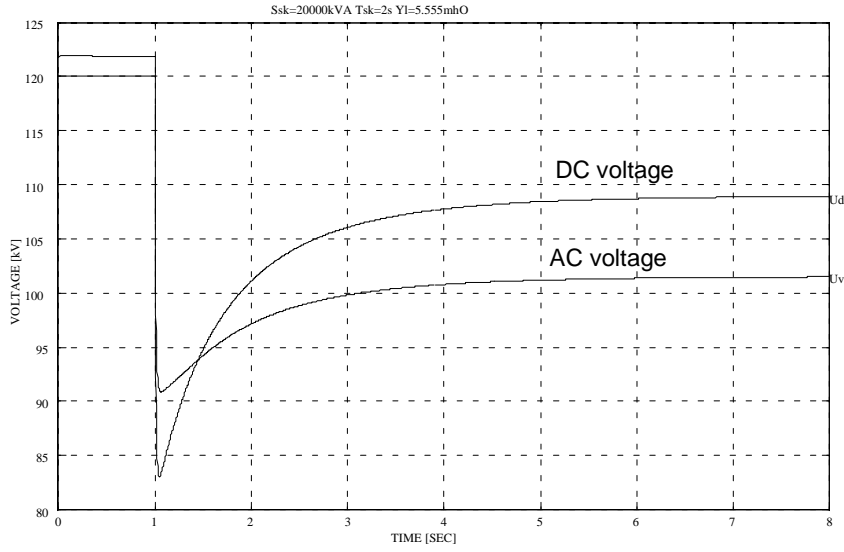


Figure 9-18 System voltages after load admittance increase corresponding to a load increase from 80 MW to 100 MW. Firing pulses referred to EMF.

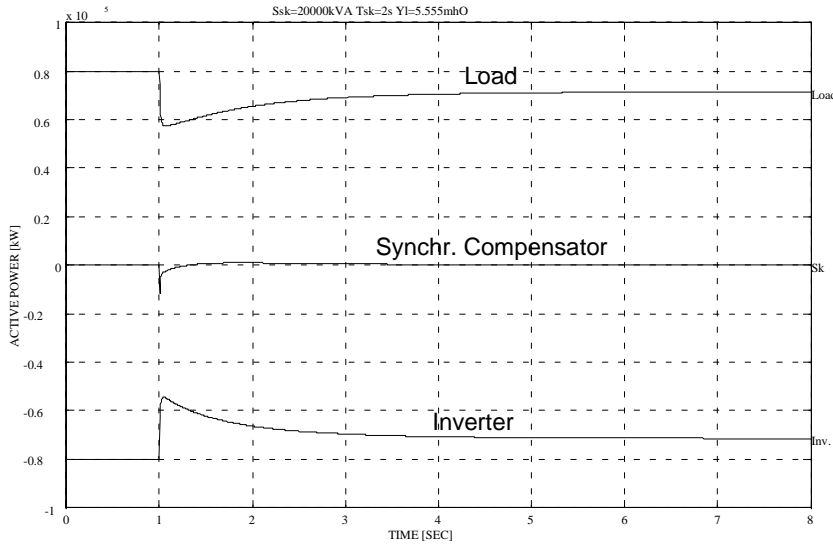


Figure 9-19 Active power balance after load admittance increase corresponding to a load increase from 80 MW to 100 MW. Firing pulses referred to EMF.

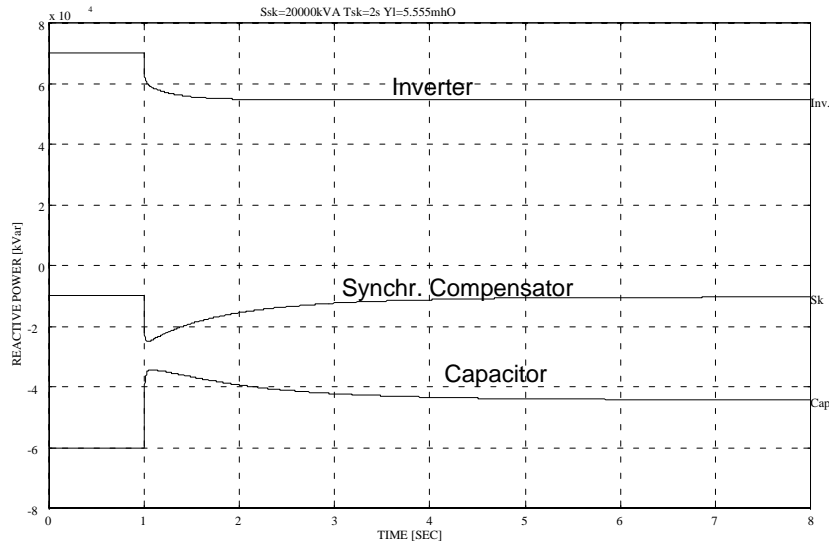


Figure 9-20 Reactive power balance after load admittance increase corresponding to a load increase from 80 MW to 100 MW. Firing pulses referred to EMF.

Figure 9-21 shows the extinction angle  $\gamma$ , and pole wheel angle  $\beta$ . It must be remembered that in this simulation the extinction angle relates to the reference for the firing pulses, the EMF of the synchronous converter which constitutes the real axis. The true extinction angle as related to the network voltage is the sum of the recorded angles  $\gamma$  and  $\beta$ . This true extinction angle is also shown in the figure. Compare to Figure 9-9

The difference between the models lies mainly in the behaviour immediately after the disturbance. In order to investigate this period closer, the same figures as in the previous case are enlarged to display a better view of the first 0.4 s after the load switch on. The electrical and mechanical frequencies are shown in Figure 9-22. In comparison to the previous simulation, see Figure 9-10, the electrical frequency rises much faster from the initial drop. The reason for this is that in this case the voltage at PCC is allowed to shift freely in phase compared to the real axis, which lies along the EMF in the q-axis of the machine. The voltage also shifts freely compared to the current, which is tied to the Q-axis by a constant firing delay time. When the voltage phasor can move swiftly, the derivative of the phase angle is large, and the variations in electrical frequency becomes large. These fast, apparent frequency changes may rather be interpreted as voltage phase-shifts. When the voltage shifts phase swiftly, it also means that the pole wheel angle  $\beta$  shifts swiftly, and the compensator can swiftly change its supply of active power. Therefore the initial increase of power is fast.



Immediately afterwards the frequencies are closely tied again and the

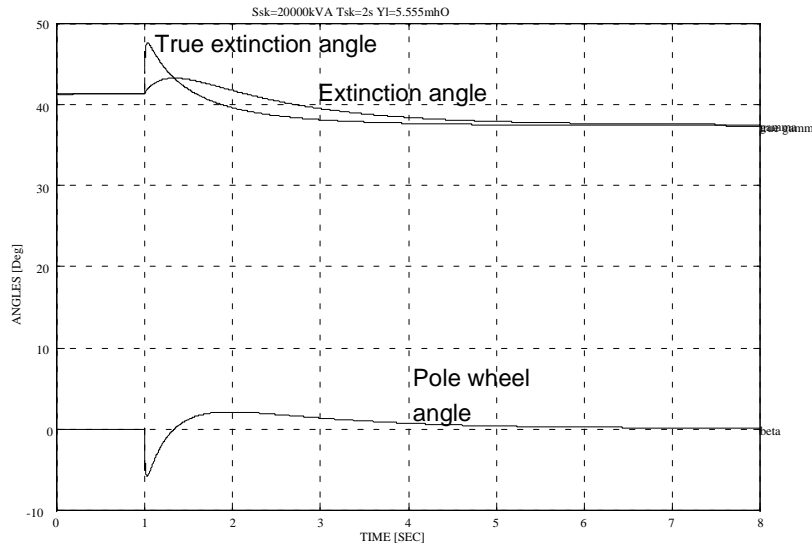


Figure 9-21 Inverter extinction angle  $\gamma$  and synchronous compensator pole wheel angle  $\beta$  after load admittance increase corresponding to a load increase from 80 MW to 100 MW. Firing pulses referred to EMF.

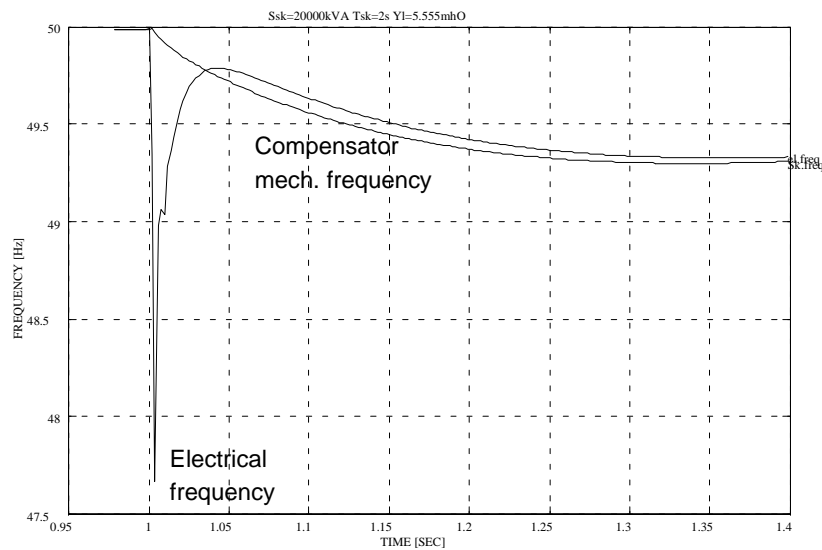


Figure 9-22 Network frequency and synchronous compensator speed the first 0.4 s after load admittance increase corresponding to a load increase from 80 MW to 100 MW. Firing pulses referred to EMF.

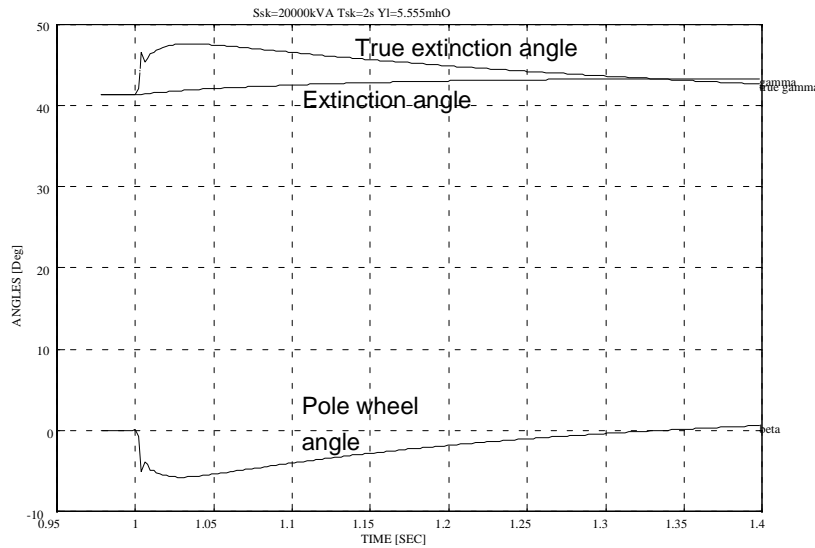


Figure 9-23 Extinction angle and pole wheel angle the first 0.4 s after load admittance increase corresponding to a load increase from 80 MW to 100 MW. Firing pulses referred to EMF.

change in pole wheel angle and supplied power is slow. This can be seen in Figure 9-23, where the extinction angle related to the EMF and pole wheel angle are shown, together with the true extinction angle as related to the voltage at the PCC. The derivative of the change in  $\beta$  is reflected as variations in the electrical voltage frequency in Figure 9-22. In Figure 9-23 it can be noted that there is no dramatic change in the extinction angle  $\gamma$ , related to the EMF. The changes are only due to the slowly varying mechanical frequency. It is also to be noted that there is even less possibilities for a lasting difference of importance between electrical and mechanical frequency in this case, as the frequency of the current is locked to the mechanical frequency. Therefore the deflection in the pole wheel angle  $\beta$  is less, and the compensator gives less contribution to keep the balance of active power. Therefore also the DC voltage has to drop further than in the previous simulation, as can be seen in Figure 9-24, which depicts the AC and DC voltages. Compare this figure with Figure 9-11. The drop in the DC voltage is reflected in a larger change in the true extinction angle as well. The phasor diagram of the load admittance is equivalent to that in Figure 9-12 but the locus plot of the change is distinctly different, as can be seen in Figure 9-25.

In this section we have modelled a second system based on quasi-phasors. This system take the reference for the firing pulses from the EMF of the compensator, and places the real axis along the voltage phasor in this point. The simulations give basically the same results. But the second system

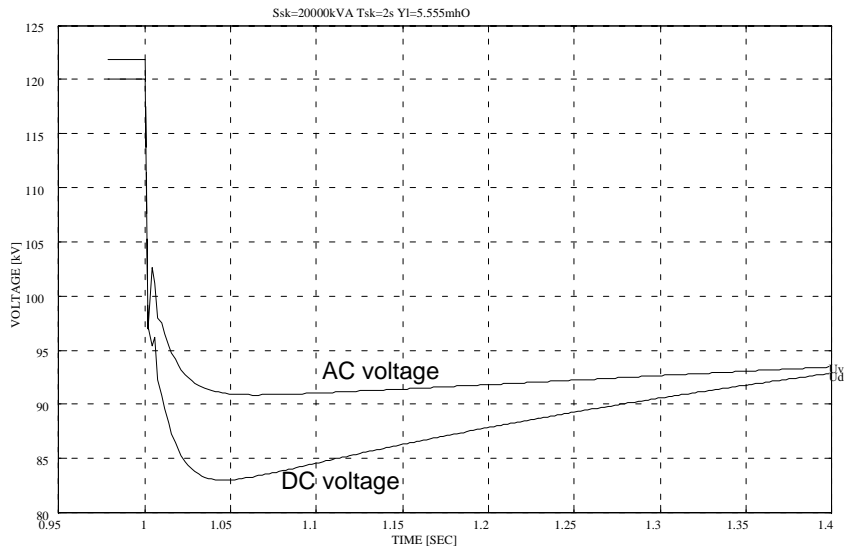


Figure 9-24 AC and DC voltages the first 0.4 s after load admittance increase corresponding to a load increase from 80 MW to 100 MW. Firing pulses referred to EMF.

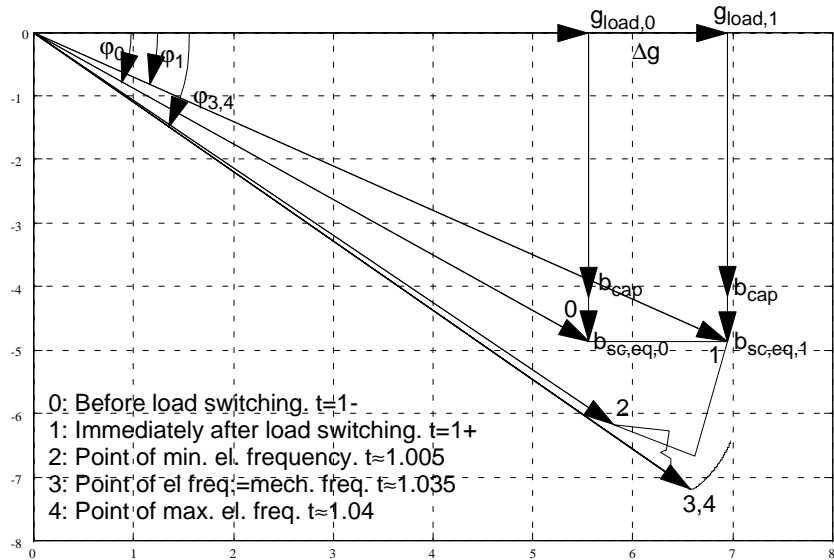


Figure 9-25 Locus plot for the resulting network impedance phasor during the first 0.4 s after load admittance increase corresponding to a load increase from 80 MW to 100 MW. Firing pulses referred to EMF.

includes the inertia of the converter in a better way, giving a more stable reference for the firing pulses to the thyristors, consequently the whole system is more stable.

### **9.4.3 Conclusion**

Both these systems are intrinsically stable for the calculated load case, at least as long as the load is not frequency dependent. For systems containing motors, however, this is not necessarily so. The motor load is dependent on the frequency. Of the two examined systems, the system which uses the EMF as reference for the firing pulses is more stable, but reacts slower than the system which takes the reference from the voltage at PCC. Both systems end in the same stationary state.

## **9.5 VERIFICATION SIMULATIONS BY KREAN**

In order to verify the results of the Matlab/Simulink simulations a corresponding model was created in KREAN, based on the KREAN models which have been used earlier. The main difference from the previous KREAN models is that the phase-locked loop, which was needed to determine zero crossings of the voltages, has been removed. In the case where the firing pulse reference is taken from the voltage at PCC, the necessary filtering of the voltage is performed by a  $60^\circ$  filter, i.e. a low pass filter with breakpoint at 28.86 Hz. This filter has a phase displacement of  $60^\circ$  and a damping of 6dB at 50 Hz. This phase displacement is compensated by a corresponding reduction of 3.33 ms of the firing delay time. This is acceptable as the network frequency do not vary much from 50 Hz. When the reference for the firing pulses is the EMF, the EMF is simulated by a three-phase voltage source with variable frequency given by the mechanical frequency of the synchronous compensator.

### **9.5.1 Voltage at PCC as reference**

The results of the KREAN simulations using the voltage at PCC as reference are shown in the following figures. Figure 9-26 depicts the electrical and mechanical frequencies in comparison to Figure 9-5. All the comparisons will be discussed later. Figure 9-27 shows the RMS line voltage and DC voltage in comparison to Figure 9-6. The RMS voltage is measured as the three line voltages rectified in a six-pulse rectifier with resistive load and damped through a low pass filter with DC damping 1/1.35 and breakpoint frequency

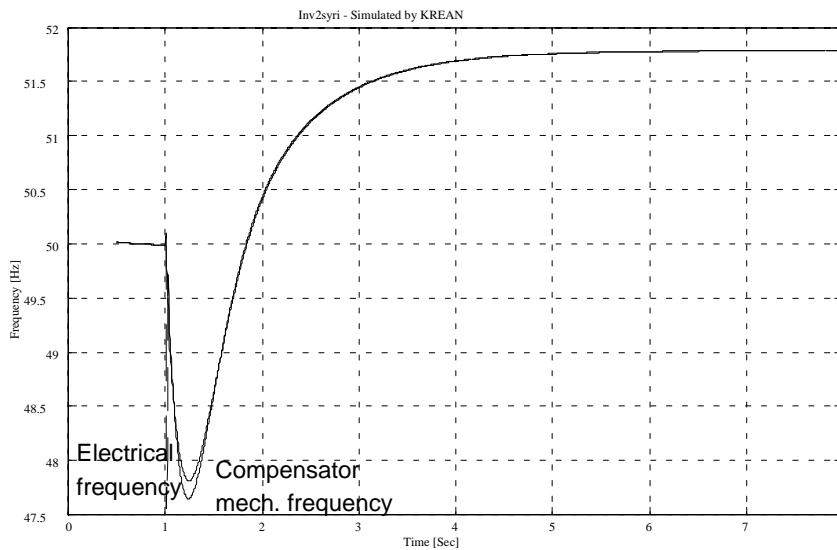


Figure 9-26 Network frequency and synchronous compensator speed after load admittance increase corresponding to a load increase from 80 MW to 100 MW. Firing pulses referred to voltage at PCC. Simulated by KREAN

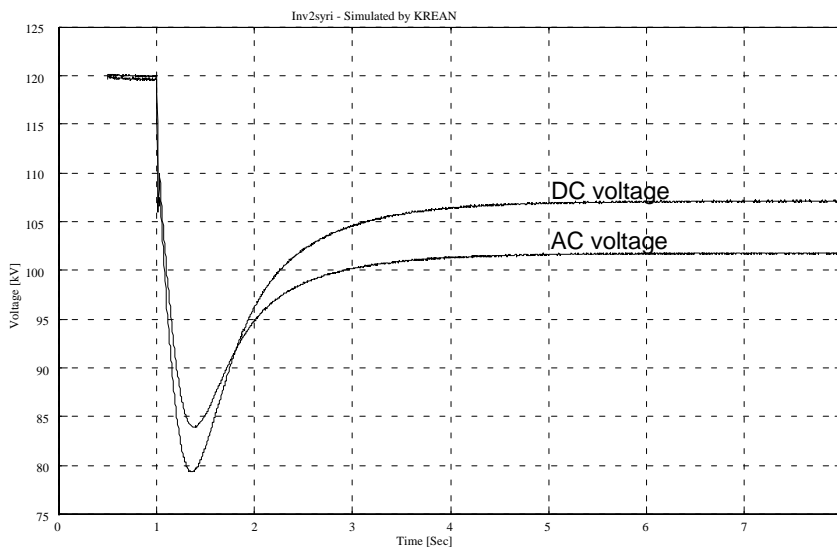


Figure 9-27 System voltages after load admittance increase corresponding to a load increase from 80 MW to 100 MW. Firing pulses referred to voltage at PCC. Simulated by KREAN

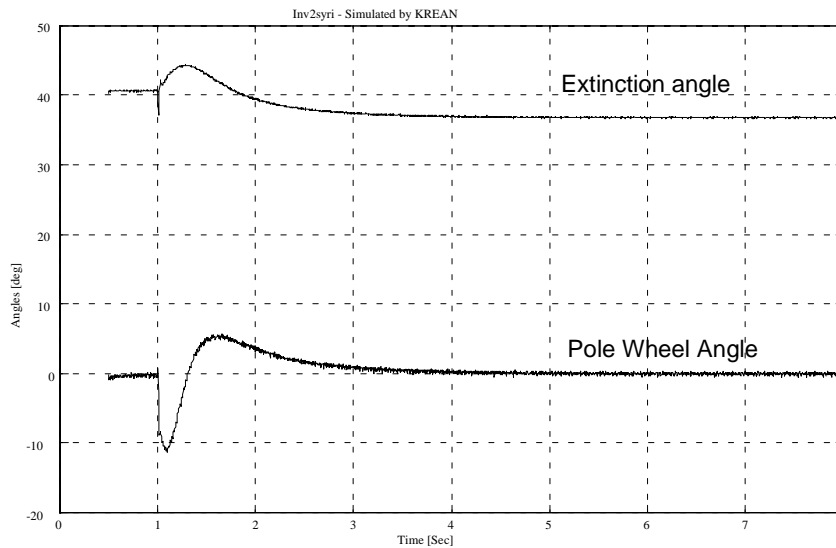


Figure 9-28 Synchronous compensator pole wheel angle  $\beta$  and inverter extinction angle  $\gamma$  after load admittance increase corresponding to a load increase from 80 MW to 100 MW. Firing pulses referred to voltage at PCC. Simulated by KREAN

50 Hz. This gives an additional damping of the 6-pulse ripple of 15.7 dB. The selection of the filter parameters is a compromise between good damping of the ripple and sufficient response to variations in RMS values. Figure 9-28 shows the pole wheel angle  $\beta$  and inverter extinction angle  $\gamma$  in comparison to Figure 9-9. The pole wheel angle  $\beta$  cannot be directly measured in KREAN and is calculated on basis of the synchronous compensator d- and q-axis voltages. The inverter extinction angle  $\gamma$  also cannot be directly measured in KREAN and is calculated from the AC and DC voltage.

As in the Matlab simulations, the first 0.4 s after the load switching has been blown up in order to see the details. The frequencies are shown in Figure 9-29, in comparison to Figure 9-10. The voltages are shown in Figure 9-30, in comparison to Figure 9-11. The pole wheel angle and inverter extinction angle are shown in Figure 9-31, in comparison to Figure 9-13. In Figure 9-32 the instantaneous phase voltage in phase R is shown, together with the RMS line voltage.

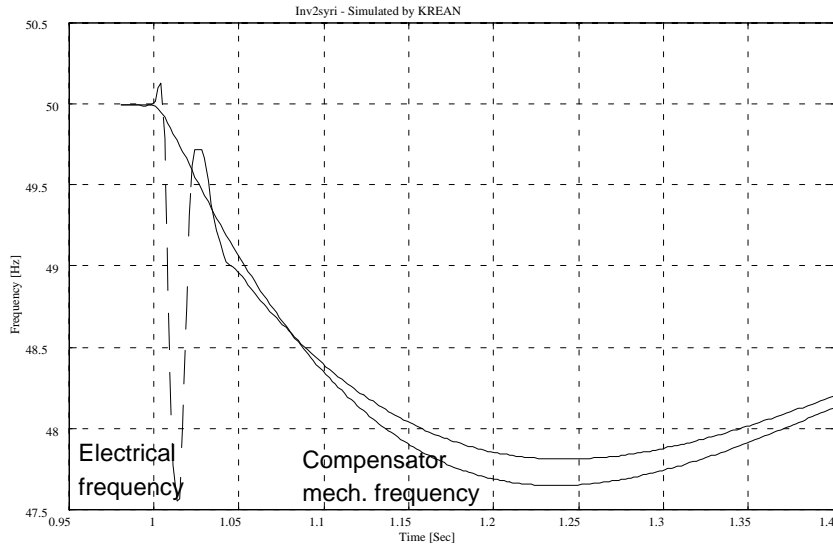


Figure 9-29 Network frequency and synchronous compensator speed the first 0.4 s after load admittance increase corresponding to a load increase from 80 MW to 100 MW. Firing pulses referred to voltage at PCC. Simulated by KREAN

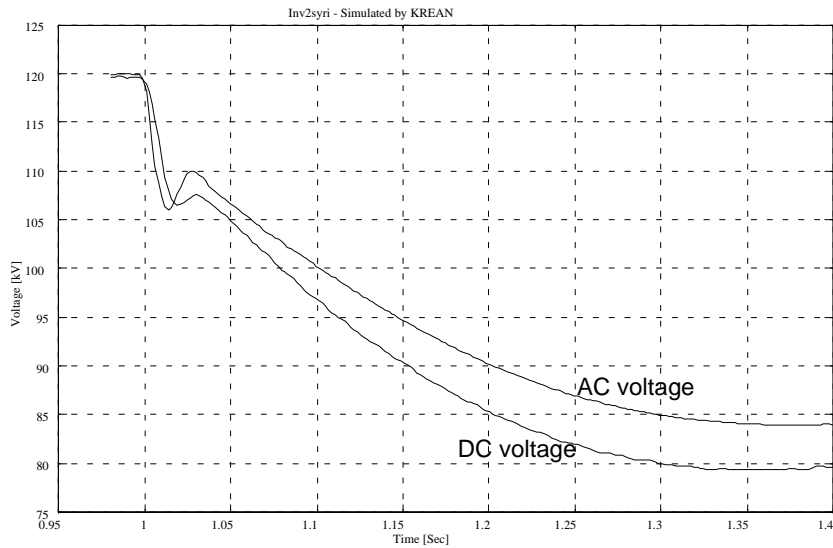


Figure 9-30 System voltages the first 0.4 s after load admittance increase corresponding to a load increase from 80 MW to 100 MW. Firing pulses referred to voltage at PCC. Simulated by KREAN

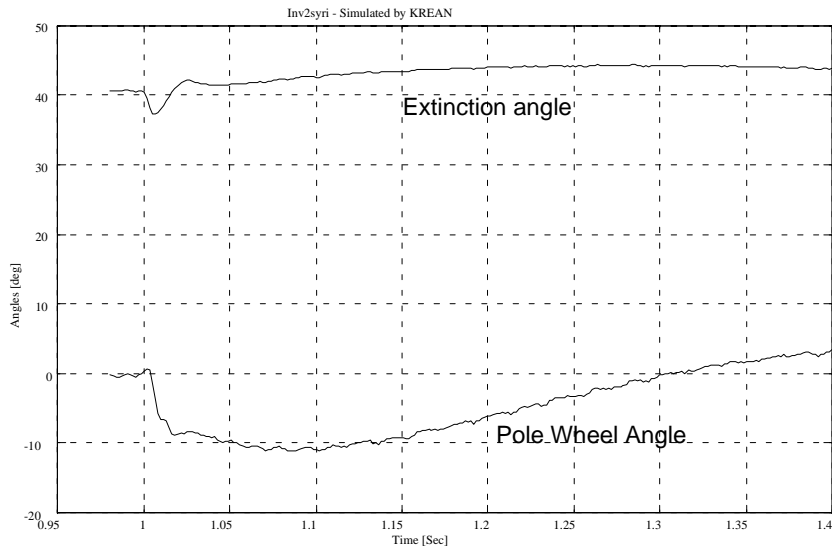


Figure 9-31 Synchronous compensator pole wheel angle  $\beta$  and inverter extinction angle  $\gamma$  the first 0.4 s after load admittance increase corresponding to a load increase from 80 MW to 100 MW. Firing pulses referred to voltage at PCC. Simulated by KREAN

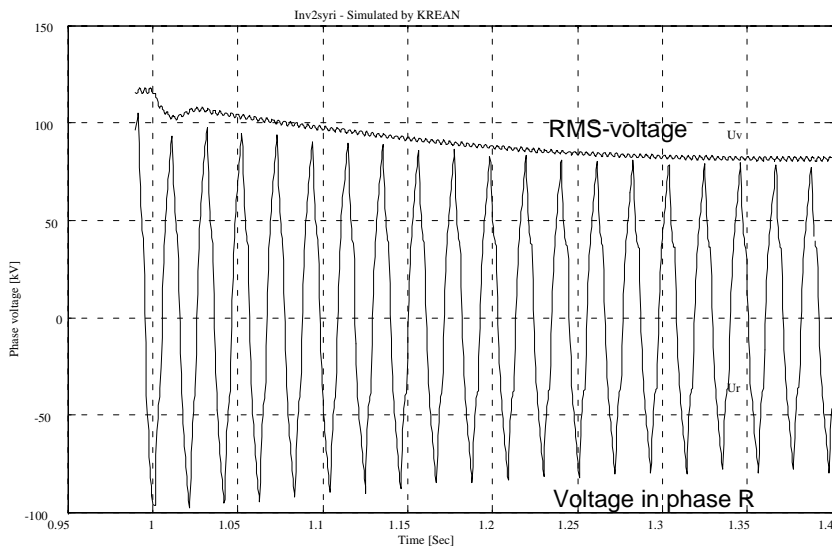


Figure 9-32 Voltage in phase R, compared with RMS line voltage the first 0.4 s after load admittance increase corresponding to a load increase from 80 MW to 100 MW. Firing pulses referred to voltage at PCC. Simulated by KREAN



### 9.5.2 EMF in the synchronous compensator as reference

The results of the KREAN simulations using the EMF in the synchronous compensator as reference are presented in the following figures, Figure 9-33 shows the electrical and mechanical frequencies in comparison to Figure 9-17. Figure 9-34 shows the RMS line voltage and DC voltage in comparison to Figure 9-18. Figure 9-35 shows the pole wheel angle  $\beta$  and inverter extinction angle  $\gamma$  in comparison to Figure 9-21.

The blown up frequencies are illustrated in Figure 9-36, in comparison to Figure 9-22. The voltages are shown in Figure 9-37, in comparison to Figure 9-24. The pole wheel angle and inverter extinction angle are shown in Figure 9-38, in comparison to Figure 9-23. The instantaneous phase voltage in phase R is given in Figure 9-39, together with the RMS line voltage.

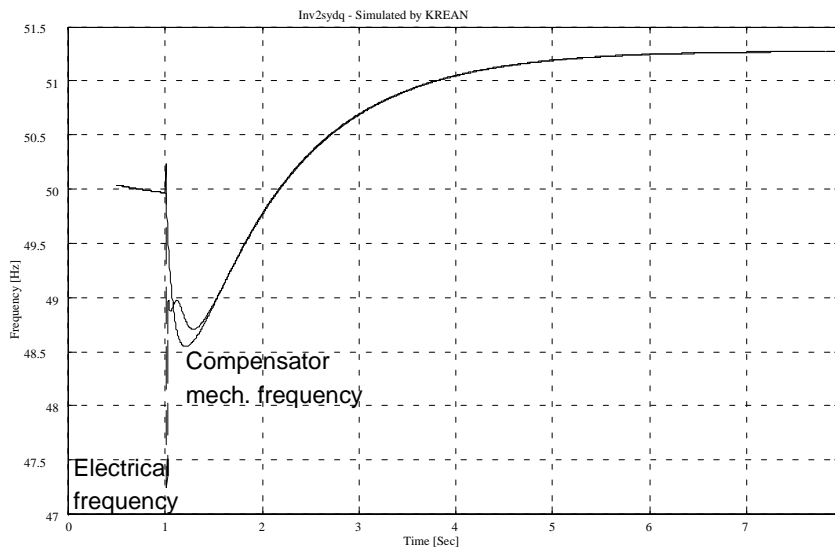


Figure 9-33 Network frequency and synchronous compensator speed after load admittance increase corresponding to a load increase from 80 MW to 100 MW. Firing pulses referred to EMF. Simulated by KREAN

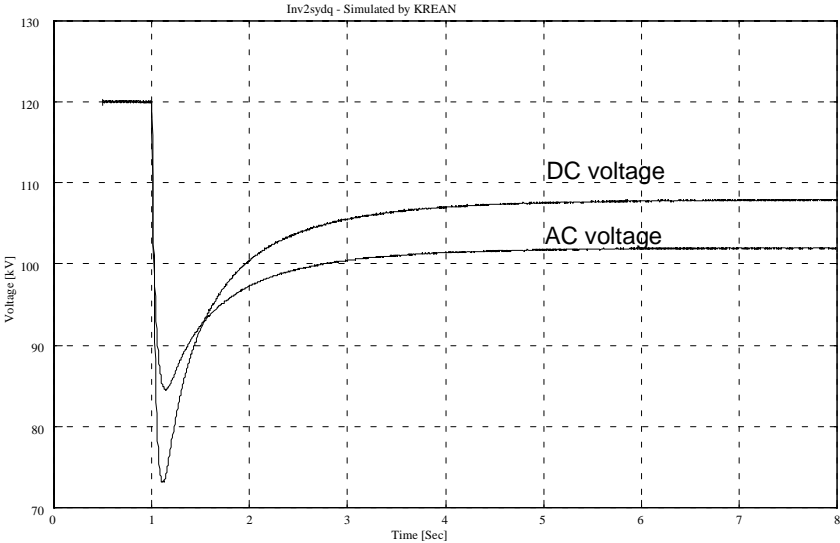


Figure 9-34 System voltages after load admittance increase corresponding to a load increase from 80 MW to 100 MW. Firing pulses referred to EMF. Simulated by KREAN

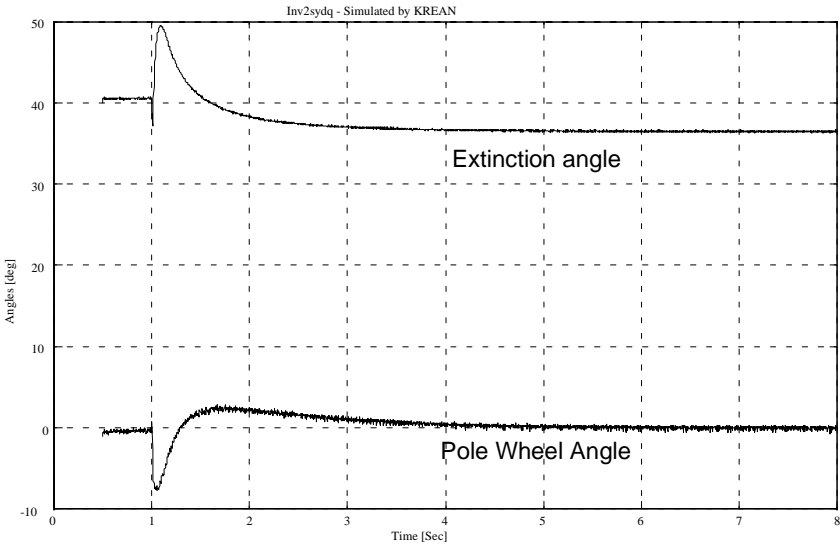


Figure 9-35 Synchronous compensator pole wheel angle  $\beta$  and inverter extinction angle  $\gamma$  after load admittance increase corresponding to a load increase from 80 MW to 100 MW. Firing pulses referred to EMF. Simulated by KREAN

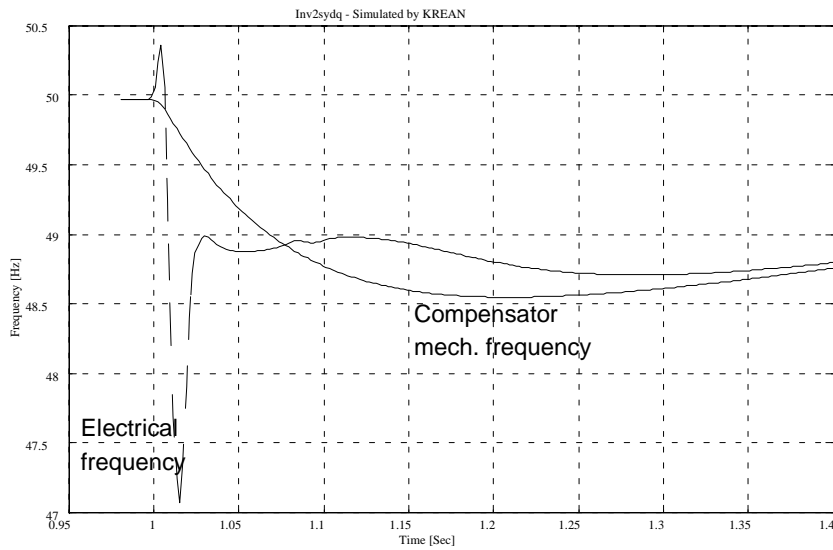


Figure 9-36 Network frequency and synchronous compensator speed the first 0.4 s after load admittance increase corresponding to a load increase from 80 MW to 100 MW. Firing pulses referred to EMF. Simulated by KREAN

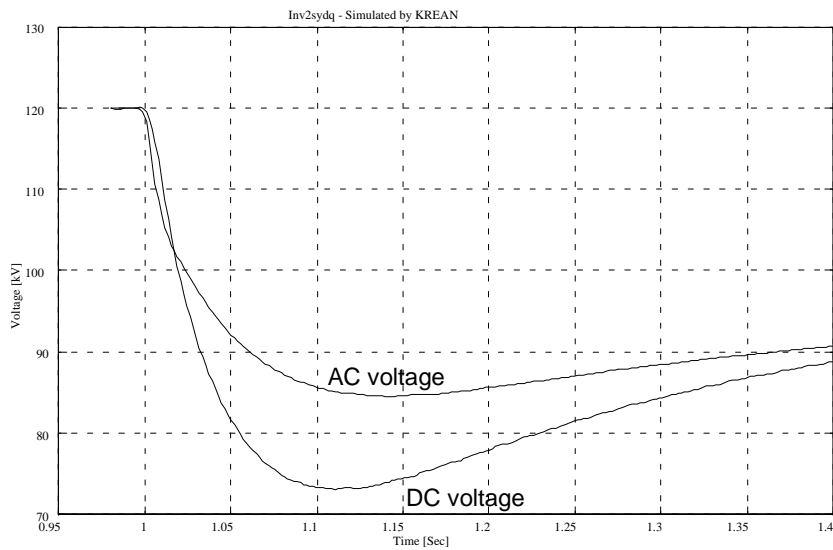


Figure 9-37 System voltages the first 0.4 s after load admittance increase corresponding to a load increase from 80 MW to 100 MW. Firing pulses referred to EMF. Simulated by KREAN

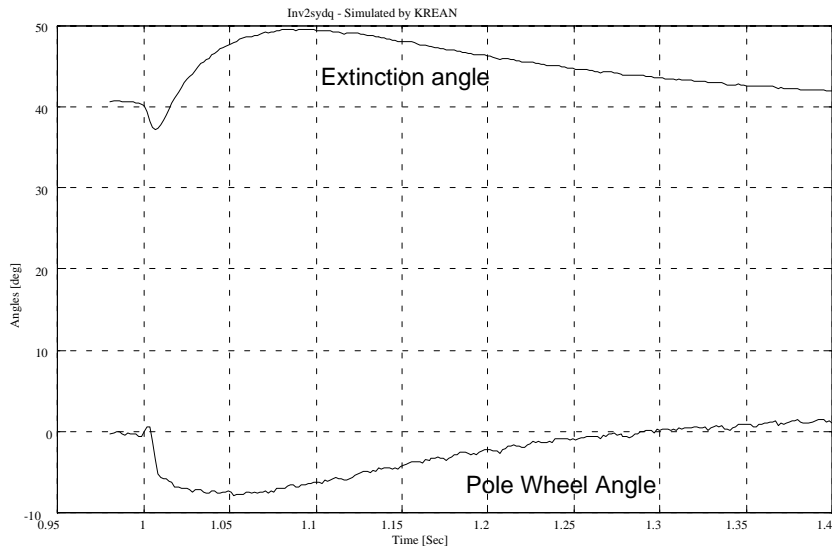


Figure 9-38 Synchronous compensator pole wheel angle  $\beta$  and inverter extinction angle  $\gamma$  the first 0.4 s after load admittance increase corresponding to a load increase from 80 MW to 100 MW. Firing pulses referred to EMF. Simulated by KREAN

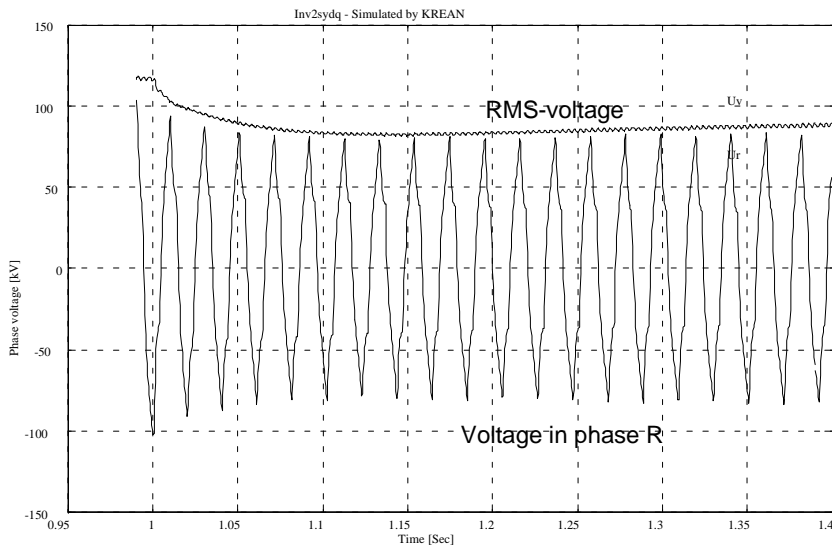


Figure 9-39 Voltage in phase R, compared with RMS line voltage the first 0.4 s after load admittance increase corresponding to a load increase from 80 MW to 100 MW. Firing pulses referred to EMF. Simulated by KREAN

### 9.5.3 Comparison of results

In order to simplify the comparison, the figures are redrawn, each figure featuring one and the same parameter from all simulations. The curves for the whole simulation time are presented, together with the details of the initial 0.4 s. Figure 9-40 shows the comparison of the line voltage during the whole simulation and Figure 9-41 shows the blow up of the initial 0.4 s. The first thing to notice is that all models arrive at the same voltage level within 2 s. after the disturbance, and the final values are equal. The KREAN models give somewhat deeper voltage drop, but the difference is tolerable, about 5 % of the initial value. The blow up shows that there is a difference between the systems taking the reference from the voltage at PCC and the models taking the reference from the EMF. Both in Matlab and KREAN, the former shows an initial drop, followed by a temporary rise and another drop. The latter shows a monotonous drop until the minimum value. Otherwise the KREAN models react slower, due to the more correct dynamic behaviour of the synchronous compensator.

Figure 9-42 shows the comparison of the electrical frequency during the whole simulation and Figure 9-43 shows the blow up of the initial 0.4 s. The curves converge to a common value, about 51.3 Hz. The exception is the KREAN simulation with reference from the PCC voltage, which ends up about 0.5 Hz higher. Looking at the blow up, however, it seems to indicate

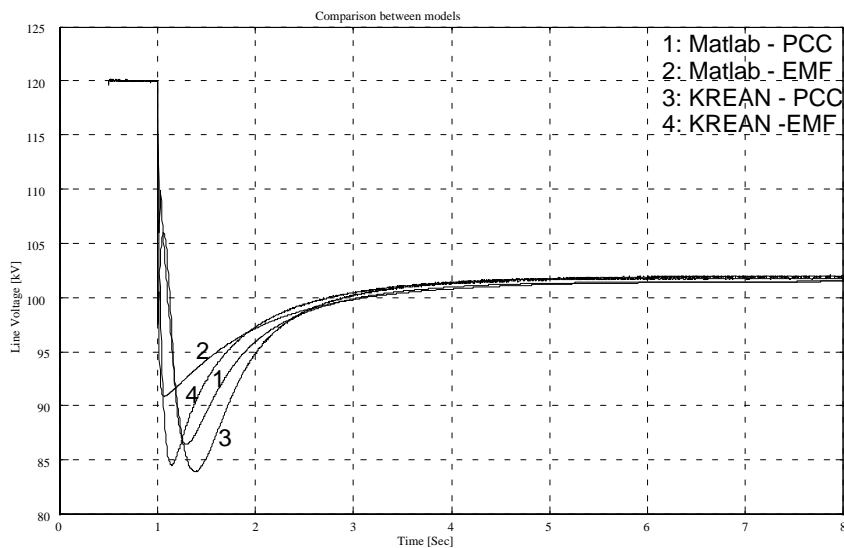


Figure 9-40 Comparison of line voltages from different models during the whole simulation of load admittance increase corresponding to a load increase from 80 MW to 100 MW

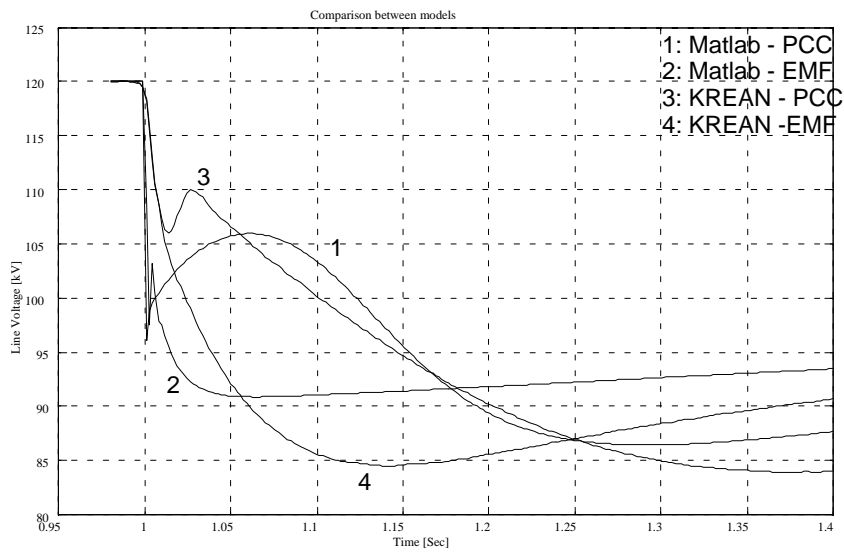


Figure 9-41 Comparison of line voltages from different models during the first 0.4 s after load admittance increase corresponding to a load increase from 80 MW to 100 MW

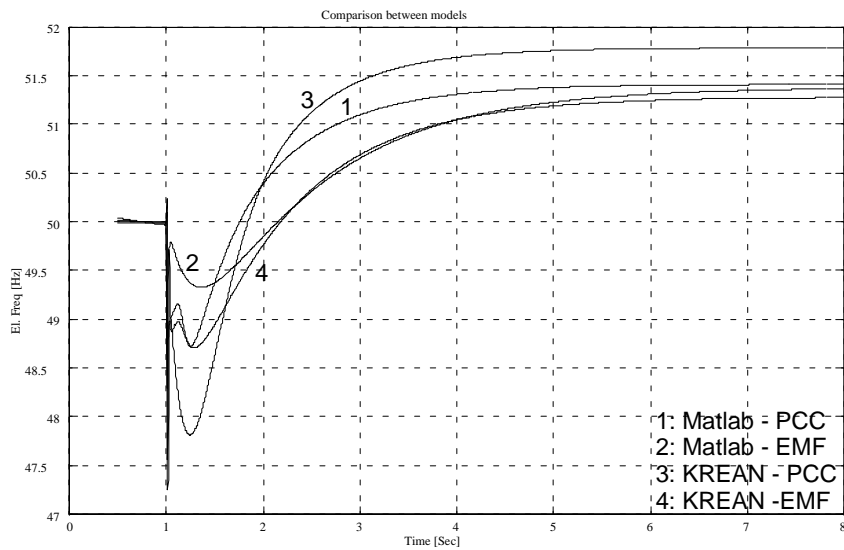


Figure 9-42 Comparison of electrical frequencies from different models during the whole simulation of load admittance increase corresponding to a load increase from 80 to 100 MW

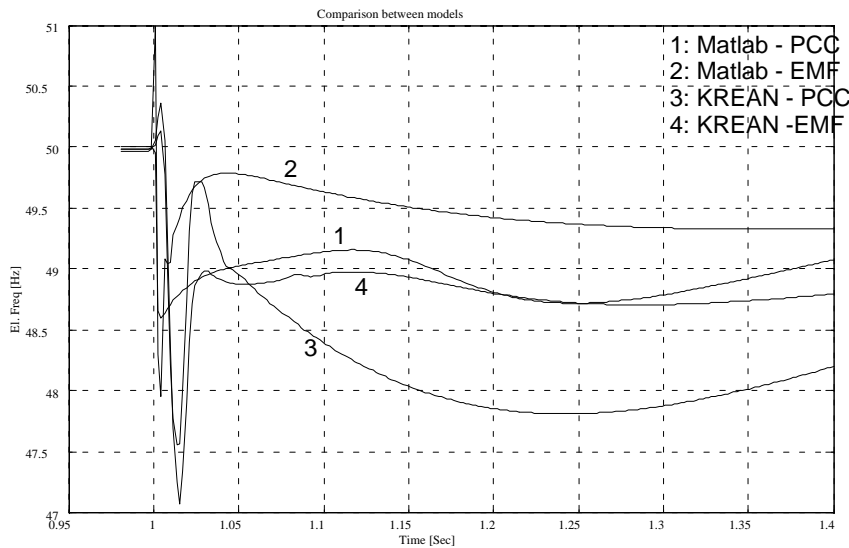


Figure 9-43 Comparison of electrical frequencies from different models during the first 0.4 s after load admittance increase corresponding to a load increase from 80 MW to 100 MW

some flaw in the Matlab models. Compare also Figure 9-10, Figure 9-22, Figure 9-29 and Figure 9-36. The greater resemblance is between the electrical frequency modelled with reference to the PCC voltage in Matlab and the electrical frequency modelled with reference to the EMF in KREAN, and between the electrical frequency modelled with reference to the EMF in Matlab and the electrical frequency modelled with reference to the PCC voltage in KREAN. The reason for this crossing is that there is a far stronger linkage between the EMF, or better the subtransient EMF of the synchronous compensator and the PCC voltage across the subtransient d-axis reactance, than the Matlab model takes into account when calculating the frequency. On the other hand, the KREAN model taking the reference from the artificial EMF, does not consider that this voltage lies fixed in the q-axis while the system really experiences the subtransient EMF, which may be situated at a considerable angle off the q-axis.

Figure 9-44 shows the comparison of the mechanical frequency during the whole simulation and Figure 9-45 shows the blow up of the initial 0.4 s. The same comments as for the mechanical frequency apply, and it can be seen that the (almost) stationary values are the same as for the electrical frequency

Figure 9-46 shows the comparison of the pole wheel angles during the whole simulation and Figure 9-47 shows the blow up of the initial 0.4 s. The pole wheel angles in the KREAN simulations are calculated on basis of the d- and q-axis voltages of the synchronous compensator. Compare Figure 9-13,

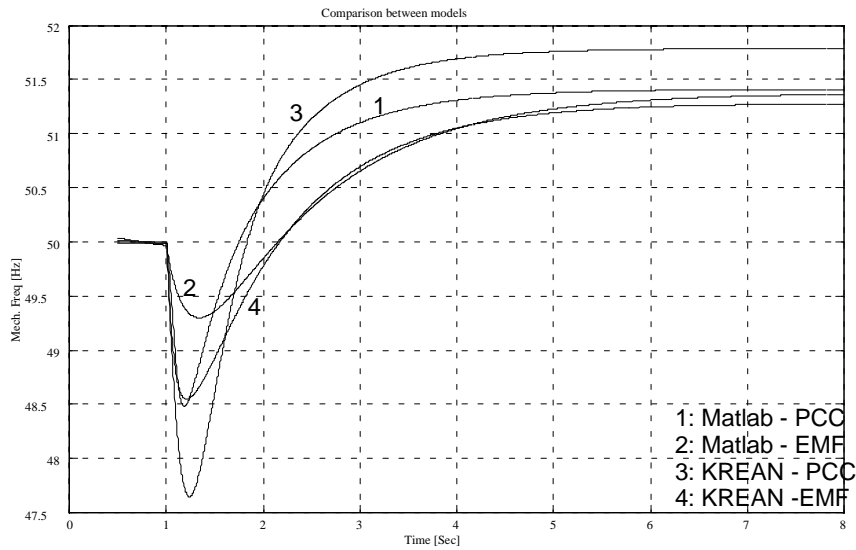


Figure 9-44 Comparison of mechanical frequencies from different models during the whole simulation of load admittance increase corresponding to a load increase from 80 to 100 MW

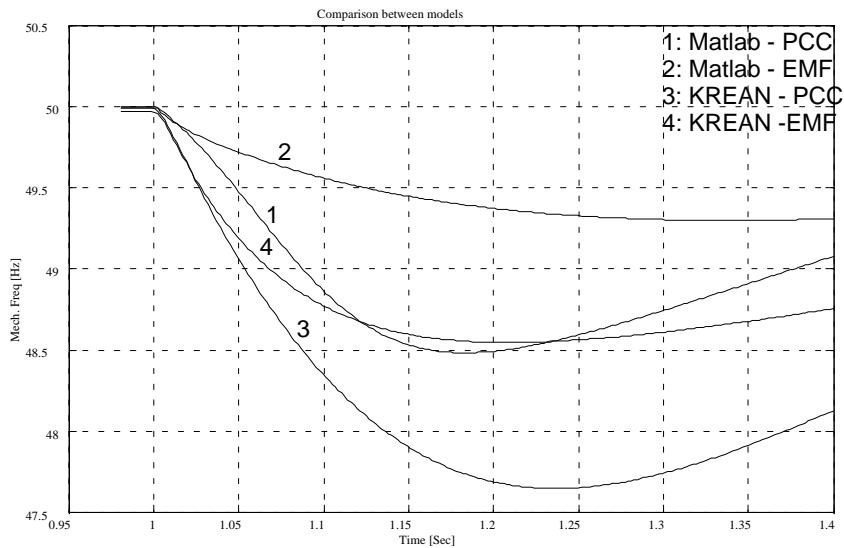


Figure 9-45 Comparison of mechanical frequencies from different models during the first 0.4 s after load admittance increase corresponding to a load increase from 80 MW to 100 MW



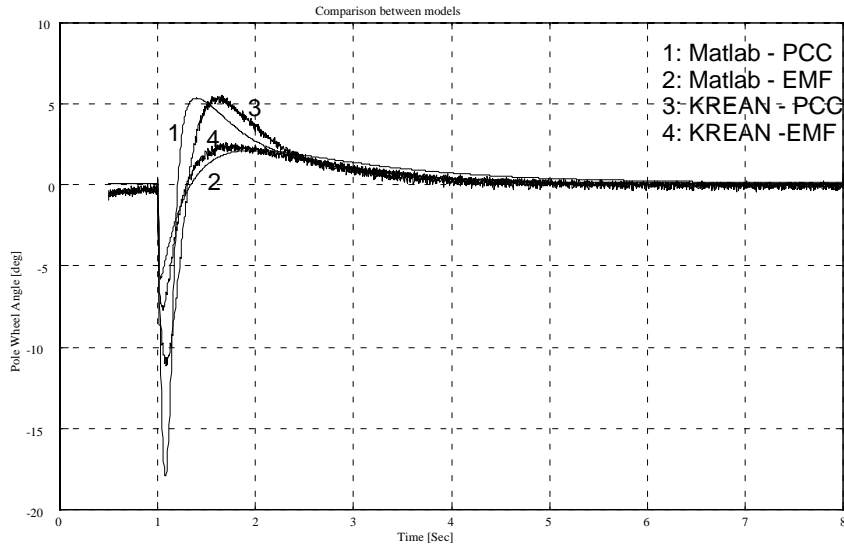


Figure 9-46 Comparison of pole wheel angles from different models during the whole simulation of load admittance increase corresponding to a load increase from 80 to 100 MW

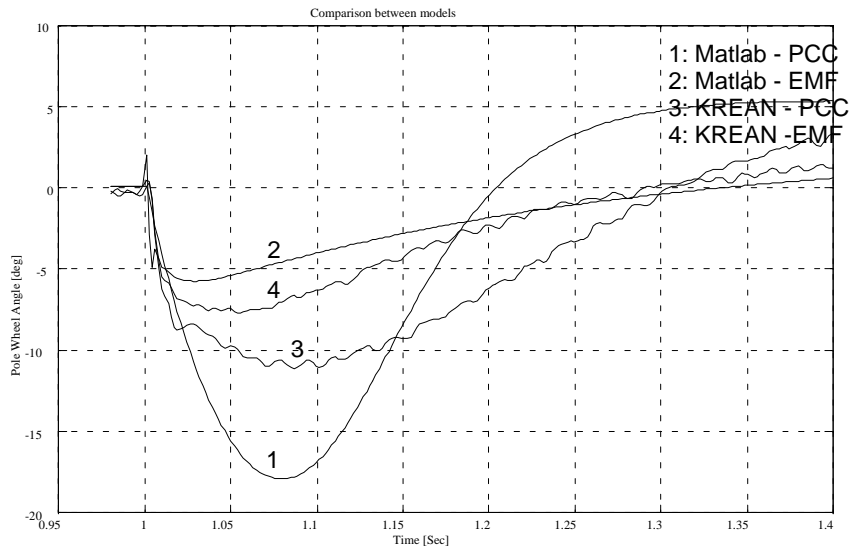


Figure 9-47 Comparison of pole wheel angles from different models during the first 0.4 s after load admittance increase corresponding to a load increase from 80 MW to 100 MW

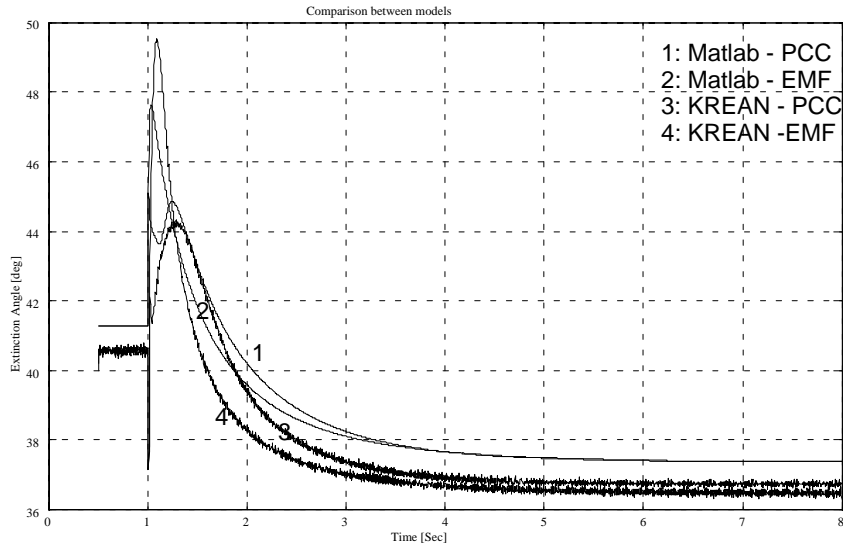


Figure 9-48 Comparison of 'true' inverter extinction angles from different models during the whole simulation of load admittance increase corresponding to a load increase from 80 to 100 MW

Figure 9-23, Figure 9-31 and Figure 9-38. There are great principal similarities between the two models using the voltage at PCC as reference and between the two models using the EMF as reference. This appears most clearly in Figure 9-46.

Finally the comparison of the inverter extinction angles are shown in Figure 9-48 for the whole simulation, and in Figure 9-49 for the initial 0.4 s. The inverter extinction angles in the KREAN simulations are calculated on basis of the AC and DC voltages. Compare Figure 9-13, Figure 9-23, Figure 9-31 and Figure 9-38. Also in this case there are great principal similarities between the two models using the voltage at PCC as reference and between the two models using the EMF as reference.

## 9.6 CONCLUSION

Two different systems have each been simulated in two different models. There are some differences between the KREAN and the Matlab model results for each system during the transients. This is natural, since the Matlab models have limited validity during transients. Qualitatively the results in KREAN and Matlab are quite similar for each system, except the frequency results. The deviations in these results are due to the fact that there is a much

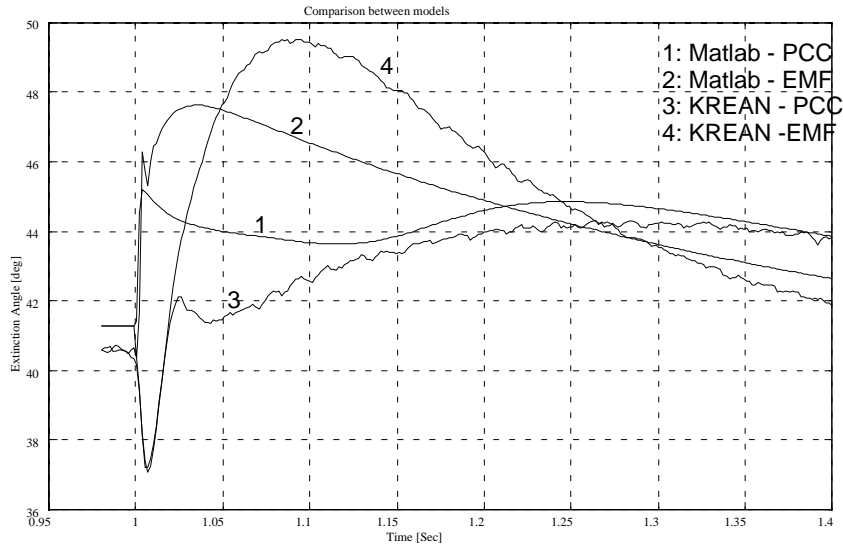


Figure 9-49 Comparison of ‘true’ inverter extinction angles from different models during the first 0.4 s after load admittance increase corresponding to a load increase from 80 to 100 MW.

stronger linkage between the EMF of the synchronous compensator and the PCC voltage than the Matlab model takes into consideration. This linkage, due to the low values of the subtransient impedance of the synchronous compensator is taken into account much better by the KREAN models.

It is noteworthy that, due to the voltage drop in this constant current system, the power dissipated in the load actually decreases when the load conductance increases.

It is to be remembered that the systems which have been treated in this chapter are only for the understanding of the principles. They do not claim to be realistic systems, furthermore all controllers are blocked. The results are way outside the allowable limits according to norms and regulations. Later, attention is turned to an investigation of the conditions where the norms and regulations can be fulfilled.



# **10 QUASI-PHASOR SIMULATIONS OF A SYSTEM WITH A SYNCHRONOUS COMPENSATOR AND INDUCTION MOTOR STARTING DIRECTLY ON LINE**

In this chapter we shall study the consequences of the introduction of an large induction motor to the network with a synchronous compensator.

## **10.1 SYSTEM TO BE SIMULATED**

The system to be simulated with the quasi-phasor-model is shown in Figure 10-1. It is identical to the system in Section 9. 3, except that the additional load is now replaced by an induction motor. The induction motor which is to be started is modelled as tables for torque and current related to relative speed, based on figures for a Siemens 1RN1804 motor, 4-pole, 10500 V, 6800 kW. This model of the motor has been scaled up to 10 MVA (9 MW), which is 10 % of the inverter rating. The model also includes the load torque of a turbo-compressor during start-up, as well as the inertia of both motor and compressor. The details of the real motor and load are found in Appendix C.

The planned course of the simulation is to allow 1 s for stabilization of initial values. Then at  $t=1$  s the induction motor is connected with zero speed. When the start is completed, some time is allowed for stabilization and then the compressor is loaded to the rated power of the motor.

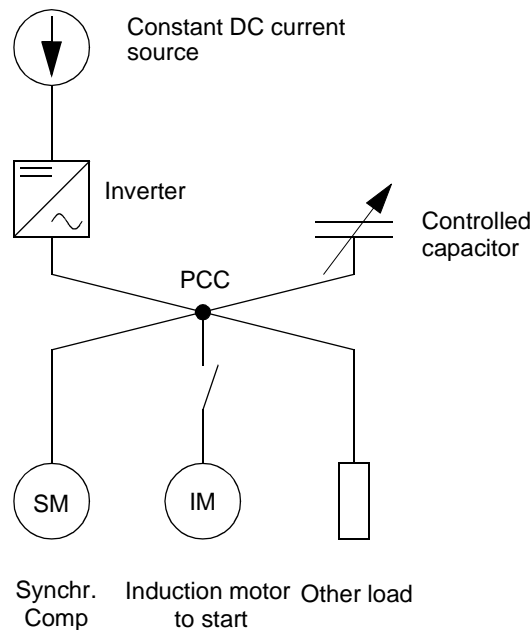


Figure 10-1 Simplified model of HVDC supply to an offshore oil-installation, to be simulated in the quasi-phasor model.

## 10.2 SIMULATIONS OF SYSTEM WITH REFERENCE FOR THE FIRING PULSES GIVEN BY THE VOLTAGE AT PCC

The block schematic from the simulations without induction motors in Section 9.4, with real axis given by the PCC voltage, can easily be extended to include an induction motor. This is done in Figure 10-2. As a minimum the same algebraic loops exist and similar filters as in the previous chapter are applied. The results of the simulations are shown in the following figures. Remember that the system is operating without controllers to check the intrinsic stability. Figure 10-3 presents the progress of the frequencies, electrical as well as mechanical for both the synchronous compensator and induction motor. Figure 10-4 shows the progress of the voltages, both AC and DC values. Figure 10-5 shows the progress of the pole wheel angle of the synchronous compensator together with the extinction angle of the inverter and the phase angle of the motor. Something negative happens when the induction motor accelerates past the pull-out frequency. Closer examination of the details of the curves reveals that the very non-linear torque curve of the induction motor, together with the positive sensitivity of the system frequency

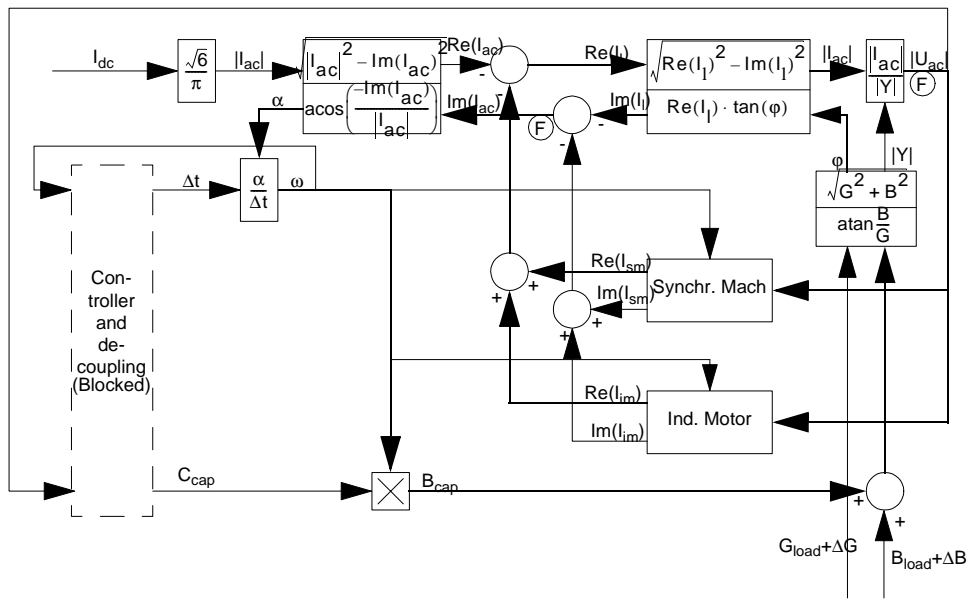


Figure 10-2 Block diagram of Simulink model including induction motor, with firing pulse reference from PCC voltage.

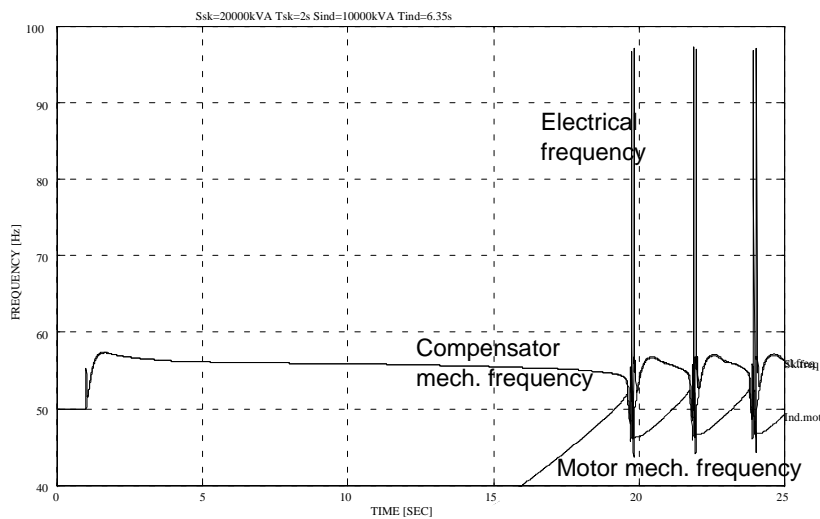


Figure 10-3 Electrical frequency and mechanical frequency for both the synchronous compensator and induction motor during DOL start of the induction motor. Firing pulse reference from voltage at PCC.

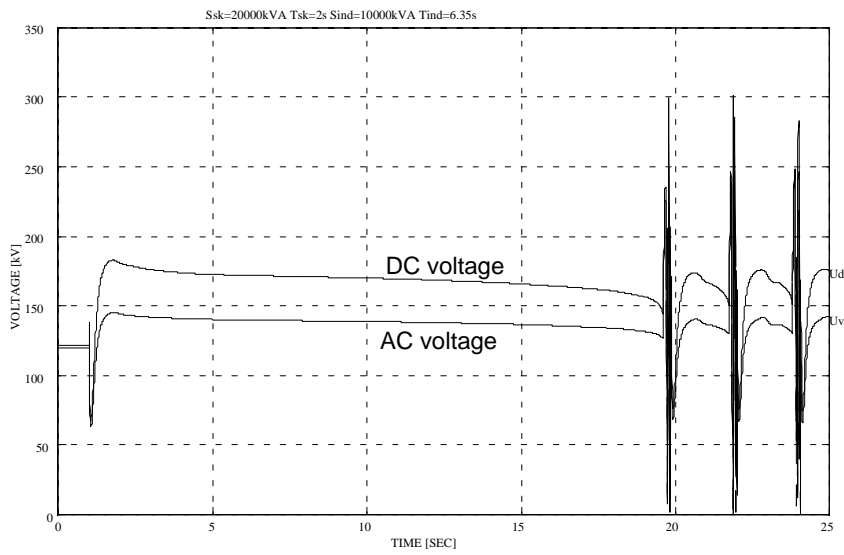


Figure 10-4 AC and DC voltage during DOL start of the induction motor. Firing pulse reference from voltage at PCC.

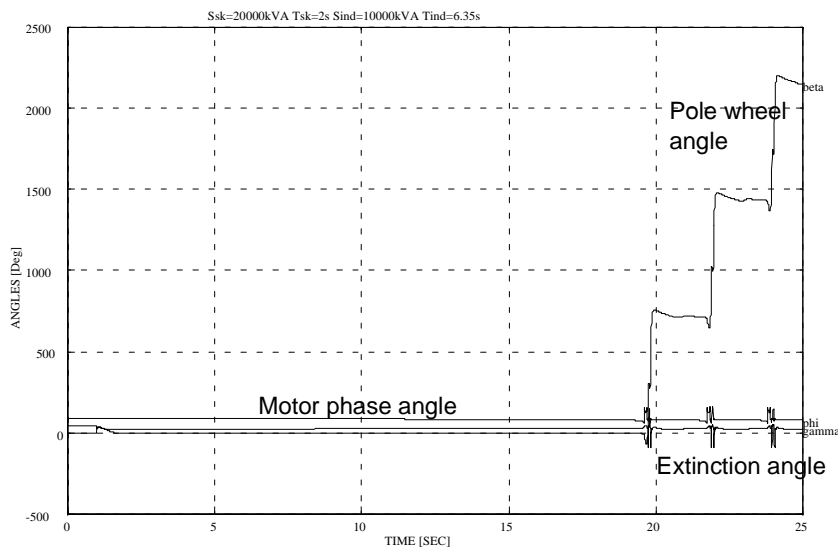


Figure 10-5 Extinction angle, pole wheel angle for the synchronous compensator and phase angle for the induction motor during DOL start of the motor. Firing pulse reference from voltage at PCC.



for variations in equivalent conductivity in the system, forces the model into non-linear oscillations. Is this a weakness of the system or the model? The results will later be compared to the results of a KREAN simulation. This comparison will show that the model is at fault, the KREAN model is stable when the motor reaches full speed, at least under the circumstances simulated in this case. It was also found in the previous chapter that the model with a control system based on firing pulse reference from the voltage at PCC gave too fast variation in the electrical frequency. This is exactly what happens in this case, the electrical frequency varies too fast and when this is combined with the strong non-linearity of the torque-curve in the motor, this creates a standing oscillation. On the other hand, this system is sensitive to the amount of load torque, also in the KREAN simulation. Under certain circumstances the electrical frequency accelerates faster than the motor can follow, causing trips in first the motor, and then the whole system. This progress was also shown in a slightly modified variant of the quasi-phasor model where the frequency-reference for the induction motor was taken from the synchronous compensator speed.

### **10.3 SIMULATIONS OF SYSTEM WITH REFERENCE FOR THE FIRING PULSES GIVEN BY THE EMF OF THE COMPENSATOR**

The block schematic from the simulations without induction motors in Section 9. 4. 2, with real axis given by the EMF voltage, can also easily be extended to include an induction motor. Figure 10-6 illustrates the extended system. As a minimum the same algebraic loops as in the model with resistive load change are present. The same filters on the real and imaginary parts of the voltages are applied to break the loops. Here too the filters are indicated by F.

The results of this simulation are presented in the following figures. Remember that the system is operating without controllers to check the intrinsic stability. Figure 10-7 shows the electrical frequency of the network and the mechanical frequency of the synchronous compensator and induction motor. Figure 10-8 gives the system voltage at the point of common coupling and the DC voltage. Figure 10-9 depicts the extinction angle  $\gamma$  and pole wheel angle  $\beta$ , together with the phase angle  $\phi$  of the induction motor.

First it can be noted that the simulations indicate a stable system, as opposed to the previous simulation. But the results may be quite astonishing at first glance. Starting a motor in the system leads to increased voltage and

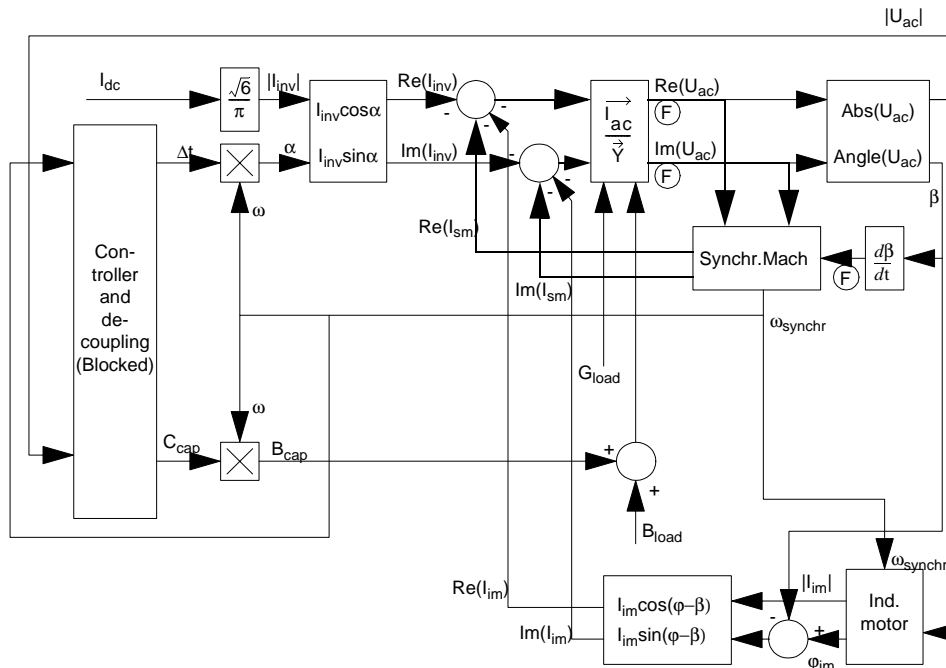


Figure 10-6 Block diagram of Simulink model including induction motor, with firing pulse reference from the EMF voltage.

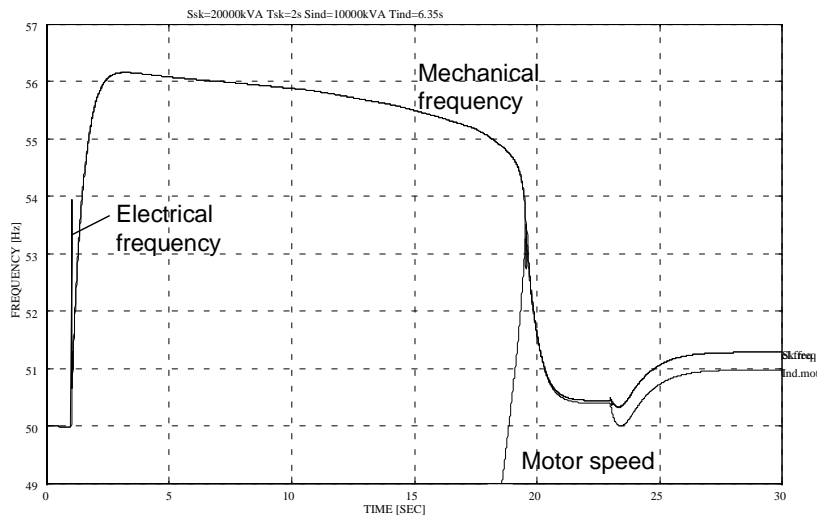


Figure 10-7 Electrical frequency as well as mechanical frequency for both the synchronous compensator and induction motor before and after DOL start of the motor. Firing pulse reference from the EMF voltage.

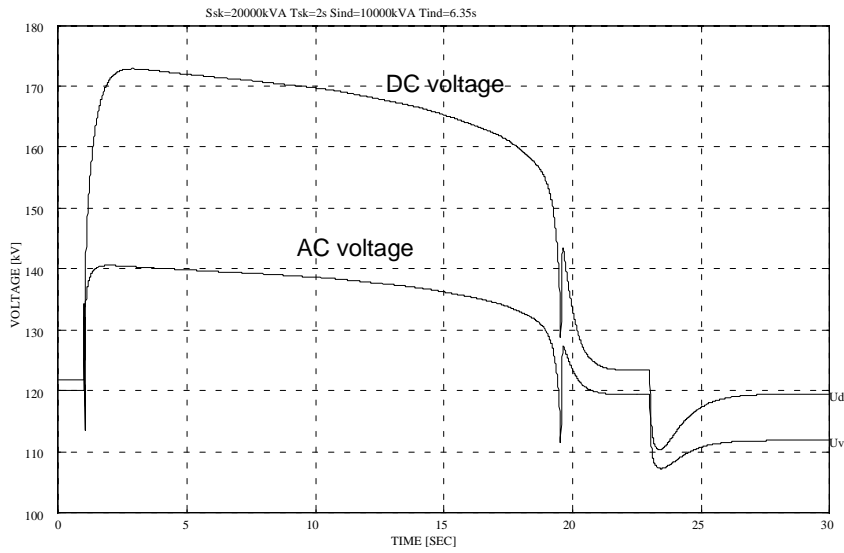


Figure 10-8 System voltage and DC voltage before and after DOL start of the induction motor. Firing pulse reference from the EMF voltage.

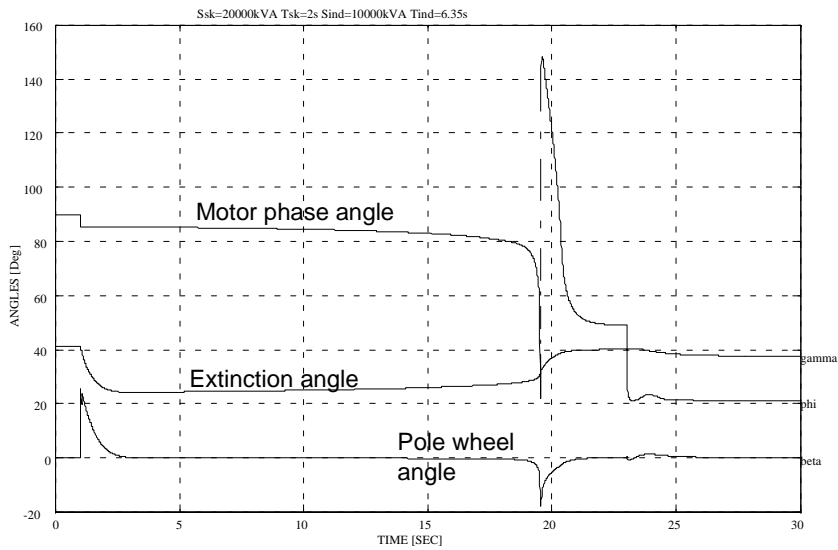


Figure 10-9 Inverter extinction angle  $\gamma$  and synchronous compensator pole wheel angle  $\beta$ , together with induction motor phase angle  $\phi$  after DOL start of the induction motor. Firing pulse reference from the EMF voltage.

frequency. In order to see what happens, we are going to investigate the three distinguished incidents:

- Connecting the motor, at  $t=1$  s
- The motor reaches full speed, at  $t\approx 19$  s.
- Loading the motor, at  $t=23$  s.

### 10.3.1 Connecting the motor, at $t=1$ s

How can we explain the increased voltage, when the motor is connected? First, we have a glance at the blow-ups of the frequencies, Figure 10-10; voltages, Figure 10-11; and angles, Figure 10-12, during the first 0.4 s after connection of the motor. Approximately the same things happen as when an active load was connected, as described in Section 9.4.2, but with opposite sign. The voltage at PCC shifts phase quickly when the inductive load of the induction motor is connected. This is registered as a pulse in the frequency, starting a similar procedure as earlier described. In order to explain the 'wrong' sign of the events, we have to take a look at the phasor diagrams.

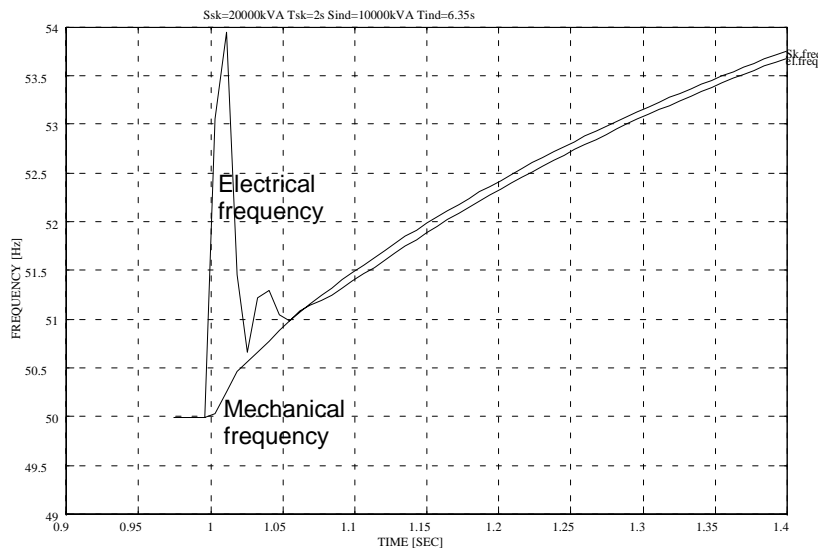


Figure 10-10 Electrical frequency and mechanical frequency for the synchronous compensator before and the first 0.4 s after DOL start of the induction motor. Firing pulse reference from the EMF voltage.

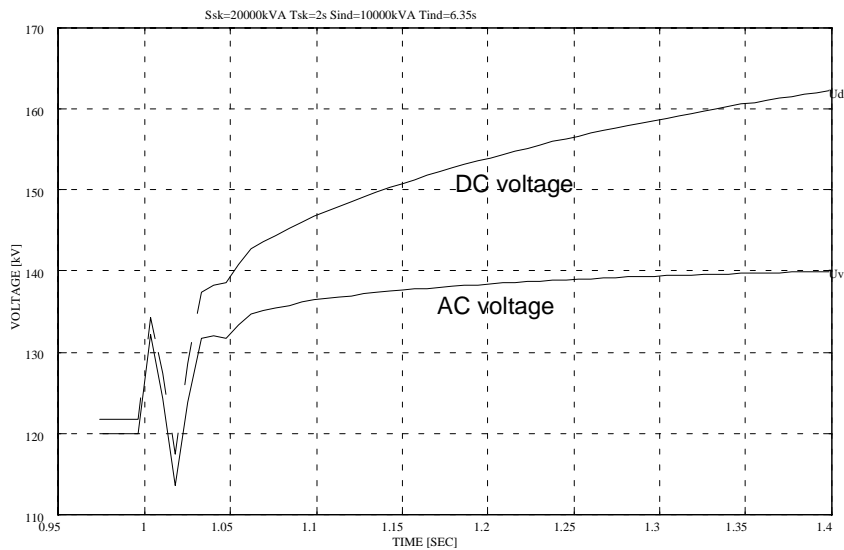


Figure 10-11 System voltage and DC voltage before and the first 0.4 s after DOL start of the induction motor. Firing pulse reference from the EMF voltage.

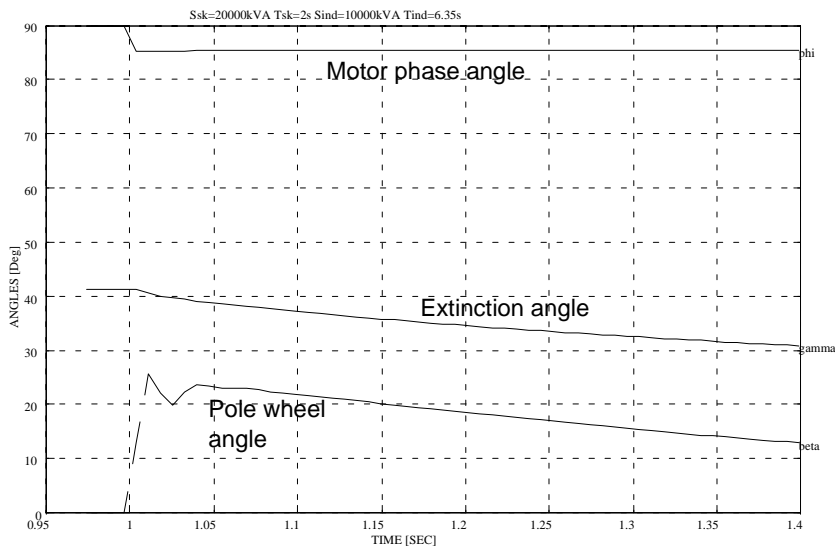


Figure 10-12 Inverter extinction angle  $\gamma$  and synchronous compensator pole wheel angle  $\beta$ , together with induction motor phase angle  $\phi$  before and the first 0.4 s after DOL start of the induction motor. Firing pulse reference from the EMF voltage.

If we compute the load at the busbar as seen from the inverter, immediately before the connection of the induction motor, we have the situation in Figure 10-13. The fundamental current from the inverter is, in complex notation:

$$I_{inv} = |I|(\cos\gamma + j\sin\gamma) \quad (10-1)$$

where extinction angle  $\gamma$  is relative to the q-axis.

The admittance of the rest of the system is:

$$Y_0 = G_{load} + j(B_{SC,eq,0} + B_{cap}) = |Y_0|(\cos\phi_0 + j\sin\phi_0) \quad (10-2)$$

If we define power consumption positive and power production negative, we have:

$$G_{load} > 0 \quad B_{SC,eq,0} < 0 \quad B_{cap} < 0 \quad (10-3)$$

The resulting voltage is

$$U_0 = |U_0|(\cos\beta_0 + j\sin\beta_0) = \frac{I}{Y_0} = \frac{|I|(\cos\gamma + j\sin\gamma)}{|Y_0|(\cos\phi_0 + j\sin\phi_0)} \quad (10-4)$$

This can be split in

$$\begin{aligned} |U_0| &= \frac{|I|}{|Y_0|} \\ (\cos\beta_0 + j\sin\beta_0) &= (\cos(\gamma - \phi_0) + j\sin(\gamma - \phi_0)) \end{aligned} \quad (10-5)$$

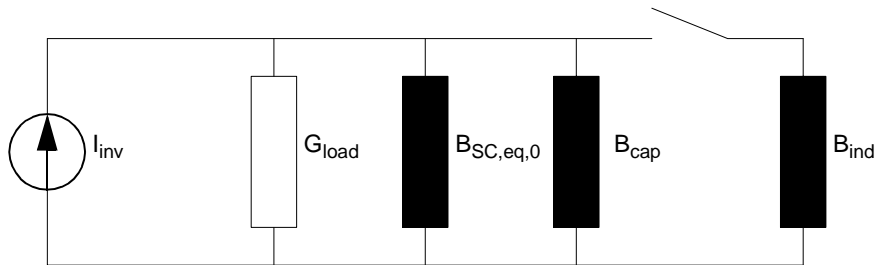


Figure 10-13 Quasi-phasor model of the load as seen from the inverter before DOL start of induction motor.

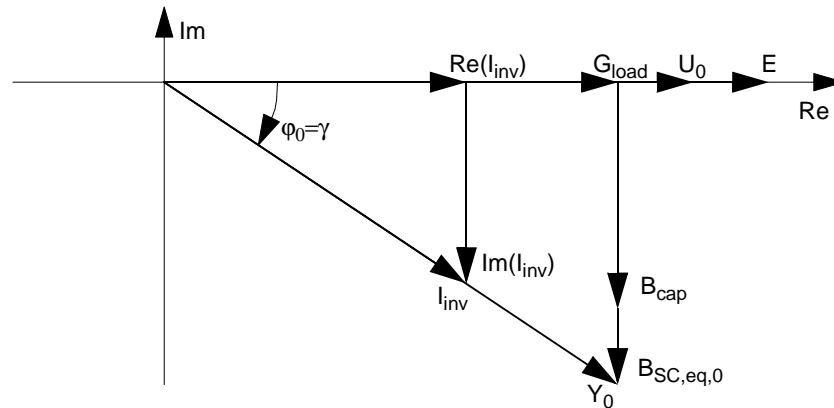


Figure 10-14 Phasor diagram of current, voltage and admittance as seen from the inverter before start of induction motor.

where

$$(\beta_0 = 0) \Rightarrow (\gamma = \phi_0) \quad (10-6)$$

because the synchronous compensator is not supplying any active power in a stable situation. This implies that the phase angle  $\phi_0$  of the admittance must be equal to the extinction angle  $\gamma_0$ . The situation is described by phasors in Figure 10-14.

After the induction motor is connected, the situation is like Figure 10-15. Bear in mind that immediately after DOL start of an induction motor the

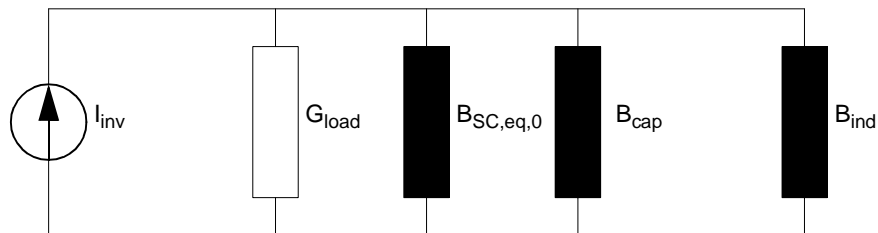


Figure 10-15 Quasi-phasor model of the load as seen from the inverter immediately after DOL start of induction motor.

motor can be approximately regarded as a pure inductive load. Now the admittance of the system is

$$Y_1 = G_{load} + j(B_{SC,eq,0} + B_{cap} + B_{ind}) \quad (10-7)$$

where

$$B_{ind} > 0 \quad (10-8)$$

The new admittance can also be expressed in phasors, Figure 10-16, and it is evident that the new admittance is less in absolute value than the old.

The extinction angle  $\gamma$  is related to the q-axis, and has not changed, therefore the current from the current source is the same, and the new voltage becomes

$$U_1 = |U_1|(\cos\beta_1 + j\sin\beta_1) = \frac{I}{Y_1} = \frac{|I|(\cos\gamma + j\sin\gamma)}{|Y_1|(\cos\phi_1 + j\sin\phi_1)} \quad (10-9)$$

where

$$|U_1| = \frac{|I|}{|Y_1|} \quad (10-10)$$

$$(\cos\beta_1 + j\sin\beta_1) = (\cos(\gamma - \phi_1) + j\sin(\gamma - \phi_1))$$

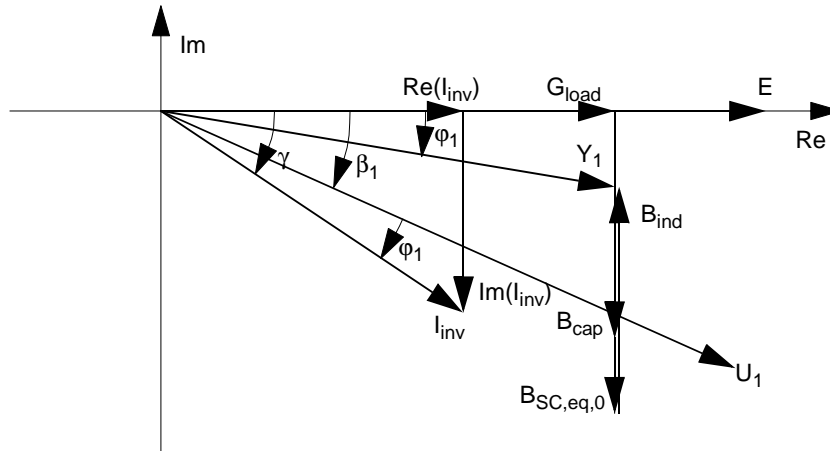


Figure 10-16 Phasor diagram of current, voltage and admittance as seen from the inverter after DOL start of induction motor.



and the new pole wheel angle

$$\beta_1 = \gamma - \varphi_1 = \varphi_0 - \varphi_1 \quad (10-11)$$

It can also be seen from the phasor diagram that the new effective extinction angle related to the voltage will be  $\varphi_1$ , giving the inverter a higher active power output than before. The increased active power is partly consumed by the active load, due to increased voltage, and partly consumed by the synchronous compensator due to the new pole wheel angle  $\beta_1$ . The power consumed by the synchronous compensator must be used for acceleration. This is the reason for the increase in frequency, when actually adding load to the system. The locus plot of the admittance phasor as result of the simulation is shown in Figure 10-17. There is a good correlation between the locus plot and the theoretical analysis, the main difference is that the plot takes the active load of the induction motor into consideration.

This frequency and voltage increase also correlates with the sensitivities found in Chapter 7. The sensitivities for voltage and frequency for a change in network capacitance are negative, predicting a reduction of voltage and frequency for an increase of capacitance. Adding inductive load is equivalent to reducing the capacitance and, as predicted, the frequency and voltage increases.

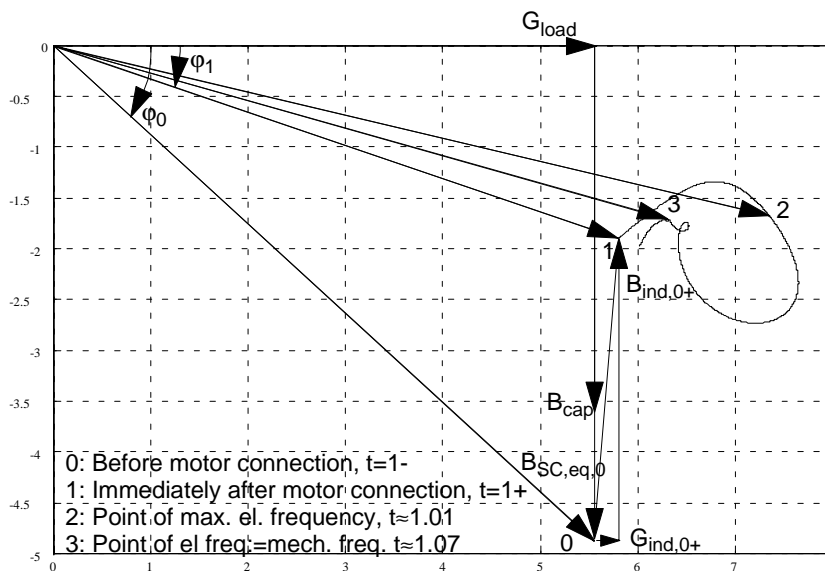


Figure 10-17 Locus plot for the resulting network impedance phasor during the first 0.4 s after connection of a 10 MVA motor. Firing pulse reference from voltage at PCC.

After the connection, the motor accelerates. This period is characterized by a slowly increasing demand for active power, combined with a slowly decreasing demand for reactive power. This results in a gradually decreasing phase angle of the total load. After the initial frequency rise, required to adapt the extinction angle to the new phase angle of the load, the frequency slowly decreases, in order to continuously adapt the extinction angle to the phase angle of the load.

### 10.3.2 The motor reaches full speed, at $t \approx 19$ s

The relevant blow-ups of the frequencies are shown in Figure 10-18, voltages in Figure 10-19, and angles in Figure 10-20. The period when the motor reaches full speed is initialized by a sharper decrease in need for reactive power. The demand for active power is still rising, but slowly in comparison, culminating somewhat later as the motor passes the pull-out point and then suddenly decreasing fast. The faster decrease of need for reactive power leads to faster reduction of speed and voltage through the reverse process of what happens at connection. The sudden decrease of need for active power as the motor passes pull-out speed acts through the opposite process of the active load increase in Chapter 9, resulting in first a frequency and voltage increase, followed by a frequency and voltage decrease. For the total system it is of no consequence that the induction motor even gets into the over-synchronous range and turns into a generator for a short while.

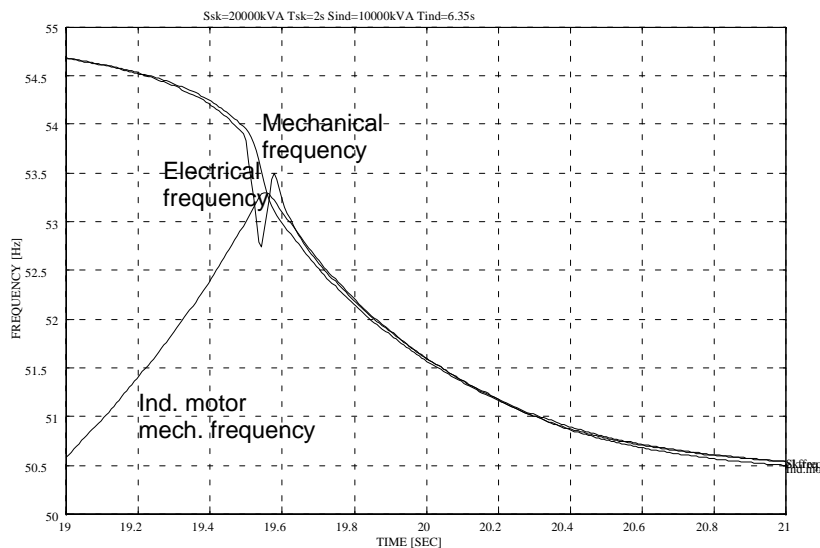


Figure 10-18 Electrical frequency and mechanical frequency for the synchronous compensator at the time when the induction motor reaches full speed. Firing pulse reference from the EMF voltage.

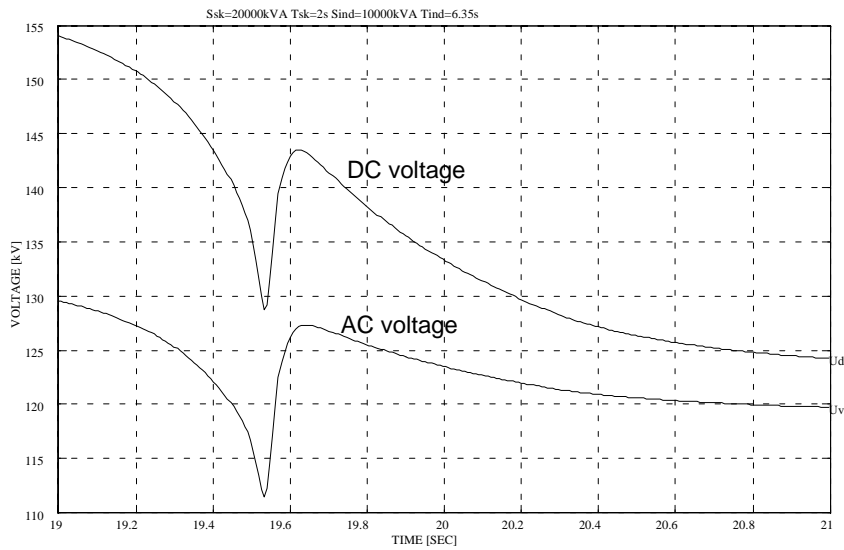


Figure 10-19 System voltage and DC voltage at the time when the induction motor reaches full speed. Firing pulse reference from the EMF voltage.

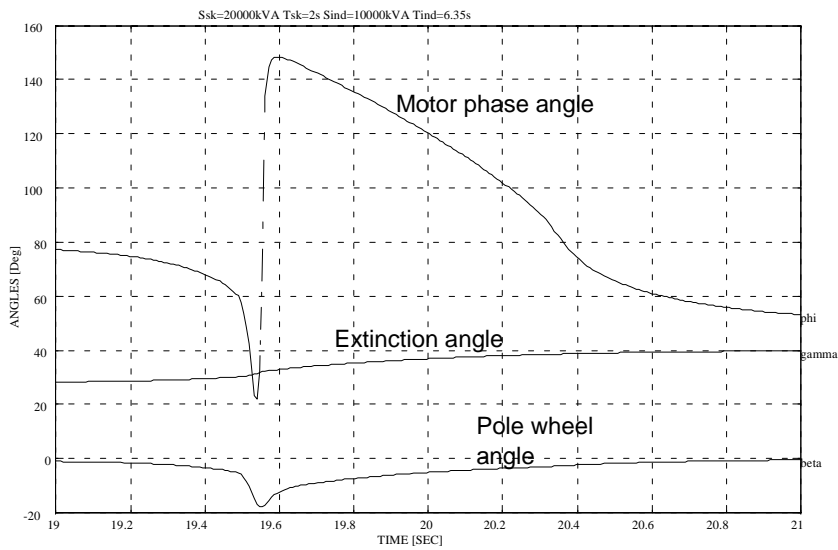


Figure 10-20 Inverter extinction angle  $\gamma$  and synchronous compensator pole wheel angle  $\beta$ , together with induction motor phase angle  $\phi$  at the time when the induction motor reaches full speed. Firing pulse reference from the EMF voltage.

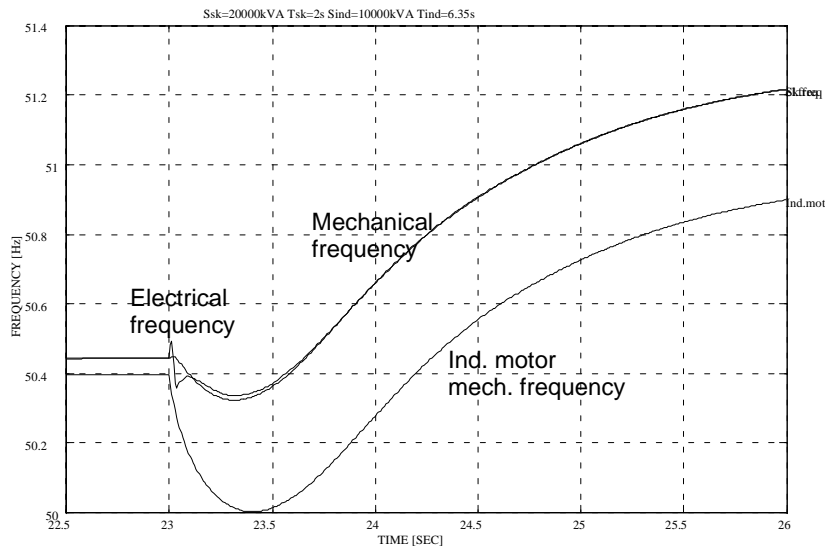


Figure 10-21 Electrical and mechanical frequency for synchronous compensator before and the first 2 s after loading of the induction motor. Firing pulse reference from the EMF voltage.

### 10.3.3 Loading the motor, at $t=23$ s

The relevant blow-ups are shown in Figure 10-21, frequencies; Figure 10-22, voltages; and Figure 10-23, angles. This event is principally the same as the load increase described in Chapter 9. Events occur somewhat slower and the deflections are less, but the same processes are present.

### 10.3.4 Conclusion

Judging by the quasi-phasor simulations, the last system, which takes the reference for the firing pulses from the EMF of the synchronous compensator, is the more stable and better suited control philosophy. This is supported by the following KREAN simulations, which confirms that the system with firing pulse reference taken from the voltage at the PCC is more inclined to lose control of the electrical frequency.

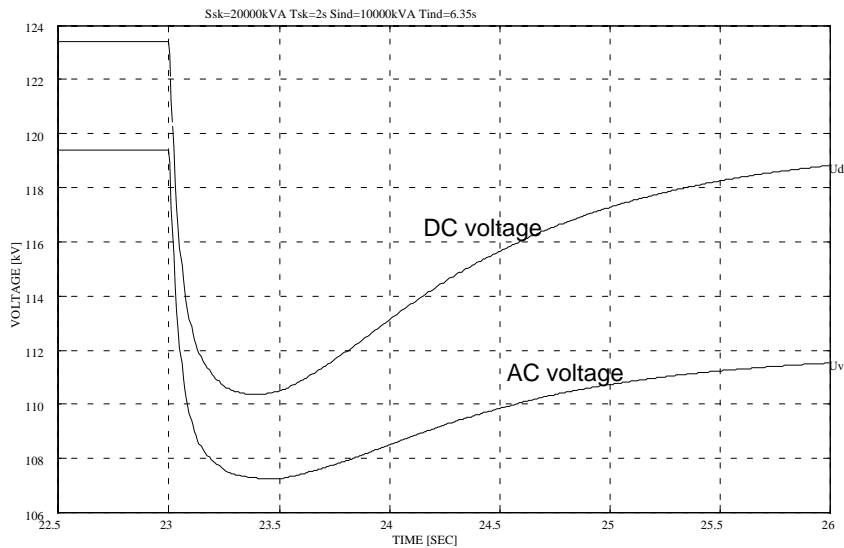


Figure 10-22 System voltage and DC voltage before and the first 2 s after loading of the induction motor. Firing pulse reference from the EMF voltage.

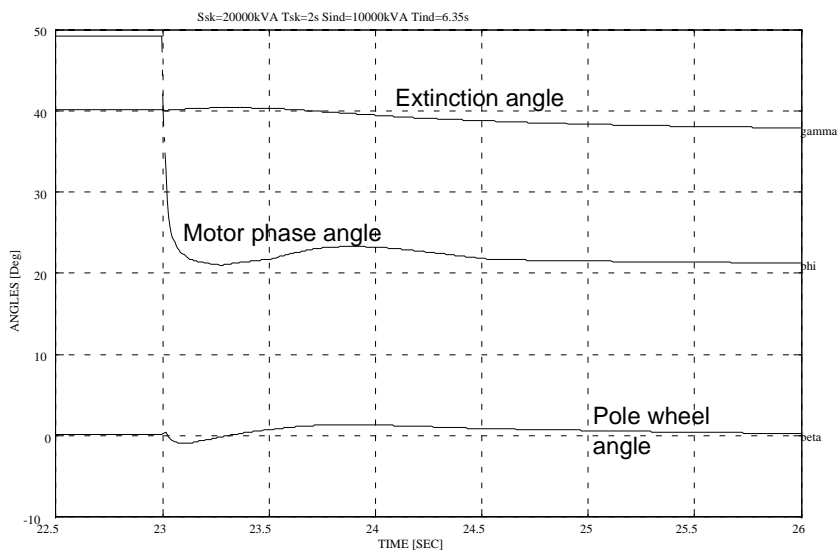


Figure 10-23 Inverter extinction angle  $\gamma$  and synchronous compensator pole wheel angle  $\beta$ , together with induction motor phase angle  $\phi$  before and the first 2 s after loading of the induction motor. Firing pulse reference from the EMF voltage.

## 10.4 VERIFICATION SIMULATIONS BY KREAN

The same KREAN-models as in Section 9.5 are applied for both firing angle references. The model is extended by a standard induction motor module from the module library. This standard induction motor module is unfortunately a linear model based on parameters that are independent of the slip frequency. The result is that when modelling a high power, high voltage motor the start-up torque is so low that the start-up time becomes unacceptable. In order to speed up acceleration, an auxiliary start-up torque is added externally. Thus the start-up time moves into the realistic range. The active load the motor draws from the network during start-up is not correct, due to this trick, but the error is considered acceptably small. The auxiliary start-up torque is gradually reduced as the speed increases and completely removed shortly before pull-out frequency is reached. The auxiliary start-up torque therefore does not interfere with the events while reaching full speed and putting on load. Sticktion and friction torque during start-up are neglected. Load torque, when added, contains these parameters. First, a control system based upon the voltage at PCC as reference for the firing pulses is simulated. Afterwards, a control system based upon using the synchronous compensator EMF as reference for the firing pulses, will be investigated.

### 10.4.1 Voltage at PCC as reference

This is the control system that went astray in the quasi-phasor simulations. It will become apparent that the system is not quite reliable in KREAN simulations either, but not for the same reasons. The results for the whole simulation period are given in the following figures. Figure 10-24 presents the frequencies in the system. Figure 10-25 displays the system voltages and Figure 10-26 depicts the angles, calculated in the same way as in the KREAN simulations in the preceding chapter. It appears that the system has no problem in handling the induction motor passing the pull-out frequency. This is the point where the quasi-phasor model failed. But when the load is applied to the motor, there are problems. These are of a physical nature. It was shown mathematically in Chapter 7 and confirmed by the simulations in Chapter 9 that the frequency rises when the load increases. For simplicity, let this dependence be expressed by:

$$\omega_{el} = f(P) \quad \frac{d\omega}{dP} > 0 \quad (10-12)$$

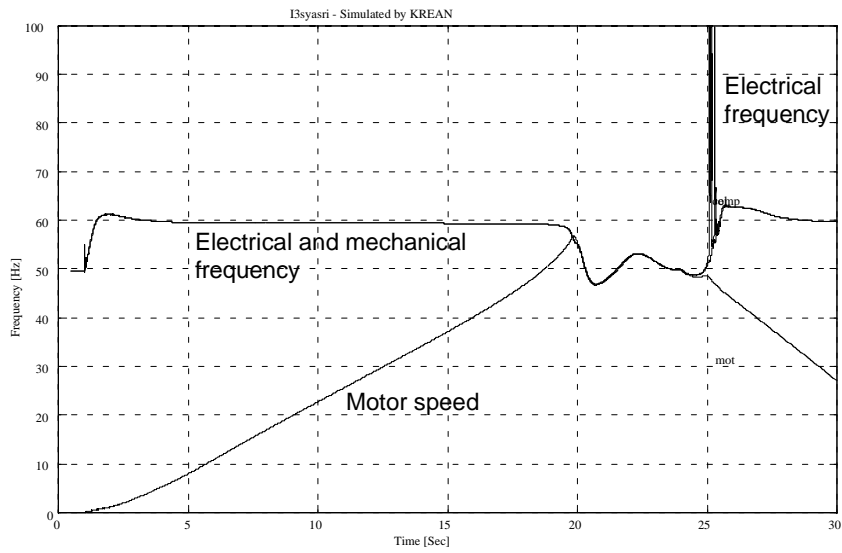


Figure 10-24 Electrical frequency and mechanical frequency for both the synchronous compensator and induction motor during DOL start of the induction motor. Firing pulse reference from PCC voltage. Simulated by KREAN.

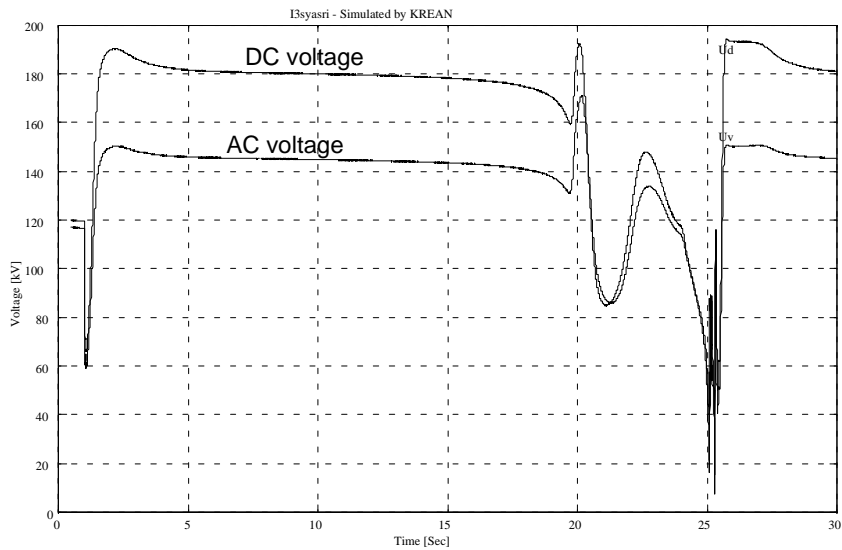


Figure 10-25 AC and DC voltages during DOL start of the induction motor. Firing pulse reference from PCC voltage. Simulated by KREAN.

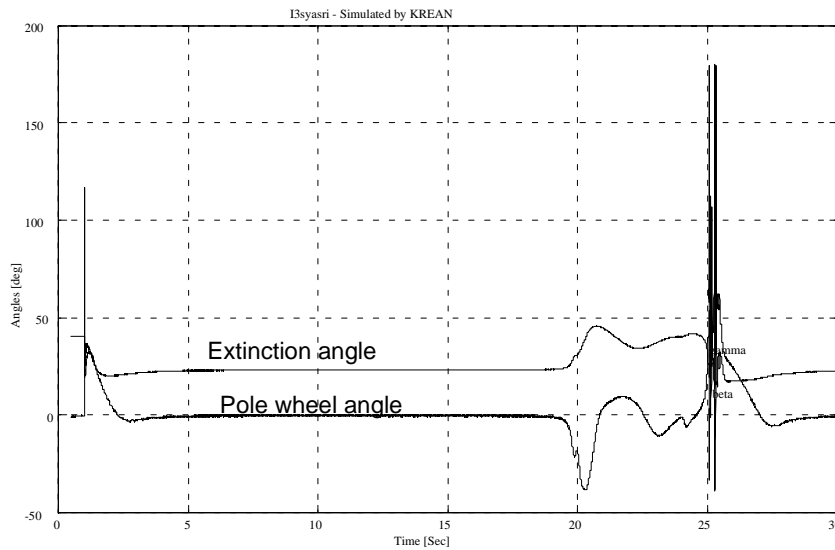


Figure 10-26 Pole wheel angle  $\beta$  and extinction angle  $\gamma$  during DOL start of the induction motor. Firing pulse reference from PCC voltage. Simulated by KREAN.

simply stating that electrical frequency is a function of the active power, and increasing the power increases the frequency. (10-12) can be modified to express the electrical acceleration:

$$\frac{d\omega_{el}}{dt} = g\left(\frac{dP}{dt}\right) \quad (10-13)$$

On the other hand, we have the mechanical acceleration equation for the motor:

$$\frac{d\omega_{mek}}{dt} = \frac{1}{T_{ma}} \cdot (m_{el} - m_l) \quad (10-14)$$

In order to have a stable system, the electrical and mechanical acceleration must be kept in pace. Normally, in a system with constant frequency, this is managed by the dependency of the torque/slip relationship, as long as the slip is below the pull-out value. But in the case simulated, there is a positive feedback, increasing the power leads to increased frequency, which leads to increased slip and further increase in power. In this simulation, the spiral ends in tripping the synchronous compensator, probably commutation failure and voltage collapse. The induction motor pulls out and finally the EMF of the



synchronous compensator manages to re-establish the system voltage and stabilize the system again.

Looking back to the comparison of simulation results in Chapter 9, Figure 9-42 and Figure 9-44, it can be seen from the curves from the KREAN simulations that the control system taking the reference for the firing pulses from the voltage at PCC, has a much sharper increase of frequency than the system using the EMF as reference. This indicates that the latter system should behave better when the load torque is increased. Which it does, as shall be shown.

### 10. 4. 2 EMF in the synchronous compensator as reference

This control system performed well in the quasi-phasor simulations, and the KREAN simulations confirm this. The results for the whole simulation period are shown in the following figures. Figure 10-27 shows the frequencies in the system. Figure 10-28 presents the system voltages and Figure 10-29 displays the angles, calculated in the same way as in the KREAN simulations in the preceding chapter. As with the corresponding quasi-phasor model the system has no problem in handling the induction motor passing the pull-out frequency. This is the point where the other quasi-phasor model failed. Also when the the load is applied to the motor, there are no problems. The same

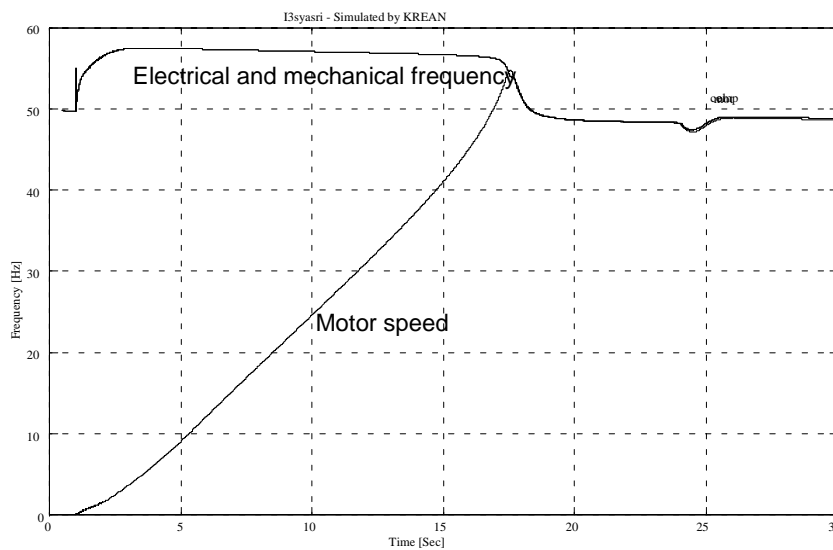


Figure 10-27 Electrical frequency and mechanical frequency for both synchronous compensator and induction motor during DOL start of the induction motor. Firing pulse reference from EMF voltage. Simulated by KREAN.

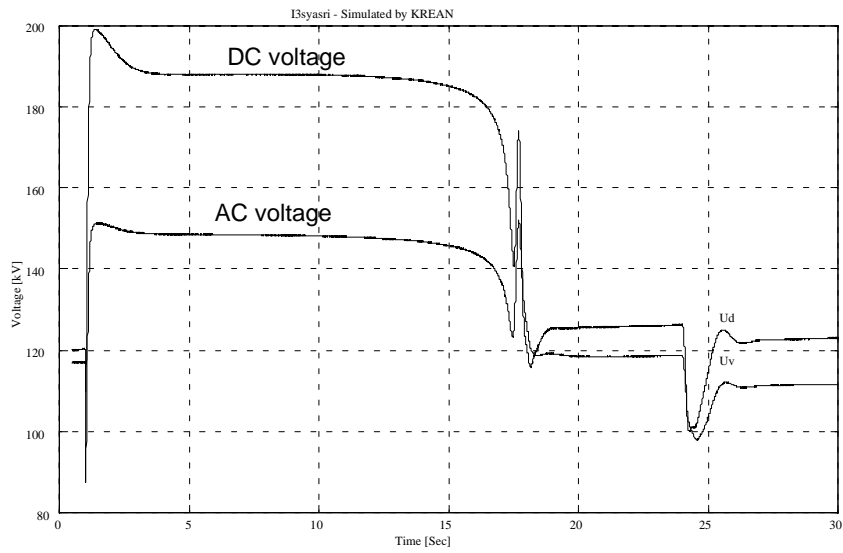


Figure 10-28 AC and DC voltages during DOL start of the induction motor. Firing pulse reference from EMF voltage. Simulated by KREAN.

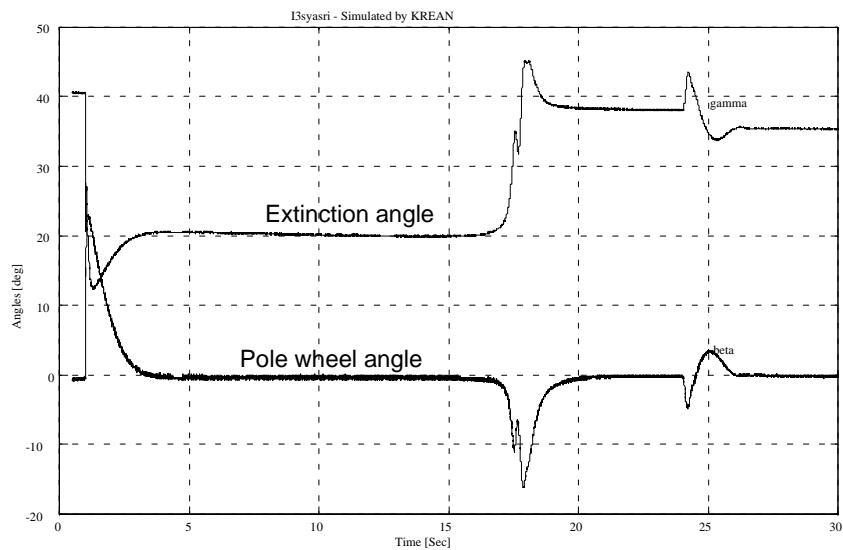


Figure 10-29 Pole wheel angle  $\beta$  and extinction angle  $\gamma$  during DOL start of the induction motor. Firing pulse reference from EMF voltage. Simulated by KREAN.

considerations regarding the frequency increase apply as in the previous case. But, as was shown, the frequency of this system is much less sensitive to load changes than the model with control system based on the voltage at PCC as reference.

Comparison of the quasi-phasor simulation and the KREAN simulations reveals first that the motor accelerates somewhat faster in the KREAN model. The immediate reason for this is that during the acceleration period the system frequency gets somewhat higher in the KREAN model. This leads to a smaller extinction angle  $\gamma$ , and thus to a higher DC voltage. A higher DC voltage means a higher supply of active power, forcing the AC voltage higher, which in turn means even higher DC voltage. The higher system voltages can be seen by a comparison of Figure 10-8 and Figure 10-28. The higher AC voltage leads to higher power consumption in the resistive load in the system, but there is also more power available for the induction motor, allowing it to accelerate faster due to higher electrical torque. The smaller extinction angle  $\gamma$  is clearly visible if the curves for the angles, Figure 10-9 and Figure 10-29, are compared.

## **10.5 CONCLUSION**

The system with control system based on firing pulse reference taken from the voltage at PCC is less stable than the second system. Possibly, good controllers with sufficient power can manage the instability of this system, the instabilities seem to have time constants that can be managed by such controllers without straining them unrealistically. That may be a topic of another study.

The system the with the control system based on firing pulse reference taken from the EMF voltage of the synchronous compensators are intrinsically stable under the given conditions. Operating without controllers, as in these simulations, the values of voltage and frequency are way outside the allowable limits according to norms and regulations. However, it will be of interest to see if simple controllers with realistic capacity can manage to keep the system closer to the norms and regulations. Then it will also be apparent how large the initial steps in voltage and frequency are. These initial steps cannot be controlled by any controllers acting on measurement of deviations, and they will probably be the dimensioning factor for the allowable load switching in the system. But they may be handled by forward feed from the switching command. After all, it is known in advance when a motor is going to be connected, and how it will influence the system.



# **11 PRACTICAL IMPLEMENTATION OF HVDC TRANSMISSION FROM LAND TO AN OFFSHORE INSTALLATION**

In this chapter the practical implementation of an HVDC transmission from land to an offshore installation will be discussed. Some figures for the required rating of the equipment will be calculated. Dimensions and weights will not be treated.

## **11.1 INTRODUCTION**

In Chapter 10 it was shown that it was possible to start an induction machine with an active power rating of 9 MW (10 MVA) in an uncontrolled inverter system consisting of a 100 MW inverter with a base resistive load of 80 MW, although the variations of both voltage and frequency were outside acceptable limits. Norms and regulations [2] call for the voltage to be kept within the limits of +20/-15 % dynamically, and the frequency to be kept within the limits of  $\pm 10$  % dynamically. The investigations were performed without active controllers in the system. The system appeared to be intrinsically stable for the chosen parameters.

It was shown in Chapter 7 that this system has a positive frequency sensitivity for increasing active load. If a considerable part of the load consists of motors, the load is frequency dependent in such a way that the load rises with increasing frequency. This type of load could easily make the system become unstable. In the simulations, the static part of the load was made up by resistors, which are frequency independent. This is the reason for the system being

intrinsically stable. A larger part of rotating machines may disturb the stability.

The simulations performed in Chapter 10 showed that the variations of AC voltage and frequency were about 25-50 % for the voltage and less than 20 % for the frequency. If we assume that the variations are proportional to the size of the motor started, these values would indicate that such a system would be within the allowable ranges when starting motors of about 6 MW. This is to my knowledge, in the range of the largest DOL induction motors that are in use offshore.

Some initial changes will happen too fast for controllers to cope with, but within a time span of less than one second most practical controllers will have ample time to react. One of the aims of this thesis is to decide if such a system will be feasible for available components, and if it will be practically possible to start the largest motor Direct-On-Line while keeping the voltage and frequency within the limits given by the norms.

In order to find out if a working system can be established to supply an offshore installation with electric power from land by means of HVDC transmission, it is reasonable first to investigate what practical possibilities there are to perform a fast control of voltage and frequency on the installation. At the same time it can be appropriate to take a brief look at the demands made on the equipment. Based on this a simple control strategy can be proposed. Then the proposed controlled system could be simulated to verify under which conditions the demands from norms and regulations regarding voltage and frequency can be obtained.

## **11.2 NECESSARY EQUIPMENT ON BOARD THE OFFSHORE INSTALLATION**

The necessary equipment to provide an HVDC power supply for a typical offshore oil installation is indicated in Figure 11-1, together with some important power consumers. As indicated in Chapter 2 and Chapter 6, the part of the load which consists of Direct-On-Line (DOL) started motors, both high voltage and low voltage, will constitute about one half of the total load. The other half consists of adjustable speed drives together with heating and lighting.

This thesis has applied an example based on a 100 MW system with nominal DC voltage of 160 kV, providing an AC voltage of 120 kV. Some typical data about the inverter and load are summarized in Table 11-1. It should be noted that these data are prepared under the assumption that drives

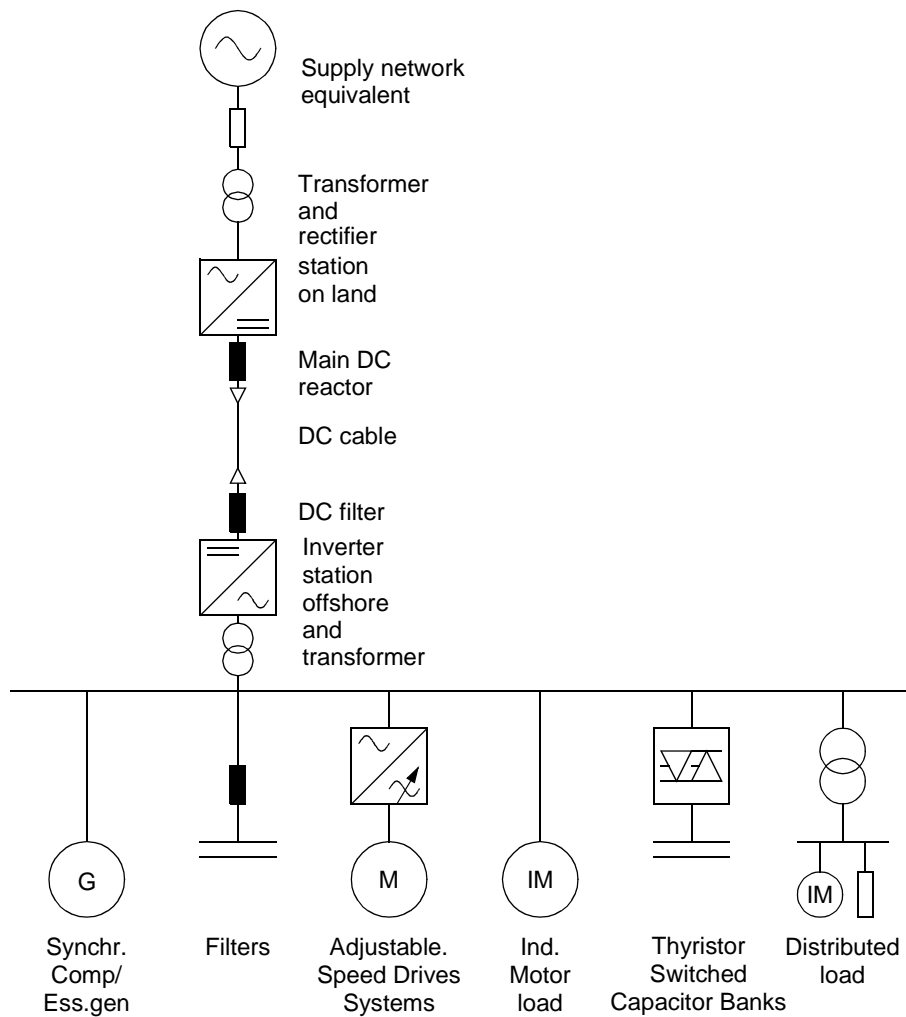


Figure 11-1 Model of HVDC supply to an offshore oil-installation.

which are directly powered by gas turbines today, will be replaced by electrically powered drives. These will mainly be adjustable speed drives due to size and process requirements. The amount of DOL-motor load on an offshore platform today is typically 80 %, and it is assumed that this part of the load will decrease to approximately 50 %. In view of stability and active and reactive power requirements, the worst case is to start the largest DOL-motor when all other loads are running. As in the previous cases it is assumed that the motor which is to be started is 10 MVA or 10 % of the inverter rating. This leaves 40 % of the load as running DOL-motors.

**Table 11-1 Data for Base Case inverter and load.**

Inverter rating [MW]	$P_N$	100
Inverter nominal extinction angle [ $^{\circ}$ ]	$\gamma_N$	20
Non-DOL load (50 %) [MW] (Power factor=1.0)	$P_{nmot}$	50
DOL motor load running at start of simulation(40 %) [MW]	$P_{mot0}$	40
Average power factor of motor load	$\cos(\phi_{av})$	0.85
Rating of motor going to be started DOL [MW]	$\Delta P_{mot}$	10
Start-up current of motor to be started [%]	$I_{0mot}/I_{Nmot}$	430
Nominal power factor of motor to be started	$\cos(\phi_N)$	0.89

### 11. 2. 1 The inverter

This thesis is based on the application of a classical line commutated thyristor inverter, to achieve the power rating required. As the AC voltage will have to be kept within the limitations given by the norms, the DC voltage and the inverter will basically require only the overdimensioning with regard to voltage which is given by the wider tolerances of the voltage on an offshore installation compared to a traditional HVDC inverter. This will amount to approximately 20 %

As has been mentioned before, an important factor in the total feasibility of such a system is the ability to preconsider large load increases, by means of increasing the extinction angle. By constant AC voltage, this will decrease the DC voltage and increase the DC current. But this will not mean a need for overdimensioning the inverter with regard to current, as the DC current only will be increased to the anticipated new level after load switch on, and this will normally not be more than the rated current. Thus it can be concluded that there will be no extraordinary requirements upon the inverter. Some overdimensioning will be necessary due to a larger extinction angle than normal.

### 11. 2. 2 Inverter transformer

Neither is there need for special considerations about the inverter transformer on the platform. The necessary overdimensioning with regard to voltage will be taken care of by the requirement of the norms for 20 % over-voltage capability. It may even be considered if the traditional tap changer can be omitted.



### 11.2.3 Harmonic filters

Harmonic filters will be needed. The dimensioning of these will have to be investigated as the content of harmonic distortion from the inverter in periods will be somewhat higher than normal. The inverter will be run for periods with a much higher extinction angle than in the case of normal HVDC transmission.

Harmonic filters will also be an important source of reactive power at network frequency.

### 11.2.4 Capacitor banks

The bulk of the reactive power required on the offshore installation will have to be produced by capacitor banks, together with the reactive power produced by the harmonic filters. The important consumers of reactive power will be the inverter itself and the DOL-motor drives. Transformers and the distribution network will consume some such power, but there will be no transmission network to consume reactive power.

The maximum need for reactive power appears when the inverter is running at nearly full load and the last and largest induction motor is to be started directly on line. According to the base case previously presented the need for reactive power can be calculated under the assumptions given in Table 11-1.

As pointed out in Section 7.3.2 the inverter has to be prepared for a load increase by increasing the extinction angle. This is done in order to decrease the DC voltage and increase the DC current supplied, such that the inverter is able to supply the required increase in power without exceeding the commutation margin. The required extinction angle  $\gamma_0$  before starting the last and largest motor (10 %) is given by:

$$\gamma_0 = \arccos\left(\frac{P_N - \Delta P}{P_N} \cos\gamma_N\right) \quad (7-84)$$

$$\gamma_0 = \arccos\left(\frac{90}{100} \cos 20\right) = 32.25[^\circ] \quad (11-1)$$

The need for reactive power to the inverter before starting the motor will then be

$$Q_{inv0} = P_{inv0} \tan(\gamma_0) = 90 \tan(32.25) = 56.8 [MVA_r] \quad (11-2)$$

The need for reactive power to the running motors will be

$$Q_{mot0} = P_{mot0} \tan(\varphi_0) = 40 \tan(\arccos 0.85) = 27.9 [MVA_r] \quad (11-3)$$

The need for reactive power to the motor to be started will be

$$\Delta Q_{mot0} = \frac{\Delta P_{mot}}{\cos(\varphi_N)} \cdot \frac{I_{0mot}}{I_{Nmot}} = \frac{10}{0.89} \cdot 4.3 = 48.3 [MVA_r] \quad (11-4)$$

Disregarding the need of transformers and distribution network, as well as necessary reserve for control purposes, the maximum need for reactive power will be the sum of (11-2), (11-3) and (11-4):

$$Q_{max} = Q_{inv0} + Q_{mot0} + \Delta Q_{mot0} = 56.8 + 27.9 + 48.3 = 133 [MVA_r] \quad (11-5)$$

After the motor has started and the system has stabilized, the need for reactive power will be:

- Inverter:

$$Q_{invN} = P_{invN} \tan(\gamma_N) = 100 \tan(20) = 36.4 [MVA_r] \quad (11-6)$$

- Just started motor:

$$\Delta Q_{mot} = \Delta P_{mot} \cdot \tan(\varphi_N) = 10 \cdot \tan(\arccos(0.89)) = 5.1 [MVA_r] \quad (11-7)$$

The rest of the motors will have unchanged needs for reactive power, and the total need will now be:

$$Q_N = Q_{invN} + Q_{mot0} + \Delta Q_{mot} = 36.4 + 27.9 + 5.1 = 69.4 [MVA_r] \quad (11-8)$$

The need for reactive power will vary widely according to the load situation, and there must be some way of controlling the production. In the earlier simulations in this thesis it has been assumed that the total network capaci-

tance was continuously controllable. This is not the case for capacitors. For our purpose they can best be switched in groups by means of thyristor switches, Thyristor Switched Capacitors (TSC). Fortunately there is the synchronous compensator which can take care of the fine tuning between the steps of the capacitor banks. The synchronous compensator can be controlled from nominal rating underexcited (i.e. inductive) to nominal rating overexcited (i.e. capacitive). Thus the range of 2 times  $S_{sc,N}$  is the theoretical maximum step size of the capacitor banks. Preferably they should be smaller.

### 11. 2. 5 Synchronous compensator

The synchronous compensator is considered to serve a dual purpose. Apart from the primary function of a compensator it may also serve as an essential generator, powered by a gas turbine. Therefore the dimensioning of the compensator has been linked to a typical, large gas turbine powered generator rated 20 MW. This rating is equivalent to an apparent power rating  $S_{sc,N}$  of 22.5 MVA for the compensator, which can be applied both over- and underexcited. This means that such a compensator can cover a maximum step size of the capacitor banks of 45 MVar. What the step size actually ought to be is just as much dependent on how the voltage and frequency controllers behave, and how much disturbance such a step initiates.

The size of the compensator is also very much determined by the necessary range in reactive power for retaining control with the voltage in the system. This dynamic rating is of short duration and may lie well outside the stationary rating of the compensator, depending on the overload capacity.

The possibility of using the synchronous compensator as a generator is also important at start-up of the system. As an offshore installation with electric power supply by HVDC transmission from land would in any case be dependent of an essential generator supply in case of transmission faults, this generator can also be applied for the start-up procedure.

It is expected that the demands to the excitation system of the generator may be greater than normal. This will have to be investigated closer.

It is not presently known to me if a gas turbine can be left running cold, or if there has to be installed some sort of clutch between the motor and the turbine. In this thesis it has been assumed that such a clutch is installed, and only the inertia of the synchronous machine itself has been considered. If the turbine is going to run along, this will not mean much difference, as the turbine is normally coupled directly on the generator shaft and does not provide much inertia.

### **11. 2. 6 The motor to be started**

Large electric motors on offshore oil installations have traditionally been limited to 5-8 MW for induction motors with DOL start. This limit has been put by the power generation system which does not allow direct starting of larger motors. Some larger drives exist, these are mainly synchronous motor drives powered by frequency converters. Controlled drives are possible to start smoothly, and represent no problem under start. The problems lie with the DOL start of large induction motors.

The large induction motors, which mostly power compressors or pumps, will normally be started with closed valves, in order to facilitate the start. Only when the motor is running at nominal speed will the valves be opened gradually, to avoid excess mechanical stresses and shocks in the system. The active and reactive load the motor draws from the network will always be given by the torque and current vs. speed curves for the motor. Different inertia and counter-torque will not influence these curves, but they will of course have a great influence on the development of the speed during start-up.

### **11. 2. 7 Running DOL motors**

This will be a mix of large and small motors. The large motors will be connected close to the inverter on the high voltage busbar, while the small motors will be distributed behind transformers. Each motor will behave individually, but seen from the supply, and for simulation purposes, they can be lumped together into a virtual motor with power rating like the sum of the individual ratings. The resulting inertia will have to be calculated from a resulting mechanical time constant, a weighed average of the individual mechanical time constants. Torque and reactive power have to be calculated from typical p.u. values for a representative motor.

### **11. 2. 8 Control strategy on board**

There are two variables that can be controlled in such an electric power system on board an offshore installation. These are the firing delay time of the inverter and the reactive power production. The firing delay time controls the DC voltage, and thus the immediate active power supply, under the assumption that the DC current cannot change swiftly. The reactive power supply is controlled by means of switching capacitors for coarse control and by the synchronous compensator for fine tuning. The result of the reactive power control can be regarded as the continuously variable capacitor which was applied in the former chapters of the thesis.

It was shown in Section 7. 2. 5, by means of sensitivities, that it would be most efficient to use the firing delay time (i.e. active power) for frequency control and leave the “variable capacitance” (i.e. reactive power) for voltage control. This is in fact similar to the way any electric power grid is controlled today.

## 11. 2. 9 Land-based rectifier

We assume that the voltage control on the platform is able to keep the AC voltage within the dynamic limits. We also assume that the inverter control on the platform is able to keep a minimum extinction angle  $\gamma$  of  $15^\circ$ . As have been seen in the previous simulations the maximum voltage and minimum extinction angle tends to coincide, so let us further assume this happens, in order to get a worst case. Then we have the maximum DC voltage of:

$$U_{d,max} = U_{vN,platform} \cdot 1.2 \cdot 1.35 \cdot \cos 15 = 1.565 \cdot U_{vN,platform} \quad (11-9)$$

The AC voltage on land is not allowed to vary, but the rectifier must be able to provide this DC voltage without getting below a minimum firing angle  $\alpha$ , which typically will be  $5^\circ$ . Thus, if we ignore the voltage drop along the cable, we have:

$$U_{d,max} = 1.565 \cdot U_{vN,platform} = U_{vN,land} \cdot 1.35 \cdot \cos 5 \quad (11-10)$$

which gives the necessary AC voltage on land:

$$U_{vN,land} = \frac{1.565}{1.35 \cdot \cos 5} \cdot U_{vN,platform} = 1.164 \cdot U_{vN,platform} \quad (11-11)$$

But, if we keep this voltage stable on land, we have to control the rectifier firing angle  $\alpha$  to a high value during normal operation, when the voltage on the platform is normal and the inverter extinction angle is normal:

$$U_{d,norm} = U_{vN,platform} \cdot 1.35 \cdot \cos 20 = U_{vN,land} \cdot 1.35 \cdot \cos \alpha \quad (11-12)$$

$$\cos \alpha = \frac{U_{vN,platform} \cdot 1.35 \cdot \cos 20}{U_{vN,land} \cdot 1.35} = \frac{1.269 \cdot U_{vN,platform}}{1.164 \cdot U_{vN,platform} \cdot 1.35} = 0.807 \quad (11-13)$$

$$\alpha = 36.2^\circ \quad (11-14)$$

Operating the rectifier in normal operation at this high firing angle requires very large phase compensating capacitor banks and large filters. As the network voltage on land is not allowed to vary, the rectifier transformer has to be equipped with a tap changer. Then the terminal voltage of the rectifier can be reduced bringing a reduction in the firing angle as well. Tap changers are normal on rectifier transformers for HVDC, and they often have a range of operation of  $\pm 15\%$ , which would be sufficient in this case.

The tap changer will not be able to operate during the start-up of a large motor on board. This means that before a start takes place, the tap changer has to be placed on one of the top steps, corresponding to the anticipated high DC voltage. As previously mentioned, the DC current will be increased and the DC voltage reduced previous to the start of a large motor. It was calculated that the extinction angle would be as high as

$$\gamma = 32.25^\circ \quad (11-1)$$

With the tap changer prepared for the coming start, we have the AC voltage calculated in (11-11) on land, and we can calculate the firing angle  $\alpha_0$  before the motor is started:

$$\cos \alpha_0 = \frac{U_{vN, platform} \cdot 1.35 \cdot \cos 32.25}{U_{vN, land} \cdot 1.35} \quad (11-15)$$

$$\cos \alpha_0 = \frac{1.142 \cdot U_{vN, platform}}{1.164 \cdot U_{vN, platform} \cdot 1.35} = 0.726 \quad (11-16)$$

$$\alpha_0 = 43.4^\circ \quad (11-17)$$

This firing angle will only be applied for a short time and need not to be the basis for dimensioning of the local phase compensation equipment at the rectifier station.

## 11. 2. 10 Rectifier control

It is not the scope of this thesis to optimize the necessary control for a HVDC transmission from land to an offshore installation, but a few points have to be indicated. Practically all controllers for thyristor-based converters in any application are built with an inner, fast current control loop and an outer, slower loop adapted to the relevant task. Also classical HVDC controllers make use of an inner, fast current control loop, as described in Chapter 4.

It has also been an assumption in this thesis that the rectifier will have an inner, fast current control loop. Together with the large smoothing inductor of the transmission line, this has been the basis for the modelling of the DC supply as a constant current source.

The outer loop, however, is an open question. It can be omitted altogether, leaving the rectifier to supply the current order from the platform. This is a fairly safe concept. As long as the current is constant, the inverter on board can control the power transmitted by means of controlling the DC voltage via the extinction angle. If there should be a loss of communication between platform and land, the rectifier will stick to the last current order received and the system will not fall apart.

A concept based on constant power supply from the rectifier will not be safe. If communication fails, and the platform at the this time reduces the need for power, the rectifier will continue to supply power the platform cannot consume.

### **11. 2. 11 Telecommunications**

This system will be extremely dependent on safe telecommunications. It has been presupposed that the system should be able to survive if the communications break down, but the system will not be able to operate for a long time without being able to control the current flowing onto the platform. Modern telecommunications based on fibreoptics are reliable and fast, this technique will be a must in a such case. It is debatable whether the optical fibres are to be integrated in the power cables, or if they are to follow separate routes. In both cases they have to have full redundancy.

### **11. 2. 12 Worst case variation of reactive power**

The worst case variation of reactive power that the system must be able to handle, is the case when the last large motor is started. Based on the figures found in Section 11. 2. 4 we can tabulate the variation of need for reactive power as shown in Table 11-2. It appears from the figures that if the synchronous compensator is to take care of all variations of reactive load during start-up of the motor, it will be heavily overloaded. Some overloading may be allowable for the relatively short duration of the start-up, but these requirements are probably too much. This means that the capacitor banks must be controlled in a way that allows fast switching during the course of the start-up. Thus at least a number of the capacitor banks should be thyristor switched.

**Table 11-2 Variation of reactive power**

Inverter rated power	100	MW
Inverter nominal extinction angle	20	°
Synchronous compensator rating	±22.5	MVAr
Heating, lighting and variable speed drives	50	MW
Sum of running DOL-motors	40	MW
Last motor to be started DOL	10	MW
Extinction angle prior to connecting last motor	32.25	°
Need for reactive power prior to connecting last motor	84.7	MVAr
Synchr. compensator load prior to connecting last motor	-22.5	MVAr
Capacitor rating prior to connecting last motor	107.2	MVAr
Need for reactive power immediately after connection	133	MVAr
Increase of reactive power	48.3	MVAr
Synchr. compensator load immediately after connection	+25.8	MVAr
Synchr. compensator load immediately after connection	115	%
Final need for reactive power after connection	69.4	MVAr
Decrease of reactive power from peak	63.6	MVAr
Decrease of reactive power from prior to connecting last motor	15.3	MVAr
Final synchr. compensator load	-37.8	MVAr
Final synchr. compensator load	-168	%

### 11. 2. 13 Procedure for starting a large motor

The procedure for starting a large motor can be:

- When it is decided to start a large motor it will be known how much power this motor will pull from the network when the start is completed.
- The required DC current to supply this power at normal DC voltage can be calculated.



- The tap changer on the rectifier transformer is placed on a sufficiently high step to handle the peak DC voltage. The firing angle  $\alpha$  has to be increased correspondingly.
- The current reference for the rectifier is adjusted such that the additional current required by the starting motor is supplied, and the inverter extinction angle adapts to the new current by increasing, so that the DC voltage is reduced. The firing angle  $\alpha$  has to be increased further.
- During the change of extinction angle, the supply of reactive power will be controlled accordingly. The system has to be prepared for a sudden rise in the demand for reactive power by selecting an extra step in the capacitor bank and running the synchronous compensator in the inductive range.
- It may be necessary to switch capacitor banks during the start-up of a motor.
- When the HVDC system has stabilized after the preparations, the switching command can be given to the circuit breaker of the motor. It may be considered if some sort of feed-forward command to the control system can be applied. One possibility could be a command to increase the excitation of the synchronous compensator at the same time or even slightly before.
- When the system has stabilized and the motor is running with load, the rectifier can start controlling the DC current in order to optimize the inverter extinction angle and the transmission DC voltage. The tap changer control can be released to find an optimal firing angle  $\alpha$  for the rectifier.

### 11.3 SUMMARY

Assuming that the voltages on the platform can be kept within the limitations given by the norms, there will be a need for 20 % voltage overdimensioning of the inverter, but no current overdimensioning. The worst problem is the control of reactive power, the change of demand under worst case load switching is calculated to be an increase of 43.8 MVar, followed by a decrease of 63.6 MVar. These are outside the supposed nominal range for the synchronous compensator,  $\pm 22.5$  MVar. Either some capacitors must be switched during the starting procedure, or the compensator has to be overloaded for a short time.



# **12 KREAN SIMULATIONS ON MODEL WITH INVERTER, SYNCHRONOUS COMPENSATOR AND LOAD**

In this chapter we shall perform the final simulations to confirm that the system may be feasible. Due to the development of the thesis it will not be the complete simulation that was foreseen in Chapter 6, but the main elements will be present.

The simulations will be performed in the time-domain by means of KREAN, not by Quasi-phasors.

## **12.1 SIMULATION CONDITIONS**

The final test is to see if a model system consisting of realistically parameterized components is able to keep voltage and frequency within the limitations specified by the norms. In order to do so the system must have active controllers. It is not the scope of this thesis to perform any optimization of the controllers involved. As a basic dimensioning the values found in Chapter 7. 3 will be applied.

The verification simulations in Chapter 10. 4 indicates that the simulations with quasi-phasors give to low dynamic variations compared to time domain simulations. Therefore it was decided to perform the final analysis with KREAN. Furthermore it was decided to perform the simulation only with a resistive base load, as the simulation time and computer resources would get beyond the available if a more detailed simulation were to be made.

## 12.2 MODEL WITH RESISTIVE BASE LOAD

The model is shown in Figure 12-1. This is the same model as was inves-

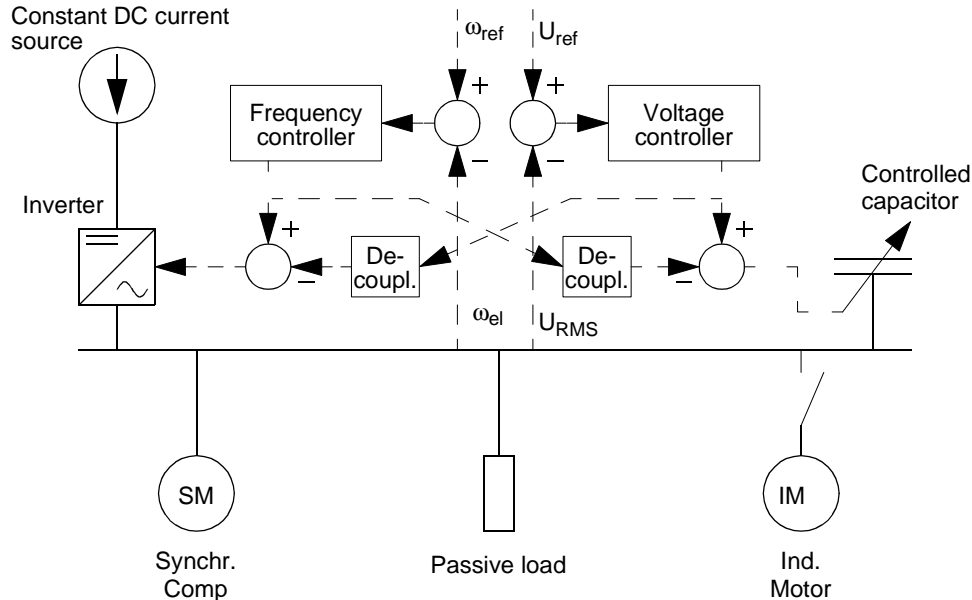


Figure 12-1 First step of model of HVDC supply to an offshore oil-installation, to be simulated in KREAN.

tigated in Section 10. 3, with reference for the firing angle taken from the EMF of the synchronous compensator. But now the simulations will be performed in the true time domain as in the verification simulations in Chapter 10. 4, not with RMS-values. Additionally the controllers will be activated. The synchronous and induction machines are modelled by state space models which belong to the standard module library of KREAN. Data for the machines will be based on p.u.-values from real machines in the relevant power range, see Appendix B and Appendix C. The controllers will be based on the values found in Chapter 7. 3. The main data for the simulation is given in Table 12-1.

The initial conditions are based on the principle of preparing the system for the additional load, such that after the load is connected, the inverter will be operating with approximately nominal extinction angle. As in all the previous simulations, the commutation is disregarded. The voltage control is performed by ideally controllable capacitors and the frequency control by firing delay control. The controllers are decoupled as it was shown in Chapter 7. 3. It must be noted that in order not to exceed the length of the available plot array, the inertia of the starting motor had to be reduced. This has no influence on the principal progress of the simulation, except for the

**Table 12-1 Main data for KREAN simulation.**

Inverter nominal power rating at 50 hz [MW]	100
Inverter nominal firing angle $\alpha$ at 50 hz [ $^{\circ}$ ]	160
AC nominal voltage at 50 hz [kV]	120
AC nominal current [A]	512
DC nominal current [A]	657
DC nominal voltage [kV]	-152.3
AC network equivalent initial load [MW]	80
AC network equivalent initial admittance, per phase $G_0$ [mho]	5.56
Initial extinction angle $\gamma_0$ [ $^{\circ}$ ]	35.4
Initial firing delay $\Delta t_0$ [ms]	8.147
Initial DC current $I_{d0}$ [A]	619
Synchronous compensator rating [MVA]	20
Initial synchronous compensator reactive power [MVA <sub>r</sub> ]	16.5
Initial value of controllable capacitance, per phase $C_0$ [ $\mu$ F]	8.71
Induction motor rating [MW]	10

oscillation when the motor reaches full speed. These will be correspondingly faster and the influence on the synchronous compensator will be less, but this is not important for the total stability of the system. And it has no influence on the transient variations of voltage and frequency due to load changes.

The results of this simulation, after some minor adjustment of the controller parameters, are shown in the following figures. The course of the simulation is apparent from Figure 12-2. First, 1 s is allowed for initial stabilization. At time  $t=1$  s, the induction motor switch is connected and the motor starts. At time  $t\approx 3.3$  s, the motor reaches full speed and oscillates a little around synchronous speed, due to the long time constant of the EMF in the motor, which makes it behave almost as a synchronous machine transiently. During the start-up, and after the motor has reached full speed, until time  $t\approx 5$  s, the controllers are working to keep voltage and frequency at required levels, as can be seen from Figure 12-3 and Figure 12-4. At time  $t\approx 7$  s, the load torque is switched instantaneously on, and the controllers adjust the system to the new power level.

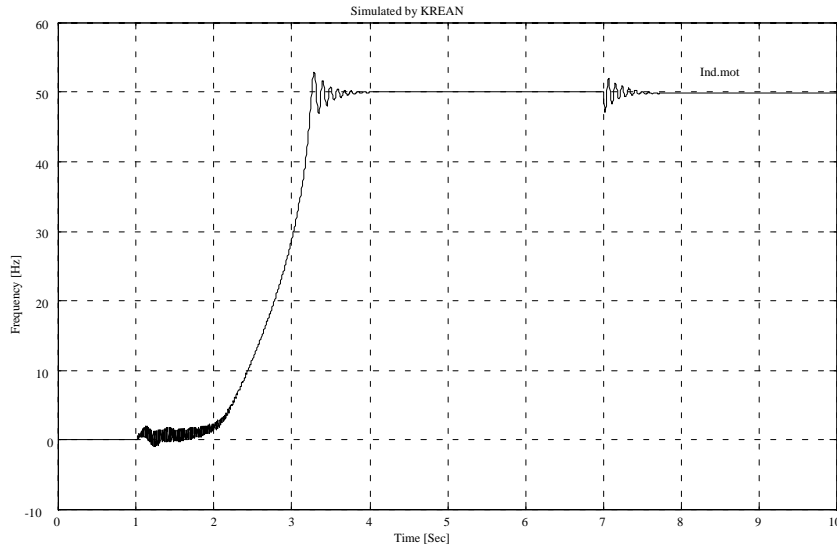


Figure 12-2 Speed of motor during start-up of a 10 MW induction motor.

Figure 12-5 presents the  $AC_{RMS}$  voltage and Figure 12-6 depicts the DC voltage during the simulations. Before the curves are discussed, it should be recalled that the controllers are not optimized and the results do not fulfil the requirements of the voltage limitations set forth in the relevant norms and regulations. The AC voltage behaves quite contrary to traditional expecta-

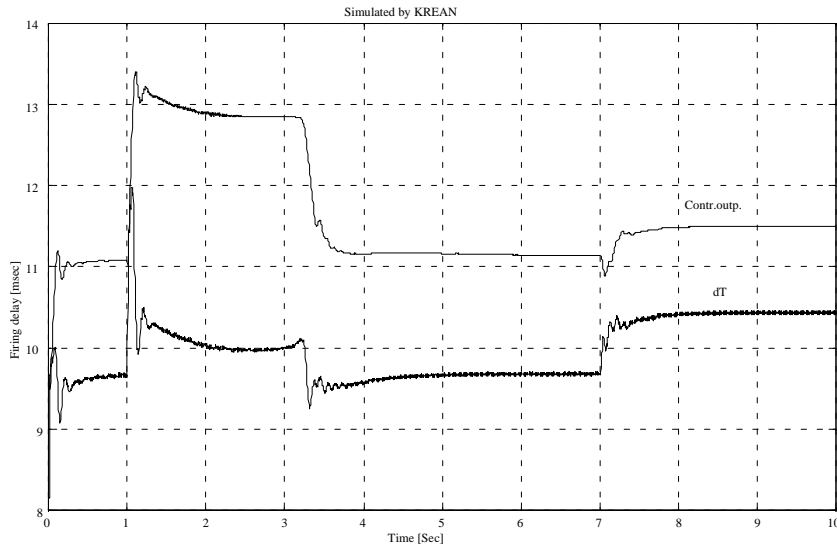


Figure 12-3 Firing delay control values before and after decoupling during start-up of a 10 MW induction motor.

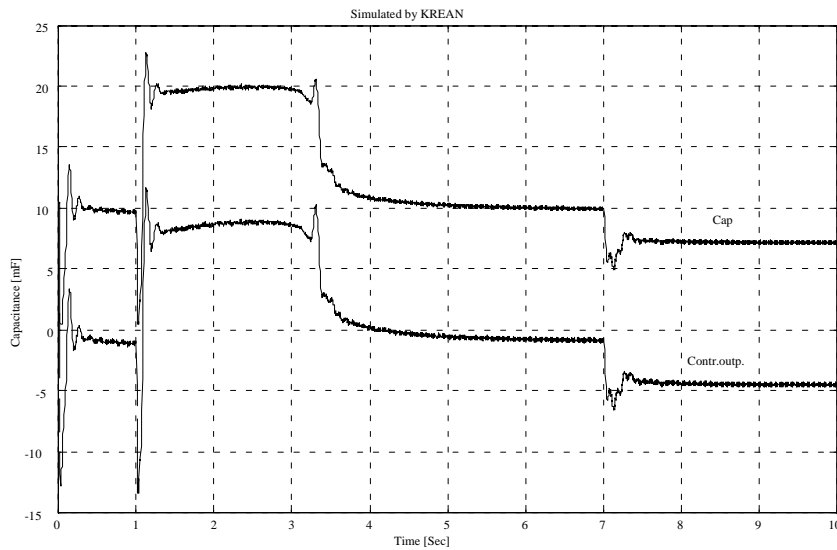


Figure 12-4 Capacitance control values before and after decoupling during start-up of a 10 MW induction motor.

tions, but in accordance with the theoretical analysis as explained in Chapter 7. The voltage rises when the initially inductive load of the induction motor is switched on, except for a transient dip due to a short DC component. The voltage rises because an increase of inductive susceptance actually decreases the admittance of the total system which is in the capacitive range.

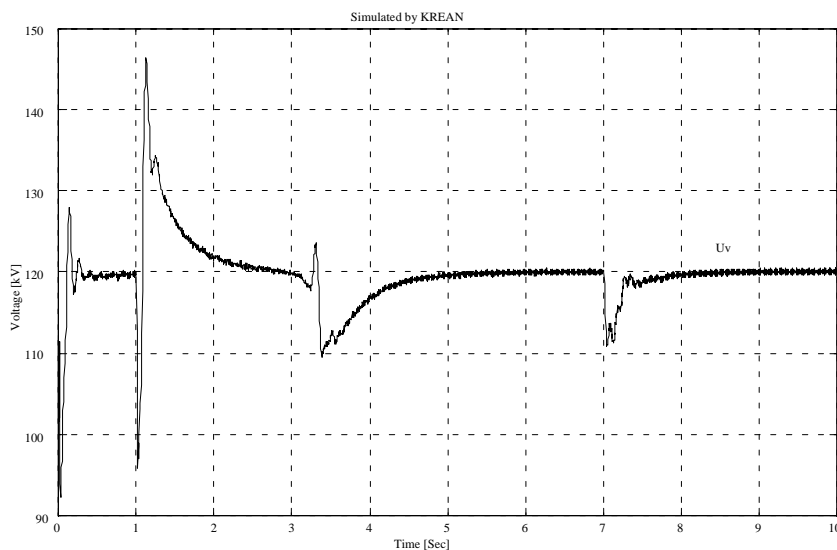


Figure 12-5 AC-RMS voltage during start-up of a 10 MW induction motor.

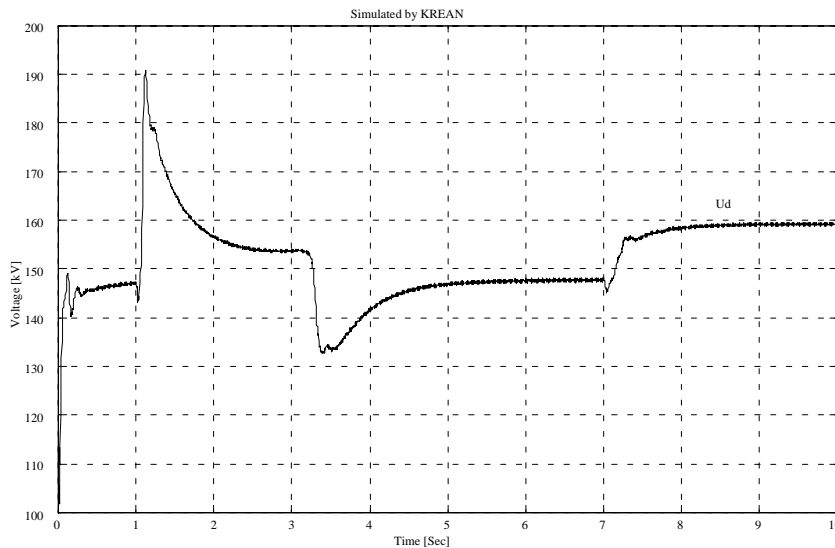


Figure 12-6 DC voltage during start-up of a 10 MW induction motor.

As the capacitance controller reacts, the capacitance, and thereby the admittance is increased and the voltage drops back to the required level. When the motor reaches full speed, the inductive load decreases abruptly and the opposite takes place. Here too, first, the voltage transiently increases due to a short DC component, then the total admittance of the system, as seen from the inverter, increases and the voltage drops again. Now the controller must counteract by decreasing the capacitance. Finally, when the load torque is applied, this can be interpreted as an increase in the resistive conductance which gives a traditional voltage drop that is corrected by a combined operation of voltage and frequency controllers.

The network frequency is shown in Figure 12-7. The frequency is measured by means of the speed of the synchronous compensator. There are good reasons for this method of measurement. As long as the synchronous machine does not fall out of synchronism, which would indicate a severe stability problem, the machine is never more than  $90^\circ$  out of phase from the voltage. The machine speed is a continuous measurement, not a sampled one, and the inertia of the machine effectively dampens transients due to phase shifting of the voltage. The consequences of this choice of frequency measurement has been discussed in Chapter 9.

The frequency deviations can be explained as follows: At time  $t=1$  s, when the induction motor is switched on, the AC voltage drops abruptly in the first instant, while the DC voltage stays almost constant. This implies that the additional active load in the AC network, which is purely resistive, drops



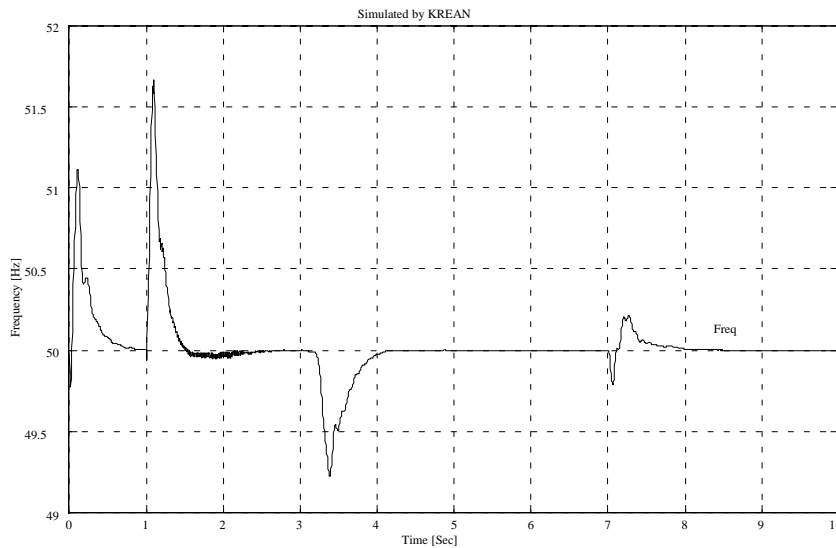


Figure 12-7 Network frequency during start-up of a 10 MW induction motor.

proportional to the square of the AC voltage. At the same time, the DC voltage drop is negligible, and this together with the constant DC current means an unchanged input of active power in the AC system. This implies a surplus of active power which has to be absorbed by the synchronous compensator, which is accelerated and the frequency increases.

After the initial drop, the AC voltage increases and pulls the DC voltage along. This implies that the increase in active load in the AC system is greater than the increase in active supply in the DC system. The deficit has to be supplied by the compensator, which decelerates again, and brings the frequency down. Meanwhile, the frequency controller tries to keep the frequency at rated value, which it manages after the time has reached approximately  $t \approx 2.5$  s.

At time  $t \approx 3.3$  s the opposite course of events takes place. Initially the AC voltage increases without the DC voltage following, pulling active power out of the compensator and slowing it down. Next, both voltages drop, leaving surplus active power to accelerate the compensator again, until the frequency controller manages to get the system back on rated frequency once more.

Both these disturbances were initiated by changes in inductive load, not active load. At the time  $t = 7$  s, when the load torque is applied, it behaves almost according to what was found in the sensitivity analysis in Chapter 7. This can also be given a physical explanation. In the first instant after the load torque is applied there is a shortage of power in the system, and the deficit is drawn from the rotating energy in the compensator, which slows down. At the

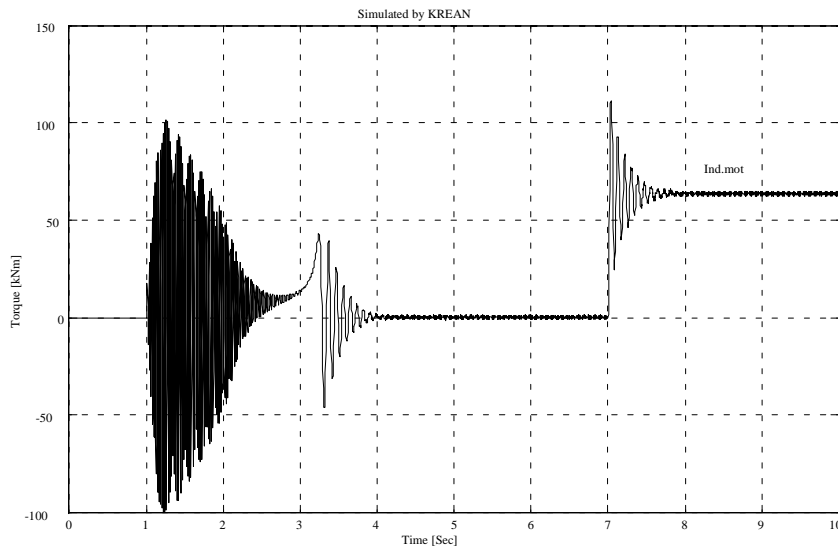


Figure 12-8 Air gap torque in motor during start-up of a 10 MW induction motor.

same time, however, the AC voltage drops significantly. The additional load in the system is resistive, thus it draws a power load proportional to the square of the voltage. The supplied power, however, is directly proportional to the DC voltage when the DC current is constant, as has been presupposed. Thus, even as the DC voltage drops practically proportional with the AC voltage, the supplied power drops less than the reduction of consumed power in the resistive load, and the surplus has to be taken up by the compensator, which accelerates again, until the controllers once more manages to get voltage and frequency back to required values.

Figure 12-8 depicts the torque variations in the motor while starting. The progress is so similar to a normal simulated start progress at any strong network, it could be mistaken. It should be noted, as mentioned earlier, that this model has linear parameters, thus the torque during start-up is to low compared to real machines. The trick with the auxiliary start-up torque has not been applied in this case.

### 12.3 CONCLUSION

These simulations indicates that with good controllers it should be possible to keep a system as investigated stable, even when starting an induction motor in the range of 10% of the total inverter rating. The extra problem of a

frequency dependent motor load is assumed to be possible to handle by means of good controllers, as this is a fairly slow acting problem and the frequency deviations even with these non-optimized controllers are within the required limits. Initial voltage deviations are in the range of  $\pm 21\%$ , which is not very far from the limits of  $+20/-15\%$ . Good controllers, perhaps including some sort of feed-forward, should be able to handle this.

It is also to be noted that the maximum DC voltage recorded is approximately 190 kV. This coincides well with the calculated required maximum DC voltage in section Section 11. 2. 9. The maximum voltage was calculated to be

$$U_{d, max} = U_{vN, platform} \cdot 1.2 \cdot 1.35 \cdot \cos 15 = 1.565 \cdot U_{vN, platform} \quad (11-9)$$

That is

$$U_{d, max} = 1.565 \cdot U_{vN, platform} = 187.2[kV] \quad (12-1)$$

which is a difference of 1.01 %



# 13 CONCLUSIONS

## 13.1 BACKGROUND

This study was initiated to investigate if it could be feasible to supply offshore oil installations in the North Sea with electrical power from land. It was clear from the beginning that the transmission would have to be by means of HVDC, as the distances are too far to reach by AC cables. Other studies indicated that conventional HVDC transmission would not be feasible due to the need for large and heavy synchronous compensators. A pre-study of alternative converter topologies indicated that the most promising solution would be to investigate a conventional system with reduced synchronous compensator rating. Classical analysis of HVDC transmission for the supply of a weak network has always assumed a Thevenin equivalent for the network, being able to accept power delivery with variable power factor. These studies indicate a minimum synchronous compensator rating of 60 % of the inverter rating.

## 13.2 FREQUENCY MUST VARY

After a summary of the state of power supply to offshore installations today, and a short review of classical HVDC transmission, this study continued by analysing how a passive network without sources influences the inverter. The transmission, with its current controlled rectifier and large inductance, is simulated as a current source. Under these circumstances the analysis shows that the network frequency has to adapt in order to keep active and reactive power balance until controllers are able to react. The concept of firing angle for a thyristor is limited in a system with variable frequency, what actually is controlled is the firing delay time. With variable frequency,

constant firing delay time before controllers react, implies a variable firing angle.

Sensitivity analysis showed some astonishing consequences. The frequency rises both by increased active and increased reactive loads. Voltage falls by increased active load, but rises by increased inductive load. It is more natural that the voltage rise and the frequency falls for increased firing delay time.

### **13.3 TWO MODELS**

Two systems of inverter, synchronous compensator and load are defined, based on two different control principles. The first takes the reference for the firing delay time from the fundamental voltage at the point of common coupling. The second takes the reference for the firing delay time from the simulated EMF of the synchronous compensator. Of these, the second is the more stable. It acts slower, both following disturbances and control commands. It also gives the smallest dynamic deflections. This should be chosen as a basis for a possible control system.

### **13.4 TWO SIMULATION TOOLS**

Two simulation tools are applied. The first is a quasi-phasor model running on Matlab with Simulink. The other is a time domain model in KREAN. The time domain model is primarily used for the verification of the quasi-phasor model, and shows that quasiphasors is still a valuable tool for making a quick analysis of the main features, when the details of the transients are of less importance. All principal features of interest were present in the quasi-phasor analysis.

### **13.5 SIMULATION RESULTS**

This study indicates that power supply by HVDC transmission from land to offshore oil installations could be technically feasible, even without the large synchronous compensators normally required. It has been shown that in a network only supplied by an inverter, variations of active and reactive loads have significant influence on both voltage and frequency. It was shown that a system with a frequency independent base load was intrinsically stable for the switching of an additional load. The system with reference for the firing

pulses taken from the synchronous compensator EMF, was also stable for the connection of an induction motor with rating that was 10 % of the inverter rating. In the case of a frequency dependent load, such as motors, the system was shown to be potentially unstable, independent of the reference voltage, due to positive frequency sensitivity to the increase of load. With very simple operating controllers it was shown that the frequency was dynamically and stationary within the limits of norms and regulations. The voltages were dynamically outside the limits, though not very far outside. Better controllers should be able to handle this.

The simulations indicate that if the inverter is used actively to control the frequency of the network on the oil platform, together with voltage control by means of reactive power, from capacitors and the “small” synchronous compensator, it should be possible to supply an oil platform with electric power from land by means of HVDC transmission. Whether this is economically feasible has not been investigated. Neither has it been considered whether the necessary equipment can actually be installed on an oil platform.

## **13.6 PRACTICAL IMPLEMENTATIONS**

Assuming that the voltages on the platform can be kept within the limitations given by the norms, there will be a need for 20 % voltage overdimensioning of the inverter, but no current overdimensioning. The worst problem is the control of reactive power, the change of demand under worst case load switching is calculated to be an increase of 43.8 MVar, followed by a decrease of 63.6 MVar. These are outside the supposed nominal range for the synchronous compensator,  $\pm 22.5$  MVar. Either some capacitors must be switched during the starting procedure, or the compensator has to be overloaded for a short time.

## **13.7 RECENT DEVELOPMENT**

This work has taken a long time to complete. Recently both ABB and Siemens have presented solutions for HVDC transmission in the lower and medium power range based on voltage source converters based on IGBTs. These solutions have already been applied to a prestudy for BP of the possibilities to supply their installations in the British Sector of the North Sea with electrical power from Scotland. This prestudy indicates that the technical solutions are available. Fully controllable voltage source HVDC converters have properties that may be better suited to supply weak or passive networks

such as offshore oil installations with electrical power rather than conventional line commutated current source thyristor inverters. But they also have some disadvantages, higher losses is one, and a complete technical and financial comparison must be performed in order to decide for any potential project.

The new technology, based on voltage source converters, introduces a better possibility of constructing multiterminal systems. It is also possible to connect these units in parallel in order to increase capacity. On the other hand, the announced possibility of providing the necessary reactive may be somewhat overstated, taking into account that this requires increased current carrying capability and consequently overdimensioning. But they may provide an interesting provider of part of the reactive power required, and at least they may be operated in a way that they do not require reactive power themselves under normal conditions.

It was not a part of the study to optimize controllers, but even with simple controllers it was possible to keep the frequency within limits given by norms and regulations, but the voltages were dynamically outside the limits, though not very far. These voltage overswings take place in the first few instances after a disturbance, so it takes unrealistically fast controllers to handle them. They are partly due to the model, where the land based rectifier and the DC reactors are simulated by a constant current source, but partly they have to be handled by overdimensioning of the system.



# **APPENDIX A    CALCULATION OF ACTIVE AND REACTIVE POWER OF AN INDUCTION MOTOR BASED ON CURVES FOR TORQUE AND CURRENT DURING START-UP**

For all electric induction motors, particularly large ones, there will be available data for torque and current during start-up. The data are usually given by relative values, Torque/Rated Torque, Current/Rated Current and Speed/Synchronous Speed in the form of curves, computed and/or measured for a given voltage, usually the nominal. From these data it is easy to calculate the active and reactive power drawn from the network during a direct on-line start. Some assumptions have to be made:

- The efficiency of the motor must be high, so the losses can be ignored. This is usually fulfilled in the case of large, modern motors, where the efficiency  $\eta$  normally is better than 97 %.
- The electric frequency should not vary wide from the nominal frequency, in order that the frequency dependent parameters should not be influenced too much. A variance of  $\pm 10\%$  as allowed transiently in the norms [2] is considered acceptable.
- The impedance of the starting motor is independent of the applied voltage.

The electric power taken from the network is, disregarding the stator losses, equal to the power transmitted through the air gap by synchronously rotating magnetic fields. That is, in p.u.:

$$p = m \left( \frac{\omega_{mek}}{\omega_{el}} \Big|_{u_n} \right) \cdot \omega_{el} \quad (\text{A-1})$$

where  $p$  is active power in p.u.

$\omega_{mek}$  is mechanical speed in p.u.

$\omega_{el}$  is electric frequency in p.u.

and  $m(\omega_{mek}/\omega_{el}|_{u_n})$  is real start-up-torque as function of relative speed at nominal voltage in p.u.

The electrical power equation at nominal voltage is:

$$p = \frac{u_n^2}{r} = \frac{1}{r} \quad (\text{A-2})$$

where  $u_n$  is nominal voltage in p.u. (=1)

and  $r$  is equivalent ohmic resistance in p.u.

Ignoring the losses, these equations have to be equal, that is

$$\frac{1}{r} = m \left( \frac{\omega_{mek}}{\omega_{el}} \Big|_{u_n} \right) \cdot \omega_{el}$$

$$r = \frac{1}{m \left( \frac{\omega_{mek}}{\omega_{el}} \Big|_{u_n} \right) \cdot \omega_{el}} \quad (\text{A-3})$$

As we have assumed that this resistance is voltage independent, we get the electric power equation for an arbitrary voltage:

$$p = \frac{u^2}{r} = u^2 \cdot m \left( \frac{\omega_{mek}}{\omega_{el}} \Big|_{u_n} \right) \cdot \omega_{el} \quad (\text{A-4})$$

and the active part of the current:

$$\Re(i) = \frac{p}{u} = u \cdot m \left( \frac{\omega_{mek}}{\omega_{el}} \Big|_{u_n} \right) \cdot \omega_{el} \quad (\text{A-5})$$

The torque, for an arbitrary voltage:

$$m\left(\frac{\omega_{mek}}{\omega_{el}}, u\right) = \frac{p}{\omega_{el}} = u^2 \cdot m\left(\frac{\omega_{mek}}{\omega_{el}} \Big|_{u_n}\right) \quad (\text{A-6})$$

We can calculate the absolute value of the impedance  $z$  from the current data:

$$|z| = \frac{u_n}{i\left(\frac{\omega_{mek}}{\omega_{el}} \Big|_{u_n}\right)} = \frac{1}{i\left(\frac{\omega_{mek}}{\omega_{el}} \Big|_{u_n}\right)} \quad (\text{A-7})$$

and from this the apparent power  $s$  at arbitrary voltage:

$$|s| = \frac{u^2}{|z|} = u^2 \cdot i\left(\frac{\omega_{mek}}{\omega_{el}} \Big|_{u_n}\right) \quad (\text{A-8})$$

From apparent and active power we can calculate the reactive power  $q$ :

$$q = \sqrt{s^2 - p^2} = u^2 \cdot \sqrt{\left(i\left(\frac{\omega_{mek}}{\omega_{el}} \Big|_{u_n}\right)\right)^2 - \left(m\left(\frac{\omega_{mek}}{\omega_{el}} \Big|_{u_n}\right) \cdot \omega_{el}\right)^2} \quad (\text{A-9})$$

*Appendix A Calculation of active and reactive power of an induction motor based on curves for torque and current during start-up*

## APPENDIX B MACHINE DATA FOR A TYPICAL OFFSHORE GENERATOR

**Table B-1: Machine data for 25.5 MVA Turbotype Generator**

Rated voltage	6	kV
Rated apparent power	25.5	MVA
Rated power factor	0.89	
Rated frequency	60	Hz
Sychr. speed	3600	RPM
Duty type	S1	
Full load power	22.7	MW
Full load current	2454	A
Sub transient reactance, saturated	14 +10/-0	%
Sub transient time constant	0.05	sec
Transient reactance, saturated	18 +10/-0	%
Transient time constant	0.1	sec
Synchronous reactance, saturated	208 +/-10	%
DC time constant	0.2	sec
Zero sequence reactance, saturated	9 +/-10	%
Short circuit current 3-phase	350	%
Short circuit current 2-phase	568	%
Thermal current rating	400	%
Thermal time rating	10	s

*Appendix B Machine data for a typical offshore generator*

# APPENDIX C MACHINE DATA FOR A TYPICAL LARGE INDUCTION MOTOR

The following pages present a copy of a typical data sheet for a typical large induction motor. Table C-1: shows the catalogue data for the actual motor. As can be seen, the figures in the data sheet differ from the catalogue data. This is also typical, catalogue data are only informative for large motors, the real motors are built to specifications.

**Table C-1: Catalogue data for SIEMENS Motor**

Manufacturer	SIEMENS
Rated voltage	9-11 kV
Rated frequency	50/60 Hz
Type of construction	IM B3
Rotor construction	Squirrel Cage
Starting characteristics	N
Degree of protection	IP545
Cooling method	IC81W
Order no.	1RN1804-4HN
Rated power at 50 Hz	7150 kW
Rated speed at 50 Hz	1494 Rpm
Rated current at 10 kV	470 A

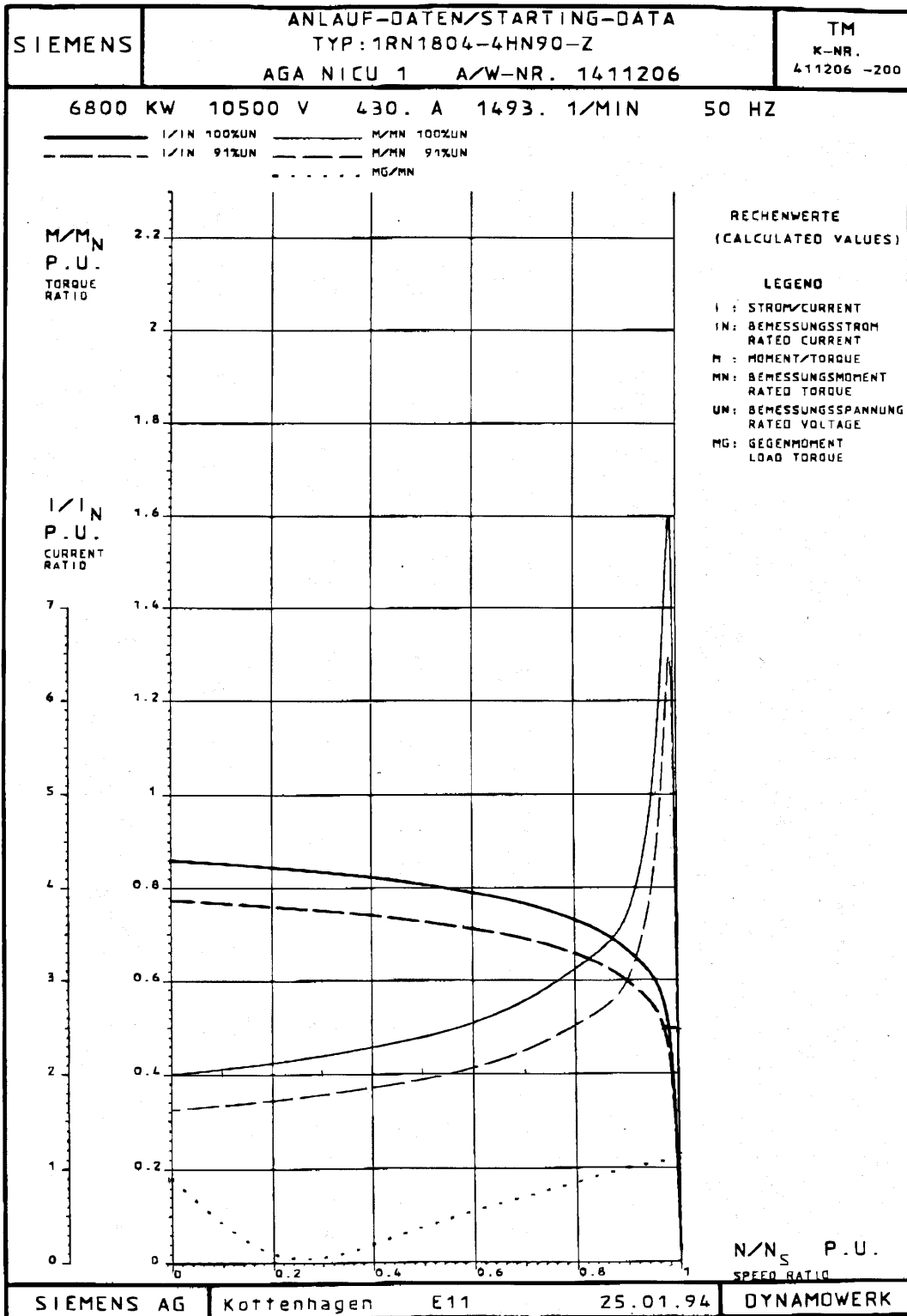
**Table C-1: Catalogue data for SIEMENS Motor**

Efficiency at 5/4 - 4/4 - 3/4 - 2/4 of rated power	97.1 - 97.5 - 97.5 - 97.0%
Cos $\phi$ at 5/4 - 4/4 - 3/4 - 2/4 of rated power	0.89 - 0.90 - 0.90 - 0.86
Rated torque	45701 Nm
Trip torque	200% of rated
Starting torque	60% of rated
Starting current	560% of rated
Moment of inertia	295 kg m <sup>2</sup>
Max. permissible external moment of inertia	2145 kg m <sup>2</sup>
Weight	17.1 t



Appendix C Machine data for a typical large induction motor

<b>SIEMENS</b>		Order Confirmation - Electrical Data		1411206	
Code Word: AGA NICU 1		Order No.: P1312-R-P131-704232		Works No.: 1411206	
		Order Date: 24.01.94		Manuf. No.: D9441120601	
1 Unit		Three-Phase Induction Motor with Laminated Squirrel Cage Rotor			
Type:	1RN1804-4HN90-Z	Mounting:	IMB3	Enclosure:	IP54
Standard:	VDE/IEC	Cooling System:	ICW37A81	Ex-Protection:	
Rotation:	ccw	Thermal Class:	F	Insul. System:	Micalastic
Duty:				Service Altitude <=	1000 m
Drive for:	Turbo-Compressor	Type:	SULZER	Required Inertia:	tm <sup>2</sup>
				Required Power:	5750 kW
<b>Operating Data:</b>					
Output	kW/HP	Rated Point			
Voltage	V	8800 / 10500		/	/
Variation	% +/-	5 / 5		/	/
Current	A	430		/	/
No Load Current	A	56			
Power Factor		0.89			
Frequency	Hz	50			
Range	% +/-	5 / 5		/	/
Speed/Over-Speed	min <sup>-1</sup>	1493 / 1800		/	/
Cooling Temp. sec./prim.	°C	28 / 43		/	/
Wdg. Limit Temp. Stator	°C <=	120 (R)			
Duty Type		S1			
Servicefactor					
<b>Starting Data</b>				<b>Counter-Torque</b>	
External Reactance	p.u.				
Voltage	p.u.	1.00	0.91	Speed p.u.	T p.u.
Locked Rotor Torque	p.u.	0.40	0.32	1.0	0.220
Pull-up Torque	p.u.	-	-	0.8	0.170
Break down Torque	p.u.	1.60	1.30	0.6	0.110
Locked Rotor Current	p.u.	4.30	3.87	0.4	0.040
Starting Time	s app.	18	23	0.2	0.020
LR-Time	cold/hot app.			0.0	0.180
Allowed Rep. Rate	cold/hot app.	3 / 2	3 / 2	TR	43.47 kNm
Method of Starting: direct-on-line		Moment of Inertia Mach./Ext. 0.293 / 1.890 tm <sup>2</sup>			
<b>Efficiency / Power Factor</b>			<b>Losses at Rated Load</b>		
Load	P.F.		Efficiency (%)	x	Bearing
0.848	0.89		97.6	x	Friction
1.000	0.89		97.6	x	Core
0.750	0.90		97.7	x	DC Stator 75 °C
0.500	0.90		97.6	x	DC Rotor 75 °C
x Marked Losses are Included in the Efficiency				x	Additional Brushes
Stator Lamination V350-85A 3.5 W/kg at 1,5 T				x	Separated Fanpower
<b>Resistances and Reactances in p.u. Ref. to ZR = Ω</b>				<b>Time Constants in s at 75 °C</b>	
F=0	F=FN		s=0	s=1	
R1		XS1			T0
R2'		XS2'			TG
		XH			T(3K)
		XK			T(2K)
Comm. React. / System (F = Hz)					
<b>Magnetic Forces</b>		<b>Therm. Time Constants</b>		<b>Sudden Short Circuit Torque (in p.u.)</b>	
		Running	20 min		
		Standstill	300 min		
		Over Current Factor	1.15		
<b>Remarks:</b>					
Sales Address: ASI1GV131 Erlangen; Mr./Mrs. OEDEGARD; Phone/Fax +186/1627					
* Guaranteed Values without Tolerance					
Date	Issued by	Dep.	Phone/Fax	Sheet: 1	
8.04.94	Kegel	E11	25231/23992	B52886	



# **APPENDIX D    COMPARISON OF SYSTEMS FOR HVDC POWER SUPPLY TO OFFSHORE OIL INSTAL- LATIONS WITH EMPHASIS ON THE DOUBLE BRIDGE INVERTER.**

Paper SPT PE 01-01-0337 presented at the IEEE/KTH Stockholm Power  
Tech Conference, Stockholm, Sweden June 18-22, 1995

*Appendix D Comparison of Systems for HVDC Power Supply to Offshore Oil Installations  
with Emphasis on the Double Bridge Inverter.*

## Comparison of Systems for HVDC Power Supply to Offshore Oil Installations with Emphasis on the Double Bridge Inverter.

Jørgen Chr. Myhre (S'95)

Department of Electrical Power Engineering  
Norwegian Institute of Technology (NTH)  
Trondheim, Norway

Tore M. Undeland (SM'92)

Henry B. Raphael (M'92)

Statoil  
Stavanger, Norway

*Abstract* - Electrical power supply from land to offshore installations is only possible by the use of HVDC, because of the long sea cables. Correct operation of conventional HVDC converters require a certain short circuit ratio in the AC-network, and this is not present on an offshore installation. The application of self commutated GTO-converters is not yet feasible due to the high power ratings required.

This paper investigates the requirements to a converter for use in the offshore end of a HVDC-transmission, together with the necessary auxiliary equipment. Different possible solutions are analysed and compared with regard to weight and volume, since they are the most important parameters in offshore applications. The most promising solution, a double bridge inverter based on forced commutated current source thyristor inverters is analysed by time domain simulation to indicate the technical feasibility of this converter..

### I. INTRODUCTION

Electrical power on Norwegian offshore installations is usually provided by local generation using gasturbines. Today, concerns regarding CO<sub>2</sub> and the greenhouse effect make it desirable to supply hydro-electrical power from land. In most cases this requires HVDC-transmission, because of the long sea-cables that have to be used.

The transmission must be able to supply the necessary power for all operations of an oil production installation. All machines that are directly powered by gas-turbines today would become electrically powered. This results in power loads from about 100 MW up to 500 MW for a large field like Ekofisk or Staffjord. Dynamically the system must withstand a direct start of an induction motor with rated power of 10 MW to 15 MW or up to 15% of the converter rating while maintaining a voltage and frequency deviation within accepted norms. In case of faults, the tolerances are wider, but system stability must be maintained.

The converter should be able to operate as a one-to-one transmission, or as a tap-station in one of the proposed HVDC-transmission projects from Norway to the European continent or Great Britain. The converter found must be based on components and technology which are available today, although the application can be unconventional, as

the era of big platforms may soon come to an end and smaller oil production units will be placed subsea.

### II. CONVENTIONAL HVDC-TRANSMISSION TO WEAK AC-NETWORKS

Conventional HVDC-converters consume reactive power in both the inverter and rectifier modes. The supply of a weak AC-network by means of a conventional HVDC-converter requires the use of capacitor banks, synchronous compensators or other sources to supply the reactive power needed both by the load and the inverter.

In the case of a weak AC-network the reactive power needed has traditionally been supplied by synchronous compensators, which has been dimensioned to supply all the reactive power needed beyond that supplied by the filters. This has given the additional benefit of improved short circuit ratio as well as increased inertia in the network, giving better voltage control and frequency stability. Usually a compensator rating of 50 to 60% of the transmission power rating or more has been applied

A typical single line diagram of a HVDC-inverter in a weak AC-network is shown on Fig. 1.

Such a compensator is heavy and space-consuming, thus making the use of conventional HVDC-transmission both expensive and impractical on an offshore installation with their severe restrictions on weight and volume.

### III. REQUIREMENTS TO HVDC-SUPPLY TO PASSIVE AC-NETWORKS

Traditional analysis of a HVDC supply to weak or passive AC-networks has focused on the reactive power problem. Some simple simulations have shown that the active power problem can be just as important.

Present research at NTH shows that by applying dq-transformation and decoupling, control techniques commonly used in advanced motor control, it has been possible to achieve a fast and accurate control of Unified Power Flow Controller (UPFC) systems with independent control of active and reactive power [1]. By applying the same control philosophy to the control of HVDC supply systems (includ-

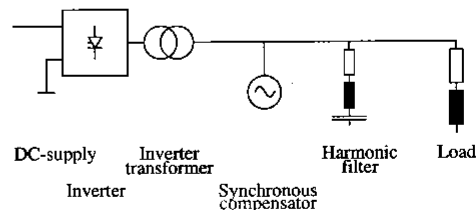


Fig. 1 Single line diagram of conventional HVDC-inverter with synchronous compensator

Paper SPT PE 01-01-0337 accepted for presentation at the IEEE/KTH Stockholm Power Tech Conference Stockholm, Sweden June 18-22, 1995

ing necessary auxiliary equipment), it is therefore possible to regard the supply of active and reactive power as two independent problems. Then the necessary elements of an offshore HVDC-inverter station can be as shown in Fig. 2

When there is a change in the active load in an offshore AC-network supplied only by traditional HVDC, there will always be a communication delay until the rectifier reacts by increasing the current, and the system can only react with a limited rate of change. This will raise a difference between required and supplied active power, leading to voltage deviations. Thus there must be some kind of energy storage that can supply or absorb the difference of active power between load and supply in order to keep the voltage within given limits. The supply of reactive power is not so critical as it can easily be produced in correct amounts on the installation itself by capacitors and fast reacting static units.

One possible solution to the active power problem is to allow the frequency to vary. Then the kinetic energy of the synchronous compensator and other motors connected to the offshore network, together with the changed need for power to the driven machines, can be used to bridge the transient difference of active power, and large voltage deviations can be reduced. A variation of this could be "flywheel" storage by frequency controlled synchronous machines.

Electrical storage of energy in inductors or capacitors is also possible. One way of doing this is to dimension the DC-capacitor of a SVC such that it is able to store sufficient energy. Another is to provide for increase of the DC-voltage while the DC-current is kept constant by the smoothing inductance and the rectifier which is operating in current control mode. This requires increased firing angle and extinction angle margins in the rectifier and inverter respectively, which leads to an increased need for reactive power in the AC-systems at both ends.

The least economical way is to always provide more active power than necessary and boil away the instantaneous surplus in a thyristor controlled dump load. This could at least be done for short periods in connection with planned switching of the load.

Not all these possibilities are equally feasible, particularly for use on offshore installations. A number of combinations has to be selected and compared to find the best.

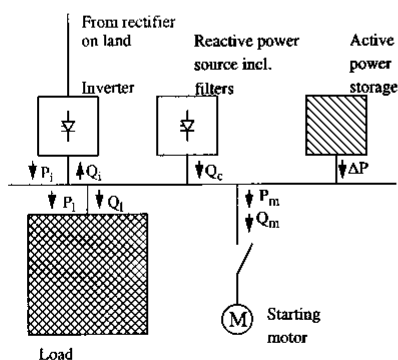


Fig. 2 Necessary elements in a HVDC supply to a weak AC-network

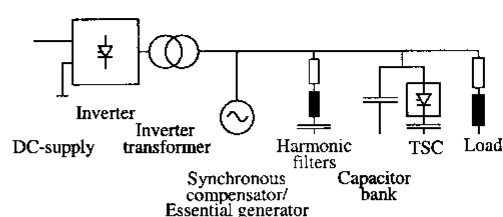


Fig. 3 Single line diagram of HVDC-transmission with minimized synchronous compensator and thyristor switched capacitor (TSC)

#### IV. POSSIBLE INVERTER TOPOLOGIES

A number of different possible inverter topologies have been analysed and compared to the conventional solution for an offshore load of 100 MVA, where the largest normal load change is caused by the starting of a 10 MW induction motor. The basis for comparison is weight and technical feasibility. In addition to the reference, the analysed converter systems are:

- HVDC-inverter with minimal synchronous compensator.
- Forced commutated, current source thyristor inverters.
- Self commutated, voltage source GTO-thyristor inverters.
- Converter system with AC-link.
- HF-base converter system.
- Double Bridge, forced commutated current source thyristor inverter system.

Some of these converter systems have been analysed both with capacitors and with synchronous compensator as means of energy storage

#### A. Conventional HVDC-inverter.

The conventional HVDC-inverter, shown in Fig. 1, with a synchronous compensator rated at 0.6 pu, has been used as reference. This solution is regarded by oil companies as too expensive, mainly due to the heavy weight of the compensator.

#### B. HVDC-inverter with minimal synchronous compensator.[2]

A single line diagram of this system is shown on Fig. 3. The compensator is dimensioned on basis of inertia in order to keep the frequency and voltage variations within the allowable limits of 2% and 10% during a load variation which is equivalent to the starting of a 10 MW induction motor. The voltage drop is caused by lack of active power due to a time delay of 30 ms (communication/data processing) and a rate of power increase limited to 0.05 pu/20 ms. The necessary reactive power is assumed to be supplied by fixed and thyristor switched capacitors. The inertia provided by the other rotating machines is ignored and the necessary inertia is provided by a synchronous machine with rating 0.1 pu by normal construction. This machine has also the capability to serve as essential generator, if it is connected to a gas turbine or diesel motor by a clutch. This solution would give a weight reduction of 20% of the total inverter station, compared to the conventional system.

#### C. Forced commutated, current source thyristor inverters.

These are not found to be feasible in their basic form as they are dependent on the current control of the rectifier in

order to control the AC-voltage. This requires a fast commutation link that must always be available. On the other hand such inverters can be applied in more sophisticated configurations like the Double Bridge inverter.

*D. Self commutated, voltage source GTO-thyristor inverters.*

These are not yet available in the necessary power range as single units, making series and/or parallel connection of units necessary. This is considered as to complex and not acceptable by the oil companies.

*E. Converter system with AC-link [3],[4].*

This system was originally proposed for traction applications. The principal features is shown on Fig. 4.. It consists of a line commutated thyristor inverter feeding into an AC-link. The voltage of the link is controlled by a forced commutated master converter operating as rectifier while supplying reactive power (4th quadrant operation). The system voltage can be adapted by the transformer to a level that allows a GTO converter to be used as master converter. Because the AC-link is not connected to the rest of the AC-network, the frequency of the link can be chosen freely. By choosing a frequency higher than the normal 50(60) Hz, the size and weight of the transformer can be considerably reduced.

This system could only be applied if a DC distribution system is used, and the third conversion can take place in separate inverter drives. Active power storage can be provided either by a capacitor in the second DC-link or by a small synchronous compensator connected to the AC-link. If all the large motors are powered by separate inverters, they can be soft started and the need for power storage can be greatly reduced.

Still there are several drawbacks with this system. It is very complex and requires conversion in 3 steps. Since all the active power has to pass through the master converter, the power rating is still to high to be handled by one single GTO- converter unit and a master converter consisting of several converters in parallel is required. A high frequency line commutated HVDC inverter is not a proven technology, neither is a high frequency transformer in the 100 MVA-class.

If the drawbacks could be overcome, the weight of the system could be as low as 30% of a conventional HVDC-inverter with synchronous compensator.

*F. HF-base converter system [5],[6].*

This system is based on a high frequency link and conversion from link to network frequency by a cycloconverter. The principle is shown on Fig. 5. The variable link frequency is determined by resonance between a capacitor and the parallel connection of the base inductor and the virtual inductances of the inverter and the cycloconverter. To

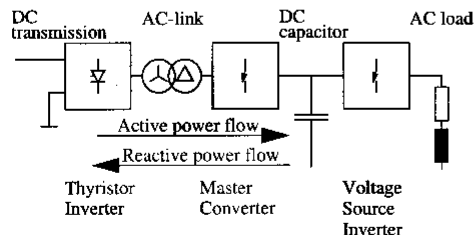


Fig. 4 Single line diagram of AC-link converter

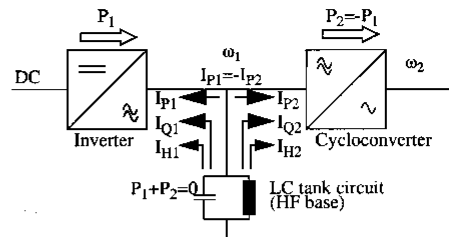


Fig. 5 Simplified functional diagram of a high frequency base DC to AC converter

achieve an output voltage from the cycloconverter with a minimum need for filtering, the tank frequency should not be less than 6 times the network frequency. The lowest frequency appears at no-load and would be 300 Hz in the case of a 50 Hz network. This is the resonant tank's auto-frequency. The upper frequency limit at max reactive load is set to 600 Hz. These frequency limits can be reduced on the cost of more filtering on the load side of the cycloconverter.

As in the previous case, a substantial weight reduction can be achieved by placing the necessary transformer in the high frequency link. The cycloconverter is able to supply an easily controlled AC-voltage with low levels of harmonics, to the load and operates with any power factor. The drawbacks are similar to the previous system: The complexity is less, but still considerable, and it requires high power high frequency technique. The system lacks inherent power storage, but this can be achieved by a small synchronous compensator (0.1 pu) connected to the supplied network. The total weight is as low as 40% of the reference HVDC converter. Further weight reduction could possibly be achieved by replacing the resonant tank with a high frequency synchronous compensator, which also gives the possibility of reducing the necessary frequency variations.

*G. Double Bridge, forced commutated current source thyristor inverter system [7],[8],[9],[10].*

This system is the most promising configuration. Here, two forced commutated current source inverters are connected in series to a DC-transmission fed by a current controlled rectifier. The inverter system is shown in Fig. 6. The two inverters are phase controlled in relation to each other to control the current being forced into the load, thus creating the correct voltage. This is indicated in the phasor diagram

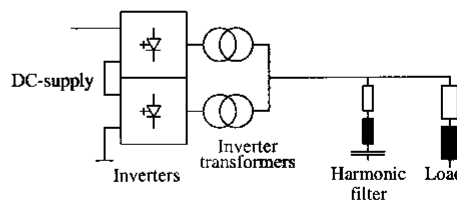


Fig. 6 Single line diagram of double bridge inverter.

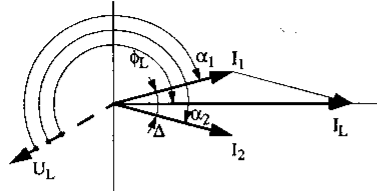


Fig. 7 Phasor diagram of voltages and currents as seen from the double bridge converter.

Fig. 7, where  $I_1$  and  $I_2$  are the currents from the two inverters, equal in magnitude but with a phase difference of  $\Delta$ . The resultant load current  $I_L$  creates the load voltage  $U_L$  when forced into the load impedance  $Z_L$ . The firing angles of the separate inverters are  $\alpha_1$  and  $\alpha_2$  respectively. Actually the idea of firing angle is irrelevant in this case as inverter 1 is timer controlled to give the fundamental frequency and only the time delay  $\Delta$  is variable. This configuration has the benefit of a fast control of the AC-current into the load, by means of controlling the phase difference  $\Delta$  between the currents from the two inverters without variation of the DC-current.

If the load varies, the delay angle  $\Delta$  between the inverter currents can be rapidly changed, adjusting the load current to restore the voltage level, while the DC-current remains unchanged. Then a slower master control can adjust the DC-current in order to get the delay angle back to the optimum. A favourable delay angle is  $30^\circ$ . The two inverters will then act as a 12-pulse connection with its beneficial influence on the harmonics. A delay angle  $\Delta$  of  $30^\circ$  leaves a control margin of only 3.4% for fast load increase. If bigger load switching is to be expected,  $30^\circ$  delay angle can still be applied if the switching can be preceded by an increase of the DC-current and a temporarily increase of the delay angle.

This system has not the need for separate energy storage elements, as it uses the transmission inductance for energy storage. By varying the phase difference between the currents the DC-voltage also is affected, thereby varying the amount of active power transmitted. Variation of the DC-voltage requires sufficient firing angle margin in the rectifier to avoid commutation failure, and thereby the rectifier requires more reactive power from the supply network.

#### H. General

All the converter systems except the last has a start-up problem, the must be energized before the inverter can be started. This is not a serious problem as there always will be an emergency power supply present on an offshore installa-

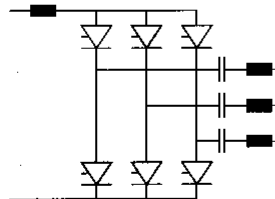


Fig. 8 Thyristor inverter forced commutated by series connected capacitors

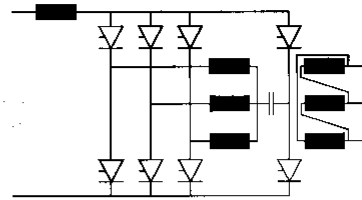


Fig. 9 Thyristor inverter forced commutated by capacitor in transformer neutral point

tion. The double bridge inverter can start on a dead network by running the two bridges with  $180^\circ$  delay angle.

The results of the analysis are summarized and compared in Table I. The best way of saving weight is to use a topology which make use of higher frequencies, but this is an uncertain technique for high power applications, also regarding transformers. The double bridge inverter is the most lightweight solution that operates with normal frequency.

#### V. FORCED COMMUTATED THYRISTOR CONVERTER FOR THE DOUBLE BRIDGE INVERTER

The double bridge inverter could be constructed on the basis of the series capacitor commutated thyristor inverter shown in Fig. 8 [7]. This topology is simple and straightforward, but it has some serious drawbacks, especially high voltages across the valves and high ratings of the capacitors, which have to carry the full load current. According to one investigation, inverters with auxiliary commutation circuits would be more feasible [8]. One such inverter is shown in Fig. 9., another, particularly promising is shown together with load and filter model in Fig. 10

The thyristor inverter with the capacitor in the transformer neutral point is thoroughly analysed and proved to be functioning [11]. Unfortunately the inverter has one drawback, it is not practically possible to operate at firing angles  $\alpha$  beyond  $205^\circ$ , due to the fact that for higher firing angles the available recovery time is getting to short for high power thyristors.

A firing angle of  $205^\circ$  corresponds to a power factor of 0.9 ind. of the load as seen from the bridge, including transformers, filters and all. This is clearly to small margin for a safe operation of the double bridge inverter. The inverter topology shown in Fig. 10 do not have this deficiency [9], [10]. As not much is found regarding dimensioning of this inverter, further investigation is necessary.

#### VI. THYRISTOR INVERTER FORCED COMMUTATED BY 4 AUXILIARY THYRISTORS AND 1 CAPACITOR

In order to investigate the inverter topology the circuit shown in Fig. 10 was modelled in Kream, a time domain simulation system developed at NTH. The DC transmission line is modelled as a current source, and the lumped motor load is modelled as a emf source behind the subtransient short circuit reactance. The filter is modelled as a high pass filter tuned at the 5th harmonic with a Q-value of 2 and a reactive power rating at fundamental frequency of 0.33pu. This provides a reasonable filtering and some phase compensation of the load. But most important is that it provides a current path without additional inductance for the commutation current from the auxiliary capacitor. It appears that the



**TABLE I: COMPARISON OF DIFFERENT CONVERTER TYPES BY WEIGHT**

	Converter type	Conventional inverter	Unconventional inverter	Capacitor (rating at 50 Hz)	Inductor/transformer (rating at 50 Hz)	Synchr. compensator	Total Weigh	Remarks
1	Conventional HVDC	84MVA 8.4t		76Mvar 53.2t	88MVA 105.6t	50MVA 110.0t	277.2t	Synchr. compensator to heavy
2	HVDC with reduced synchr. compensator	134MVA 13.4t		117Mvar 81.9t	88MVA 105.6t	10MVA 22.0t	222.9t	Conventional technique
3	Conv. system with AC-link and cap. energy storage.	94MVA 9.4t	194 <sup>a</sup> MVA 19.4t	1200Mvar 840.0t	18MVA 21.6t		890.4t	Prohibitive capacitor rating. To complex. High frequency techn.?
4	Conv. system with AC-link and synchr. comp	94MVA 9.4t	194MVA 19.4t	10Mvar 7.0t	18MVA 21.6	10MVA 22.0t	79.4t	To complex, to many conversion steps. High frequency techn.?
7	HF-base converter	84MVA 8.4t	157 <sup>b</sup> MVA 15.7t	11.9Mvar 8.4t	37.4MVA 45.6t		78.1t	No active power storage. Resonant circuit? High frequency techn.?
8	HF-base converter with synchr. compensator	84MVA 8.4t	157MVA 15.7t	11.9Mvar 8.4t	37.4MVA 45.6t	10MVA 22.0t	100.1t	Synchr comp. in resonant circuit may stabilize. High freq. techn.?
9	Double bridge converter		142 <sup>c</sup> MVA 14.2t	73.4Mvar 51.8t	100MVA 120.0t		186.0t	Technique possible but untried. Most lightweight with normal freq.

- a. GTO-rating
- b. Cycloconverter equivalent thyristor rating
- c. Equivalent thyristor rating

critical factor to get the commutation times down is the value of the commutation inductivity which decides how fast the DC-current can be shifted from the load circuit to the auxiliary circuit. The model has the following parameters, adjusted to achieve a load fundamental voltage of 100% and a load fundamental current of 100%, with a power factor of 0.8ind:

- Load inductance  $L_L: 3.68 \times 10^{-4}$
- Load resistance  $R_L: 9.23 \times 10^{-3}$
- Load emf  $e_L: 0.51e^{j67.1^\circ}$
- Transformer leak inductance  $L_T: 2.2 \times 10^{-4}$
- Filter inductance  $L_F: 3.8 \times 10^{-4}$
- Filter resistance  $R_F: 1.2$
- Filter capacitance  $C_F: 1.1 \times 10^{-3}$
- Auxiliary capacitance  $C_H: 2.5 \times 10^{-4}$
- Auxiliary inductance  $L_H: 1 \times 10^{-8}$

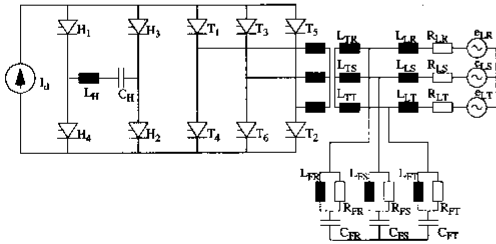


Fig. 10 Krean model of forced commutated inverter with motor load and high pass filter added

- DC current  $I_d: 1.64$

Some results of the simulations are shown. Fig. 11 shows the auxiliary capacitor voltage and current. For the chosen circuit, the voltage reaches as high as 350%. This voltage also appears as peaks in the DC-voltage, Fig. 12, and AC terminal voltage, Fig. 13, but the peaks are substantially damped by means of the commutation inductivity and the filter circuit before reaching the load, Fig. 14. Max.  $di/dt$  is found to be  $0.01I_{TM}/\mu s$  and max.  $dV/dt$  is  $1.7V_{DRM}/ms$ . Reverse recovery time for the main thyristors is  $400\mu s$ . The total rms value of the current in the auxiliary capacitor is 86%.

It must be noted that this circuit is chosen only to investigate the commutation properties, and it is not optimized in any way. But it is apparent that the circuit operates and the component stresses are not prohibitive, even without optimization.

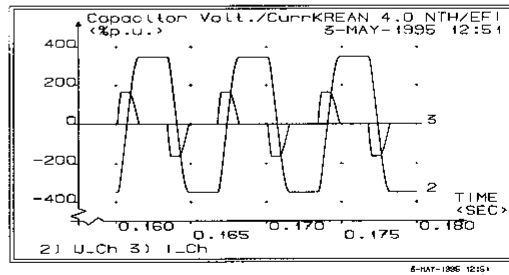


Fig. 11 Auxiliary capacitor voltage and current as result of Krean simulation

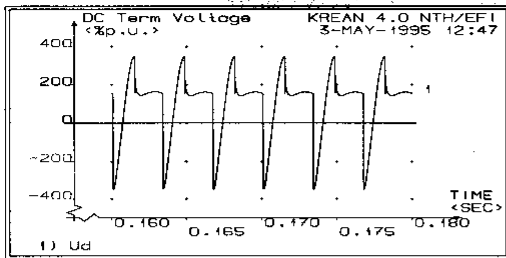


Fig. 12 DC terminal voltage as result of Kream simulation

#### VII. CONCLUSIONS

If offshore oil installations shall be supplied with electrical power from land, HVDC transmission is necessary. The inverter station must be able to operate on a passive AC-network, and synchronous compensators are not desirable due to the weight. Two ways are possible, either reduce the size of the compensator and accept increased frequency variations, or apply a forced commutated inverter system, which must have two control variables in order to control both AC voltage and frequency. GTO inverters are not yet available with the ratings necessary, but the double bridge inverter can probably be used. A forced commutated current source thyristor inverter with 4 auxiliary thyristors and 1 capacitor is simulated in the time domain to investigate the commutation, and found feasible. Further simulations are necessary to optimize the inverter circuit for use in the double bridge inverter. Further system analysis is also necessary to determine the necessary requirements for a stable operation under fault conditions.

#### VIII. REFERENCES:

- [1] Q. Yu, S. D. Round, L. E. Norum and T. M. Undeland, "A New Control Strategy for a Unified Power Flow Converter," to be published in Proceedings of the 6th European Conference on Power Electronics and Drives, Sept. 1995
- [2] Gjerde/Gjengedal/Fleto: "Stability in weak power systems supplied by HVDC" EFL/NTH 1994
- [3] H. Mennicken, "Stromrichtersystem mit Wechselspannung-Zwischenkreis und seine Anwendung in der Traktionstechnik." Dr.ing-dissertation, Aachen, June 1978.
- [4] S. Ostlund, "A Primary Switched Converter System for Traction Applications." Dr.ing-dissertation, Stockholm, December 1992
- [5] Gyugyi/Cibulka: "The high frequency base converter - a new approach to static high power conversion" IEEE/IAS ISPC-77
- [6] P. M. Espelage and B. K. Bose, "High frequency link power conversion." Proceedings of IEEE-IAS Ann. Meeting 1975, pp 802-808

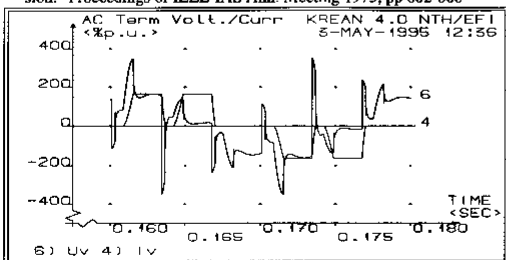


Fig. 13 AC terminal voltage and current as result of Kream simulation

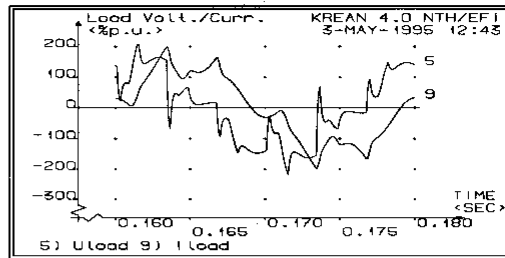


Fig. 14 Load voltage and current as result of Kream simulation

- [7] Turani/Menzies/Woodford: "Feasibility of DC transmission with forced commutation to remote loads" IEEE-PAS 103 no. 6, June 1984
- [8] Tam/Laseter: "Implementation of the hybrid inverter for HVDC/weak AC system interconnection" IEEE-PWRD 1 no. 4, Oct. 1986
- [9] V. K. Sood and J. P. Bowles, "Forced Commutated HVDC Inverters", Paper prepared for the System planning and Operating Section, Canadian Electrical Association Spring Meeting, Vancouver March 1979
- [10] V. K. Sood "A Novel DC Line-side Force-commutated HVDC Inverter for Feeding Remote Loads", IEEE international Communications and Energy Conference, Montreal 2-4 Oct. 1984, pp 86-89.
- [11] R. Jötten and W. Michel, "Feeding into a weak AC-system by a forced commutated HVDC converter and the associated control." D.O.E. Symposium on Urban Application of HVDC Power Transmission, Philadelphia, Oct. 24-26, 1983.

Jørgen Chr. Myhre (S'95) graduated from Dept. of Electrical Machines, NTH, in 1975. Then he was with the Norwegian Electric Power Research Institute (EFI), before joining Siemens Norway in 1977. He is currently on leave from Siemens, pursuing a Dr.ing degree at Dept. of Electrical Power Engineering, NTH. The studies are funded by the Norwegian Research Council.

Tore M. Undeland (M'86, SM'92) graduated in 1970 and received the Dr.ing degree in 1977, both from NTH. From 1970 he has been with NTH, from 1984 as Professor in Power Electronics at the Dept. of Electrical Power Engineering. He is also a Scientific Adviser to EFI. He has been a Visiting researcher at ASEA Sweden in 1979 and at Siemens Norway in 1991/92. He was a Visiting Professor in the Dept. of Electrical Engineering at the Univ. of Minnesota, Minneapolis, in 1982. He has worked on many industrial R&D projects in the power electronics field. He has numerous publications and is a co-author of a recent textbook in power electronics. Prof. Undeland is a member of the IAS Industrial Power Converter Committee (IPCC) and its European Subcommittee (EWG), and of European Power Electronic Association (EPE).

Henry B. Raphael (M'92) received the M.S. and Ph.D. degrees from the NTH and Univ. of Toulouse in 1959 and 1968 respectively. He worked with the NTH from 1960 to 1978, except for two sabbatical years at the Univ. of Toulouse and at Siemens Erlangen respectively. In 1979 he joined EFI, and from 1987 he has been with the Norwegian oil company Statoil. His field of work deals with offshore and onshore electrical power systems, especially large adjustable speed drives. Dr. Raphael still holds an adjunct professorship at the NTH. He has been an author or co-author of more than 40 conference, seminar and journal papers.

## REFERENCES

- [1] H. B. Raphael.  
"Bruk av turtallsregulerte elektromotorer og kompresjon" ("The use of controllable speed drives and compression")  
NIF-TIR, Stavanger 1991
- [2] FEA-M 1990  
Regulations for electrical installations on board ships, mobile drilling platforms, dredgers, floating cranes etc. of 1 March 1990.....  
Prepared by the Norwegian Water Resources and Electricity Board 1990
- [3] NPD 1993  
Regulations relating to electrical installations in the petroleum activities.  
Norwegian Petroleum Directorate 1993
- [4] E. W. Kimbark.  
"Direct Current Transmission"  
John Wiley & Sons, Inc. 1971
- [5] Å. Ekstrøm  
"High power electronics. HVDC and SVC."  
The Royal Institute of Technology, Stockholm June 1990.
- [6] H. Mennicken  
"Stromrichtersystem mit Wechselspannungs-Zwischenkreis und seine Anwendung in der Traktionstechnik."  
Dr.ing-dissertation, Aachen, June 1978.

*References*

- [7] S. Östlund  
“A Primary Switched Converter System for Traction Applications.”  
Dr.ing-dissertation, Stockholm, December 1992  
(TRITA-EMK-9201)
- [8] L. Gyugyi and F. Cibilka  
“The high frequency base converter - a new approach to static high power conversion.”  
IEEE/IAS ISPC 1977 Conference Papers, pp137-146.
- [9] R. Jötten and W. Michel  
“Feeding into a weak AC-system by a forced commutated HVDC converter and the associated control.”  
D.O.E. Symposium on Urban Application of HVDC Power Transmission, Philadelphia, Oct. 24-26, 1983.
- [10] K. Tam and R. Lasseter  
“Implementation of the hybrid inverter for HVDC/ weak AC system interconnection.”  
IEEE PRWD-1 no 4 1986.
- [11] A. Tromm  
“Self-commutated converter circuit for offshore HVDC-supply.”  
Study project NTH/TU Darmstadt 1993/94.
- [12] J. C. Myhre  
“Converter system with AC-link.”  
Project notes KEM.95.009 NTH 1995.
- [13] J. C. Myhre  
“HF-base converter for DC/ weak AC conversion.”  
Project notes KEM.95.010 NTH 1995.
- [14] J. C. Myhre  
“Forced Commutated Thyristor Inverter for the Double Bridge inverter.”  
Project notes KEM.95.013 NTH 1995.
- [15] J. C. Myhre  
“Comparison of possible converters for DC/ weak AC conversion.”  
Project notes KEM.95.011 NTH 1995.

- [16] H. M. Turanli, R. W. Menzies and D. A. Woodford  
“Feasibility of DC transmission with forced commutation to remote loads.”  
IEEE PAS-103 no 6 1984
- [17] O. J. Figved  
“Høgspenning - likestrømforsyning fra land”  
 (“High voltage direct current supply from ashore”)  
NIF-TIR, Stavanger 1992
- [18] J. O. Gjerde, T. Gjengedal and R. Flølo.  
“Stability in weak power systems supplied by HVDC”  
International Conference on Power System Technology, Beijing 1994
- [19] D. Povh.  
“Special Report for Group 14 (DC Links and Power Electronic Equipment)” for Study Committee 14, 1994 Session
- [20] Siemens AG  
“Catalog M27 High voltage motors H-module”, 1990
- [21] B. Ärnlov.  
ABB Power Systems, Ludvika, Sweden  
Private communications, Sept. 1994
- [22] L. Rolfseng.  
“Generelle betingelser for vekselstrømsforsyning fra land” (“General conditions for alternating current supply from ashore”)  
NIF-TIR, Stavanger 1992
- [23] J. C. Myhre  
“Active power condition during startup of a big induction motor on an offshore installation supplied by HVDC”  
Project notes KEM.95.012 NTH 1995.
- [24] S. Gilje.  
“Energisystemene på plattformer sett i et totalperspektiv” (“Energy system on platforms seen in a total perspective”)  
NIF-TIR, Stavanger 1992

## References

- [25] A. Haines.  
"Plattformens elektrisitetssystemer" ("Electricity systems of the platform")  
NIF-TIR, Stavanger 1992
- [26] B. K. Bose.  
"Power electronics and ac drives"  
Prentice-Hall 1986
- [27] H. H. Faanes, A. T. Holen, K. J. Olsen.  
"Stabilitet for kraftsystemer og motordrifter. Del 3; effekt og spenningsregulering" ("Stability for power systems and motor drives. Part 3; Power and voltage control")  
NTH Trondheim, 1992.
- [28] Joint Task Force, Cigré 14.07/ IEEE15.05.05.  
"Guide for Planning DC-Links Terminating at AC Locations Having Low Short-Circuit Capacity. Part I: Interactions"  
Cigré/IEEE 1991.
- [29] B. Frankén.  
"An Analysis of HVDC in Weak AC-Systems"  
Lic Techn.-dissertation, Stockholm, March 1989  
(TRITA-EES-8901)
- [30] G. Andersson.  
"Some Considerations on the Short-Circuit Capacity Requirements for a HVDC Terminal"  
KTH Stockholm, June 1992. (TRITA - EES - 9203)
- [31] Q. Yu, S. D. Round, L. E. Norum, T. M. Undeland.  
"A New Control Strategy for a Unified Power Flow Controller"  
NTH Trondheim, 1995
- [32] "KREAN Reference Manual"  
NTH Trondheim, 1994
- [33] "KREAN Module Manual"  
NTH Trondheim, 1994
- [34] "KREAN Module Library"  
NTH Trondheim, 1994
- [35] OLF  
Letter of 13 Oct. 1995

- [36] J. G. Balchen  
"Reguleringsteknikk Bind I" ("Control Theory, Volume I")  
Tapir, Trondheim 1971
- [37] J. G. Balchen  
"Reguleringsteknikk Bind I" ("Control Theory, Volume I")  
Tapir, Trondheim 1988
- [38] H. Bühler  
"Einführung in die Theorie geregelter Drehstromantriebe, Bd. I u. II"  
Birkhäuser, 1977
- [39] A. K. Ådnanes, T. M. Undeland.  
Stabilitet for kraftsystemer og motordrifter. Del 2; Modelling av synkronmaskinen" ("Stability for power systems and motor drives. Part 2; Modelling of the synchronous machine")  
NTH Trondheim, 1993.
- [40] A. T. Holen, I. Johansen, N. A. Selseth.  
"Elektriske kretser Bind II" ("Electrical Circuits, Volume II")  
Tapir, Trondheim 1968.
- [41] ABB Pamphlet POW-0017, rev 3  
HVDC Light Applications - Transmission with simplicity  
ABB Power Systems AB.
- [42] Siemens AG HVDC<sup>PLUS</sup> Workshop  
Siemens AG Dept EV HA 7M, Erlangen,  
12-13 December 2000.

*References*